R. & M. No. 2222
(10,324 & 10,325)
A.R.C. Monograph

MINISTRY OF SUPPLY

AERONAUTICAL RESEARCH COUNCIL
REPORTS AND MEMORANDA

Research on High Speed Aerodynamics at the Royal Aircraft Establishment from 1942 to 1945

By

THE STAFFS OF THE HIGH SPEED TUNNEL
AND HIGH SPEED FLIGHT SECTIONS

EDITED BY
W. A. MAIR

LONDON: HIS MAJESTY'S STATIONERY OFFICE
1950

LONDON
PRINTED AND PUBLISHED BY HIS MAJESTY'S STATIONERY OFFICE
To be purchased directly from H.M. Stationery Office at the following addresses:
York House, Kingsway, London, W.C.2; 13a Castle Street, Edinburgh, 2;
39 King Street, Manchester, 2; 2 Edmund Street, Birmingham, 3;
1 St. Andrew's Crescent, Cardiff; Tower Lane, Bristol, 1;
80 Chichester Street, Belfast
OR THROUGH ANY BOOKSELLER
1950
Price £1 10*s* 0*d* net

Research on High Speed Aerodynamics at the Royal Aircraft Establishment from 1942 to 1945

By

The Staffs of the High Speed Tunnel and
High Speed Flight Sections

Edited by W. A. Mair

Communicated by the Principal Director of Scientific Research (Air),
Ministry of Supply

Reports and Memoranda, No. 2222
*September, 1946**

Summary.—A brief description of the Royal Aircraft Establishment (R.A.E.) High Speed Wind Tunnel is given, together with an account of the methods used for calibrating the tunnel and for testing models in it. This is followed by a survey of the more important results obtained from tests on models in the tunnel. An account is then given of the technique which has been used at the R.A.E. for the investigation of compressibility effects in flight. Flight experiments at high speeds are described, and some comparisons are made with the results of wind tunnel tests. Future developments in wind tunnel and flight research at high speeds are briefly discussed.

Acknowledgments.—This report was written by W. J. Charnley, D. J. Higton, W. A. Mair, F. Smith, A. Thom and J. S. Thompson. In addition to these, many other members of the R.A.E. staff contributed to the work described in the report. It is not possible to include the names of all who took part, but important contributions were made by E. P. Bridgland, J. Caldwell, J. Y. G. Evans, S. P. Hutton, G. F. Midwood, R. Smelt and A. W. Thom. Mention should also be made of the pilots of the Aerodynamics Flight, R.A.E., particularly Squadron Leaders A. F. Martindale, B. H. Moloney and J. R. Tobin, on whose skill and courage the whole of the high-speed flight research depended.

LIST OF CONTENTS

* R.A.E. Report No. Aero. 2155 (A.R.C. 10,324) received 3rd February, 1947.
R.A.E. Report No. Aero. 2152 (A.R.C. 10,325) received 3rd February, 1947.

LIST OF CONTENTS—*continued*

LIST OF CONTENTS—*continued*

LIST OF ILLUSTRATIONS

LIST OF ILLUSTRATIONS—*continued*

LIST OF ILLUSTRATIONS—*continued*

1. *Introduction.*—In aerodynamic theory as applied to the design of aeroplanes it has been usual, until the last few years, to neglect the effects of the compressibility of the air. This simplification is justified if the flight speed is not too high, because it can be shown that if the velocity of the air relative to a body is small compared with the velocity of sound, the general features of the air flow past the body are very nearly the same as they would be if the air were incompressible. However, when the flight speed exceeds about 0·6 or 0·7 of the velocity of sound the changes of air density which occur in the flow round a wing become very important, and the compressibility of the air can then no longer be neglected. The velocity of sound in air depends on the temperature, and in the standard atmosphere it is 762 m.p.h. at sea level, 707 m.p.h. at 20,000 ft., and 660 m.p.h. at 36,000 ft. or above. Thus we may expect compressibility effects to become important at flight speeds above about 400 or 500 m.p.h. These speeds have frequently been reached in dives during the last 5 or 6 years and, more recently, they have been exceeded in level flight. Thus the effects of compressibility in aeronautics have become increasingly important during the last few years.

The dimensionless parameter which determines the effect of the compressibility of the air is the Mach number, the ratio of the velocity of air relative to a body to the velocity of sound in the air. As mentioned above, compressibility effects usually become important (on conventional aircraft) at Mach numbers above about 0·6 or 0·7. At some Mach number in this region, the local air velocity at a point on the wing usually becomes equal to the local velocity of sound. At higher Mach numbers a local region of supersonic flow is formed on the wing, and a shock wave is formed at the downstream boundary of this region. Shock waves formed in this way have large and important effects on the aerodynamic characteristics of aerofoils and aircraft at high speeds.

High-speed wind tunnels, designed to run at Mach numbers approaching unity, have been in use for a considerable time[1, 2]. Most of these tunnels have been fairly small, however, with working sections about 1 ft. in diameter, and have been used mainly for tests on two-dimensional aerofoils. Early in 1937 it was realised that there would be an urgent need in this country for a high-speed wind tunnel large enough for testing complete aircraft models. Proposals for the construction of such a tunnel were considered about that time, and in 1938 detail design work was started for a large high-speed wind tunnel at the Royal Aircraft Establishment (R.A.E.). The construction of the tunnel began in 1939, and three years later it was ready for use.

Until about 1943 no quantitative flight measurements at high speeds were available in this country which could be used to check the results of high-speed wind tunnel tests. At about that time, aircraft were becoming available with highly supercharged engines and fairly high wing loadings which were able to reach very high Mach numbers in dives from high altitudes. A series of dive tests was therefore started at the R.A.E., to provide quantitative information at high flight speeds which could be compared with the results of high-speed wind tunnel tests, and to investigate the handling characteristics of aircraft at high speeds.

This report describes experiments on high-speed aerodynamics which have been made at the R.A.E., in the wind tunnel and in flight. Descriptions of the High Speed Wind Tunnel and of the technique used for high-speed flight tests are also included.

2. *Description of High Speed Tunnel and Equipment.*—The R.A.E. High Speed Wind Tunnel is a variable density tunnel with a closed working section 10 ft. by 7 ft. The fan power is 4,000 H.P., and a top speed of 600 m.p.h. ($M = 0·8$), or slightly greater, can be obtained at a pressure of a sixth of an atmosphere, while with a tunnel pressure of four atmospheres the maximum Reynolds number is about ten million per foot chord at 250 m.p.h. The air in the tunnel is kept very dry, and the temperature is kept down by cooling the tunnel walls.

2.1. *Construction.*—An outline sketch of the tunnel structure is given in Fig. 1, and a pictorial view in Fig. 2. The settling chamber, the working section, and the expansion cone leading up to the fan lie along the axis of the cylindrical shell, and are surrounded by the return circuit which is of annular cross-section. This arrangement gives a dead space within the tunnel which is not part of the air circuit but is at about the same pressure.

2.11. *Buildings.*—The buildings are of reinforced concrete, and the general layout is shown in Fig. 3. At one end of the long room housing the tunnel is a room for the electrical plant, including the fan driving motors, and at the other end are the compressors and refrigerating plant, including brine storage tanks. In front of the tunnel is the block which contains a workshop at ground level, and above this the observation room at the level of the tunnel door (Fig. 1), these rooms being connected by a lift for moving models. The rest of the front block is used for offices, and it may be remarked that during the war years the output of tunnel work so far exceeded expectation that this office accommodation was not nearly adequate for the staff required.

The tunnel room is lined all over with a five-inch thick layer of cork for heat insulation. This also provides such effective sound-proofing that there is no unpleasant noise in the offices even when the tunnel is running at its maximum speed.

2.12. *Steelwork.*—The outer steel shell of the tunnel, which is 37 ft. diameter and 130 ft. long, is designed for internal absolute pressures from a tenth of an atmosphere to four atmospheres. The general construction can be seen from Fig. 4, a photograph taken during erection in 1941. The shell rests on four concrete foundations, and at three of the supports provision is made for sliding to allow for expansion. The inner wall of the return circuit is mounted on six struts at each end (*see* Fig. 1), and the rest of the internal structure is fixed to this shell. The balance, just below the working section, is mounted quite independently of the tunnel structure ; its supports pass through streamlined shields in the return circuit and rubber seals in the outer shell.

Access to the working section is obtained through the three doors shown in the middle section in Fig. 1. The outermost door is 7 ft. by 7 ft., and is of massive construction to withstand a load of 140 tons when the tunnel is under full pressure.

Most of the walls are of steel plate $\frac{3}{8}$ in. thick, but the outer shell is $\frac{9}{16}$-in. thick, and the working section is made of machined cast iron to ensure accuracy. Brine jackets for cooling are fitted to all the wind-swept surfaces, except the settling chamber, contraction cone, and working section.

2.13. *Air Circuit.*—The working section of the tunnel is 15 ft. long, and the cross-section at the upstream end is in the shape of a rectangle 10 ft. broad and 7 ft. high, with the corners rounded off to a radius of 2·4 ft. The height increases uniformly to 7 ft. 2 in. at the downstream end, giving an expansion of $2\frac{1}{2}$ per cent. in area to compensate for increasing boundary layer thickness. (It is shown below that this is rather more than is needed.) The air circuit is vented to the dead space through 38 holes $2\frac{1}{2}$-in. diameter at the downstream end of the working section.

Between the working section and the fan the area of the passage is doubled, and the expansion in the diffuser, which is very gradual at first, finally gives an area gradient equivalent to that of a cone of about 8 deg. included angle. The air after passing through the fan is turned through 180 deg. (without guide vanes), and along the annular return circuit the area expands from twice to seven times the working section area. In order to eliminate certain velocity fluctuations, mixing vanes have recently been installed in the return circuit. These are described in more detail below.

At the end of the return circuit the air makes a second 180 deg. turn to pass through the honeycomb into the settling chamber. At this point there was originally some breakaway of flow, and a double ring of turning vanes was installed to prevent this. The honeycomb is built up of hexagonal cells one inch across flats and five inches long. From the settling chamber to the working section the area ratio is seven, and the final stage of the contraction into the beginning of the working section is made very gradual.

2.14. *Fan.*—The fan (Fig. 5) is of one stage, with fixed guide blades upstream and downstream. There are 13 moving blades, and the normal maximum speed is 850 r.p.m., although the fan was originally designed for a higher speed. The hub diameter is 9 ft. 9 in. and the overall diameter 15 ft. 11 in., which gives a rotational tip speed of 710 ft./sec. at 850 r.p.m. This imposes severe stressing conditions on the fan ; the design, in fact, probably gives the maximum output that it is practicable to obtain from a single stage. The blades are made of " Hiduminium " RR 56, mounted on a solid steel hub (*see* Fig. 6).

2.2. *Operating Machinery.*—2.21. *Fan drive.*—The fan is driven by two direct current motors of 2,000 H.P. each, mounted in tandem as shown in Fig. 7. Some flexibility is provided by a cardan shaft with a Bibby coupling at each end, in order to allow for distortion or movement of the whole tunnel structure produced by pressure and temperature changes. Where the shaft passes through the tunnel shell, an oil seal is provided to prevent leakage when the tunnel is under pressure or vacuum. The oil pressure is adjusted automatically as the air pressure in the tunnel is changed.

The driving motors are supplied from two D.C. generators coupled to a synchronous motor on the 6,600 volt A.C. mains. The fan speed is controlled on the Ward Leonard system by adjusting the generator field ; in this way a smooth variation can be obtained over the whole speed range. This control is operated from the observation room. For keeping the fan speed steady, an automatic control is used, in which the voltage from a tachometer generator on the fan shaft is compared with a pre-set standard voltage, and the difference, amplified by thyratrons, is fed to an auxiliary field on the generators.

2.22. *Pressure control.*—The tunnel pressure is varied by two compressors, which can also be used as vacuum pumps, of 400 H.P. each. These two machines, working in parallel, can pump the tunnel up to an absolute pressure of four atmospheres in about 80 minutes, or down to a tenth of an atmosphere in 45 minutes. A control set of 80 H.P. is used for holding the pressure steady at any given value. Provision was made for this control to be automatic, but it is found more convenient to keep the pressure constant by hand, using an adjustable air leak operated by remote control from the observation room.

A diagram of the piping connections is included in Fig. 8.

2.23. *Cooling.*—The tunnel is cooled by circulating brine at about 4 deg. C. in jackets on the walls of the tunnel circuit. The brine itself is cooled by passing through heat exchangers refrigerated by an ammonia plant of normal type.

At full load, the 4,000 H.P. supplied to the fan has to be removed from the tunnel in the form of heat, and as the refrigerating machinery cannot handle this continuously, large brine tanks containing 460 tons of calcium chloride brine (density 1·23) at about —10 deg. C. are used as low temperature reservoirs. These consist of two steel tanks supported one above the other on reinforced concrete columns. These two storage tanks supply the jackets in the top and bottom halves of the tunnel through two independent systems, in order to avoid large hydrostatic pressures. Each system has 23 parallel circuits which can be controlled separately to obtain the best cooling conditions in the tunnel. The outer brine jackets and some of the piping can be seen in Fig. 4. The brine is circulated by a number of 7 H.P. centrifugal pumps, and thermostatically controlled mixing valves are arranged so that cold brine from the reservoirs and warm brine from the jackets can be mixed to produce any required circulating temperature. A small quantity of sodium dichromate added to the brine has been found effective in preventing excessive corrosion.

A schematic diagram of the cooling system is given in Fig. 8. There are four 65 H.P. two-stage ammonia compressors running at 300 r.p.m. and delivering at about 170 lb./in.^{2}. The high pressure ammonia vapour from these compressors is first cooled and condensed, then passed through a reducing valve to the brine coolers, and finally returned to the compressors. A separate brine cooler is used for each storage tank, and the brine is circulated by pumps. The water used for the compressor intercoolers and the ammonia coolers is pumped to a spray pond where it is finely diffused and allowed to cool before re-entering the system.

The capacity of the cooling plant is 30,000,000 B.Th.U. per 24 hours, which represents the cooling required for about 3 hours' continuous tunnel running on full load. This is in excess of normal requirements, since full tunnel power is used only for short periods, but during the war years, when the tunnel was in constant use, the cooling plant was only just able to meet the heavy demands made on it.

2.24. *Air drying.*—The tunnel air is dried before being admitted to the tunnel by passing through a drier which operates by cooling the air to about —18 deg. C. and condensing out most of the moisture. This lowers the moisture content sufficiently, as explained below, to prevent condensation inside the tunnel for all running conditions.

The drier is supplied from a separate brine cooler fed from the same ammonia coolers as the tunnel brine coolers. This brine circuit works at a slightly lower temperature than the others, and brine of slightly greater density (1·24) is used.

For removing accumulated ice from the brine coils in the drier, an electric brine heater can be put into the circuit, and warm brine circulated till all the ice has melted off.

A small air-conditioning plant is installed in the tunnel room, to keep the air there dry and to avoid condensation on the brine pipes or on the outside of the tunnel shell.

2.3. *Instruments and Equipment.*—2.31. *Balance.*—Measurements of the forces on a model in the working section are made on a balance mounted in the dead space, on which the six components, lift, drag, pitching moment, rolling moment, yawing moment, and side force can be measured. (The weighbeams for the last three components have only recently been installed, and no experience has yet been gained of their use.) The model is mounted on three struts fixed to the balance and passing up through the floor of the working section. The incidence is varied by raising or lowering the rear strut, and the model is yawed by turning the whole upper part of the balance, both these adjustments being operated by remote control.

A diagram of the linkage arrangements for the three weighbeams measuring lift, drag, and pitching moment is given in Fig. 9. The drag frame is mounted on a Watts linkage which constrains it to move horizontally, and the frame is connected to the drag weighbeam by a cranked lever. The lift unit is mounted entirely on the drag frame, and the pitching moment from the model is transmitted through a parallel motion linkage to a sector member, and thence to the pitching moment weighbeam on the lift frame. The same parallel motion linkage is used for changing incidence ; a worm at the end of the pitching-moment arm engages with a rack on the arc of the sector member.

In Fig. 9, the two main struts are shown rigidly fixed to the lift frame, but for measuring rolling moment, yawing moment, and side force, the struts are connected to the frame through a linkage mechanism. The pitching-moment unit remains mounted directly on the lift frame, and a universal joint is provided at each end of the rear strut, to make it quite independent of these three components. The principle of the method of measuring rolling moment, yawing moment, and side force is shown in Fig. 10. Each strut is fixed to a fore-and-aft member at its lower end, thus making two inverted T-frames, and the ends of these are connected by flexible joints to two cross-frames which are pivoted on a common fore-and-aft axis at their mid-points. The two T-frames are also linked by a horizontal member, and the whole system, which has three degrees of freedom, is kept in equilibrium by applying measured forces A, B, and C at the points shown. With suitable factors, $A + B$ gives the rolling moment, $A - B$ the yawing moment, and C the side force on the model. Fig. 11 shows the linkages for the side force weighbeam and for obtaining the forces A and B from the cross frames ; and Fig. 12 shows the mechanism for adding and subtracting A and B so that rolling and yawing moments can be measured directly on the appropriate weighbeams. The rolling moment weighbeam effectively measures the lift on the member connecting the A and B links, and the yawing-moment weighbeam the pitching moment.

Fig. 13 gives a general view of the balance. In the middle of the picture is the incidence-changing mechanism, and below it, in the foreground, is the lift weighbeam. The side-force weighbeam can be seen on the left, and part of the roll-yaw weighbeams on the right.

The whole balance is mounted on eight pillars, which are clear of the tunnel structure and rest on solid foundations beneath. All parts of the balance are of massive construction, to minimise distortion, and it is designed so that such distortion as does occur will produce negligible errors.

Instead of moving pivots or knife-edges, flexible steel connections of various kinds are used throughout : single flat strips for taking direct tension, two crossed flat strips for cross loads (or where a definite centre is required), and round wires where freedom in two directions is needed. This arrangement eliminates all sliding friction, and the small necessary deformations occur elastically. An exception occurs in the pivots where the strut heads are attached to the model, and where the lower end of the rear strut is attached to the pitching moment arm. These pivots are used for incidence variation, and bearings must be used to get the necessary range. The sector member, however, which carries the pitching-moment arm, is mounted on spring centres.

The forces and moments are measured by weighbeams, each with a rider weight on a leadscrew and a series of dropweights operated by cams, all remotely controlled from a panel in the observation room. This arrangement of leadscrews and dropweights gives a high accuracy over the wide range required. Fig. 14 gives a schematic diagram of one weighbeam, which may be compared with the photograph in Fig. 15.

The two motors driving the rider leadscrew and the dropweight cam are each coupled to a selsyn transmitter which operates the corresponding dial on the balance panel in the observation room. On the end of the weighbeam arm is an electrical balance indicator consisting of a search coil moving between two opposed A.C. magnetic fields. This operates a pointer on the panel which shows when the weighbeam is in balance. The rider and dropweight may be manually adjusted by pushbuttons on the panel, but it is generally more convenient to use an automatic device by which the out-of-balance voltage from the indicator is amplified and used to turn the leadscrew in the appropriate direction. When the rider reaches the end of its travel, a relay adds or removes a dropweight, thus making the balancing entirely automatic.

Variable damping is provided by an oil dashpot on the weighbeam, with a remote control adjustment and position indicator.

There are six of these weighbeams, differing only in minor details, for the six components of the balance, and a seventh weighbeam is used for a manometric balance. This instrument, which is installed outside the tunnel, measures the pressure difference between the settling chamber and the working section, and so, by suitable calibration, gives the wind speed. The principle of operation is shown in Fig. 16. Two cast iron mercury pots with a connecting pipe are mounted at the ends of the weighbeam. The pressure difference to be measured displaces the mercury and produces a load on the weighbeam which is balanced out by a rider and dropweights in the usual way. The dials on the panel are arranged to read the pressure difference in inches of water.

The ranges and sensitivities of the balance components are as follows :—

Lift	—100 lb.	to	1,200 lb.	by 0·1 lb.
Drag	—150 lb.	to	300 lb.	by 0·01 lb.
Pitching moment . .	—500 lb.-ft.	to	500 lb.-ft.	by 0·1 lb.-ft.
Rolling moment . .	—400 lb.-ft.	to	400 lb.-ft.	by 0·2 lb.-ft.
Yawing moment . .	—500 lb.-ft.	to	500 lb.-ft.	by 0·25 lb.-ft.
Side force	—400 lb.	to	400 lb.	by 0·2 lb.
Wind speed . .	0	to	80 in. water	by 0·01 in.

The values given for the sensitivities are those of the smallest dial graduations, and represent the accuracy with which a dead load can be measured. In practice, for normal aerodynamic measurements the limiting factor is the unsteadiness of the flow in the tunnel, and not the sensitivity of the balance.

The balance control panel can be seen towards the left in the photograph of the observation room, Fig. 17. The various control buttons and switches are on the sloping desk, and the indicating dials on the vertical panel. For photographic recording, duplicate dials are provided on the back of the panel. These are graduated in white on a black ground, and are photographed by a remote-controlled F.24 aircraft camera.

2.32. *Manometers.*—The tunnel wind speed is measured as the pressure difference between two reference holes, one in the settling chamber and the other just upstream of the working section, using the manometric balance described above. To obtain the Mach number, it is also necessary to know the absolute pressure in the working section. Pressures below atmospheric are measured with a special barometer which covers a range down to 2 in. of mercury (absolute), and can be read to within 0·01 in. without difficulty. For pressures above atmospheric a Bourdon type pressure gauge gives sufficient accuracy.

For such measurements as the pressure distribution over an aerofoil, or the total head across a wake, multitube manometers are used. About a hundred copper pipes are permanently connected to manometers in the observation room, and go from there to a distribution board inside the tunnel, from which they can be connected to a model in the working section as required.

In a tunnel of this kind, working over a wide range of speeds and pressures, there are special difficulties in the design of manometers. Those at present in use have alcohol as the working liquid, with heights up to 110 in., which gives adequate range and sensitivity for nearly all purposes. Alcohol gives a clear meniscus, and has the merit of being harmless if it should be sucked into the tunnel, an accident which may easily occur if a connection comes off or becomes blocked.

At low tunnel pressures two difficulties were encountered. Air which had been dissolved in the alcohol came out of solution and tended to form bubbles which blocked the manometer tubes. This was avoided by providing a vent pipe and using glass tubes of large enough bore for any bubbles to rise freely. The other difficulty was that very small air leaks to atmosphere in the connecting pipes caused large errors in the readings ; the remedy for this was to take the greatest possible care in testing the pipes.

The manometer readings are recorded photographically, the distance of the camera being altered according to the range and accuracy required. A projector is used for reading the films.

2.33. *Other instruments.*—The Mach number, as explained below, is obtained from the ratio of the wind speed pressure difference (measured on the manometric balance) to the absolute pressure in the tunnel, and a special device is used to give a direct indication of this ratio. The tunnel pressure is connected to a mercury gauge, and a selsyn motor electrically coupled to the leadscrew of the manometric balance is used to rotate a reflecting prism about a vertical axis. There is an illuminated slit behind the mercury column, and a lens throws an image of this, via the prism, on to a cylindrical frosted perspex screen. The vertical position of the end of the image of the slit thus gives the tunnel pressure, and its horizontal position the wind speed, so that lines of constant pressure ratio, which are lines of constant Mach number, can be drawn as sloping lines on the screen. The effect of dropweights is allowed for by rotating the screen by hand, and a system of contacts switches off the light if the screen is not in the position corresponding to the value of the dropweight on the balance.

It is occasionally necessary to measure the humidity of the air in the tunnel, and this is done with a modified version of a hygrometer developed for measuring the moisture content of samples from compressed air cylinders. Air from the tunnel is drawn over a polished steel mirror, which can be cooled by liquid oxygen. An optical system throws an image of a small filament on to this mirror ; the image is invisible when the mirror is clean, but appears when a deposit of hoar-frost is formed. The dew point of the air is measured by cooling the mirror gradually, and observing the temperature at which the image just becomes visible.

In addition to those already described, other instruments in the observation room include a fan speed indicator, a fan motor ammeter, a resistance thermometer giving the air temperature in the settling chamber, and thermocouples indicating the bearing temperatures.

2.34. *Propeller testing gear.*—Special equipment is provided for testing propellers in the tunnel at high forward speeds. A 3-phase variable frequency induction motor is used for the drive, with a rating of 200 h.p. at 4,000 to 8,000 r.p.m., and by careful design it has been made small enough to be accommodated in a nacelle 19·2 in. diameter. A solid steel rotor is used, with copper squirrel-cage bars.

This unit is mounted on three struts as shown in Fig. 18. These struts are fixed to the balance in the tunnel, so that the thrust can be measured directly on the balance. The torque is obtained from the speed and electrical power input. The motor losses are derived from a previous calibration covering a range of loads, speeds, and winding temperatures ; for this calibration the motor is coupled to an induction brake, and the torque is measured with a weighbeam.

The motor is cooled by circulating brine from the main tunnel supply, and the temperature is measured with a resistance mat in the stator winding.

2.4. *Acknowledgements to Firms.*—It is not possible to give the names of all the manufacturers who have contributed to the construction of the tunnel. Special acknowledgements, however, are due to the following firms for the design and development work they have done to produce the specialised plant and equipment required.

Sir William Arrol and Co., Ltd.—Tunnel structure.
Holst and Co., Ltd.—Buildings and foundations.
The British Thomson Houston Co., Ltd.—Fan, fan motors and electrical gear.
Sir Howard Grubb, Parsons and Co.—Balance.
J. & E. Hall, Ltd.—Refrigeration plant.
J. Browett Lindley (1931) Ltd.—Compressor-evacuators.
Metropolitan-Vickers Electrical Co., Ltd.—Propeller motor and control gear.

3. *Method of Using the High Speed Tunnel.*—3.1. *Calibration and Characteristics.*—3.11. *Method of calibration.*—For calibrating the tunnel, separate pitot and static tubes were mounted on a steel strut of 8 in. chord and 0·8 in. thickness. This gave satisfactory readings up to a Mach number of about 0·85 ; above this speed the tunnel blockage effects (*see* below) on static pressure became serious, even for this small strut, and for the highest speeds of all a single static tube, 18 ft. long and half an inch diameter at the end, was mounted on wires in such a way as to cause insignificant blockage in the working section.

This calibration gives the total head H_0 and the static pressure P_0 in the working section, in terms of the pressures p_1 and p_2 at two reference holes in the tunnel walls, one in the settling chamber and one just before the working section. The absolute pressure p_2 is measured on the mercury gauge referred to above, and the difference $p_1 - p_2$ on the wind speed manometric balance. The total head H_0 is of the same order as p_1, and P_0 is of the same order as p_2, so that it is convenient to express the calibration in terms of the ratios

$$\frac{H_0 - p_1}{p_1 - p_2} \text{ and } \frac{p_2 - P_0}{p_1 - p_2}.$$

These are both small quantities which are practically independent of Reynolds number and can be expressed as functions of Mach number only. The Mach number M is given by

$$\frac{H_0}{P_0} = (1 + \tfrac{1}{5}M^2)^{7/2} \quad .. \quad .. \quad .. \quad .. \quad .. \quad .. \quad (1)$$

and it follows that the ratio $(p_1 - p_2)/p_2$ is also a function of M, and the same applies to $\frac{1}{2}\rho V^2/(p_1 - p_2)$. These calibration curves are given in Fig. 19. It is interesting to notice the effect on $(H_0 - p_1)/(p_1 - p_2)$ of installing the turning vanes in front of the honeycomb. The reduction of this ratio implies an increase in the effective area of the settling chamber, confirming that there was a dead region round the outer part of the honeycomb before the turning vanes were put in.

The Mach number and $\frac{1}{2}\rho V^2$ can be obtained from pressure measurements only, but to obtain velocity or Reynolds number the temperature T in the working section must be known. For this purpose it is sufficiently accurate to assume that a thermometer in the settling chamber gives the stagnation temperature T_0. T is then given by the equation

$$\frac{T_0}{T} = 1 + \tfrac{1}{5}M^2 \quad .. \quad .. \quad .. \quad .. \quad .. \quad .. \quad (2)$$

3.12. *Velocity distribution.*—The velocity distribution across the working section is good, and does not vary by more than $\pm 0 \cdot 25$ per cent. over the part of the tunnel occupied by a normal model (Fig. 20).

The tunnel was designed with a slight expansion down the working section, to allow for the thickening boundary-layer. This was intended to give a uniform longitudinal velocity distribution, but there is actually a slight falling velocity gradient, indicating that the expansion is rather too great. Fig. 21 shows the geometrical expansion in the working section compared with the equivalent expansion calculated from the velocities along the tunnel walls. The rate of increase of boundary-layer displacement thickness deduced from these results is about $0 \cdot 02$ in. per ft., and is nearly independent of Mach number up to $M = 0 \cdot 85$.

Fig. 22 shows velocity distributions measured along the tunnel walls at the highest fan speeds with the tunnel empty. The speed of sound is first reached at the beginning of the working section, where the cross-sectional area is least, and there is a supersonic region for some distance aft of this. In ordinary tunnel tests, however, the speed is limited by other factors discussed below, and the speed attained in the empty tunnel does not indicate its useful range.

3.13. *Steadiness and turbulence.*—Before the turning vanes were installed in front of the honeycomb, the separation occurring on the wall of the settling chamber produced considerable unsteadiness in the flow in the working section, causing irregularities in the balance readings. The turning vanes, by guiding the flow round the corner into the edge of the honeycomb, made the conditions very much steadier, and improved the operation of the balance considerably.

Observations with hot wires, however, still showed velocity fluctuations in the return circuit, which were of a surprisingly regular character. The period of these fluctuations was about five seconds at $M = 0 \cdot 7$, and was generally about three times the period of a complete circuit of the air round the tunnel. The velocity was high at the top and bottom of the return circuit annulus when it was low at the sides, and vice versa, thus forming a symmetrical pattern with four nodes. A series of tests[3] made on a $\frac{1}{16}$-scale model of the tunnel showed a similar effect. It was found on the model that a set of sinuous mixing vanes round the return circuit annulus, arranged as in Fig. 23, completely eliminated the fluctuations. Similar mixers have recently been installed in the full size tunnel, and the fluctuations have been reduced, but the mixing is not thorough enough to make them completely effective.

Hot wire technique involves difficulties at high speeds, but at low tunnel speeds the small scale turbulence, as given by a wire in the working section, is about $0 \cdot 4$ per cent. This value is fairly high, as would be expected in a tunnel of this kind with a low contraction ratio (7 to 1). Measurements[4, 5] of the drag of a laminar flow aerofoil (EQH1260 section) show a fairly low critical Reynolds number, thus confirming the high turbulence.

3.14. *Power factor.*—Some measurements of the power factor of the tunnel, defined as :

$$\frac{\text{shaft power supplied by fan motor}}{\frac{1}{2}\rho V^3 \times \text{area of working section}},$$

are given in Fig. 24. The reduction of power factor with increasing Mach number in the empty tunnel is to be expected, but with a model in the tunnel the effect of the rise in drag above $M = 0 \cdot 7$ more than counterbalances this. The improvement in the flow produced by the turning vanes in front of the honeycomb gave an appreciable reduction in power factor.

3.15. *Humidity.*—It is important to keep the moisture content of the air in the tunnel low enough to avoid condensation in all conditions. The worst case occurs in high-speed tests, when the air undergoes a sudden expansion associated with a large drop in temperature. For instance, if the tunnel Mach number is $0 \cdot 8$, and the stagnation temperature of the air is 35° C., the temperature of the air in the working section is 0° C., and near the surface of the model, where the local Mach number may be $1 \cdot 4$, the corresponding temperature is −52° C.

The air entering the tunnel, after passing through the drier described above, has a dewpoint of about −18° C. at atmospheric pressure, corresponding to a moisture content of $0 \cdot 075$ per cent. At the reduced tunnel pressure for normal running conditions, the dewpoint is therefore

about $-35°$ C. at $M = 0{\cdot}8$ and $-43°$ C. at $M = 1{\cdot}4$. The air in the free stream (at $0°$ C.) is thus completely dry and, although slight supersaturation may occur locally at $-52°$ C., the condition is probably too transient for condensation to take place.

When the tunnel is pumped up to four atmospheres, the dewpoint rises from $-18°$ C. to just below $0°$ C., but since no high-speed runs are made in this condition, the air temperature never falls low enough to produce saturation.

3.2. *Construction of Models.*—3.21. *Requirements.*—The models used in the tunnel have to satisfy somewhat exacting requirements. The wing loading is about 200 lb./ft.^{2}, with severe buffeting in some conditions, and it is essential to run no risk of structural failure, which would probably cause extensive damage to the fan and tunnel. The atmospheric conditions in the tunnel are severe, and the combination of extreme dryness, low pressure, and wide temperature range causes warping or cracking in any but the best seasoned woods. Every effort is made to keep the tunnel free from dust, by systematic vacuum cleaning with a special plant, and by making everyone wear overshoes when going into the tunnel ; but in spite of these precautions the airstream always carries round the circuit a small amount of dust and grit, which may cause considerable abrasion of model surfaces at high speeds.

3.22. *Typical construction.*—A typical model of a complete aircraft is about 6 ft. span with a mean chord of 1 ft. It is usually made of teak, which resists the atmospheric conditions well, but the wing may have to be made of steel or dural if the thickness/chord ratio is less than about 11 per cent. The wood is varnished with " Pheenorock ", which gives a smooth and durable finish. The tail plane and fin are of laminated wood. No hinges are used for elevator adjustments ; the elevators are screwed to rigid steel plates let into the tail plane and previously bent to the required angle. Plastics are used for certain applications, for example, perspex for radiator cowls, and tufnol for a sharp trailing edge on a wooden wing.

For jet aircraft models an open duct is generally used, which gives a fair representation of the flow at the entry but does not, of course, represent the high velocity jet. When radiator ducts are represented, a slotted metal baffle plate is used to give the required flow[6]. In a few cases windmilling propellers have been fitted, but no power-driven propellers have yet been tested on complete models.

3.23. *Method of rigging.*—A complete model is rigged on the three balance struts referred to above, two under the wing and one at the rear of the body. The general arrangement can be seen from the photograph of a model in the tunnel, Fig. 25, and more details are given in a sketch of a typical rig, Fig. 26. The struts are of EC1240 section (12 per cent. thick), with a chord of 4 in. on the parallel portion tapering down to about $1\frac{1}{4}$ in. at the point of attachment to the model. The lower part of each front strut is shielded by a guard fixed to the floor, and elliptical bracing wires $\frac{3}{8}$ in. by $\frac{1}{8}$ in. are used to restrain the lateral movement. The strut head fitting is shown in Fig. 26 ; in some cases ball-bearings are used, but it is found that even with plain bearings the friction can be kept down to about $0{\cdot}2$ lb.-ft., which is small enough for most purposes. (The sensitivity of the pitching-moment balance is $0{\cdot}1$ lb.-ft.)

These struts produce considerable aerodynamic interference on the model, particularly at high Mach numbers, and modifications are being made to improve this. It has been found better in some cases to use heavier struts, so that the guards and bracing wires can be dispensed with.

For rolling and yawing-moment measurements ball-ended struts must be used, and when the model is to be yawed the struts must be of circular cross-section. No tests of this kind have yet been done, but some difficulty is anticipated in correcting the moments for the effects of strut deflection and interference.

Plain wings are mounted in the same way as complete models, except that the end of the rear strut is connected to a steel sting fixed to the after part of the wing at the middle of its span. For wings of rectangular plan form it is important not to have the struts at the positions of the nodes of a natural mode of vibration ; if this happens, large amplitudes of vibration may be set up, particularly in metal wings. The most dangerous strut spacing is $0{\cdot}55$ of the span ; $0{\cdot}67$ of the span is generally used.

For two-dimensional tests an aerofoil 7 ft. long is mounted vertically in the tunnel and fixed to the roof and floor. Unless the chord is very small such models are made of wood, and if necessary they are braced with wires to the side walls. Pressure-plotting holes are made with copper pipes about $\frac{1}{16}$ in. bore, the ends being flush with the model surface. Wake traverses are made with a comb of pitot tubes mounted on a horizontal aerofoil 4 in. chord and 72 in. long. The pitot tubes are of hypodermic tubing 0·04 in. outside diameter and projecting 0·3 in. from the aerofoil leading edge ; the spacing varies from 0·1 in. at the middle of the span to 6·4 in. at the ends.

Most model tests are included in the categories described above, but various special rigs have been used for certain jobs. For instance, in tests on control surfaces the wing is mounted rigidly on the balance, and the rear strut is connected to a sting on the hinged elevator, so that hinge moments can be measured on the pitching-moment balance.

3.3. *Method of Testing.*—The majority of the tests made in this tunnel have been either force measurements with the balance or pressure measurements with the manometers. In addition, some flow observations have been made by photographing tufts on models, but up to the present no special optical methods have been used.

3.31. *Range of tests.*—For all types of test, a variety of tunnel conditions can be obtained by changing the speed and pressure. The possible range is defined by various limitations arising from different causes, of which the most important are discussed below.

For high-speed tests on a model of normal size, it is not practicable to operate at Mach numbers above about 0·8 to 0·85, the ultimate limitation being the choking speed of the tunnel, and the practical one the uncertainty of the blockage corrections when this speed is approached. This limiting Mach number depends on the size of the model, and is discussed in more detail later. A second limitation is the interference effect of the model supports, which becomes large at high Mach numbers and is difficult to measure. This effect increases as the model size is reduced, and makes it impracticable to extend the speed range by reducing the scale of the model.

The fan power and speed do not enter into the above considerations, but the power does affect the Reynolds number obtainable in high-speed tests. For a given Mach number M, the Reynolds number R is proportional to the tunnel pressure, and it is usual to adjust this pressure to keep R constant over a range of M. The maximum R which can be obtained at $M = 0{\cdot}8$ is about 1·2 million per foot chord, with the available fan power of 4,000 H.P.

For low-speed tests at high tunnel pressures, the Reynolds number may be limited for various reasons, such as the capacity of the lift balance, the strength of the model, and in some cases the desirability of avoiding compressibility effects. In practice, each of these considerations limits the maximum Reynolds number to about 4 or 5 million for a typical complete model.

3.32. *Typical procedure.*—The typical procedure in a normal balance test is as follows. A range of Mach numbers is selected, generally about ten values ranging from 0·4 to 0·8, and the tunnel pressures required to give a constant Reynolds number are estimated. (In these estimates, an allowance must be made for the drop in pressure in the working section when the fan is run up to speed. This change, which is produced by the redistribution of the air in the tunnel circuit, may be as much as 20 per cent. of the absolute pressure, for high values of M.) The tunnel is then pumped down to the required pressure, and the fan is run up to the appropriate speed and kept at constant r.p.m. by the automatic control while the balance forces are measured for a range of incidences. Running at constant fan speed is roughly equivalent to running at constant Mach number, but not exactly, chiefly because as the model incidence is raised the drag increases and the Mach number falls. It is found, however, that the tunnel conditions are steadier when the fan speed is kept constant than when an attempt is made to keep the Mach number constant by raising the fan speed as the drag increases.

The balance works automatically. It is only necessary for the operator to take a photograph when the indicators are steady, and then to move the model to the next incidence. Some time can be saved, however, if the operator anticipates the dropweight changes, and makes them manually before the rider weight gets to the end of the balance arm.

When the incidence range is completed, the fan is stopped, and the tunnel pressure is reduced for the next speed. The time taken is about 15 to 20 minutes for a run involving measurements at about 12 incidences at constant speed, and the total time for a series of runs covering a range of ten speeds is about three hours, including the time for pressure changes.

3.4. *Reduction of Results.*—The reduction of the balance readings to coefficient form is laborious, partly because of the large number of readings, and partly because the value of $\frac{1}{2}\rho V^2$ depends on both the Mach number and the tunnel pressure, and it is not practicable to keep both of these exactly constant during a run.

The first stage in the calculations, after reading the films, is to obtain the Mach number M from the wind speed reading $p_1 - p_2$ and the tunnel pressure p_2, as described above, for each photograph. The value of $\frac{1}{2}\rho V^2$ is obtained by multiplying $p_1 - p_2$ by a factor which is a nearly constant function of M (Fig. 19), and the coefficients C_L, C_D, and C_m are computed. Next, since the Mach number is not exactly the same at each incidence, each coefficient must be plotted against M at constant incidence, and interpolated values obtained for selected values of M. Finally, various corrections have to be applied, which are discussed in more detail below. Electric calculating machines are used for most of the arithmetical operations, and the computing is generally done to four significant figures, the final results being given to three. The analysis of a day's running in the tunnel will occupy two computers for about a week.

3.41. *Tunnel constraint and blockage.*—In all tunnel tests, the constraining effect of the tunnel walls must be allowed for. For low-speed tests the corrections are well established[7], and involve corrections to the incidence, drag, and tail-setting of the model, and to the speed and static pressure in the free stream. For high-speed tests, the corrections are calculated in the same way, but, to allow for compressibility, some of them must be increased by a factor depending on Mach number M. It can be shown by linear perturbation theory[8] that this factor is $1/\beta$ (where $\beta = \sqrt{(1 - M^2)}$), or some power of $1/\beta$, according to the type of correction. Most of the corrections are quite small, even with this factor, and can be estimated with sufficient accuracy. A special difficulty arises, however, in the blockage correction to the tunnel speed, because this involves a correction to M, and at high speeds, where force and moment coefficients may change rapidly with M, an error of one or two per cent. in M is very much more serious than an equal error in a coefficient.

The blockage correction (for which typical values are given in Fig. 27) depends partly on the size of the model (solid blockage), and partly on its drag (wake blockage). It is usually calculated by the method given in Ref. 9. The correction includes a compressibility factor (generally $1/\beta^3$), based on linear perturbation theory[8], which becomes unreliable when the disturbances are large or when shock waves are present.

There is another limitation to the speed at which reliable results can be obtained, arising from the phenomenon of choking. The tunnel is said to be choked when the Mach number (as indicated by reference pressures upstream) cannot be increased by raising the speed of the fan. The effect can be roughly represented by regarding the tunnel as a channel with uniform flow over any cross-section, for which it is well known that the Mach number cannot exceed unity at the throat, or section of minimum area. Normally the throat occurs at the model, and if the presence of the model reduces the tunnel cross-sectional area from A to A_m, the choking Mach number M is given (for $\gamma = 1{\cdot}40$) by

$$\frac{A}{A_m} = \frac{1}{M}\left(\frac{5 + M^2}{6}\right)^3 \quad \ldots \quad \ldots \quad \ldots \quad \ldots \quad \ldots \quad \ldots \quad (3)$$

This crude theory gives surprisingly good agreement with the measured choking speeds for various models plotted in Fig. 28, but this agreement may be partly fortuitous, because the velocity distribution is very far from uniform round a model in the tunnel[10]. In Fig. 28 the model frontal area plotted is the maximum value occurring at any cross-section. For normal complete models the struts and guards contribute 20 to 30 per cent. of the blocked area.

The choking speed for a particular model gives an upper limit to the Mach number at which any tests can be made, but measurements near this speed are not of much use, because the blockage corrections are uncertain; in fact it is doubtful whether the conditions in the tunnel

can be represented by any equivalent infinite stream. Further theoretical and experimental work is going on[10], but at the present state of our knowledge it is not considered reliable to use measurements at values of M within about 0·03 of the choking speed. For a model of average size (frontal area about 2 sq. ft.) this limits the Mach number to about 0·8 (corrected).

3.42. *Support corrections.*—The struts supporting the model produce interference effects which must be measured and allowed for in deducing the results of tests. No difficulty arises at low speeds, where the drag of the struts themselves is the only important item, but at high speeds the interference effect between the strut and the wing becomes large. For strength reasons the strut fitting must be near the maximum thickness of the wing, where the local speed may be supersonic ; in this condition the strut head can produce large changes in the flow pattern over the wing.

The interference effect of a strut depends on the size and shape of the wing section where it is fitted, and no standardised corrections can be used. It is not usually possible to measure strut interference on the model itself, because of support difficulties, but tests have shown that the effect of wing plan form is not important. The interference is therefore measured on a wing of rectangular plan form with a uniform cross-section which is the same as that of the wing of the model at the position of the struts. The method of rigging is shown in Fig. 29. The wing is mounted upside-down on three supporting struts fixed to the balance in the usual way. The dummy strut, the interference of which is to be measured, is hung from outside the top of the tunnel, and is attached to the wing lower surface with the normal type of fitting. The forces on the model are measured for a range of speed and incidence, with and without the dummy strut and guard in position, and the difference between the two sets of readings gives the total interference effect of the strut and guard on the wing. (An allowance must be made for the fact that part of the drag of the dummy strut is taken on the upper hinge, but this effect is small.)

The effect of the bracing wires is measured independently, by fitting temporary bracing wires outboard of the struts and comparing measurements made with and without the normal inboard wires in position.

The above procedure for measuring support interference is not entirely satisfactory, but no better method has so far been devised. For some of the earlier tests a less reliable method was used ; however, most of the results given in this report have been corrected by the above method.

A typical set of strut corrections is given in Fig. 30. The values for lift and pitching moment are probably reliable up to about $M = 0{\cdot}8$, and for drag up to $M = 0{\cdot}75$.

3.5. *Organisation.*—Running a tunnel of this size and complexity involves the co-operation of many workers of different kinds. First a test has to be planned, then a model must be designed, drawn, and made. The model must then be rigged in the tunnel, the fan must be run, the pressure adjusted, and the cooling plant kept working, while the tunnel operators make their measurements. The photographic records must be developed and read, the results computed, and curves plotted. Finally the test results must be examined and digested, and described in a written report. A failure at any point in this chain of operations would make the whole test useless, and credit is due to all the workers concerned for the successful way in which the whole plant has been run.

From the time when the tunnel was first put into operation (late in 1942) till the end of the war in the summer of 1945, the tunnel was in use almost continuously for seven days a week. Between 70 and 80 workers, classified roughly as follows, devoted all their time to the tunnel.

Technical and scientific staff	16
Assistants (chiefly computers)	18
Designers and draughtsmen	9
Wood and metal workers	15
Fitters and riggers	5
Compressor and refrigerator staff	9
Electricians	3

The proportions of the different kinds of staff must be carefully balanced to keep the tunnel working satisfactorily at its full capacity. The ultimate limitation of output is in the cooling plant; even with this running 24 hours a day the tunnel cannot be used for more than about 12 hours, including rigging time. This limit was not quite reached, but any increase in running time would have required more wood-workers to keep the tunnel supplied with models, and more computers to work out the results. An increase in the output of test data would have involved a further limitation, more insidious because less obvious; this is that the scientific staff would not have time to give full consideration to the meaning and significance of the results.

4. *Tests on Models in the High Speed Tunnel.*—The tunnel was run for the first time in August, 1942. The next three months were occupied in balancing the fan and in preliminary calibrations and strut interference measurements. Tests on models were started in November, 1942. In June, 1945, the tunnel was shut down for installation of mixers in the return circuit and erection of a six-component balance.

In the following pages, a summary is given of the results of tests made in the tunnel between November, 1942 and June, 1945. A large proportion of this time was spent in testing complete models of aircraft, but tests on aerofoils, controls, and other miscellaneous models were also made. A brief analysis of the work done in the tunnel during this period is given in Table 1, below.

TABLE 1

Work Done in Tunnel from November, 1942 to June, 1945

Type of work	*No. of days*	*Per cent. total*
Complete aircraft models*	435	67·6
Aerofoils	85	13·2
Controls	69	10·7
Miscellaneous	55	8·5
	644	100·0

In addition to the above items, about 180 days were spent in calibrations, support interference measurements, and alterations and repairs to the tunnel.

In discussing the results of high-speed tunnel tests, the properties of aerofoils and controls at high Mach numbers are considered first, in order to illustrate the fundamental phenomena affecting the behaviour of a complete aircraft. Since comparatively few aerofoil tests have been made in the R.A.E. High Speed Tunnel, it is necessary to make use of some results obtained in other high-speed tunnels, but except where otherwise stated, the results given are from tests in the R.A.E. High Speed Tunnel at a Reynolds number of about 1×10^6.

4.1. *Aerofoil Tests.*—A few measurements of lift, drag, and pitching moment have been made on rectangular aerofoils (6 ft. × 1 ft.) mounted on the balance. Similar measurements have also been made on tapered wings, as part of the programme of tests on complete models of aircraft. In addition, some measurements of pressure distribution and profile drag have been made on two-dimensional aerofoils mounted vertically in the tunnel. The profile drag measurements on these aerofoils were made by the wake traverse method. Measurements of profile drag have also been made at one section of a three-dimensional half wing, mounted vertically from the floor of the tunnel.

The results of all these aerofoil tests, together with some results from other high-speed tunnels, are summarised and discussed below.

4.11. *Aerofoil pressure distributions.*—Figs. 31 to 33 show pressure distributions at various Mach numbers on three different aerofoil sections. The results given in Fig. 31 were obtained from tests on a two-dimensional aerofoil of "Mustang" section[11]. This was an early type of low-drag section having the maximum thickness at about 40 per cent. chord and a cusped trailing

*This includes tests of nacelles, etc. on a rectangular wing, required for the development of aircraft which were tested in the tunnel as complete models.

edge. The maximum thickness and camber are $0{\cdot}145c$ and $0{\cdot}012c$ respectively. The model aerofoil was made to represent a particular section of the wing on an aircraft which was being used for high-speed flight research (*see* § 6.81). This wing section has a slight hump on the upper surface at about 40 per cent. chord, and the high local suction due to this hump can be seen clearly in Fig. 31.

Fig. 32 shows pressure distributions on the aerofoil section NACA23021 at a fairly high incidence[12]. This section is of course much thicker than any likely to be used for the wing of a modern high-speed aircraft, but the results are of interest in showing the severe loss of lift that occurs at high Mach numbers with a thick section. With increase of Mach number above about $0{\cdot}6$, the suction on the lower surface continues to increase, while that on the upper surface decreases. Thus the lift falls as the Mach number rises above $0{\cdot}6$, and is about zero at $M = 0{\cdot}75$ and $\alpha = 5$ deg.

Fig. 33 shows the results of some measurements of pressure distribution on an aerofoil of EC1250 section[13], in the 20 in. × 8 in. Rectangular High Speed Tunnel at the N.P.L. This section is an early type of low-drag aerofoil, with the maximum thickness at 50 per cent. chord and zero camber. The trailing edge angle is exceptionally large for an aerofoil of this thickness, and this unusual feature should be remembered in considering the results.

The pressure distributions in Figs. 31 to 33 show that the value of $(-C_p)$ tends to increase with Mach number up to some critical value, and then decreases with further increase of Mach number. These effects are illustrated in Figs. 34 and 35, where $(-C_p)$ is plotted against Mach number.

The variation of C_p with Mach number, for speeds up to that at which local sonic velocity is first reached, can be calculated theoretically by several approximate methods[14, 15]. It has been found that the approximate theory which gives the best agreement with experiment is that due to Temple and Yarwood[14], although the Karman formula[15] also gives fairly good agreement. The dotted curves in Fig. 34 have been calculated from the equation given in Ref. 14, and show good agreement with the experimental results, for the range of Mach numbers in which the flow is everywhere subsonic. At higher Mach numbers, the experimental curves diverge from the theory, even when the local velocity at the point under consideration is still subsonic.

Fig. 35 shows that there is apparently an upper limit to the local Mach number that can be reached in the flow round an aerofoil, and that this limit is roughly the same for all incidences. The limiting local Mach number has been found[12], from tunnel tests on several aerofoils, to be about $1{\cdot}3$. There is some evidence[12] that the value increases slightly with Reynolds number, but the limiting local Mach number is probably not greater than $1{\cdot}4$ even at full scale Reynolds numbers[16, 17].

In general, the variation of the suction coefficient $(-C_p)$ with Mach number, at a given point on an aerofoil, may be summarised as follows. As the Mach number increases from zero $(-C_p)$ increases as predicted by the Temple and Yarwood theoretical relationship, up to the Mach number at which local sonic velocity is first reached at some point on the aerofoil surface. (At this Mach number, the local Mach number at the point under consideration is in general less than 1.) At higher Mach numbers, the Temple and Yarwood theory is not applicable, and $(-C_p)$ rises more steeply with Mach number (except at positions near the leading edge), until the limiting local Mach number is reached. If the stream Mach number is increased still further, the local Mach number remains approximately constant at the points where the limiting value has already been reached, and at these points $(-C_p)$ decreases with increase of Mach number. At other points on the aerofoil, where the local Mach number is still below the limiting value, $(-C_p)$ continues to increase with stream Mach number until the limiting local Mach number is reached. The result of this is a flattening out of the pressure distribution curve at high Mach numbers, as shown in Fig. 33.

The value of the free stream Mach number at which local sonic velocity is first reached at some point on an aerofoil or body is sometimes known as the " critical Mach number ". Until recently, it was usual to regard this critical Mach number as a warning of the approach of serious compressibility effects, such as increase of drag, loss of lift, and movement of centre of pressure.

This had some theoretical justification, because the formation of stationary shock waves is obviously impossible at Mach numbers below the critical value, and it is known that most of the serious compressibility effects observed on aerofoils at high Mach numbers are due to the formation of shock waves. However, it is now known that in many cases the " critical " Mach number of an aerofoil can be exceeded by quite a large amount before any serious compressibility effects appear. In these cases, the shock waves which are formed at the critical Mach number, or slightly above it, do not cause any serious changes of aerodynamic force or moment until considerably higher Mach numbers are reached. In particular, when the pressure distribution at low speed shows a high suction peak extending over a comparatively small area near the nose, as in the case of a thin symmetrical aerofoil at a fairly high incidence, the critical Mach number as defined above is usually fairly low, but serious compressibility effects on forces and moment do not appear until much higher Mach numbers are reached. For example, in the curves for $\alpha = 5{\cdot}75$ deg. in Fig. 33, the critical Mach number is only about $0{\cdot}52$, yet the pressure distribution at a Mach number of $0{\cdot}654$ is nearly the same as at low Mach numbers. Other high speed tunnel tests on aerofoils (*e.g.* Refs. 18 and 19) have shown that, when there is a high local suction peak near the nose, the drag coefficient does not start to rise appreciably until Mach numbers considerably greater than the critical value are reached.

As discussed above and in Refs. 20 and 21, the critical Mach number, defined as the stream Mach number at which sonic velocity is first reached locally at some point on the aerofoil, may be very misleading as an indication of compressibility effects on force or moment coefficients, especially when there is a high local suction peak near the nose of the aerofoil. The thickness ratio of an aerofoil is usually a more satisfactory indication of the Mach number at which serious compressibility effects may be expected than the critical Mach number (defined as above). In the case of aerofoils having nearly " flat " pressure distributions the two alternative criteria, thickness ratio and critical Mach number, are almost equivalent. However, the critical Mach number is very unsatisfactory as a basis for comparison between one aerofoil having a " flat " pressure distribution and another having a high local suction near the nose. One important consequence of this is that the effect of increasing incidence, on the Mach number at which serious compressibility effects occur on a thin aerofoil of small camber, is not as great as is indicated by the variation of critical Mach number with incidence.

In Fig. 33, the curves for $\alpha = 5{\cdot}75$ deg. show clearly the sudden rise of pressure at the shock wave on the upper surface of the aerofoil. In other cases, for example in the curves for $M = 0{\cdot}75$ in Fig. 32, the rise of pressure at the shock wave appears to be much more gradual. Possible explanations of a gradual rise of pressure at a shock wave instead of a sudden one are :—

(*a*) Fore-and-aft oscillation of the shock wave. (The pressures measured by the usual methods are time averages.)

(*b*) The main shock wave may break up near the surface of the aerofoil into a series of shock waves of smaller intensity. Shadow photographs, taken at the N.P.L. and elsewhere, have indicated that this sometimes occurs.

(*c*) The pressure distribution at the aerofoil surface may be smoothed out because of the presence of the boundary layer, especially if this is very thick.

Of these three alternatives, the last is the most probable explanation of the gradual pressure rise shown in Fig. 32 for the higher Mach numbers. In this case the shock wave probably causes considerable thickening (and possibly separation) of the boundary layer. Because of the thick boundary layer the pressure rise, as measured at the aerofoil surface, is a gradual one, although outside the boundary layer there may be the usual sudden pressure rise at the shock wave.

Wind tunnel tests by Göthert at the D.V.L.[22] have shown that the steepness of the pressure rise at the shock wave on an aerofoil increases with Reynolds number. However, the few measurements of wing pressure distribution which have been made in flight (*see* 6.82 and Ref. 16), at Reynolds numbers of 20×10^6 or more, have not shown a steeper rise of pressure at the shock

wave than has been commonly found in wind tunnel tests at Reynolds numbers of about 1×10^6.* A possible explanation of this is that the effect of the increased Reynolds number in the flight tests was obscured by greater fore-and-aft oscillations of the shock waves.

The changes of lift and pitching moment that occur on an aerofoil at high Mach numbers are often associated with fore-and-aft movements of the shock waves on the upper and lower surfaces. In general, on an aerofoil at a fixed incidence, the shock waves on both surfaces tend to move back and grow in intensity with increase of Mach number. With increase of incidence at a constant Mach number, the upper surface shock wave moves forward and becomes stronger, while the lower surface shock wave moves back and becomes weaker. Since there is usually a region of roughly constant suction in front of a shock wave, rearward movement of the upper surface shock wave will tend to give an increase of lift and a reduction of (nose up) pitching moment. In the same way, rearward movement of the lower surface shock wave will tend to give a reduction of lift and an increase of pitching moment. The combined effects of shock wave movements on both surfaces may cause a large reduction, or even reversal, of lift curve slope, and a large movement of the aerodynamic centre at high Mach numbers. There is some evidence from German tests[19] that these movements of shock waves may be more serious for an aerofoil which is convex at the rear, and hence it may be possible to reduce the undesirable effects of the shock wave movements on lift and pitching moment by lessening the convexity at the rear of the aerofoil.

In some of the pressure distribution measurements which have been made in high-speed tunnels, there is some indication of a partial separation of flow behind the shock wave, *e.g.* Figs. 31 and 32 at the highest Mach numbers. These results show negative pressure coefficients near the trailing edge, which are usually associated with separation and high drag. A complete separation would appear as a region of constant (negative) pressure coefficient behind the shock wave, and hence it is probable that the separation is only a partial one in most cases. However, the pressure measurements which have so far been made in flight, *e.g.* Ref. 16, have not given any indication of suction at the trailing edge, and hence it is possible that the tunnel conditions, *i.e.* presence of the walls, turbulence, or low Reynolds number, may have some effect on the separation behind a shock wave.* An alternative possibility is that suction at the trailing edge (and partial separation) normally occur on an aerofoil at high Mach numbers, either in flight or in a wind tunnel, but sufficiently high Mach numbers may not have been reached in the flight tests to show the effect, and the tunnel Mach numbers may be underestimated at present on account of uncertainties in the corrections.

Little has been said so far about the effect of aerofoil section shape on the pressure distribution at high Mach numbers. There is not much information available on this subject, because no really systematic tests on families of aerofoils at high Mach numbers have been made in this country. The small amount which is known will be discussed later in connection with the variation of forces and moments at high Mach numbers.

4.12. *Lift.*—High-speed tunnel tests have shown that the lift curve slope of an aerofoil $\left(\frac{dC_L}{d\alpha}\right)$ usually increases with Mach number up to some critical value, then falls sharply with further increase of Mach number. The Mach number at which the lift gradient is a maximum depends mainly on the thickness ratio of the aerofoil, being greater for thinner aerofoils. Glauert[23] has shown theoretically that the lift gradient of a two-dimensional thin aerofoil of infinite aspect ratio should be proportional to $(1 - M^2)^{-1/2}$, for small incidences and for Mach numbers at which the speed of sound is not exceeded locally. In Ref. 24 Young gives a modified theory, allowing for the effects of finite aspect ratio.

*More recently, it has been shown by Ackeret, Feldmann, and Rott (Mitt. Inst. Aerodynamik, E.T.H., Zurich, 10, 1946, ARC 10044), and by Liepmann (*Journ. Aero. Sci.* 13, 12, 1946, ARC 10479), that the shock wave formation and pressure distribution on an aerofoil depend on whether the boundary layer is laminar or turbulent at the position of the shock wave. It was also shown that separation occurred much further forward on the aerofoil when the boundary layer was laminar than when it was turbulent, and in the former case the increase of boundary-layer thickness at the shock wave was much greater. These results may explain some of the variations with Reynolds number which have been found in aerofoil pressure distributions at high Mach numbers.

Figs. 36 and 37 show the effect of Mach number on the lift gradients of several two-dimensional aerofoils, tested in the 1-ft. Circular High Speed Tunnel at the N.P.L.[25] These results show that, for aerofoils less than about 18 per cent. thick, the experimental values agree fairly well with the $(1 - M^2)^{-1/2}$ law given by Glauert[23]. For very thick aerofoils, the increase of lift gradient with Mach number is less than that given by the Glauert law.

Fig. 38 shows the lift gradients of several wings of finite aspect ratio, tested in the R.A.E. High Speed Tunnel[26, 27, 28, 29, 30]. The aspect ratio of all these wings was about 6, and the theoretical curve from Ref. 24 for aspect ratio 6 is included for comparison. Agreement with the theory is fairly good, but for the thinner wings the lift gradient at high Mach numbers tends to be rather greater than is indicated by the theory. However, the theories of Refs. 23 and 24 are only applicable below the Mach number at which the local speed of sound is first reached at some point on the wing, and this Mach number is nearly always considerably lower than that at which the lift gradient starts to fall. Thus the high lift gradients shown in Fig. 38 for some of the wings at Mach numbers of 0·7 to 0·75 can be explained by the fact that the flow is supersonic at some parts of the wing, so that the theory of Ref. 24 is not applicable.

Figs. 36, 37 and 38 show the effect of wing thickness ratio on the Mach number at which the lift gradient starts to fall. This Mach number decreases by about 0·015 for an increase of 0·01 in t_w/c. There is also some evidence from Figs. 36 and 37 that for a given thickness ratio the lift gradient starts to fall at a lower Mach number on a cambered aerofoil than on a symmetrical one. This effect of camber has been confirmed by some systematic tests in Germany[18].

Fig. 39 shows the effect of Mach number on the zero-lift incidence of several cambered aerofoils[26, 28, 29, 30]. The zero-lift incidence, which is negative at low Mach numbers for a cambered aerofoil, increases fairly suddenly to about zero at high Mach numbers. Since a cambered aerofoil at supersonic speeds gives zero lift at approximately zero incidence, it is probable that no important changes of zero lift incidence will occur at Mach numbers above those included in Fig. 39. The systematic German tests described in Ref. 18 show that the zero-lift incidence of an aerofoil at high subsonic Mach numbers is between 0 deg. and +1 deg. for all cambers between 0 and 4 deg. For a symmetrical aerofoil the zero-lift incidence is of course zero at all Mach numbers, and the change of the no-lift incidence at high Mach numbers is approximately proportional to the camber of the aerofoil. The increase of zero-lift incidence at high Mach numbers is a very objectionable feature of a cambered wing for use on a high-speed aircraft, because it causes a nose down change of trim. This effect will be discussed later in more detail.

It has been shown that, for a cambered aerofoil, the lift gradient decreases and the zero-lift incidence increases at high Mach numbers. These two effects are additive in causing a loss of lift at high Mach numbers, for a given incidence. For thick aerofoils ($t_w/c > 0{\cdot}18$), the loss of lift gradient at high Mach numbers is very severe, and usually has a more important effect than the increase of zero-lift incidence. For thinner aerofoils, however, the loss of lift gradient is less severe, and for thin cambered aerofoils the change of zero-lift incidence is usually more important than the loss of lift gradient.

The effect of Mach number on the lift of an aerofoil can be explained qualitatively in terms of the change of pressure distribution with Mach number. The increase of lift gradient with Mach number, for low and moderate Mach numbers, is due to a general increase in the suction coefficients all over the aerofoil. To a first approximation, the suction (and pressure) coefficients on a two-dimensional aerofoil at a fixed incidence increase with Mach number and are proportional to $(1 - M^2)^{-1/2}$. This gives a corresponding increase of lift, leading to the well-known Glauert law[23].

When the Mach number is increased to such a value that the velocity of sound is exceeded locally on the surface of the aerofoil, the suctions usually increase more rapidly with Mach number in the local supersonic region than at other parts of the aerofoil. Since the local velocity of sound is usually exceeded first on the upper surface of the aerofoil, this gives a steeper rise of lift gradient at these Mach numbers than is predicted by the Glauert law.

With still further increase of free stream Mach number, the limiting local Mach number of about 1·3 to 1·4 is reached on the upper surface of the aerofoil. Any further increase of stream Mach number then gives a reduction of suction coefficient in front of the shock wave on the upper surface, while for an aerofoil at a positive lift coefficient the lower surface suction coefficients

usually continue to increase. These effects cause a reduction of lift coefficient with increasing Mach number, for a given fixed incidence. The pressure distributions given in Fig. 32 show the causes of the loss of lift at high Mach numbers on a thick aerofoil at a fairly high incidence. The loss of lift on such a thick aerofoil is much more severe than that on a thin one, but the causes of the lift loss are similar in all cases, except that on thick aerofoils separation of flow behind the shock wave probably plays a more important part.

The increase of zero-lift incidence for a cambered aerofoil at high Mach numbers is due to similar causes. For a cambered aerofoil at zero incidence the average suction on the upper surface at low Mach numbers is greater than that on the lower surface, giving a positive lift. With increase of Mach number, the suction coefficients on the upper surface start to decrease when the limiting local Mach number is reached, while the suctions on the lower surface continue to increase until the pressures on upper and lower surfaces are roughly equalised, thus reducing the lift to zero. This effect is shown in the curves for $\alpha = -0{\cdot}5$ deg. in Fig. 31.

Ref. 19 describes some German high-speed tunnel tests on the aerofoil NACA 23015, in which a reversal of lift gradient was found at high Mach numbers, caused by fore-and-aft movements of the shock waves with changing incidence. As already explained, increase of incidence causes forward movement of the upper surface shock wave and rearward movement of the lower surface shock wave, and these shock wave movements may lead to a reduction of lift with increasing incidence. The German tests showed that the adverse effects of these shock wave movements on the lift gradient could be considerably reduced by making the rear part of the aerofoil more concave and reducing the trailing edge angle.

All the undesirable lift changes at high Mach numbers can be reduced, or at least delayed to higher Mach numbers, by decreasing the thickness and camber of the section. For a symmetrical section the incidence for zero lift is always zero and is independent of Mach number. There is also some evidence, from tests at the N.P.L. and in Germany, that while the lift gradient of a thick section may fall to a value very near zero at high Mach numbers, that of a thin section does not fall to such a low value at any Mach number.

The effect of Mach number on the maximum lift coefficient of an aerofoil may be fairly large in some cases, especially for thick aerofoils. Unfortunately, this effect is difficult to investigate in a wind tunnel because it is known to depend on Reynolds number to a large extent. This is shown in Fig. 40, in which the maximum lift coefficient of a Welkin aircraft is plotted against Mach number. The two lower curves are derived from high-speed tunnel tests[31] at two different Reynolds numbers, while the upper curve is from flight tests[32]. The curves show that there is a very serious reduction of maximum lift coefficient with increase of Mach number, but they also show that no more than a very rough estimate of this loss of lift can be made from wind tunnel tests at low Reynolds numbers.

Fig. 41 shows some results from other model tests in the high speed tunnel (mostly at $R = 1{\cdot}1 \times 10^6$)[28, 29, 31, 33, 34, 35, 36]. The maximum lift coefficients at high Mach numbers are reasonably large in most cases, especially when it is remembered that there may be scale effects similar to that shown in Fig. 40. The exceptional behaviour of the Welkin is attributed to its unusually thick wing (21 per cent. at the nacelles).

4.13. *Pitching moment.*—Fig. 42 shows the effect of Mach number on C_{m_0}, for several cambered wings[27, 28, 29, 37] of finite aspect ratio. The dotted curves show for comparison the variation of C_{m_0} with Mach number given by Hilton's empirical law[38]. This empirical law is based on the well-known Glauert factor $(1 - M^2)^{-1/2}$, with an additional term depending on the thickness ratio of the wing, to give better agreement with results of high-speed tunnel tests. For a wing of zero thickness, the Hilton and Glauert factors are identical. In drawing the dotted curves in Fig. 42, the mean wing thicknesses have been used for calculating the Hilton factors. The Hilton empirical law was originally designed to give good agreement with tunnel tests on two-dimensional aerofoils, but as Fig. 42 shows, the law also gives very good agreement with the results of tests on wings of finite aspect ratio. The Hilton law is of course only intended to give the variation of C_{m_0} with Mach number up to the point at which $(-C_{m_0})$ starts to decrease suddenly. The Mach number at this point decreases with increasing wing thickness, and is approximately equal to the Mach number at which the zero-lift incidence starts to increase.

For aerofoils with reflexed camber lines, designed to have C_{m_0} nearly zero at low Mach numbers, the increase of $(-C_{m_0})$ with Mach number is usually much greater than that given by the Hilton law of Ref. 38. For example, the tests described in Ref. 39, on a thick aerofoil with a reflexed camber line, showed that C_{m_0} was $-0{\cdot}007$ at $M = 0{\cdot}2$ and $-0{\cdot}032$ at $M = 0{\cdot}72$. The probable explanation of this large increase of $(-C_{m_0})$ with Mach number is that the reflexed trailing edge, which reduces $(-C_{m_0})$ at low Mach numbers, becomes ineffective at high Mach numbers because of thickening of the boundary layer at the rear of the aerofoil.

Fig. 43 shows the variation of aerodynamic centre position with Mach number, for a number of aerofoils[40] tested at the R.A.E. and at the N.P.L. In general, the movements of aerodynamic centre are fairly small, up to the Mach number at which large changes of lift and moment occur ($M = 0{\cdot}75$ to $0{\cdot}85$ for aerofoils of small or moderate thickness). At higher Mach humbers, the aerodynamic centre moves suddenly forward on most of the aerofoils, but on some of the thinner aerofoils the movement at these Mach numbers is in a backward direction. It may be noted that the aerodynamic centre of an aerofoil in supersonic flow is known from theory[41], to be approximately at the half-chord point, so that the forward movement shown for most of the aerofoils in Fig. 43 must be followed by a backward movement at still higher Mach numbers.

These changes of C_{m_0} and aerodynamic centre position can be partially explained in terms of the known variations of aerofoil pressure distribution with Mach number and incidence. The increase of $(-C_{m_0})$ with Mach number, in the range where the Hilton law is applicable, is analogous to the well-known Glauert effect on lift, and is due to a general increase in the suction coefficients at all parts of the aerofoil. The sudden reduction of $(-C_{m_0})$ at high Mach numbers is probably due mainly to a rearward movement of the lower surface shock wave with increase of Mach number, possibly combined with separation or thickening of the boundary layer. These effects cause a rearward movement of the "centre of suction" on the lower surface, giving a positive increase of pitching moment. This is shown, for example, by comparing the curves for $M = 0{\cdot}774$ and $M = 0{\cdot}794$ in Fig. 31 at $\alpha = -0{\cdot}5$ deg. At $M = 0{\cdot}774$ there is a small negative lift on the front part of the aerofoil and a larger positive lift on the rear part, giving a fairly large value of $(-C_m)$. When the Mach number is increased to $0{\cdot}794$, the lower surface shock wave moves back and the positive lift on the rear part of the aerofoil disappears, giving a positive increase of C_m and a slight decrease of C_L. If the incidence were increased to counteract the loss of C_L, a still greater increase of C_m would occur.

The sudden forward movement of aerodynamic centre at high Mach numbers, shown for example by the curves for NACA 0015 and 2417 in Fig. 43, may be due to fore-and-aft movements of the shock waves with changing incidence. As the incidence is increased from the zero-lift position, the shock wave on the upper surface tends to move forward, while that on the lower surface moves back. Since the greatest suction, on either upper or lower surface, occurs in front of the shock wave, these shock wave movements tend to give a positive pitching moment which increases considerably with incidence, *i.e.* a far forward position of the aerodynamic centre. If the shape of the aerofoil is such that the shock waves remain at approximately the same chordwise position over a range of incidences, then this large forward movement of aerodynamic centre does not occur. If the shock waves are near the trailing edge on both surfaces, the pressure distribution probably begins to resemble that found at supersonic speeds and the aerodynamic centre is then in a far back position.

From the experimental results available at present it is not possible to predict, for a new aerofoil section, whether the aerodynamic centre will move forward or back at high Mach numbers. It is generally assumed for stressing purposes that, as the Mach number increases, the aerodynamic centre first moves forward (to about $0{\cdot}1\bar{c}$), and then moves back to about $0{\cdot}45\bar{c}$ at still higher Mach numbers. The German tests[19] already mentioned in connection with lift gradient reversal suggest that fore-and-aft movements of the shock waves with changing incidence, and the associated forward movement of aerodynamic centre, may be more serious for aerofoils which are convex towards the rear than for aerofoils with flat sided or cusped trailing edges.*

*Tests made at the R.A.E. since this report was written have shown that the large forward movement of the aerodynamic centre at high Mach numbers can be avoided by using a thin aerofoil with a fairly small trailing edge angle.

4.14. *Drag.*—Fig. 44 shows the variation of profile drag coefficient with Mach number for a two-dimensional wing of Mustang section[11]. Fig. 45 gives similar results for a section of a three-dimensional Spitfire half wing[42]. The slight increase of drag with Mach number, up to about $M = 0{\cdot}67$ in Fig. 44 and $M = 0{\cdot}74$ in Fig. 45, is probably due mainly to forward movement of the transition points with increasing tunnel speed. As the Mach number increases above these values the drag coefficient rises rapidly due to the formation of shock waves. The Mach number at which the drag coefficient starts to increase rapidly is sometimes known as the " drag critical Mach number ". This Mach number is about 0·69 for the Mustang wing and about 0·75 for the Spitfire wing.

It has been shown by numerous high-speed tunnel tests[43, 20] that the drag critical Mach number increases as the thickness ratio of the aerofoil is reduced. Figs. 44 and 45 also illustrate this point. Analysis of some systematic German tests on aerofoils of different thicknesses[44] has shown that for zero lift and for thickness ratios less than about 18 per cent., the change of Mach number with thickness ratio, for a given value of the drag coefficient, is given approximately by :—

$$\frac{dM}{d(t_w/c)} = -1{\cdot}2$$

where t_w/c is the ratio of thickness to chord.

Figs. 44 and 45 show that, for a cambered aerofoil, the drag critical Mach number is greatest at an incidence just below zero, not at what is usually known as the " design incidence ". For example, the drag critical Mach number of the Spitfire wing section (Fig. 45) is a maximum at an incidence of about — 1 deg. or — 2 deg. (the exact value depends on the definition used), whereas the " design incidence " of the section is about + 1 deg. German tests[18] have confirmed this, and have shown that the lift coefficient for minimum profile drag on a cambered aerofoil changes from a positive value at low Mach numbers to about zero at a Mach number just above the drag critical, becoming negative at still higher Mach numbers. The same German tests[18] show that the drag critical Mach number decreases with increase of camber, for all lift coefficients up to about 0·6, and hence within this range of lift coefficients the drag of a symmetrical aerofoil at high Mach numbers is less than that of a cambered one. These results provide further illustration that the Mach number at which the local speed of sound is first reached has very little practical significance, especially on an aerofoil having a high suction peak near the nose, *e.g.* a thin symmetrical aerofoil at a fairly high incidence.

Some drag measurements have been made on aerofoils of different sizes[45], to investigate the effects of Reynolds number and tunnel wall interference on drag at high Mach numbers. Fig. 46 shows the results of these tests, corrected for the effects of tunnel wall interference by comparing results for different sizes of model at the same Reynolds number. It appears that there is a large scale effect on drag at high Mach numbers, especially at Reynolds numbers below about 1×10^6. However, the scale effect appears less serious when the results are plotted as a ratio of drag coefficients at high and at low Mach number (Fig. 47).

Beavan has analysed the results of a number of high-speed tunnel tests at the N.P.L.[43] to find the rate of rise of drag with Mach number above the critical value. Defining the rate of rise as the mean rate of change between $C_D = 0{\cdot}015$ and 0·030, $(\partial C_D/\partial M)_a$ was found to be about 0·45 for the N.P.L. tests and about 0·42 for the R.A.E. results reproduced here in Fig. 46 (at $R = 1{\cdot}4 \times 10^6$).

When the profile drag of an aerofoil is measured at high Mach numbers by the wake traverse method[46, 47], it is sometimes possible to estimate roughly the proportion of the drag rise due to direct shock wave loss. In Fig. 48, which shows curves of total head loss behind a Spitfire wing[42] at high Mach numbers, the central part of the wake, with a relatively sharp peak, represents the loss of total head in the boundary layers. The outer parts of the wake are due to direct total head losses at the shock waves. The total increase of drag due to the shock waves may be considered in two parts, as follows :

(*a*) The drag due to direct loss at the shock waves, and

(*b*) The increase of drag due to the effect of the shock waves on the boundary layers.

The drag given by the area of the central part of the wake includes item (*b*) above and may be called, for convenience, the basic drag. Item (*a*) is given by the area of the outer parts of the wake, and this part of the drag is sometimes known as the shock drag. It should be noted, however, that this so-called shock drag does not represent the whole of the drag increase due to the shock waves, because the indirect effect of the shock waves on drag is included in the basic drag. The sum of the basic drag and the shock drag is of course equal to the total drag.

Figs. 49 and 50 show the relative importance of the basic drag and the shock drag for the Spitfire wing at two different incidences. At the incidence for minimum drag at high Mach numbers ($\alpha = -1$ deg.), most of the drag rise at high Mach numbers is due to direct shock wave loss (Fig. 49). At a higher incidence (Fig. 50) the rise of basic drag with Mach number is considerably greater. Flight measurements on a Spitfire[17] have also shown that the increase of basic drag at high Mach numbers is comparatively small, the greater part of the drag rise being due to direct shock wave loss (*see* §6.9). These conclusions are important, because if most of the drag rise at high Mach numbers is due to direct shock wave loss, only a small improvement can be expected by such devices as sucking away the boundary layer after the shock wave. It should be noted, however, that the thickness ratio of the Spitfire wing section was only 0·113, and for greater thicknesses the rise of basic drag with Mach number may be more important.

4.2. *Tests on Controls.*—The reliability of control tests in the High Speed Tunnel at fairly low Reynolds numbers is still very uncertain. It was shown in some tests on an EC 1540 aerofoil with 20 per cent. control flap[48], that the addition of transition wires at about 5 per cent. chord caused large changes of control effectiveness and hinge moment at all Mach numbers. It is not known, however, whether these changes were due mainly to the movement of transition point produced by the wires, or to the direct effects of the wires on the pressure distribution at high Mach numbers. It should be noted also that these tests with transition wires were made on a rather unusual aerofoil section, with an exceptionally large trailing edge angle, and it is possible that the effects of the wires would have been less serious on a more normal aerofoil section.

A further cause of uncertainty in high-speed tunnel tests on controls is the large effect of a gap between the control flap and the aerofoil on the control effectiveness at high Mach numbers. Until fairly recently, all tests on controls in the R.A.E. High Speed Tunnel were made with a gap of about $0{\cdot}002\bar{c}$, but some recent tests have shown that the loss of control effectiveness due to this gap is considerably greater at high Mach numbers. All future tests will therefore be made with the gap sealed.

A summary of the results of control tests in the High Speed Tunnel is given below, but in view of the uncertainties mentioned above, the results should only be considered qualitatively.

Fig. 51 shows the variation of control effectiveness (a_2) with Mach number, for three different models[48, 49, 50]. One of these models, a tail plane of Typhoon plan form with EC 1240 section, was tested with a gap of $0{\cdot}002\bar{c}$ and also with the gap sealed. The curves show that the loss of control effectiveness with increasing Mach number is considerably reduced by sealing the gap. The other two models, the Typhoon tail plane and the EC 1540 aerofoil, were only tested with a gap of $0{\cdot}002\bar{c}$.

The results given in Fig. 51 show that in most cases a_2 remains roughly constant up to a Mach number of 0·75 or more, although theory[24] indicates a rise of a_2 with Mach number. At high Mach numbers there is a fairly sudden collapse of a_2, and the Mach number at which this begins is lower for the thicker aerofoil sections. This loss of a_2 at high Mach numbers would have very serious results if it occurred on the elevator of a full-scale aircraft. However, at high flight Mach numbers, the local Mach number in the region of the tail of an aircraft is usually considerably less than the flight Mach number, so that in practice the shock stalling speed of the tail plane is usually not reached in flight. This point will be discussed later in more detail.

Figs. 52, 53 and 54 show the variation of hinge moment coefficient with control angle, for three different models at several Mach numbers[49, 50, 51]. In Figs. 52 and 53, which show results for a control with a set-back hinge, the control becomes lighter (for small control angles) with increase of Mach number up to about 0·75. For the thicker tail plane (Fig. 52), the control becomes heavier again at still higher Mach numbers. Fig. 54 shows that similar changes occur on a Frise

type aileron[51], but in this case the control becomes heavier, for large negative angles, at quite low Mach numbers. The results given in Fig. 54, at an incidence of + 0·1 deg., do not show any increase of heaviness at high Mach numbers for small control angles, at least up to $M = 0{\cdot}78$, but for higher and lower incidences an increase of heaviness was found at high Mach numbers[51].

4.3. *Tests on Complete Models.*—A summary has now been given of the effects of compressibility, as far as they are known, on the properties of aerofoils and controls. By consideration of these results, most of the compressibility effects which have been observed on complete aircraft can be explained, because on conventional present day aircraft the behaviour at high Mach numbers is determined mainly by compressibility effects on the wing and tail plane. In most cases the compressibility effects on the fuselage are relatively unimportant, but excrescences on the wing such as engine nacelles and radiators may have considerable effects on the behaviour of the aircraft at high Mach numbers.

Tests on a large number of complete model aircraft have been made in the High Speed Tunnel (Refs. 27 to 31, 33 to 36, and 52 to 57), and one of these models, the Mustang I[52], has been selected for the purpose of illustrating the typical behaviour of a complete aircraft at high Mach numbers. The results of the tests on the Mustang will be discussed fairly fully, and any important differences between these results and those of other complete model tests in the High Speed Tunnel will be mentioned.

The Mustang I is a low-wing, single-engine, fighter monoplane aircraft of U.S.A. design. Fig. 55 shows a sketch of the model as tested in the tunnel. The wing sections are an early low-drag type, the thickness ratio being 0·151 at the root and 0·114 at the tip. The camber is 3·0 per cent. at the root and 0·8 per cent. at the tip. The thickness ratio of the tail plane is 0·10. The pitching moments have all been reduced to a C.G. position at $0{\cdot}280\bar{c}$.

4.31. *Properties of wing and fuselage at high Mach numbers.*—For conventional aircraft designs, the variations with Mach number of lift, drag, and pitching moment on the wing are usually not much affected by the addition of the fuselage. This means that the effects of the fuselage on the forces and moments can in most cases be assumed to be roughly independent of Mach number. This is shown, for the Mustang, in Figs. 56 to 61. In some other cases it has been found that the addition of a fuselage to a wing causes a small change in the Mach number at which critical changes of C_L, C_m and C_D occur.

Fig. 56 shows the variation of lift coefficient with Mach number at constant incidence, for the Mustang wing alone and also for the wing and body together. Fig. 57 shows the variation of zero-lift incidence with Mach number for the same models, and Fig. 58 shows the variation of lift gradient. All these diagrams show that the effect of the body on the relationship between lift and incidence is comparatively unimportant at all Mach numbers up to 0·8.

Fig. 59 shows the variation of drag coefficient with Mach number for the complete model of the Mustang. A curve for the wing alone at zero lift is also included. (The drag curves for the complete model are nearly the same as those for the wing and body, the drag of the tail surfaces being small.) The drag curves for the complete model in Fig. 59 are similar to those discussed earlier for wings (*e.g.* Figs. 44 and 45), but the variation of C_D with C_L is much greater in Fig. 59 because induced drag is included.

The curves for zero lift in Fig. 59 show that the " apparent body drag " is almost independent of Mach number up to $M = 0{\cdot}8$. This " apparent body drag " depends on the difference between the drag of the body and the drag of the portion of the wing which is normally covered by the body. On some other models it has been found that this " apparent body drag " decreases slightly at high Mach numbers, *i.e.* that the increase of drag of the portion of the wing which is normally covered by the body is greater than the increase of drag of the body itself. The true body drag, as measured on the isolated body, may increase at high Mach numbers even in cases where the apparent body drag decreases.

Figs. 60 and 61 show the variation of pitching-moment coefficient with Mach number for the Mustang wing alone and also for the wing and body without tail. These curves show similar characteristics, but the spacing of the curves is wider in Fig. 61 than in Fig. 60 because of the destabilising effect of the body. In both diagrams there is a gradual decrease of C_m with increase

of Mach number up to about 0·75, followed by a rise of C_m with further increase of Mach number. These effects are similar to those shown in Fig. 42, where C_{m_0} is plotted against Mach number for several wings.

It is well known that $(-C_{m_0})$ for a wing and body at low Mach numbers can be considerably reduced by fitting a reflexed wing root fillet. On one complete aircraft model[57], the effects of a reflexed wing root fillet have been investigated at high Mach numbers. It was found in this case that the reduction of $(-C_{m_0})$ due to the reflexed fillet was nearly independent of Mach number up to $M = 0{\cdot}8$. This result is surprising, since it is known that the effect of a reflexed wing camber line in reducing $(-C_{m_0})$ tends to disappear at high Mach numbers[39].

The variation of aerodynamic centre position with Mach number for a wing and body is generally similar to that found on the wing alone. In most cases there is a slight forward movement (about $0{\cdot}02\bar{c}$ to $0{\cdot}03\bar{c}$) with increase of Mach number up to some critical value, followed by a sudden forward or backward movement with further increase of Mach number. On the Mustang and most of the other models which have been tested in the tunnel this sudden movement of aerodynamic centre at high Mach numbers has been in the forward direction. The behaviour of the Mustang at moderate Mach numbers is exceptional; in this case there is a slight backward movement of the aerodynamic centre with increase of Mach number (Fig. 65).

4.32. *Trim changes.*—On most of the aircraft models which have been tested in the High Speed Tunnel, a fairly large reduction of (nose-up) pitching-moment coefficient has been found at high Mach numbers. This is shown in Fig. 62, for the Mustang, and Fig. 63 shows the corresponding reduction of elevator angle to trim. This nose-down trim change at high Mach numbers has caused considerable trouble in flight at high speeds (*see* 6.4). The trim change is caused mainly by the increase of incidence required to maintain a given wing lift coefficient at high Mach numbers. This gives an increase of tail plane incidence, and therefore an increased tail plane lift, so that there is a reduction of pitching moment at high Mach numbers. The causes of the trim change are discussed in Ref. 40, and it is shown there that in certain conditions it is theoretically possible for the change of pitching moment due to the tail to be balanced approximately by the change of pitching moment on the wing. In practice, however, the nose-down trim change due to increase of tail plane lift is nearly always much greater than the nose-up change of pitching moment on the wing, so that there is a resultant nose-down trim change on the complete aircraft.

Considering the results of the tests on the Mustang, comparison of Figs. 61 and 62 shows that the nose-down trim change at high Mach numbers is caused by a reduction of pitching moment due to the tail, *i.e.* an increase of tail plane lift. The increase of pitching moment on the wing and body, occurring at Mach numbers above about 0·75, tends to reduce the nose-down trim change, but this effect is small in comparison with the change due to increase of tail plane lift. Since the effective tail plane lift gradient a_1 (Fig. 64) does not vary much with Mach number, at least up to $M = 0{\cdot}8$, the increase of tail plane lift coefficient at high Mach numbers must be mainly due to an increase of effective tail plane incidence. Fig. 66 shows that the downwash angle at the tail, for a given (small) wing lift coefficient, falls by about $\frac{1}{2}$ deg. as the Mach number increases from 0·7 to 0·8. This partly explains the increase of effective tail plane incidence. However, a much more important effect is due to the increase of zero-lift angle for the wing (Fig. 57), which amounts to about 1·8 deg. between $M = 0{\cdot}7$ and $M = 0{\cdot}8$. In addition, there is a reduction of lift gradient at high Mach numbers which makes the increase of incidence, for a given positive lift coefficient, even greater than the increase of incidence for zero lift.

We may now analyse the change of trim on the Mustang, as follows:

Consider the change between $M = 0{\cdot}7$ and $M = 0{\cdot}8$, at a constant lift coefficient of 0·2. (For steady flight at a constant altitude the lift coefficient would fall with increase of Mach number, but the effect of this is unimportant.)

Between $M = 0{\cdot}7$ and $M = 0{\cdot}8$, the incidence for zero lift (wing and body) increases by 1·85 deg. (Fig. 57). For the same change of Mach number, the lift gradient falls from 5·5 to 4·3 per radian (Fig. 58).

$\therefore$ For $C_L = 0{\cdot}2$, the increase of wing incidence is given by

$$\Delta\alpha_w = \underset{\text{(no-lift angle)}}{1{\cdot}85} + \underset{\text{(lift gradient)}}{0{\cdot}6} \text{ degrees}$$

The reduction of downwash angle at the tail is $0{\cdot}55$ deg., so that the total increase of effective tail plane incidence is

$$\begin{aligned}\Delta\alpha_T &= \Delta\alpha_w + 0{\cdot}55 \text{ deg.}\\ &= \underset{\text{(no-lift angle)}}{1{\cdot}85} + \underset{\text{(lift gradient)}}{0{\cdot}6} + \underset{\text{(downwash)}}{0{\cdot}55} \text{ degrees,}\\ &= 3{\cdot}0 \text{ degrees.}\end{aligned}$$

(Note that 60 per cent. of this change of tail plane incidence is due to the increase of no-lift angle.)

The change of aircraft pitching-moment coefficient due to the tail plane is given by

$$\Delta C_{m_T} = -\bar{V}a_1\Delta\alpha_T$$

where $\bar{V}$ = tail volume coefficient

$= 0{\cdot}438.$

Neglecting the small change of a_1 between $M = 0{\cdot}7$ and $M = 0{\cdot}8$, and taking a mean value of $a_1 = 3{\cdot}4$ (Fig. 64)

$$\begin{aligned}\Delta C_{m_T} &= -0{\cdot}438 \times \frac{3{\cdot}4}{57{\cdot}3} \times 3{\cdot}0\\ &= -0{\cdot}078.\end{aligned}$$

Also, the increase of pitching-moment coefficient for the wing and body, between $M = 0{\cdot}7$ and $M = 0{\cdot}8$, is given by :

$$\Delta C_{m_w} = +0{\cdot}019.$$

$\therefore$ The resultant change of C_m on the complete aircraft is :

$$\begin{aligned}\Delta C_m &= \Delta C_{m_w} + \Delta C_{m_T} = +0{\cdot}019 - 0{\cdot}078\\ &= -0{\cdot}059\end{aligned}$$

(which is the amount shown in Fig. 62).

The numerical values given above are fairly typical of the results of high-speed tunnel tests on conventional low-wing monoplanes with cambered wing sections. Excrescences on the wing, such as nacelles and radiators, may have considerable effects on the trim change at high Mach numbers, and these will be considered later. The effect of wing camber is considered below.

It has been shown that the nose-down trim change on the Mustang at high Mach numbers is caused by an increase of effective tail plane incidence, and that 60 per cent. of this change of tail plane incidence is due to the increase of no-lift angle of the wing and body. This change of no-lift angle could be reduced to zero by the use of a symmetrical arrangement of wing and body, with zero camber on the wing. In practice, it is usually not possible to make the body exactly symmetrical, but the change of no-lift angle with Mach number can be made very small.

If the change of no-lift angle with Mach number is reduced to zero, the nose-down trim change due to increase of tail plane lift is reduced from

$$\Delta C_{m_T} = -0{\cdot}078 \quad \text{to} \quad \Delta C_{m_T} = -0{\cdot}030$$

However, if the wing and body are made symmetrical, the change of C_m with Mach number for the wing and body probably disappears, so that the total change of trim is altered from :

$$\Delta C_m = -0{\cdot}078 + 0{\cdot}019 = -0{\cdot}059 \text{ (with cambered wing)}$$

to $$\Delta C_m = -0{\cdot}030 + 0 \quad = -0{\cdot}030 \text{ (with symmetrical wing and body)}$$

Thus the change of trim between $M = 0{\cdot}7$ and $M = 0{\cdot}8$ could be halved by altering the original Mustang design to a symmetrical arrangement of wing and body.

The advantages of symmetrical wing sections over cambered ones for aircraft to fly at high Mach numbers are now fairly well known. The nose-down trim change at high Mach numbers will always be less with a symmetrical wing than with a cambered one.* Considering the particular case of a vertical dive (or climb) at zero lift, it is clear that with a symmetrical aircraft there can be no change of trim with Mach number. Also, German high-speed tunnel tests[18] have shown that the drag of a symmetrical wing at high Mach numbers is less than that of a cambered one, at all lift coefficients up to 0·6. Symmetrical wings have the further advantage of making C_{m_0} numerically small.

Other possible methods of reducing the nose-down trim change at high Mach numbers will now be considered. In some cases the trim change is increased by a loss of downwash angle at the tail for a given wing lift coefficient (*e.g.* Fig. 66). This loss of downwash is probably due to the thickness ratio of the wing being greater at the root than at the outer parts of the wing, so that the shock stall occurs at a lower Mach number at the root. Thus for a given overall wing lift coefficient the local lift coefficients at the sections near the root are reduced, giving a loss of downwash at the tail. The change of downwash can be minimised by keeping the thickness ratio of the wing constant along the span. However, a possible objection to this is that the part of the wing in front of the ailerons would then shock stall at about the same Mach number as the rest of the wing, so that compressibility troubles on the ailerons might be experienced which would not occur on an aircraft having thinner wing sections at the tip than at the root.

On the Mustang, if the reduction of downwash with increasing Mach number could be eliminated, the trim change (with the cambered wing) would be reduced from :

$$\Delta C_m = -0{\cdot}059 \qquad \text{to} \qquad \Delta C_m = -0{\cdot}043$$

If, in addition, the wing and body were made symmetrical, the trim change between $M = 0{\cdot}7$ and $M = 0{\cdot}8$ would be reduced to

$$\Delta C_m = -0{\cdot}014$$

This remaining trim change is entirely due to loss of wing lift gradient. This can be delayed to higher Mach numbers by the use of thinner wing sections, but it cannot be completely avoided.

So far, only the changes of trim at Mach numbers up to about 0·8 have been considered. The change of trim to be expected in passing from a moderate subsonic speed ($M = 0{\cdot}7$) to a fairly high supersonic speed ($M = 1{\cdot}3$) has been investigated theoretically by Smelt[58]. It was shown that a nose down change of trim would always occur with a conventional design of aircraft ; the principal causes of this trim change are given below :—

(*a*) For a positively cambered wing, the no-lift angle is negative at subsonic speeds and is approximately zero at supersonic speeds. Consequently, the incidence required to maintain a given lift increases as the speed rises through the speed of the sound. This gives an increase of tail plane lift and hence a nose-down change of trim. In some cases, this effect may be augmented by a change of wing lift curve slope, but the importance of this depends on the aspect ratio and the Mach numbers considered.

(*b*) With increase of speed, through the speed of sound, the aerodynamic centre of a wing moves back from a position near the quarter-chord point to one near the half-chord point. Thus the downward load required on the tail plane to trim the aircraft at a positive lift is greater at supersonic than at subsonic speeds.

(*c*) The mean downwash angle at the tail, for a given wing lift coefficient, may be considerably smaller at supersonic speeds than at subsonic speeds, thus causing a nose-down change of trim as the speed rises through the speed of sound. (The importance of this effect depends on the lay-out of the aircraft and on the Mach numbers considered.)

*The discussion given here refers only to low lift coefficients. If the operating altitude is very high, the lift coefficient may be fairly large even at top speed, and the reduction of lift gradient at high Mach numbers may then have a more important effect than the change of no-lift angle.

(*d*) The effectiveness of an elevator is considerably less at supersonic speeds than at subsonic speeds. For an aircraft whose elevator angle to trim at subsonic speeds is near zero, this effect increases the change of elevator angle to trim in passing through the speed of sound, because in this case the elevator angle to trim is negative at supersonic speeds, and the loss of elevator effectiveness causes a numerical increase of this negative elevator angle.

(*e*) For a cambered wing there is a change of C_{m_0} in passing through the speed of sound, but the effect of this on the trim change is relatively unimportant.

It has been shown that the first of these causes, the change of no-lift angle, can be avoided by using a symmetrical arrangement of wing and body. The other important cause of the trim change, the movement of aerodynamic centre, can probably be delayed to high subsonic Mach numbers by using thin wing sections but must inevitably occur at some Mach number in the transonic range. In theory, considering only the overall change of trim in passing from a moderate subsonic speed to a fairly high supersonic speed, the trim change could be avoided altogether by using a wing section with negative camber. The change of no-lift angle would then tend to give a nose-up trim change, and this could be made to counteract the other effects. The use of a negatively cambered wing is not recommended, however, because in any case the trim change could only be avoided for one lift coefficient. Also, although at the design lift coefficient the elevator angle (or tail setting) to trim would be the same for a moderate subsonic speed as for a fairly high supersonic speed, there would probably be fairly large and irregular changes of trim at speeds nearly equal to the speed of sound.

It has been suggested by Benson and Philpot[59] that the trim change on a symmetrical aircraft, in passing from subsonic to supersonic speeds, could be avoided by the use of a front wing of small aspect ratio and a tail plane of large aspect ratio. The ratio a_1/a would then decrease in passing from subsonic to supersonic speeds, and this could be made to counteract the effects of movement of aerodynamic centre and loss of downwash. Unfortunately, with conventional values of wing and tail area the aspect ratios required are not practicable. If the aircraft is made with a fore plane, however, *i.e.* with the main lifting surface at the rear, the required conditions can be satisfied with more normal aspect ratios.

A possible alternative method of avoiding the change of trim in passing through the speed of sound is to use a tailless aircraft of unconventional plan form. This subject has not yet been investigated, but there are indications from German tests that the change of centre of pressure position with Mach number may be fairly small on a wing of very low aspect ratio, having large sweepback on the leading edge and small sweep forward on the trailing edge.

Most of the complete aircraft models which have been tested in the High Speed Tunnel have shown a nose-down trim change at high Mach numbers, similar to that found on the Mustang (Fig. 62). The magnitude of the nose-down trim change, and the Mach number at which it starts, depend mainly on the camber and thickness of the wing and vary from one model to another. Some exceptional cases have been found in which the trim change is almost zero, or is even in the nose-up direction. Most of these exceptional cases can be explained by the presence of nacelles or radiators under the wing. The effects of these on the trim change at high Mach numbers will be discussed later. In all the cases where a nose-up trim change has been observed in the tunnel, it is probable that a nose-down change would occur at still higher Mach numbers, but it has not yet been found possible to test complete models in the tunnel at Mach numbers above about 0·8.

One exceptional case which has been found is the Meteor IV (with extended nacelles)[60, 61, 62]. On this model a nose-up trim change was found at high Mach numbers, and this has been confirmed by flight tests (*see* §6.4 and Ref. 63). A nose-up trim change was also found in the tunnel tests on the model without nacelles, showing that the effect was not caused by the nacelles. On the Meteor I with the original short nacelles, the nacelles caused a breakaway of flow on the upper surface of the wing at high Mach numbers, giving a nose-down trim change. On the model with extended nacelles (or without nacelles), the changes of pitching moment on the wing and body, and of downwash at the tail, were very small at all Mach numbers up to 0·82. The nose-up trim

change was apparently due to a *reduction* of the incidence for no lift at high Mach numbers, instead of the increase usually found on other models. The explanation of this reduction of no-lift angle with increasing Mach number is not yet clear, but it is very probable that at still higher Mach numbers there would be an increase of no-lift angle, accompanied by the usual nose-down change of trim.

Some tests made on a flying boat of high wing design showed a slight nose-up change of trim at high Mach numbers. In this case the effect was due mainly to an increase of the downwash angle at the tail. The large hull underneath the wing probably caused a separation of flow on the lower surface of the central part of the wing. This would cause a local increase of lift coefficient at the wing root and hence an increase of downwash angle at the tail. Similar effects caused by underslung nacelles will be discussed later.

It has been found that the nose-down change of trim discussed above can be counteracted by the use of small flaps on the lower surface of the wing[64]. These are known as dive recovery flaps, and when opened they cause an increase of wing lift coefficient, for a given incidence, and also in some cases an increase of wing pitching moment. On a complete aircraft, these effects cause an increase of pitching moment for a given lift, or an increase of lift at a given pitching moment, and thus assist recovery from a high-speed dive. It is shown in Ref. 65 that the behaviour of an aircraft, during recovery from a dive with constant elevator angle, may be calculated approximately by assuming that the lift coefficient at any instant has the value required to make $C_m = 0$, provided that the stability margin of the aircraft $-\left(\frac{\partial C_L}{\partial C_m}\right)_M$ is fairly large. Since the nose-down trim change at high Mach numbers is usually accompanied by an increase of longitudinal stability, the required condition that the stability margin should be large is usually satisfied in cases where dive recovery flaps are required. This means that the normal acceleration produced by opening dive recovery flaps can be calculated roughly (assuming that the elevator angle remains constant) from the increase of C_L at constant C_m due to opening the flaps. In practice, the pilot may change the elevator angle during the recovery in either direction, so that the normal acceleration actually achieved may be either greater or less than the amount calculated in this way.

Dive recovery flaps are usually placed on the lower surface of the wing at about 20 to 40 per cent. of the local chord. They are more effective if they are placed on the inboard part of the wing, in front of the tail plane, because they then give an increase of downwash at the tail for a given mean wing lift coefficient, in addition to the other effects mentioned above.

High Speed Tunnel tests have been made on several models fitted with dive recovery flaps (e.g. *see* Ref. 66). The results of the tests on one of these models are shown in Fig. 68. On this model the wing sections were very thin (11 per cent. at the root), and any nose-down change of trim would probably occur at Mach numbers greater than the highest value reached in the tunnel tests (0·82). With increase of Mach number up to about 0·8 there was a slight nose-up change of trim, and thus the dive recovery flaps could not be investigated at the Mach numbers at which they would be required in flight. However, the results given in Fig. 68 show that the flaps give a positive increase of C_m at constant C_L and that the effectiveness of the flaps increases with Mach number. At Mach numbers between 0·7 and 0·8 the tunnel results show that the aircraft is unstable (without flaps), so that at these Mach numbers the normal acceleration produced by the flaps cannot be estimated from the increase of C_L at constant C_m. At a Mach number of 0·82, however, $-\left(\frac{\partial C_m}{\partial C_L}\right)_M$ has a reasonably large positive value at low incidences, and at this Mach number the flaps increase C_L by about 0·2 at constant C_m. This is equivalent to an increase of normal acceleration of about 3g at 10,000 ft.

4.33. *Longitudinal stability.*—Gates and Lyon[67] have given an account of a generalised theory of longitudinal stability which takes into account variations of the aerodynamic force and moment coefficients with speed. The theory can be applied to the analysis of longitudinal stability at high Mach numbers, but it should be remembered that it is a first order theory, and its application to conditions above the shock stalling Mach number is therefore doubtful. Gates and Lyon define four important criteria of longitudinal stability and handling qualities.

These are the static margins (stick-fixed and stick-free), and the manœuvre margins (stick-fixed and stick-free). In discussing the results of high-speed tunnel tests, only the stick-fixed static and manœuvre margins can be considered at present, because there is not enough reliable information on the variation of elevator hinge-moment coefficients with Mach number, to enable any estimates of the stick free margins to be made from the tunnel tests.

The stick fixed static margin is proportional to the change of stick position required to trim in steady flight at a higher or lower speed than the initial trimmed speed, and is defined as:

$$K_n = -\frac{dC_m}{dC_R} \qquad (4)$$

where $C_R = \sqrt{(C_L^2 + C_D^2)} = \dfrac{w}{\frac{1}{2}\rho V^2}$ (w = wing loading).

In the absence of aero-elastic distortion effects, the static margin may be expressed as:

$$K_n = -\left(\frac{\partial C_m}{\partial C_R}\right)_M + \frac{M}{2C_R}\left(\frac{\partial C_m}{\partial M}\right)_{C_R}$$

$$= -\left(\frac{\partial C_m}{\partial C_R}\right)_M + \frac{\gamma P_0 M^3}{4w}\left(\frac{\partial C_m}{\partial M}\right)_{C_R} \qquad (5)$$

where P_0 is the atmospheric pressure at the altitude under consideration and γ is the ratio of the specific heats of air. At low Mach numbers, the second term in equation (5) is zero and C_R is usually very nearly equal to C_L, so that the static margin is given simply by:—

$$K_n = -\left(\frac{\partial C_m}{\partial C_L}\right)_V \qquad (6)$$

At high Mach numbers, the static margin is determined mainly by the second term in equation (5). This is because the trim changes discussed above make the term $\left(\frac{\partial C_m}{\partial M}\right)_{C_R}$ numerically large, and also because M^3 becomes relatively large. If there is the usual nose-down trim change with increase of Mach number K_n tends to have a large negative value, but if there is a nose-up trim change K_n usually has a large positive value.

Because of the important effects of the term $\left(\frac{\partial C_m}{\partial M}\right)_{C_R}$, the static margin becomes, at high Mach numbers, merely an indication of the magnitude and direction of the trim change with speed. For nearly all the complete models which have been tested in the High Speed Tunnel, K_n assumes numerically large values at Mach numbers above about 0·7. At these Mach numbers K_n is usually negative, indicating a nose-down trim change with increase of speed. In some cases, there is a slight nose-up change of trim at moderate Mach numbers (M = 0·6 to 0·65), giving a large positive value of K_n, and at higher Mach numbers a nose-down trim change develops, making K_n negative.

These large changes of static margin at high Mach numbers may not be important in practice, because at high flight speeds the change of stick position (or force), corresponding to a fairly large change of speed, may be quite small even for a numerically large static margin. In fact, quite a large negative static margin may be acceptable at high speeds, provided the manœuvre margin is positive, because the divergence that develops in these conditions is a slow one. However, the condition that the manœuvre margin should be positive is a very important one, because with a negative manœuvre margin a rapid divergence is likely to occur. Thus at high speeds the manœuvre margin is a more important criterion of longitudinal stability and handling qualities than the static margin.

The stick fixed manœuvre margin is proportional to the " stick movement per g " in a recovery from a trimmed dive. It is shown in Ref. 67 that the manœuvre margin is given by:

$$H_m = -\left(\frac{\partial C_m}{\partial C_L}\right)_M + \frac{a_1 \bar{V}}{2\mu_1} \qquad (7)$$

where a_1 is the effective tail plane lift gradient, $\bar{V}$ is the tail volume coefficient, and

$$\mu_1 = \frac{w}{\rho l} \quad .. \quad .. \quad .. \quad .. \quad .. \quad .. \quad .. \quad .. \quad (8)$$

In equation (8), w is the wing loading, ρ is the air density, and l is the tail arm of the aircraft.

For the range of Mach numbers covered by high-speed tunnel tests (*i.e.* up to about 0·8), the variations of the tail plane lift gradient a_1 with Mach number are usually small. Hence, for a given altitude, the variations of stick-fixed manœuvre margin with Mach number are approximately equal to the variations of the term $-\left(\frac{\partial C_m}{\partial C_L}\right)_M$, as found from high-speed tunnel tests. It may be noted that for a typical modern fighter aircraft, the value of the term $\frac{a_1 \bar{V}}{2\mu_1}$ varies from about 0·03 at sea level to about 0·01 at 33,000 ft., and the manœuvre margin therefore exceeds the value of the term $-\left(\frac{\partial C_m}{\partial C_L}\right)_M$ by these amounts.

Fig. 65 shows the variation of $-\left(\frac{\partial C_m}{\partial C_L}\right)_M$ with Mach number for the Mustang I model. For the model with tail there is a steady decrease of stability with increasing Mach number up to about 0·67, followed by an increase at still higher Mach numbers. This behaviour is similar to that found on most of the other models which have been tested, but as already mentioned the changes of $-\left(\frac{\partial C_m}{\partial C_L}\right)_M$ with Mach number for the Mustang model without tail are unusual. In most other cases the aerodynamic centre of the model without tail moves forward slightly with increase of Mach number up to the shock stalling speed, while on the Mustang the aerodynamic centre moves back slightly. As the Mach number is increased above the shock stalling speed, the aerodynamic centre (without tail) moves forward on the Mustang and also on most of the other models tested.

The decrease of manœuvre margin with increase of Mach number up to the shock stalling speed has been predicted theoretically by Owen[68], and has also been found in nearly all the high-speed tunnel tests on complete aircraft models. However, in many cases the loss of stability found in the tunnel tests has been rather greater than that given by the theory. The explanation of this discrepancy is that Ref. 68 is based on the linear perturbation theory[8], whereas the variations of lift gradient, downwash, and wing pitching moment with Mach number do not always follow the linear perturbation theory exactly.

The theoretical explanation of the loss of manœuvre margin with increasing Mach number, up to the shock stalling speed, can be seen by considering the equation :

$$-\left(\frac{\partial C_m}{\partial C_L}\right)_M = (h_0 - h) + a_1 \bar{V}\left(\frac{1}{a} - \frac{d\varepsilon}{dC_L}\right) \quad .. \quad .. \quad .. \quad .. \quad (9)$$

In this equation, h_0 and h define the positions of the aerodynamic centre of the wing and body and of the aircraft C.G., a and a_1 are lift gradients for the wing and body and for the tail plane respectively, and ε is the downwash angle at the tail. Below the shock stalling Mach number, $d\varepsilon/dC_L$ remains approximately constant, so that the tail plane contribution to stability depends on a term of the form

$$a_1 \bar{V}\left(\frac{1}{a} - Z\right) \quad .. \quad .. \quad .. \quad .. \quad .. \quad .. \quad (10)$$

where $\bar{V}$ and Z are constants. This term will obviously become less as a increases with Mach number, even if a_1 increases in the same ratio. In most cases, the proportional increase of a_1 with Mach number is considerably less than that of a, on account of aspect ratio and wake effects, so that the reduction of the tail plane contribution with increasing Mach number is exaggerated.

For most of the models which have been tested, h_0 decreases slightly with increasing Mach number up to the shock stalling speed, so that the net loss of manœuvre margin is slightly greater than the loss of tail plane contribution. As already mentioned, the Mustang is an unusual case in which h_0 increases with Mach number (Fig. 65).

It can be shown theoretically that the loss of manœuvre margin with increasing Mach number, below the shock stalling speed, can be avoided by making the aspect ratio of the tail plane greater than that of the wing. If this is done, and if the wing aspect ratio is fairly small, the ratio a_1/a will increase with Mach number, and this increase can be made to counteract the increase in the term $a_1\bar{V}\left(\frac{d\varepsilon}{dC_L}\right)$. There are of course many objections to a layout of this kind, but the aspect ratios required are rather more practicable than those required to give zero change of trim (or stability) in passing through the speed of sound (*See* § 4.32 and Ref. 59).

An alternative method of avoiding the change of stability with Mach number, below the shock stalling speed, has been suggested in Germany. If the wing has a fairly large sweepback while the tailplane has no sweepback, a_1/a will increase with Mach number, even for conventional values of the wing and tail aspect ratios, and thus the change of stability can be reduced to zero. The objection to this arrangement is that unless the tail plane is made much thinner than the wing it will shock stall at a lower Mach number, and this early shock stall of the tail will give a serious loss of stability.

Neither of the above methods of avoiding the change of stability with Mach number, below the shock stalling speed, can be considered satisfactory. Since this change of stability is due mainly to variations of the tail plane contribution with Mach number, it seems that ultimately the best solution of the problem is likely to be some form of tailless aircraft.

Above the shock stalling Mach number, high-speed tunnel tests on complete models usually show a fairly large increase of manœuvre margin, often much larger than that shown for the Mustang in Fig. 65. This effect is nearly always due to a large increase in the tail plane contribution to stability. In many cases the aerodynamic centre of the wing and body moves forward at high Mach numbers, but the increase of tail plane contribution is more than enough to counteract this. This is shown, for example, in Fig. 65.

The increase at high Mach numbers of the tail plane contribution to stability is caused by the shock stalling of the main wing at a Mach number at which no shock stalling occurs on the tail plane. On most aircraft, the shock stalling speed of the tail plane is considerably higher than that of the main wing, because the thickness ratio of the tail plane is usually less than that of the wing, and also because at high Mach numbers the local speed near the tail is usually less than the flight speed. The latter effect is discussed in detail below in connection with elevator control. When the wing shock stalls, the lift gradient a falls and, if no shock stalling occurs on the tail plane, the term $\frac{a_1\bar{V}}{a}$ increases, thus increasing the tail plane contribution to stability. In some cases, the effect is exaggerated by changes of downwash. For, if the wing thickness ratio is greater at the root than at the outer sections, the term $\frac{d\varepsilon}{dC_L}$ will decrease as the Mach number rises above the stock stalling speed. Equation (9) shows that this will increase the tail plane contribution to stability.

In Ref. 58, Smelt considers the changes of longitudinal stability to be expected in passing from subsonic to supersonic speeds. It is shown that, for conventional plan forms and aspect ratios, a large increase of stability will always occur. The increase of stability at high subsonic speeds, discussed above, may be considered as the beginning of the change that occurs in passing through the speed of sound. For an aircraft having a wing of zero camber and a symmetrical arrangement of wing and body, the increase of stability in passing through the speed of sound is due to exactly the same causes as the nose-down change of trim which has already been discussed, because in this case the aerodynamic centre coincides with the centre of pressure. Theoretically, the change of stability in passing through the speed of sound can be avoided in the same way as the trim change, by making the aspect ratio of the tail plane much greater than that of the wing, but, as already remarked, the dimensions required for this arrangement are not practicable unless a " tail first " design is adopted. As suggested in discussing trim changes, a tailless design will probably be the best ultimate solution.

4.34. *Elevator control.*—It has already been shown that when an elevator is tested on an isolated tail plane in a high-speed tunnel it usually shows a serious loss of effectiveness at high Mach numbers (Fig. 51). However, when the same tail plane and elevator is tested as part of a complete aircraft model, with the tail in the conventional position, no loss of control effectiveness is found until considerably higher Mach numbers are reached. For example, the results given in Fig. 51 show that the Typhoon elevator[49] begins to lose its effectiveness at a Mach number of about 0·77, whereas the tests on the complete model of the Typhoon[27] showed no loss of elevator effectiveness at any Mach number up to at least 0·8.

It has also been noticed that complete aircraft models with rather high tail planes (e.g. Ref. 34) have shown a greater loss of elevator effectiveness at high Mach numbers than models with conventional low tail planes. This naturally suggested that the difference of behaviour at high Mach numbers, between a tail plane and elevator tested alone and as part of a complete model, might be caused by the wake of the wing or body. Some tests were therefore made to investigate these effects by exploring the velocity distribution in the neighbourhood of the tail on several aircraft models[69]. Fig. 67 shows a typical result, the distribution of local Mach number in the region of the tail of the Typhoon at a wing incidence of 3·5 deg. and a free stream Mach number of 0·8. It may be noted that, although this incidence is fairly high, the results given in Ref. 27 show that the corresponding lift coefficient for the Typhoon at this Mach number is about zero. The results given in Fig. 67 show that the mean local Mach number in the region of the tail plane is less than 0·69 when the free stream Mach number is 0·8. The diagram also shows that the reduction of local Mach number at the tail would be considerably less for a high tail position. The reduction of speed at the tail is rather greater for the Typhoon than for most other high speed aircraft, because the Typhoon wing is unusually thick. Also, the effect is exaggerated on the Typhoon by the loss of lift at the wing root, causing a reduction of downwash at the tail. This makes the centre of the wing wake pass very near the tail at high Mach numbers, whereas at low Mach numbers the wing wake is lower and passes clear of the tail plane.

It may be concluded that, on conventional aircraft with low tail planes flying at high Mach numbers, the local Mach number in the region of the tail will usually be less than the flight Mach number. Thus, if the thickness ratio of the tail plane is not greater than that of the wing, shock stalling of the tail plane and loss of elevator control are not likely to occur. However, for an aircraft with the tail plane in a high position the relieving effect of the wing and body wake is less than with a low tail plane, and shock stalling of the tail plane, with consequent loss of elevator control, may occur unless the tail plane thickness ratio is considerably less than that of the wing.

The information that is available from flight tests confirms the above conclusions. A Spitfire has been dived up to a Mach number of about 0·9 without any indications of loss of elevator control, although at this Mach number the aircraft drag coefficient was about 3 or 4 times the low speed value, showing that severe compressibility effects were occurring on the wing.

In the future, with aircraft developing very high propulsive thrusts at high altitudes, it may be possible to reach Mach numbers so high that, even with a low tail, the effects of the wing and body wake are not sufficient to prevent shock stalling of the tail plane. For these aircraft, all moving tail planes will probably be required in order to provide longitudinal control at very high Mach numbers.

4.35. *Effects of Nacelles.*—For an engine nacelle mounted on a wing, compressibility usually produces a considerable increase of drag, beginning at a lower Mach number than that at which the wing drag starts to rise. The Mach number at which the nacelle drag starts to increase can be raised by increasing the fineness ratio of the nacelle. In addition to these drag changes, a nacelle whose centre line is above or below the wing chord line has important effects on the lift and pitching moment of the wing at high Mach numbers.

Fig. 69 shows the variation with Mach number of the drag of several alternative nacelles for the Meteor[60]. It was found that the drag of the original nacelles started to rise fairly steeply at a Mach number of about 0·65. Also, buffeting had been experienced in flight at Mach numbers above about 0·74, and it was suspected that this was caused by separation of flow near the nacelles. High-speed tunnel tests were therefore made for the purpose of improving the

nacelle design. Observations of surface tufts on the model in the tunnel showed slight signs of flow separation at the rear of the nacelle, even at low Mach numbers. As the Mach number increased above about 0·6 the separation, as shown by disturbance of the tufts, spread forward on the wing and became more severe. This separation probably explained the drag rise at a comparatively low Mach number and also the buffeting which had been experienced in flight. Measurements of pressure distribution on the original Meteor nacelles showed that sonic velocity would be reached locally in the nacelle-wing junction at a Mach number of about 0·675. Since the nacelle drag starts to rise at a lower Mach number than this, the separation is probably caused more by the steep adverse pressure gradient in the nacelle-wing junction than by shock waves.

Extending the nose and tail of the Meteor nacelles to increase the fineness ratio gave a considerable reduction of drag at high Mach numbers (Fig. 69), and also reduced the flow separation as shown by the surface tufts. This improvement has been confirmed by flight tests (*see* § 6.3 and Ref. 63). It is interesting to note that measurements of pressure distribution on the nacelle with extended nose and tail[70] showed that, for wing incidences greater than 1 deg., the critical Mach number (at which sonic velocity was first reached locally) was less than for the original nacelle, and even at lower incidences the critical Mach number was only slightly greater than for the original nacelle. Thus the critical Mach number, defined as the Mach number at which local sonic velocity is first reached, does not give a reliable indication of the improvement due to lengthening the nacelle.

The only important effect, other than drag, of a nacelle having its centre line on or near the wing chord line, is the loss of longitudinal (and directional) stability due to the nacelle. This effect is present at low Mach numbers, and in some cases it may increase slightly with Mach number. Underslung nacelles also have this destabilising effect, but in addition these nacelles usually cause changes of lift and pitching moment which vary considerably with Mach number, and these variations have important effects on C_{m_0} and on trim changes at high Mach numbers.

At low Mach numbers, an underslung nacelle usually gives a reduction of lift and pitching moment for a given incidence. At high Mach numbers, however, separation of flow occurs at low incidences under the wing in the region of the nacelle, and the lift increment at constant incidence due to the nacelle increases to zero or even becomes positive[35] (Fig. 70). The pitching-moment increment at constant incidence usually becomes more negative with increase of Mach number.

As a result of the effects described above, the variation of C_{m_0} with Mach number is usually very large for an aircraft with underslung nacelles. For example, Fig. 71 shows that C_{m_0} for the complete model of the Hornet at a Mach number of 0·8 is about three times the low-speed value. For the wing and body without nacelles, however, the numerical increase of C_{m_0} with Mach number is no more than that found on other models without nacelles, and is of the same order as that given by Hilton's empirical law[38]. Thus the exceptionally large numerical value of C_{m_0} at high Mach numbers is due to the effect of the nacelles.

Fig. 72 shows an analysis of the effect of the nacelles on C_{m_0} for the Hornet. In order to explain this diagram, consider first the wing and body with no nacelles, at zero lift. Then let the nacelles be added, keeping the incidence constant, and let $(\Delta C_L)_\alpha$ and $(\Delta C_m)_\alpha$ be the changes of C_L and C_m. If the incidence is now changed to bring C_L back to zero, the corresponding change of C_m is

$$-\left(\frac{\partial C_m}{\partial C_L}\right)_M (\Delta C_L)_\alpha$$

where $\left(\frac{\partial C_m}{\partial C_L}\right)_M$ is a mean value over the range $C_L = 0$ to $C_L = (\Delta C_L)_\alpha$ for the wing and body with nacelles.

Thus the total change of C_{m_0} due to the nacelles is given by

$$\Delta C_{m_0} = (\Delta C_m)_\alpha - \left(\frac{\partial C_m}{\partial C_L}\right)_M (\Delta C_L)_\alpha \quad .. \quad .. \quad .. \quad .. \quad .. \quad (11)$$

Fig. 72 shows that $(\Delta C_m)_\alpha$ varies with Mach number in a fairly normal way, the numerical increase being only a little greater than that given by the Glauert factor $(1 - M^2)^{-1/2}$. However, at low Mach numbers the nacelles give a negative lift increment, and consequently the change of C_m at constant incidence $(\Delta C_m)_\alpha$ is exactly counteracted by the other term $-\left(\frac{\partial C_m}{\partial C_L}\right)_M (\Delta C_L)_\alpha$. At high Mach numbers, there is a small positive lift increment due to the nacelles, and hence the term depending on $(\Delta C_L)_\alpha$ augments the term $(\Delta C_m)_\alpha$, instead of counteracting it.

Observation of surface tufts on the lower surface of the Hornet model wing[71] confirmed that there was a separation in the region of the nacelle at high Mach numbers, thus explaining the change of nacelle lift increment shown in Fig. 70. Since the exceptionally large value of $(-C_{m_0})$ at high Mach numbers was caused by this change of nacelle lift increment, attempts were made to reduce the separation at high Mach numbers by lengthening the nacelles[71]. Unfortunately, this modification gave very little improvement in C_{m_0}, probably because the greatest increase of nacelle length which was practicable on the full-scale aircraft was not enough to affect appreciably the separation at high Mach numbers. It was found that the value of $(-C_{m_0})$ could be reduced, at all Mach numbers up to 0·82, by turning up the tails of the nacelles, but this modification only slightly reduced the change of C_{m_0} with Mach number.

For underslung nacelles, in addition to the effect on C_{m_0} discussed above, the change of nacelle lift increment at high Mach numbers has an important effect on the longitudinal trim of the aircraft. It has been shown already that the nose-down trim change, which occurs on most aircraft at high Mach numbers, is mainly due to an increase of effective tail plane incidence. For an aircraft with underslung nacelles, the lift increment due to the nacelles increases at high Mach numbers, so that the increase of wing incidence required to maintain a given lift coefficient is less than for a similar aircraft without nacelles. Thus the nose-down trim change at high Mach numbers is usually smaller for an aircraft with underslung nacelles than for one with chordline nacelles or without nacelles, because the increase of tail plane incidence is smaller. Alternatively, the effects of underslung nacelles on the trim change may be explained by considering them as local regions of negative camber on the wing, and it has already been pointed out that a negatively cambered wing tends to reduce the nose-down trim change at high Mach numbers, or give a nose-up trim change.

The influence of underslung nacelles on trim changes at high Mach numbers is illustrated in Fig. 73. For the Mosquito model without nacelles at $C_L = 0$, there is hardly any change of C_m with Mach number up to $M = 0{\cdot}8$, but in the presence of the nacelles there is a considerable increase of C_m above a Mach number of about 0·75. This effect is mainly due to the increase of nacelle lift increment at high Mach numbers, shown in Fig. 74. At $C_L = 0{\cdot}2$, the effect of the nacelles on the trim change is much smaller than at zero lift, because at this lift coefficient the increase of downwash, which occurs at high Mach numbers on the model without nacelles, is reduced by the presence of the nacelles. This may be due to a separation occurring on the upper surface of the wing, as well as on the lower surface.

It would be expected that on an aircraft of high-wing design the fuselage would have effects on C_{m_0} and trim changes at high Mach numbers similar to those found for underslung nacelles. There is not yet sufficient information from high-speed tunnel tests to confirm this, since only one high-wing design, a flying boat, has been tested in the High Speed Tunnel. On this model, the hull appeared to have the expected effect of causing a nose-up trim change at high Mach numbers, instead of the nose-down trim change found on other models, but the measurements of C_{m_0} gave unexpected results. For the wing alone, the variation of C_{m_0} with Mach number was normal, but in the presence of the hull C_{m_0} was nearly independent of Mach number up to $M = 0{\cdot}8$. The difference between the observed effect of the hull on C_{m_0} and the effect which would be expected from tests on underslung nacelles was probably due to the sharp chine lines of the flying boat hull.

4.36. *Effects of radiators.*—It has been found that large underwing radiators have effects similar to underslung nacelles, on lift, C_{m_0}, and trim changes at high Mach numbers. For example, Fig. 75 shows the variation with Mach number of the lift increment due to the underwing radiators on the Spiteful[29]. The increase of ΔC_L at high Mach numbers is probably due to a separation on the lower surface of the wing or underneath the radiators, the effect being similar to that already described for underslung nacelles. Because of this change of radiator lift increment, the radiators tend to cause a nose-up trim change at high Mach numbers (Fig. 77). The presence of the radiators also causes an exceptionally large numerical increase of C_{m_0} with Mach number (Fig. 76). The explanations of these radiator effects on C_{m_0} and longitudinal trim are similar to those already discussed for nacelles; at low Mach numbers the radiators give negative increments of lift and pitching moment (at constant incidence), but at high Mach numbers the lift increment becomes positive.

Fig. 78 shows the variation with Mach number of the drag of the underwing radiators on the Spiteful[29]. Although the Mach number at which local sonic velocity is first reached is moderately low, the rise of drag that occurs is fairly small until a Mach number about 0·1 above this critical value is reached. The rather low theoretical critical Mach number is due to a high local suction peak near the front of the radiator[29] and, as already mentioned, the theoretical critical Mach number has little significance when this occurs[21].

4.37. *Tailless aircraft.*—The only tailless aircraft model which has so far been tested in the High Speed Tunnel is the AW52G glider[55]. High Mach number tests were made on this model in order to give some general information on the behaviour of tailless aircraft at high speeds. The model has a sweepback (at the quarter-chord line) of 16 deg. on the inboard part of the wing and 29 deg. on the outboard part. The thickness ratio of the wing is 20 per cent. at the centre line and 16·4 per cent. near the tip. The wing camber is 1·5 per cent. at the centre line and 0·1 per cent. near the tip. The tests in the High Speed Tunnel showed a fairly severe nose-down change of trim at Mach numbers above about 0·68, caused by loss of lift (for a given incidence) on the inboard part of the wing, without any corresponding loss on the outboard part. This difference of behaviour between the inboard and outboard parts of the wing is probably due to the greater thickness ratio and camber, and smaller sweepback, of the inboard part of the wing. It may be concluded that a nose-down trim change at high Mach numbers is to be expected on any tailless aircraft with a layout similar to this one. The trim change could probably be reduced considerably by making the wing sections symmetrical, and keeping the angle of sweepback and thickness ratio constant along the span. However, a full discussion of the behaviour of swept-back wings at high Mach numbers is beyond the scope of this report.

4.4. *Tests on Propellers.*—Fig. 79 shows the results of some tests on a 2-blade, 6 per cent. thick, Clark Y section propeller[72]. The revised thrust corrections given in the addendum to Ref. 72 have been applied, but in view of the uncertainty of these corrections at high Mach numbers, no results at forward Mach numbers above 0·75 are included in Fig. 79. The results show that the efficiency falls rapidly at forward Mach numbers above about 0·6, but at a given forward Mach number this fall of efficiency is less serious for the larger blade angles. It may be possible to obtain greater efficiencies on this propeller at high forward speeds by operating at still greater blade angles. This propeller was selected for tests in the High Speed Tunnel as the first of a systematic series. There is little doubt that other propellers could be designed which would give greater efficiencies at high forward Mach numbers.

Equipment is not yet available for testing aircraft models with power driven propellers in the High Speed Tunnel. However, some measurements on a Typhoon model with a freely rotating propeller[73] showed that the pitching and yawing moments due to the propeller were not appreciably affected by Mach number, up to $M = 0{\cdot}8$. Hence, until further information is available from tests on powered models, it may be assumed that changes of longitudinal and directional stability due to the presence of propellers are unaffected by variation of Mach number.

4.5. *High Reynolds Number Tests.*—In addition to the tests at high Mach numbers, measurements have also been made at low Mach numbers, over a range of Reynolds numbers, on most of the complete models which have been tested in the High Speed Tunnel. Fig. 80 shows some

results of measurements of maximum lift coefficient on complete aircraft models at low Mach numbers. In most cases there is a favourable scale effect, but there are a few exceptions. An interesting case is that of the Sturgeon[30]. For this model there is a fairly large favourable scale effect when the wing radiators are removed and the entries faired in, but on the complete model with radiators the maximum lift coefficient is almost independent of Reynolds number. Investigations with surface tufts showed that, at high Reynolds numbers with flaps down, the part of the wing behind the radiators stalled at a much lower incidence than the rest of the wing. At lower Reynolds numbers, this difference of stalling incidence was less. This means that the adverse effect of the radiators on the maximum lift coefficient of the model with flaps down increases greatly with Reynolds number, so that tests at low Reynolds numbers on the model complete with radiators are misleading.

The tests which have been made on complete models at low Mach numbers, over a range of Reynolds numbers, have usually shown a slight forward movement of the neutral point with increasing Reynolds number, for the model with tail. The amount of this forward movement was usually about $0{\cdot}01\bar{c}$ or $0{\cdot}02\bar{c}$ between Reynolds numbers of $1{\cdot}5 \times 10^6$ and $4{\cdot}5 \times 10^6$. This shift of neutral point with increasing Reynolds number is in the same direction as that given by Owen[74], but the effect is small and comparatively unimportant.

4.6. *Miscellaneous Tests at High Mach Numbers.*—4.61. *Tests on armaments and external stores.*—Some tests made on a mock-up 20 mm. cannon[75] showed that the resultant-force coefficient increased slightly with Mach number up to $M = 0{\cdot}7$, but the increase above the low-speed value was never more than 30 per cent. These tests were made just below the critical Reynolds number for a cylinder.

Tests made on a full-size model of a 3-in. rocket projectile also showed very little compressibility effect on the forces and moments, at all Mach numbers up to $0{\cdot}8$. The drag coefficient remained roughly constant over the Mach number range $0{\cdot}2$ to $0{\cdot}8$, and the lift and moment coefficients were only about 10 per cent. greater at $M = 0{\cdot}8$ than at low speed.

Several tests have been made to investigate the effects of compressibility on the force and moment changes caused by bombs and drop tanks mounted beneath the wings of aircraft[76, 77]. In all cases the effects of bombs or drop tanks on the lift and pitching moment of the aircraft were found to be fairly small, but the drags were usually very large at high Mach numbers. Fig. 81 and 82 show some typical results. Fig. 81 shows the important effect of engine nacelle interference on the Mach number at which the drag of underwing drop tanks starts to rise steeply. Fig. 82 shows the effect of wing thickness on the drag at high Mach numbers of a bomb mounted under a wing.

4.62. *Other miscellaneous tests.*—Fig. 83 shows the variation with Mach number of the drag of several alternative cabins for the Spiteful.[78] These results show that increasing the radius of curvature at the sides of the flat windscreen gives almost as much improvement as fitting a curved front screen. Flight tests[79] to compare the curved front screen with the flat windscreen with $0{\cdot}3$ in. radius corners showed a rather greater difference of drag than that given in Fig. 83.

Fig. 84 shows the variation with Mach number of the position error of an under-wing pitot-static head on the Typhoon.[80] The speed recorded by the A.S.I. at high Mach numbers is much too large, the sudden increase of position error at $M = 0{\cdot}73$ being due to rearward movement of the lower surface wing shock wave past the static holes. These results show that under-wing pitot-static heads are quite unsuitable for use on high-speed aircraft ; this has also been shown in flight tests (*See* § 5.11).

Tests made on a two-dimensional wing of NACA 0012 section, to determine the effect of roughness on drag over a range of Reynolds and Mach numbers[81], showed that the effect of compressibility on the drag increase due to roughness was negligible at Mach numbers up to $0{\cdot}7$.

5. *Technique of High-Speed Flight Tests.*—Until very recently, it has only been possible to reach the high Mach numbers at which shock waves are formed on an aircraft by diving steeply from a high altitude. Most of the high-speed flight tests at the R.A.E. have therefore been made by this method. The tests have usually been made at the highest possible altitude, for two reasons. The first is that the tests can be made more safely at high altitudes, because for a given Mach number the dynamic pressure $\frac{1}{2}\rho V^2$ is directly proportional to the atmospheric static pressure, so that the pilot's control forces and the stresses in the aircraft structure are less at high altitudes. Making the tests at high altitudes also increases the safety by giving the pilot more time in which to recover from the dive, after reaching the required Mach number. The second reason for making the tests at the highest possible altitude is that, for a given angle of dive, a greater Mach number can be reached at a high altitude, because when the air pressure is lower the drag coefficient at the terminal velocity is greater.

The dives were started by accelerating to maximum level speed at a height which was usually within about 2,000 ft. of the ceiling, trimming the aircraft there and then easing the stick forward to give a normal acceleration of about $\frac{1}{2}g$. A normal acceleration of about this amount was maintained until a Mach number within about 0·1 of the maximum value was reached ; the stick was then eased back to prevent the Mach number from increasing too rapidly. The maximum angle of dive was usually about 45 deg., but in a few cases dives as steep as 60 deg. were made. The highest Mach number was usually reached about 11,000 ft. below the starting height, and the recovery from the dive was usually made in a pull out at 2 to 3g. Before putting the nose down to start the dive, the engine controls were set to a position which would give the maximum permissible continuous boost at the end of the dive.

The technique required for measurements in dives at high Mach numbers differs in some respects from that used in flight tests at lower speeds. Special instruments and methods of measurement have been developed for use in flight research at high speeds, and the more important of these are described below. Some of these methods have not been described in other reports, and are therefore given here in considerable detail.

5.1. *Corrections to Aircraft Pitot-Static Systems.*—The air speed, altitude, and Mach number of an aircraft in flight are usually obtained from measurements of pitot and static pressure. Even at low speeds, corrections must be applied for the effect of the aircraft on the pressures recorded by the pitot and static tubes (position error). At high speeds, the position error may be changed by compressibility effects, and there is also an additional compressibility correction depending on the known theoretical relationship between pitot pressure, static pressure, and air speed. Further, when the measurements are made in a steep dive, there is an important error caused by pressure lag in the tubing connecting the pitot-static head to the recording instruments, and corrections must be applied to eliminate this error. The methods which have been used for determining the corrections for position error, compressibility, and lag are described below.

5.11 *Position error, including compressibility effects.*—In correcting the results of flight tests at low or moderate speeds for the effects of position error and compressibility, it has been usual to assume that the static pressure at the head varies with Mach number according to a relation of the Glauert form :

$$S_c \text{ (compressible)} = \frac{S_c \text{ (incompressible)}}{\sqrt{(1 - M^2)}}$$

Methods of determining the corrections, using this assumption, are given in detail in Refs. 82, 83 and 84. In Refs. 82 and 83, but not in Ref. 84, the additional assumption is made that the pitot tube measures the full total pressure correctly. The latter assumption, that the total pressure is measured correctly by the pitot tube, is known to be correct at subsonic speeds for an unyawed head which is not either in a low speed wake or behind a shock wave, and may be accepted within 1 per cent. for angles of incidence up to about 10 deg.

The other assumption, that the pressure coefficient at the static head is proportional to $(1 - M^2)^{-1/2}$, cannot be justified theoretically at Mach numbers above that at which shock waves are first formed on the aircraft, and the assumption is known to be incorrect at Mach numbers approaching unity. Some flight tests were therefore made at the R.A.E. to investigate position error and compressibility corrections at high Mach numbers. At the same time, a comparison was made between a static vent and leading edge and under-wing pitot-static heads, because it was suspected that the error in measuring air speed with an under-wing pitot-static head would become very large at high Mach numbers (*see* § 4.62).

For these flight tests, a Spitfire XI was fitted with leading-edge and under-wing pitot-static heads on the port wing. In addition, a static vent was fitted on the starboard side of the fuselage. The static vent only measured static pressure, and was used in conjunction with the pitot tube of the leading-edge head. Fig. 85 shows the exact positions of the pitot-static heads and the static vent. The position of the under-wing head was the standard one for Spitfire aircraft. The leading-edge head was fitted near the wing tip, with the static holes 60 per cent. of the local chord ahead of the wing leading edge, this position being chosen to give a very small position error at high speeds. The static vent was fitted in the optimum position as determined from previous low-speed tests. Separate air speed indicators were connected to the two pitot-static heads and the static vent, and the readings of these three instruments were compared by photographing them in an automatic observer.

The position error at ground level was determined by the standard aneroid method, the static position error of the leading-edge head being obtained from the difference between the actual height of the aircraft above the ground, as found from a photograph, and the recorded height given by the aircraft altimeter. Having determined the error of the leading-edge head, the under-wing head and static vent errors could be found directly by comparison, and these are shown in Fig. 86 as corrections to the indicated speed.

The standard aneroid method can only be used at speeds up to the maximum in level flight at ground level, and in order to extend the measurements to higher Mach numbers it was necessary to make further tests at high altitudes. For these high altitude tests a calibrated Lancaster, flying at constant height and speed, was used as a datum instead of the ground. For tests at moderate speeds the Spitfire was flown level in formation with the Lancaster, but for higher speeds it was necessary to dive the Spitfire past the Lancaster. From recordings of the altimeter readings in the Lancaster and in the Spitfire, and a photograph of the Spitfire from the Lancaster, all taken at the same instant, the actual height of the Spitfire could be found and compared with the height recorded by the altimeter. The difference between these two heights gave the error in the static pressure as recorded by the leading edge head. (As explained above, the pitot tube error can be assumed to be negligible.) The static pressure errors of the under-wing head and the static vent were determined directly by comparing the readings of the three air speed indicators.

For photographing the Spitfire from the Lancaster, an F.24 camera with a lens of 20 in. focal length was installed in the rear turret. The camera pointed aft with the optical axis inclined upwards at $4\frac{1}{2}$ deg. to the aircraft datum, so that when the aircraft was flying slowly at a fairly high incidence the camera axis was approximately horizontal. A small automatic observer in the Lancaster was used to record the altitude, air speed, and attitude of the aircraft. For the measurement of attitude, an artificial horizon was used, suitably modified to measure small angles of pitch. From the measured attitude of the Lancaster, and the known camera angle, the exact inclination (θ_c) of the camera axis to the horizontal could be found. Clocks were included in the automatic observers of both the Lancaster and the Spitfire, so that the readings of air speed and altitude in the two aircraft could be correlated.

The two cameras in the Lancaster, one photographing the automatic observer, the other photographing the Spitfire from the rear turret, were operated from the rear turret when the Spitfire was judged to be in the field of view of the rear turret camera. At the same time a radio signal was transmitted from the Lancaster, received in the Spitfire, and used to operate the automatic observer camera in the latter aircraft. A "Queen Bee" remote control radio set, normally used for controlling pilotless target aircraft, was used as the radio link between the two aircraft.

The static vent of the Lancaster was first calibrated against a trailing static head over a range of indicated air speeds about 160 m.p.h. By keeping this speed fairly low, all uncertain compressibility effects on the " datum aircraft " were eliminated, and thus the true pressure altitude of the Lancaster was always known accurately. After these preliminary calibrations, the Lancaster was flown at constant speed (160 m.p.h. I.A.S.) and constant altitude (12,000 ft.), while the Spitfire flew past at several different speeds. In the tests at moderate speeds, with the Spitfire flying level, it was possible to take several photographs from the rear turret as the Spitfire approached, while the distance between the two aircraft decreased from about 700 ft. to 100 ft. In the tests at higher speeds, however, when the Spitfire was diving past the Lancaster, the Spitfire was only in the field of view for about $\frac{1}{3}$ second, so that only one photograph could be taken. For this one photograph, the aircraft was usually about 900 ft. away. The highest speed recorded at 12,000 ft. was 425 m.p.h. I.A.S. ($M = 0{\cdot}7$). In order to extend the results to still higher Mach numbers, the measurements were repeated at 25,000 ft. At this altitude, an indicated air speed of 399 m.p.h. was recorded ($M = 0{\cdot}82$, fully corrected).

From the photographs taken by the rear turret camera, the height h_1 of the Spitfire above the camera axis (as given by the cross-wires) could be found, and also the distance D_a between the two aircraft could be obtained. The true difference of height between the two aircraft was then given by $h_2 = h_1 + D_a\theta_c$, where θ_c is the angle between the camera axis and the horizontal. The difference between the altimeter readings in the two aircraft, when compared with the true height difference h_2, then gave the error in altitude due to the static pressure error on the Spitfire. The Lancaster altimeter readings had to be corrected for position error and compressibility, but these corrections were given directly by the trailing static calibration. The Spitfire altimeter readings had to be corrected for lag of several kinds ; pressure lag in the pipes, mechanical lag in the cameras, and time lag in the radio relays. All these lag corrections are of course only important in the dive tests, when the height is changing rapidly. The correction for pressure lag in the pipes was determined by the normal methods which are described later in this report. In order to determine the other lag corrections, a " mock-up " was made of the whole arrangement of cameras and radio, and each camera was focussed on a stop watch. By comparing the photographs taken by the three cameras when the main control switch was closed, it was found that there was a delay of 0·02 seconds on the Spitfire camera, equivalent to a maximum height correction of 15 ft.

From the measurements described above, the static pressure error of the leading edge head on the Spitfire was found, for a range of Mach numbers up to 0·82. The static pressure errors of the under-wing head and the static vent could then be found quite simply by comparing the readings of the air speed indicators. No tests with the Lancaster were made at Mach numbers above 0·82, but in order to obtain a comparison between the two heads and the static vent at higher Mach numbers the Spitfire was dived, without the Lancaster, up to a Mach number of 0·89. The dive was very steep, and the loss of oil pressure to the constant speed unit resulted in severe overspeeding of the propeller. The reduction gear and propeller were torn away, thus preventing any further tests from being made on this aircraft.

The results of the measurements of position error and compressibility correction on the Spitfire are given in Figs. 86 to 92. Fig. 86 shows the corrections to air speed at ground level, for the two types of pitot-static head and for the static vent. Figs. 87 and 88 show the static pressure corrections for the leading-edge head, at ground level, 12,000 ft., and 25,000 ft. In Fig. 87, the corrections are expressed as differences of static-pressure coefficient, and in Fig. 88 the corresponding corrections to altitude are given. In both Figs. 87 and 88, only static pressure errors are considered, and thus the results given are independent of pitot error and " calibration compressibility error ". The latter error is caused by the variation with Mach number of the (known) relationship between pitot pressure, static pressure, and equivalent air speed ($V\sqrt{\sigma}$).

The results obtained in the tests at 12,000 ft. were only approximate, because the rear turret camera failed to operate, and thus the height of the Spitfire relative to the Lancaster could only be estimated visually. In the level flight tests this estimate could be made fairly easily, because the Spitfire approached at roughly the same height as the Lancaster, but in the dives the error in estimating the height of the Spitfire may have been as much as $\pm$ 70 ft. For this reason

more " weight " should be attached to the results obtained at 25,000 ft. In the level flight tests at this height, visual judgment could be used to check the results obtained from the rear turret camera, and an agreement within about $\pm$ 20 ft. was obtained. It is doubtful whether such good accuracy was obtained in the dives, when the altimeter mechanisms were moving rapidly, but it is considered that the error in determining the altitude of the Spitfire in the dive tests at 25,000 ft. was probably not greater than $\pm$ 40 ft.

In correcting for the effects of compressibility in flight tests at moderate speeds, it is usual to assume[82, 83, 84] that S_c, the static-pressure coefficient at the head, is directly proportional to the Glauert factor $(1 - M^2)^{-1/2}$. Using this assumption, the static pressure corrections for the leading-edge head at 12,000 ft. and 25,000 ft. have been calculated from the ground level results. The corrections obtained in this way, using the Glauert factor, are shown as dotted curves in Figs. 87 and 88. The full lines in Figs. 87 and 88, for altitudes of 12,000 ft. and 25,000 ft., show the corrections deduced from the ground level results, assuming that the static-pressure coefficient S_c is independent of Mach number. The curves show that, at both altitudes, the assumption that the static-pressure coefficient at the head is independent of Mach number (for a constant lift coefficient), gives better agreement with the experimental results than the use of the Glauert factor as in Refs. 82, 83, and 84. In the tests at 25,000 ft., where the results are more reliable than at 12,000 ft., the full line curves in Figs. 87 and 88 agree very well with the experimental results at all speeds up to 365 m.p.h. ($M = 0{\cdot}75$, corrected). The sudden reduction of static-pressure correction at higher speeds is probably caused by shock stalling of the wing ; this is discussed more fully below.

These investigations of position error and compressibility corrections are still proceeding, and the information is not yet complete. However, it appears from the results available at present (Figs. 87 and 88), that the static pressure coefficient at a leading-edge head is nearly independent of Mach number, instead of following the Glauert law as is usually assumed. It may be noted here that the Glauert relation strictly applies only at a constant incidence, and not at a constant lift coefficient. In Ref. 84, a small correction is applied to allow for the variation of lift-curve slope with Mach number, but in practice this additional correction makes very little difference because the lift coefficient is usually small at high Mach numbers.

Figs. 87 and 88 show that for the leading-edge head at 25,000 ft. there is a sudden reduction of static-pressure correction as the indicated speed increases from 365 m.p.h. to 400 m.p.h. The one experimental point on which this sudden change depends was obtained in a very steep dive, but there is no reason to suspect that this point is less accurate than any of the other dive points ; certainly neither the 230 ft. difference from the full line (constant S_c), nor the 500 ft. difference from the dotted line (Glauert law), could be explained by experimental errors. The most probable explanation is that the sudden reduction of static-pressure correction is due to the formation of shock waves on the wing at a Mach number of about $0{\cdot}8$. If there were a loss of lift on the wing (for a given incidence) as a result of the shock wave formation, an increase of incidence would be required to restore the lift, and the position error would then be altered to a value corresponding to a higher incidence (*i.e.* lower E.A.S.,) exactly as is shown in Figs. 87 and 88. An attempt was made to measure the change of incidence on this Spitfire at high Mach numbers, by means of an incidence vane mounted in front of the leading edge. This was not successful, because any definite changes of incidence, due to compressibility effects, were obscured by vibrations of the aircraft and movements of the arm supporting the incidence vane. Incidence measurements made on the Gloster E.28/39 were more successful[85], and a considerable increase of incidence was recorded on this aircraft at high Mach numbers. These measurements will be discussed later.

Fig. 89 shows the static-pressure corrections for the under-wing head, compared with the corrections deduced from the ground level results, using the two alternative assumptions for the variation of the static pressure coefficient with Mach number. In this case the dotted curves, based on the Glauert law, are nearer to the experimental results than the full line curves, except at the highest speeds at 25,000 ft., where it will be shown later that the discrepancy can again be explained by the increase of aircraft incidence which occurs when shock waves are formed on the wing. One very fast dive was made without the Lancaster, starting at 40,000 ft. and reaching a Mach number of $0{\cdot}89$, and in this dive a very interesting effect

was observed on the under-wing head. The time history of the dive, given in Fig. 92, shows the readings of the leading-edge and under-wing air-speed indicators, and the fully corrected "leading-edge" Mach number. It can be seen that the readings of air speed given by the leading-edge head show no sudden variation at high Mach numbers, but the under-wing head reads much too high a speed at Mach numbers above about 0·87. At the peak Mach number of 0·89, the air speed reading given by the under-wing head is 95 m.p.h. too high, the corresponding indicated Mach number being 1·14. As the Mach number falls, the under-wing A.S.I. reading returns to its normal value, and then continues to rise to a peak with the leading-edge A.S.I. reading, showing that the unusual behaviour of the under-wing head at Mach numbers above 0·87 is due to the high Mach number and not to the high indicated air speed.

The sudden increase of air speed reading given by the under-wing head at high Mach numbers is probably caused by the rearward movement of the shock wave on the lower surface of the wing past the static holes on the head. When the shock wave is first formed it is probably in front of the head and then has a comparatively small effect on the observed static pressure. With increasing Mach number the shock wave moves back, and when it passes behind the static holes the recorded pressure falls suddenly. As the Mach number decreases again, the shock wave moves forward past the static holes, and the recorded static pressure returns to its normal value. The air speed recorded by any pitot-static head is nearly equal to the local speed at the static holes, and in the case of an under-wing head this local speed becomes supersonic when the lower surface wing shock wave moves back past the static holes. In the case of the Spitfire, the lower surface wing shock wave moved behind the static holes on the under-wing head as the flight Mach number rose above 0·87, and the apparent Mach number recorded by the under-wing head was then greater than 1. (The loss of total head at a shock wave has only a small effect on the pitot pressure.) A similar effect has been observed in tunnel tests on an under-wing head on a model Typhoon (*see* § 4.6 and Ref. 80). In this case the sudden change of position error occurred at a lower Mach number than in the Spitfire flight tests, because the thickness ratio of the Typhoon wing is considerably greater than that of the Spitfire.

In Fig. 91 the speed correction for the under-wing head due to the effect of compressibility on the static pressure is plotted against (corrected) flight Mach number. In this diagram the speed corrections at low Mach number, obtained from the tests at ground level, have been subtracted from the results, so that the corrections given are due to compressibility effects only. The corrections are given for altitudes of 25,000 ft. to 30,000 ft.; for lower altitudes the corrections (in m.p.h.) would be greater. The speed corrections were only measured directly, using the Lancaster as a datum, at Mach numbers up to 0·82. The curve in Fig. 91 for higher Mach numbers has been derived from the results given in Fig. 92, using a rough extrapolation of Fig. 88 to give the correction for the leading-edge head at Mach numbers above 0·82. Because of the uncertainty of this extrapolation, and because the results do not refer to an exactly constant altitude, the curve given in Fig. 91 is only an approximate one, but it is good enough to give a qualitative indication of the changes that occur on an under-wing pitot-static head at high Mach numbers.

It has already been shown (Fig. 89) that the variation with Mach number of the static-pressure coefficient at the under-wing head agrees fairly well with the Glauert law, up to moderately high Mach numbers. This is also shown by the first part of the curve in Fig. 91, up to a Mach number of about 0·77. As the Mach number increases above 0·77, the speed correction due to compressibility changes sign from negative to positive. This change is probably due to the increase of incidence required to maintain lift on the wing as shock waves develop; the increase of incidence reduces the local velocity at the head and so makes the speed correction more positive. As the Mach number increases above about 0·87, the correction shown in Fig. 91 falls suddenly to a large negative value. As already explained, this sudden change is caused by rearward movement of the lower surface wing shock wave past the static holes.

Fig. 90 shows the static-pressure correction for the static vent on the Spitfire, at ground level, 12,000 ft. and 25,000 ft. In this case the full line curves, deduced from the ground level results by assuming that the static-pressure coefficient is independent of Mach number, agree more closely with the experimental values than the dotted curves based on the Glauert law. It may

be noted that the corrections shown in Fig. 90 are fairly small at all air speeds and altitudes covered by the tests. There is no noticeable effect due to change of incidence at high Mach numbers, probably because the static vent was on the side of the fuselage, behind the wing, and would therefore not be affected much by changes of incidence. A discussion of the relative merits of static vents and pitot-static heads is given in Ref. 86.

These investigations of position error and compressibility corrections in flight at high Mach numbers have not yet been completed, but the results available at present lead to the following conclusions :—

(1) It appears that the static-pressure coefficient at a leading-edge pitot-static head, or at a static vent, does not vary with Mach number according to the Glauert law. Corrections deduced from measurements at ground level, for a leading-edge head or static vent, agree more closely with experimental results if it is assumed that the static-pressure coefficient at the head (or static vent) is independent of Mach number, than if the Glauert law is assumed. For an under-wing pitot-static head, better agreement with experimental results is obtained by using the Glauert law than by assuming that the static-pressure coefficient at the head is independent of Mach number.

(2) There are indications from tests on leading-edge and under-wing pitot-static heads that, when shock waves are formed on the wing of the aircraft, an increase of incidence occurs which alters the position error corrections considerably. Further tests are required to confirm the nature and magnitude of this effect.

(3) An A.S.I. connected to an under-wing pitot-static head may give a reading which is as much as 100 m.p.h. too high, when the speed is high enough for the lower surface wing shock wave to move back behind the static holes, so that the local speed at the head is supersonic. On the Spitfire (which has a thin wing) this effect does not occur until a Mach number of about 0·87 is exceeded, but on aircraft with thicker wings it probably occurs at much lower Mach numbers. Leading-edge pitot-static heads are much less affected by shock waves on the wing, and it is recommended that the leading edge type of head should always be used on high-speed aircraft.

In order to apply these results to the correction of air speed and altitude readings obtained in flight at high Mach numbers, a general method of determining the position error and compressibility corrections is given below. In this general method, any arbitrary law can be assumed for the variation with Mach number of the static-pressure coefficient at the head. If the Glauert law is assumed, the method is equivalent to that given in Ref. 84. However, the results of the flight tests described above show that it is probably better, for a leading-edge pitot-static head or a static vent, to assume that the static-pressure coefficient at the head is independent of Mach number.

It will be assumed that the pitot tube reads true total head, *i.e.* that the pitot position error and pitot compressibility error are zero. For leading-edge heads this assumption is probably very nearly correct for angles of yaw up to $\pm$ 10 deg. and for Mach numbers up to 1. For an under-wing head, if there is a shock wave formed on the wing in front of the head, the pitot tube reading may be slightly less than the true total head, but in any case under-wing pitot static heads are not suitable for use on high-speed aircraft.

Using the notation given in the list of symbols, it can be shown (Refs. 82 and 84) that

$$\tfrac{1}{2}\rho_0 V_r^2 (1 + \tfrac{1}{4}M_{r_0}^2) = \tfrac{1}{2}\rho_0 V_i^2 (1 + \tfrac{1}{4}M^2 + \tfrac{1}{40}M^4 + \ldots) - \tfrac{1}{2}\rho_0 V_i^2 S_c$$

or

$$V_r^2(1 + \tfrac{1}{4}M_{r_0}^2) = V_i^2 [f(M) - S_c] . \quad \ldots \quad \ldots \quad \ldots \quad \ldots \quad \ldots \quad \ldots \quad (12)$$

This is the fundamental equation for all calculations on position error and compressibility corrections.

The relation between the altitude correction and the static-pressure coefficient at the head is given by

$$P_s - P_0 = \tfrac{1}{2}\rho_0 V_i^2 \cdot S_c = \rho g \Delta h_c \quad \ldots \quad \ldots \quad \ldots \quad \ldots \quad \ldots \quad \ldots \quad \ldots \quad (13)$$

$$\therefore \qquad S_c = \frac{2g\sigma\Delta h_c}{V_i^2} = \frac{2g\sigma\Delta h_c}{V_r^2(1 + \frac{1}{4}M_{r0}^2)}\,[f(M) - S_c] \qquad \ldots\ldots \qquad (14)$$

or if we put $$E = \frac{2g\sigma\Delta h_c}{V_r^2(1 + \frac{1}{4}M_{r0}^2)} \qquad \ldots\ldots \qquad (15)$$

$$\frac{S_c}{f(M)} = \frac{E}{E + 1} \qquad \ldots\ldots \qquad (16)$$

Since S_c is usually small, it is sufficiently accurate to use the uncorrected air speed and altitude readings in calculating $f(M)$, *i.e.* to put

$$f(M) = f(M_r)\,.$$

Equation (16) then becomes

$$\frac{S_c}{f(M_r)} = \frac{E}{E + 1} \qquad \ldots\ldots \qquad (16a)$$

Figs. 93 and 94 show the variation of $\frac{S_c}{f(M_r)}$ with $\sigma\Delta h_c$, for various values of V_r, as calculated from equation (16a). These diagrams may be used to determine the altitude correction when the static-pressure coefficient has been found.

The correction to air speed may conveniently be considered in two parts, as follows :—

(1) $\Delta_1 V = V_c - V_r$ due to the calibration compressibility error.

(2) $\Delta_2 V = V_i - V_c$ due to the position error and compressibility error.

These two corrections may be applied separately, and their sum gives the total correction. The first correction ($\Delta_1 V$) can be found from equation (12) by putting $S_c = 0$, giving

$$V_c^2 f(M_c) = V_r^2(1 + \tfrac{1}{4}M_{r0}^2) \qquad \ldots\ldots \qquad (17)$$

The solution of this equation has been given in Fig. A1 of Ref. 84 and is also included as Fig. 95 in this report. The speed correction $\Delta_1 V$, and also the Mach number M_c corresponding to the speed V_c and height h_c, can be determined directly from Fig. 95.

Now, to determine the correction $\Delta_2 V$, combine equations (12) and (17), giving

$$V_c^2 f(M_c) = V_i^2\,[f(M) - S_c] \qquad \ldots\ldots \qquad (18)$$

Put $V_i - V_c = \Delta_2 V$ and let $v_2 = \frac{\Delta_2 V}{V_c}$.

Then $$V_i = V_c(1 + v_2) \qquad \ldots\ldots \qquad (19)$$

Therefore $$\frac{V_i^2}{V_c^2} = (1 + v_2)^2 = \frac{f(M_c)}{f(M) - S_c}\,. \qquad \ldots\ldots \qquad (20)$$

Also $$f(M) - f(M_c) = \tfrac{1}{4}(M^2 - M_c^2) + \tfrac{1}{40}(M^4 - M_c^4)$$

$$= \frac{V_i^2 - V_c^2}{4pV_{s0}^2}\left[1 + \frac{V_c^2(2 + 2v_2 + v_2^2)}{10pV_{s0}^2}\right]$$

$$= \left[\frac{V_c^2 v_2}{2pV_{s0}^2}\left(1 + \frac{v_2}{2}\right)\right]\left\{1 + \frac{V_c^2}{5pV_{s0}^2}\left(1 + v_2 + \frac{v_2^2}{2}\right)\right\}$$

Since $M_c^2 = \frac{V_c^2}{pV_{s0}^2}$ and since $\frac{M_c^2}{5}$ is small compared with 1, so that the terms in v_2 at the end of the equation can be neglected, this may be written

$$f(M) - f(M_c) = \frac{M_c^2 v_2}{2}\left(1 + \frac{v_2}{2}\right)\left(1 + \frac{M_c^2}{5}\right). \qquad \ldots\ldots \qquad (21)$$

Therefore from equation (20)

$$\frac{f(M_c)}{(1+v_2)^2} = \frac{M_c^2 v_2}{2}\left(1+\frac{v_2}{2}\right)\left(1+\frac{M_c^2}{5}\right) + f(M_c) - S_c$$

Therefore
$$S_c = 2v_2\left(1+\frac{v_2}{2}\right)\left[\frac{M_c^2}{4}\left(1+\frac{M_c^2}{5}\right) + \frac{f(M_c)}{(1+v_2)^2}\right] \quad .. \quad .. \quad .. \quad .. \quad (22)$$

In Fig. 96 v_2, as calculated from the above equation, is plotted against Mach number for several values of the static-pressure coefficient S_c.

In order to apply this method to the determination of the corrections to air speed and altitude at any height, the position error at ground level is measured first by the standard aneroid method. From these measurements a curve showing the variation of the height correction Δh_c (at ground level) with indicated air speed V_r can be obtained. This height correction is then converted to static-pressure coefficient S_c, using the curves given in Figs. 93, 94 and 97 and putting $\sigma = 1$.

Before proceeding any further with this method, it is necessary to decide what assumption is to be made for the variation of static-pressure coefficient S_c with Mach number (at constant lift coefficient). It has been usual in the past (Refs. 82, 83 and 84) to assume that S_c is proportional to $(1 - M^2)^{-1/2}$, but the flight tests described above show that it is probably more nearly correct, for leading-edge heads and static vents, to assume that S_c is independent of Mach number for a given lift coefficient. For under-wing heads it appears to be better to use the $(1 - M^2)^{-1/2}$ factor.

In order to determine the correction to altitude, values of S_c for a given altitude are calculated from the ground level results for several values of V_r. The correction Δh_c can then be found from Figs. 93, 94 and 97.

To determine the correction to air speed, Fig. 95 is used to find, for a given height, the values of $\Delta_1 V$ and M_c for several values of V_r . V_c is then known from the equation

$$V_c = V_r + \Delta_1 V$$

and Fig. 96 is used to obtain values of $\Delta_2 V$ for the previously determined values of S_c. The equivalent air speed V_i is then found from

$$V_i = V_c + \Delta_2 V \ .$$

After calculating the altitude and air speed corrections for a range of speeds at several altitudes, charts similar to those shown in Fig. 98 can be constructed, and these can be used to determine the corrections for all flight conditions.

5.12. *Lag corrections.*—In recording air speed and altitude by the usual pressure instruments on an aircraft in a high-speed dive, there is a lag effect due to the rapid change of pressure during the dive, causing errors in the readings of the instruments. This lag has been investigated both theoretically and experimentally, and a method of correcting the instrument readings has been developed[87]. The theoretical and experimental results are given below, and the method of applying the corrections is explained.

It has been found that the lag may be considered in two parts ; the pressure lag in the tubes connecting the instruments to the pressure holes, and the mechanical lag in the recording instruments.

Considering first the pressure lag in the tubes, it can be shown that in all practicable pitot-static systems in aircraft, the Reynolds number of the flow in the tubes (due to the pressure changes) is no more than a few hundred, and thus is always less than the critical Reynolds number for transition from laminar to turbulent flow. A simple theory of pressure lag is given below, assuming that the flow in the tubes is always laminar, and that the radius of curvature of any bend in the tube is large compared with the internal radius.

Fig. 99 shows diagrammatically an altimeter connected by a long tube to a pitot-static head or static vent. The volume of the altimeter Q is relatively large, and the instrument is connected to the static holes, at which the pressure is changing rapidly during the dive, by a tube of internal

diameter d, length l_T, and internal cross-sectional area S_T. An altimeter has been chosen for this example, but the theory given below applies equally well to any other pressure instrument, connected by a long tube to a source of changing pressure.

If P is the pressure in the tube at a distance z from the closed end, then it can be shown (Ref. 88) that the pressure gradient is given by

$$\frac{dP}{dz} = \frac{32\mu v}{d^2} \qquad (23)$$

where v is the mean velocity in the tube (towards the closed end) and μ is the coefficient of viscosity.

If dm/dt is the rate of mass flow from the tube into the volume Q, and if ρ is the air density at a distance z from the closed end of the tube, then the equation of continuity is

$$\rho v S_T - \frac{dm}{dt} = S_T z \cdot \frac{d\rho}{dt} \qquad (24)$$

Now if we put $d\rho/dt = \rho'$ and assume that it is independent of z, for a given value of t, we obtain

$$\rho v = \rho' z + \left(\frac{1}{S_T} \cdot \frac{dm}{dt}\right) = \rho' \left(z + \frac{Q}{S_T}\right) \qquad (25)$$

since $$\frac{dm}{dt} = Q\rho'$$

The relation between the pressure P and the density ρ is given by the general gas law

$$P = B\rho^N \qquad (26)$$

and, differentiating this equation with respect to z, we obtain

$$BN\rho^N \frac{d\rho}{dz} = \rho \cdot \frac{dP}{dz} = \frac{32\mu v \rho}{d^2}$$

$$= \frac{32\mu\rho'}{d^2}\left(z + \frac{Q}{S_T}\right). \qquad (27)$$

Integrating from $z = 0$ to $z = l_T$ (for a constant value of t),

$$\frac{BN}{N+1}\left[\rho_l^{n+1} - \rho_0^{n+1}\right] = \frac{32\mu\rho'}{d^2}\left(\frac{l_T^2}{2} + \frac{Ql_T}{S_T}\right), \qquad (28)$$

where ρ_l and ρ_0 are the values of ρ for $z = l_T$ and $z = 0$ respectively.

Then, it can be shown that the pressure drop in the tube is given by

$$\Delta P = \left(\frac{\rho'}{\rho}\right)\left(\frac{128\mu l_T}{\pi d^4}\right)\left(\frac{l_T S_T}{2} + Q\right)$$

$$= \frac{\rho'}{\rho} \cdot \mu K \text{ where } K = \frac{128 l_T}{\pi d^4}\left(\frac{l_T S_T}{2} + Q\right). \qquad (29)$$

This is the fundamental equation for the pressure lag in any system. The pressure difference ΔP can easily be converted to a difference of either altitude or air speed.

For practical purposes it is more convenient to express the pressure lag ΔP in terms of the rate of descent, given by

$$\text{Rate of Descent} = v_d = -\frac{dh_c}{dt} \text{ (where } h_c \text{ is height).}$$

(It is assumed here that the pressure lag in a dive is due entirely to the rate of change of static pressure. This is not strictly correct, because there is a small lag due to increase of total head as the speed increases, but this effect is small compared with that due to change of static pressure and may usually be neglected.)

If σ is the relative density at an altitude h_c,

$$\frac{\rho'}{\rho} = \frac{1}{\rho} \cdot \frac{d\rho}{dt} = -\frac{v_d}{\sigma} \cdot \frac{d\sigma}{dh_c} \quad \ldots\ldots\ldots\ldots\ldots\ldots\ldots \quad (30)$$

and for the standard I.C.A.N. atmosphere,

$$\sigma = (1 - 6{\cdot}88 \times 10^{-6}\, h_c)^{4{\cdot}256}$$

therefore

$$\frac{\rho'}{\rho} = \frac{2{\cdot}93 \times 10^{-5}}{1 - 6{\cdot}88 \times 10^{-6}\, h_c} \times v_d \,. \quad \ldots\ldots\ldots\ldots\ldots\ldots \quad (31)$$

Substituting in equation (29) we obtain

$$\Delta P = v_d \mu K \times \frac{2{\cdot}93 \times 10^{-5}}{1 - 6{\cdot}88 \times 10^{-6}\, h_c} \quad \ldots\ldots\ldots\ldots\ldots\ldots \quad (32)$$

and, since μ is a function of height, this may also be written as

$$\Delta P = v_d K \times G(h_c) \,. \quad \ldots\ldots\ldots\ldots\ldots\ldots\ldots \quad (33)$$

To correct the pressure lag to a height lag, we use the relation

$$\Delta P = -\rho g \Delta h_c$$

i.e.

$$\begin{aligned} -\Delta h_c &= v_d \times \frac{2{\cdot}93 \times 10^{-5}\,\mu}{\rho g(1 - 6{\cdot}88 \times 10^{-6}\, h_c)} \times K \\ &= v_d \times \frac{3{\cdot}83 \times 10^{-4}\mu}{\sigma(1 - 6{\cdot}88 \times 10^{-6}\, h_c)} \times K \\ &= v_d \times F(h_c) \times K \,. \quad \ldots\ldots\ldots\ldots\ldots\ldots \quad (34) \end{aligned}$$

The curves given in Figs. 101 and 102 show the variation of $\frac{\Delta P}{v_d}$ and $\frac{\Delta h_c}{v_d}$ with altitude, for several values of the factor K. It may be noted that the quantity $\frac{\Delta h_c}{v_d}$ has the dimension of time, and depends on the time taken for a pressure change at the open end of the tube to reach the recording instrument (*e.g.* the altimeter).

In order to convert the pressure lag ΔP into an air speed lag correction ΔV_i, we use the calibration formula for an air speed indicator,

$$\text{Pressure Difference} = \tfrac{1}{2}\rho_0 V_i^2 \,(1 + \tfrac{1}{4}M_0^2)$$

If the indicated air speed V_i is expressed in m.p.h. instead of ft. per sec., we obtain from this by differentiation,

$$\Delta V_i = \frac{-\Delta P}{2{\cdot}15\rho_0 V_i \,(1 + \tfrac{1}{2}M_0^2)} \,,$$

where ρ_0 is the air density at sea level, V_i is the indicated air speed in m.p.h., and M_0 is the Mach number at sea level corresponding to the speed V_i.

Thus if we record altitude, air speed, and time in a high speed dive, a rough value of the rate of descent v_d can be found and, provided the factor K for the system of tubes is known, the lag can be determined from the simple theory given above, and applied as a correction to the measured height and speed.

The lag factor K is given in equation (29) as

$$K = \frac{128 l_T}{\pi d^4}\left(\frac{l_T S_T}{2} + Q\right).$$

Thus K depends only on the length and diameter of the tubing, and on the volume of any instruments which are connected to it. The term inside the brackets in the above expression is the sum of the volume of the instruments Q and one-half the volume of the tube, and is therefore the volume "downstream of the mid-point of the tube". It should be noted that the lag factor K is dimensionless, and hence in determining its value any consistent units of length may be used for the dimensions of the tubing and instruments.

If the system of tubing is more complex than the simple case considered above, the relationships still apply but each piece of tubing of different diameter has to be treated separately, and the values of K are then added. Any losses of pressure at junctions between tubes of different diameter are neglected. As an example, we may consider the system shown in Fig. 100, consisting of a number of different instruments connected by tubes of different lengths and diameters; by treating the lengths 1–2, 2–3 and 2–4 separately, it is possible to evaluate the factors K for the lags at the three instruments. The three lag factors are given by

$$K_{12} = \frac{128 l_{T1}}{\pi d_1^4}\left[\tfrac{1}{2}\cdot\frac{\pi}{4}\cdot d_1^2 l_{T1} + \frac{\pi}{4} d_2^2 l_{T2} + \frac{\pi}{4} d_3^2 l_{T3} + Q_1 + Q_2 + Q_3\right]$$

$$K_{23} = \frac{128 l_{T2}}{\pi d_2^4}\left[\tfrac{1}{2}\cdot\frac{\pi}{4}\cdot d_2^2 l_{T2} + Q_1 + Q_2\right]$$

$$K_{24} = \frac{128 l_{T3}}{\pi d_3^4}\left[\tfrac{1}{2}\cdot\frac{\pi}{4} d_3^2 l_{T3} + Q_3\right].$$

By addition, we find that the lag factor for either of the instruments (1) or (2) is $K_{13} = K_{12} + K_{23}$, and for instrument (3) it is $K_{14} = K_{12} + K_{24}$. By working successively through the tubing system in this manner, it is possible to determine the lag factor for any point within the system.

For the particular case of an altimeter connected to a static head or vent, the height lag can be computed directly by the above method, if the volume of the altimeter casing is known. For an air speed indicator, however, the lags in the pitot and static lines have to be considered separately, although in normal installations, using $\frac{5}{16}$ in. o.d. dural tubing, the lag in the pitot line can be neglected because of the relatively small internal volume of the capsule. For other instruments the methods of determining the lag corrections are similar; the volumes of the standard instruments in use at present are given below.

Instrument	*Volume (cubic inches)*
Sensitive Altimeter	13·8
A.S.I. (large type)—static side	9·6
A.S.I.—pitot capsule	0·5
Machmeter—static side	13·8
Machmeter—pitot capsule	1·5
Rate of climb indicator	9·6

The above figures are only approximate, and different makes of instrument have slightly different volumes. The largest variations in volume occur in air speed indicators; the volume of 9·6 cubic ins. given above for the static side corresponds to the deepest English type.

The expression for the lag factor K shows clearly that the main causes of the lag are the d^4 term and the volume Q of the instruments connected to the end of the tube. It follows that the lag can be reduced by increasing the diameter of the tubing or by reducing the volume to be filled. Increasing the tube diameter also increases the volume, but the effect of this is small compared with the powerful effect of the d^4 term. For a typical aircraft system, consisting of a standard pressure head at the wing tip, connected by $\frac{5}{16}$-in. o.d. dural tubing to one air speed indicator, one altimeter, and one rate of climb indicator in the cockpit, the factor K for the static pressure line which is connected to each instrument is about 1×10^8. This gives a lag correction which is fairly small, but if $\frac{3}{16}$-in. o.d. tubing were used, as was common in American aircraft at one time, the value of K would be increased to 16×10^8. In practice the lag corrections would not be 16 times as great, for reasons which will be explained later, but nevertheless much greater care would be necessary in determining the corrections. The effect of the pressure head static holes on lag is usually negligible.

A rather similar theoretical treatment of the lag problem has been carried out in the U.S.A.[89] However, in Ref. 89 no experimental evidence is given to support the theoretical results, and it is considered that the results given there are not presented in such a convenient form as those described here.

For a complete investigation of lag corrections, it is necessary to make some experimental measurements in addition to the theoretical work already described. This is because only the pressure lag is considered in the theory, whereas in fact there may also be some mechanical lag in the recording instruments. This mechanical lag is particularly noticeable in the standard altimeter, where in a high-speed dive the pointer moves in a series of jerks. It is difficult to express the mechanical lag mathematically, although attempts have been made to do so[90], and it was therefore decided to investigate the problem experimentally, and modify the theoretical results by an empirical relation which, for normal cases, would allow for the mechanical lag in the instruments.

Before describing the tests, it should be explained that they were kept as simple as possible, and were only intended to provide a rough basis for estimating the corrections to be applied to flight results at high rates of descent. No effort was made to set up apparatus for examining all the variables in the theoretical formulae, and only sufficient work was done to establish a reliable working method.

The system to be investigated, consisting of instruments and tubing, was first evacuated to a known pressure. The end of the tube was then opened, and the rate of rise of pressure was measured. If P_0 is the atmospheric pressure, and P is the pressure at a given instrument at a time t, we have from equation (29)

$$P_0 - P = \frac{K\mu}{\rho} \cdot \frac{d\rho}{dt} . \qquad (35)$$

It may be assumed that the flow is isothermal, because the time taken for the pressure to rise is usually fairly long (several seconds to reach atmospheric pressure). Equation (35) then becomes

$$\frac{1}{K\mu} \cdot dt = \frac{dP}{P(P_0 - P)} \qquad (36)$$

Integrating, we obtain

$$\frac{P_0}{K\mu} \cdot t = -\log_e\left(\frac{P_0 - P}{P}\right) + (\text{constant}) . \qquad (37)$$

Hence if we plot the logarithmic function $\log\left(\frac{P_0 - P}{P}\right)$ against time, the curve should be a straight line whose slope is $-\frac{P_0}{K\mu}$, and thus K can be found. In the description given below the experimental lag factor found by this method will be called K_1, to distinguish it from the theoretical factor K, since the two values do not usually agree.

The curves given in Figs. 103 and 104 show the logarithmic pressure function plotted against time, for various different systems of tubing and instruments. It can be seen that the slopes of the curves are determined fairly accurately by the experimental points, even in cases where the whole experiment only takes 1 or 2 seconds. The values of the experimental lag factor K_1 are shown for each arrangement, together with the theoretical factors K. It can be seen that the values of K_1 and K do not agree, but there appears to be some correlation between them. In order to investigate this correlation further, K_1 is plotted against K in Fig. 107. It can be seen that there is always a discrepancy between K_1 and K, the latter being consistently smaller. The results given in Fig. 107, obtained from a series of tests over a large range of K, show that there is a definite linear relationship between the two factors, which may be expressed by the equation

$$K_1 = 1{\cdot}5K + (1{\cdot}1 \times 10^9) . \qquad (38)$$

It is not yet understood why the relationship between the two factors should take this form, but it is probable that the constant of $1{\cdot}1 \times 10^9$ is due to mechanical lag in the instruments. Possibly the factor of $1{\cdot}5$ in equation (38) is due to the effects of bends, junctions, etc. in the tubing system. In any case, there is little doubt that equation (38) applies with reasonable accuracy to all systems of tubing and instruments likely to be used in practice.

A few laboratory measurements of K_1 were made in systems containing either pressure-plotting orifices or small bore pitot tubes such as are used in wake-traverse drag measurements. It was found that the pressure-plotting orifices had a negligible effect on the lag, because of their small length. In systems containing small bore pitot tubes, the length of small bore tubing is often as much as 4 ft. This has an appreciable effect on the lag, but it was found that equation (38) still applied in cases of this kind.

It may be concluded, therefore, that if the theoretical factor K is calculated for any system, the experimental factor K_1, calculated from equation (38), may be used to determine the lag corrections.

The laboratory tests described above enable the factor K_1 to be determined for any system, but they do not give any check on the functions $G(h_c)$ and $F(h_c)$ in equations (33) and (34). These functions depend on the density and viscosity of air at different altitudes, and can best be investigated in flight.

Some flight tests were therefore made in which a length of small bore copper tubing ($\frac{1}{16}$-in. i.d.) was connected between two altimeters, one of which was connected directly to a static head on an aircraft used for high-speed dive tests. The altimeters were mounted in an automatic observer and photographed during the dive. The difference in height reading between the two instruments then gave the pressure lag in the length of tubing.

In these flight tests the altimeters moved in jerks which were often not in phase with one another; consequently the height difference Δh_c showed large fluctuations about a mean value. The correct mean value was found by plotting Δh_c against time for the whole of the dive and drawing a faired curve through the points. The rate of descent v_d was found by differentiating the altitude-time curve graphically (the altitude need not be fully corrected for this), and $\frac{\Delta h_c}{v_d}$ was then plotted against height.

Figs. 105 and 106 show the results of some tests on two different Spitfires. When $\frac{\Delta h_c}{v_d}$ is plotted against height, the results agree fairly well with the theoretical curve for $K_1 = 2 \times 10^9$, except at the beginning and end of the dive where both the rate of descent and the lag are changing very rapidly, and a small error in time may produce a large error in $\frac{\Delta h_c}{v_d}$. In these experiments, the theoretical lag factor for the tubing between the altimeters was $1{\cdot}34 \times 10^9$, while the factor K_1 found by laboratory tests was $3{\cdot}7 \times 10^9$. These values are roughly consistent with equation (38). In the flight tests the lag is measured as a difference between two altimeter readings, and if we apply equation (38) to each we obtain the simple relation $K_1 = 1{\cdot}5K$. Alternatively, this may be explained by assuming the constant of $1{\cdot}1 \times 10^9$ to be due to mechanical lag in the instruments. As we are measuring the difference between the readings of two similar instruments, we may expect this constant to disappear. Thus we should expect the observed value of K_1 in the flight tests to be about

$$1{\cdot}5 \times 1{\cdot}34 \times 10^9 = 2 \times 10^9,$$

and, as explained above, this was the value actually found.

Experiments on a Mustang, with a different piece of tubing between the two altimeters, gave similar results; showing that the general application of equation (38) is justified, and verifying the form of the variation of lag with height, as given by equations (33) and (34).

It was shown earlier that for a normal cockpit installation K is about 1×10^8, making $K_1 = 1{\cdot}3 \times 10^9$ (from equation (38)). In this case K_1 is mainly due to the instrument lag, as given by the constant $1{\cdot}1 \times 10^9$ in equation (38). With this installation, in a typical high-speed dive at 30,000 ft., with a rate of descent of 600 ft. per sec., $\frac{\Delta h_c}{v_d}$ will be about $0{\cdot}54$ seconds (Fig. 102) and the lag in altitude will be about 320 ft. If $\frac{3}{16}$-in. o.d. tubing is used in the installation, instead of the more usual $\frac{5}{16}$-in. o.d. tubing, K becomes $1{\cdot}6 \times 10^9$, K_1 is $3{\cdot}5 \times 10^9$ and the lag in altitude under the same conditions is about 850 ft. Thus although the theoretical factor

K is 16 times as great with the thinner tubing, K_1 and the altitude lag are only about $2\frac{1}{2}$ times as great. Nevertheless, these figures illustrate the importance of keeping the tube diameter fairly large in order to minimise the lag corrections.

In estimating the lag at an air speed indicator, the pitot and static sides must be considered separately because of the different volumes. Having found K for both pitot and static sides of the A.S.I. the formula $K_1 = 1{\cdot}5K + (1{\cdot}1 \times 10^9)$ is applied to the difference $(K_{\text{static}} - K_{\text{pitot}})$. In this case, although a pressure difference is being measured, the conditions are not the same as in the case of the two altimeters because we are using only one instrument. For this reason, the constant term $1{\cdot}1 \times 10^9$ does not disappear. In a typical cockpit installation, at indicated air speeds of the order of 400 m.p.h., the lag is seldom more than 1 or 2 m.p.h. and thus is usually negligible.

The numerical examples given above show that corrections for altitude lag should always be applied to results of high-speed dive tests, although if $\frac{5}{16}$-in. o.d. tubing is used the corrections will usually be fairly small. When small bore tubing has to be used for connecting up special apparatus, *e.g.* a pitot comb mounted behind a wing, lag effects may be large, and it is then very important that the corrections should be determined accurately. The lag may be increased unnecessarily by unsuitable methods of connecting the instruments, *e.g.* by connecting the static sides of a large number of air speed indicators all to the same static-pressure source for use as a datum pressure. A better method is to leave the static sides of most of the instruments open to the fuselage static pressure, and to use a single instrument to compare the fuselage static pressure with the pressure given by the aircraft static head.

In flight experiments where it is necessary to apply lag corrections, it is usually found convenient to install two altimeters, connected together by a 4-ft. length of small bore tubing, as a standard piece of equipment. The experimental factor K_1 is then calculated for each of the instruments connected to the system, and the factor for the piece of " lag tubing " between the altimeters is also calculated. The height difference given by the two altimeters is measured throughout the tests, and the height lag at any other instrument is then given by

$$\frac{K_1 \text{ (for instrument)}}{K_1 \text{ (between altimeters)}} \times \text{(Difference between altimeter readings)}.$$

The advantage of this method is that the effect of the rate of descent is included in the measured lag between the altimeters. The value of K_1 for the piece of " lag tubing " between the altimeters is usually made about double that for a normal aircraft instrument system. The order of the height (or pressure) correction to any instrument is then immediately obvious from the altimeter readings.

In future high-speed flight tests, lag corrections are likely to be less important, because with the increasing thrusts available from jet propulsion units it will be possible to reach very high speeds in level flight, or at least at fairly small rates of descent.

5.2. *Alternative Methods of Measuring Speed and Height.*—In the last section, the corrections which must be applied to readings of air speed and altitude obtained from a pitot-static head in a high-speed dive have been considered in some detail. These corrections have been minimised as far as possible by fitting the leading edge type of pitot-static head and by using large diameter tubing, but there is still a considerable uncertainty in estimating the compressibility correction to position error at high Mach numbers, when shock waves have developed on the wing. Uncertainties of this kind will be present in any method which depends on measurements of static pressure, and other methods of determining aircraft speed and height are therefore being considered. Two such methods have so far been tried.[91] In the first of these, " tape measure height " was found by comparing a photograph of the ground, taken from the aircraft, with a map of the same area. In the second method, the speed and height of the aircraft were determined by Radar " tracking " from the ground. In both cases a Spitfire was used for the tests, and a comparison was obtained between the results given by the aircraft pitot-static system and the alternative method.

For the photographic method a standard F.24 camera, with a lens of 20 in. focal length, was mounted in the fuselage of a Spitfire XI. The camera was mounted with its axis at 45 deg. to the aircraft datum, so that the axis would be roughly vertical in a typical steep dive. Photographs of the ground were taken at regular 2-second intervals, and at the same time the aircraft instruments in an automatic observer were photographed by another camera. The photographs of the ground were compared with Ordnance Survey maps (scale 6 in. to 1 mile) of the same area, and thus the " tape measure " heights of the aircraft were obtained for comparison with the aircraft altimeter readings. Fig. 108 shows a reproduction of a typical photograph, together with the map of the same area.

One of the difficulties of the method is the exact location of the cross-wires on the map, but in some cases this is made easy by relating their position to obvious road intersections or corners of fields. Once the position of the cross-wires on the map has been established, the analysis consists of choosing suitable reference points and substituting in the following formulae (*see* notation given in Figs. 109 and 110).

$$\tan\theta' = f\left\{\frac{\Sigma\frac{X_2}{x_2} - \Sigma\frac{X_1}{x_1}}{\Sigma X_2 + \Sigma X_1}\right\} \quad .. \quad .. \quad .. \quad .. \quad .. \quad .. \quad .. \quad (39)$$

and slant range $= S_R = f\cos\theta'\dfrac{\Sigma\frac{X_1^2}{x_1}}{\Sigma X_1} + \sin\theta'\dfrac{\Sigma\frac{X_1^2}{x_1}}{\Sigma\frac{X_1}{x_1}}$ .. .. (40)

θ' is an angle measured in the pitching plane, but it is not equal to the angle of pitch of the aircraft. An angle ϕ' measured in the rolling plane (not equal to the aircraft angle of roll) can also be found by replacing θ', X_1, X_2, x_1, x_2, in equation (39) by ϕ', Y_1, Y_2, y_1, y_2. The slant range S_R can then be determined independently using ϕ', Y_1, *etc.* instead of θ', X_1, *etc.* in an equation similar to (40). Altogether, four values of the slant range S_R were found for each photograph, and the " tape measure height " H_T was then calculated from the mean value of S_R, using the equation

$$H_T = \frac{S_R}{\sqrt{1 + \tan^2\theta' + \tan^2\phi'}} \quad .. \quad .. \quad .. \quad .. \quad .. \quad .. \quad (41)$$

The equations used in the analysis are developed in detail in Apprendix I of Ref. 91.

Before the " altimeter height " and the " camera height " can be compared, the former has to be corrected for position error, lag, and compressibility error, for temperature, and for the zero setting of the altimeter; while the camera height has to be corrected for ground altitude to give the height above sea level. The order of the corrections to the altimeter reading is shown by the typical numerical values given in Table 2, below.

TABLE 2

Typical corrections to altimeter readings

Altimeter reading (corrected for instrument error) ..	= 29,460 ft.
Lag correction	= − 140 ft.
Position error and compressibility correction	= + 130 ft.
Temperature correction	= + 580 ft.
Ground level pressure correction (for altimeter set at 1,013 millibars)	= + 340 ft.
∴ Total correction to altimeter reading	= + 910 ft.
∴ Corrected aircraft height above sea level	= 29,460 + 910 ft. = 30,370 ft.

Fig. 111 shows a comparison between the " camera height " and the " altimeter height " in a dive from 32,000 ft. Only the first part of the dive is shown, because the photographs in the later part were obscured by clouds. At the beginning of the dive the discrepancy between the two methods of measurements is about 600 ft. (2 per cent.), but later, as the angle of dive increases, the camera becomes more nearly vertical and the agreement between the two methods is better. The results given in Fig. 111 suggest that, by careful choice of camera setting in the aircraft, and by diving at the angle required to keep the camera axis nearly vertical, it should be possible to measure altitude within $\pm$ 300 ft. (1 to $1\frac{1}{2}$ per cent.) by the camera method.

There are two factors limiting the accuracy of this photographic method ; one is the difficulty of taking measurements from the film and the map, and the other is the doubtful nature of the corrections to be applied in order to convert true altitude into pressure altitude[92] (or *vice versa*). An accuracy of $\frac{1}{2}$ per cent. was aimed at in measuring the distances on the film and on the map, but this was not always realised because lines which were quite sharply defined on the map sometimes appeared on the photograph only as vague boundaries, with a thickness too great to give the accuracy required. In this connection it should be explained that the Spitfire on which these tests were made was being used primarily for measurement of wing pressure distribution, and no particular attention was paid to diving the aircraft over an area most suitable for the height analysis. For the estimation of temperature corrections to altitude, meteorological observations over Farnborough had to be used, because no thermometer was fitted to the aircraft for measuring air temperature. Since an error of 1° C. in air temperature gives a height error of 120 ft. at 30,000 ft., it is clear that accurate measurements of air temperature are most important in this method of measuring height.

The increased accuracy at lower altitudes is due to the decrease in slant range S_R from 44,000 ft. at the beginning of the dive to about 24,000 ft. as the camera axis approaches the vertical position, with a corresponding increase in the size of the image on the film.

It is concluded from the tests described above that, because of the inherent inaccuracies of the photographic method, it can only give a rough check on the reading of the aircraft altimeter, even under most carefully chosen conditions.

For the measurement of aircraft speed and height by Radar, a standard S.C.R. 584 Radar gun laying equipment was modified by Radio Dept., R.A.E. and used to provide ciné records of the elevation θ, azimuth ϕ, and range S_R of a Spitfire in a high-speed dive. From these records the height and true air speed of the aircraft were calculated, and compared with the results given by the instruments in the aircraft auto-observer. The Radar tracking in elevation and azimuth was automatic, readings being obtained to the nearest minute on two theodolite vernier scales attached to the rotating paraboloid on top of the van, but the tracking in range was manually operated. The range was found by means of a disc, arranged to move in sympathy with the fine adjustment cathode-ray tube, a line on the disc indicating the position of the echo. The extreme range of the equipment was limited by the coarse cathode-ray tube to 32,000 yards.

With the notation given above for elevation, azimuth, and range, the formulae used in the reduction of the results were :—

" Tape measure height " $= S_R \sin\theta$.

The plan position of the aircraft is given by the co-ordinates (x_p, y_p) where

$$x_p = S_R \cos\theta \cos\phi$$

and

$$y_p = S_R \cos\theta \sin\phi \quad . . \quad . . \quad . . \quad . . \quad . . \quad . . \quad . . \quad . . \quad (42)$$

The resultant true speed relative to the earth (*i.e.* neglecting the effect of wind) is given by

$$V_E = \sqrt{\left(\frac{dS_R}{dt}\right)^2 + S_R^2\left(\frac{d\theta}{dt}\right)^2 + S_R^2 \cos^2\theta \left(\frac{d\phi}{dt}\right)^2} \quad . . \quad . . \quad . . \quad . . \quad (43)$$

Before discussing the results of the Radar measurements in dives, it may be useful to consider the results obtained in level flight tests at the A. & A.E.E.[93] (Figs. 112 and 113). These results

show that there are periodic variations in the speed and height given by the Radar, leading to errors of about 5 m.p.h. ($1\frac{1}{2}$ per cent.) in speed and about 300 ft. (1 per cent.) in altitude. It was not expected that the errors would be any less in the high-speed dive tests at the R.A.E.

Fig. 114 shows a plan view of the aircraft flight path during a dive, as found from the Radar results using equation (42). The scatter of the results from the straight line (about $\pm$ 50 ft.) is probably due entirely to lag in the manual operation of the range tracking.

In Fig. 115 the " Radar height " during a dive is compared with the height given by the aircraft altimeter, the latter being corrected for position error, compressibility, lag, temperature, and air pressure at ground level. The temperatures had to be estimated from figures supplied by the Meteorological Office, because no air thermometer was fitted on the aircraft, and thus the temperature corrections to altitude were not very reliable. Fig. 115 shows that the Radar height is consistently less than the altimeter height by about 400 ft. This discrepancy is of the same order as that found in the level flight tests at A. & A.E.E. (Fig. 112).

In order to compare the true air speeds given by the Radar and the aircraft A.S.I., it was necessary to correct the Radar results for the effects of wind speed. For this purpose the aircraft was assumed to be diving in the direction given by Fig. 114, and the estimated wind speeds and directions at the appropriate altitudes were obtained from the Meteorological Office. Fig. 116 shows the true air speed comparison, after making all the corrections. The agreement between the two methods of measurement is fairly good, except at the beginning of the dive where the aircraft is accelerating rapidly and the results given by the aircraft instruments are known to be rather unreliable. The aircraft A.S.I. results are more scattered than the Radar results, probably on account of the severe vibration of the aircraft. However, if smooth curves are drawn through both sets of results, the two methods of measurement agree within about $1\frac{1}{2}$ per cent., except at the beginning of the dive. Better agreement might be possible if more accurate estimates of the wind speed and direction could be made.

From the Radar measurements of true air speed, and the air temperatures obtained from the Meteorological Office, values of the " Radar Mach number " were calculated. These values were found to be within 0·01 of the Mach number given by the aircraft instruments, up to the highest Mach number reached (0·76).

The discrepancies in the measurements of speed and height by the aircraft instruments and by Radar could be explained by assuming that the corrected static pressure given by the aircraft pitot-static head is too low. It is unlikely that this is the correct explanation, however, because the discrepancies between the Radar and the aircraft instruments also occur at low air speeds, when the static pressure error can be measured very accurately.

It may be concluded that air speed and Mach number can be measured within $1\frac{1}{2}$ per cent., using S.C.R. 584 Radar equipment. This does not represent the best possible accuracy obtainable by this method, because speed measurement by Radar was not the primary object of these dive tests, and it is felt that with an improved technique and more care in determining the necessary corrections, better results would be possible. The reliability of the Radar method will not decrease with increasing Mach number, as with methods depending on measurements of static pressure, and thus Radar should be a suitable method of measuring speed in the transonic range. Perhaps the main disadvantage of the Radar method is the large amount of computing involved in deriving the results, since ciné records of all three variables, elevation, azimuth, and range, are essential.

5.3. *Automatic Recording during Dives.*—For nearly all of the high-speed flight research which has been done at the R.A.E. during the last few years, single-seat fighter aircraft have been used. In these aircraft it is of course not possible to carry an observer, and in a high-speed dive, when altitude and air speed are changing rapidly, satisfactory instrument readings cannot be taken by the pilot. Automatic observers have therefore been used in all cases for recording the readings of the instruments.

In principle, an automatic observer consists simply of one or more instrument panels which can be photographed by cameras controlled by the pilot. For dive tests, a T.35 camera control was usually installed, so that photographs could be taken automatically at regular time intervals. Whenever possible, F.24 aircraft cameras were used, but in some cases where the available space in the aircraft was very restricted, " Robot " 35 mm. cameras were used. Ciné cameras have also been used, especially for the investigation of oscillations, where it was essential to obtain continuous records.

The instruments in automatic observers are mounted as close together as possible and illuminated by filament lamps. In choosing the positions of these lamps, care must be taken to avoid shadows and reflections on the faces of the instruments.

Fig. 117 shows a typical set of photographs taken in an automatic observer in the E.28/39.[85] In this aircraft, only a small space was available for the automatic observer and it was necessary to use three separate instrument panels, each photographed by a " Robot " camera.

For recording a large number of pressures on an aircraft (*e.g.* the pressure distribution on a wing) a recording multi-capsule manometer has been designed. The general arrangement of this instrument is shown in Figs. 118 and 119, and Fig. 120 shows details of the capsules, linkages, and mirrors. There are 32 capsules, each capable of measuring positive or negative pressure relative to the datum. Each of these capsules is connected by a linkage to a small mirror, which rotates when the capsule is deflected. There is a separate light source focussed on each mirror, giving a line on a film whose position depends on the deflection of the capsule. A graticule, used for reading the films, is calibrated by subjecting all the capsules to equal increments of pressure, and observing the position of the film records on the graticule.

In using the multi-capsule manometer for measuring wing pressure distributions,[16] one capsule is connected to the aircraft pitot tube, another to the aircraft static tube, and the remainder to the pressure orifices. The case of the instrument is left open to the internal fuselage pressure, in order to reduce the lag in the pressure measurements. The instrument is rather bulky for use in small aircraft, the width of the film being 11 in.

In practice, an automatic observer with a large number of air speed indicators has usually been found more satisfactory for pressure plotting than the multi-capsule manometer described above. Air speed indicators are effectively more compact, because they can be distributed in the fuselage of the aircraft in the most convenient way. They also give better accuracy than the multi-capsule manometer, because the range of each instrument can be selected according to the pressure it is expected to measure, whereas in the multi-capsule manometer all the capsules are designed to cover the maximum possible range. When A.S.I's. are used, the required pressures (*e.g.* on the wing) are measured directly relative to the internal fuselage pressure, and one instrument is used to measure the pressure difference between the inside of the fuselage and the aircraft static tube. If possible, each instrument is connected in such a way that it will give a positive reading on the dial for all flight conditions.

5.4. *Miscellaneous Apparatus.*—Other apparatus which has been developed for use in high-speed flight tests is described below. In some cases, the apparatus described is similar to that used in tests at lower speeds, but modifications have been introduced to make it suitable for use at high speeds.

In flight investigations of compressibility effects, the Mach number can be calculated from the readings of the aircraft A.S.I. and altimeter, after applying corrections for position error, compressibility, and lag. This method is quite satisfactory for computing the experimental results, but the pilot cannot easily determine the Mach number in this way, because in a dive the A.S.I. and altimeter readings are usually changing rapidly. Thus it is very desirable to have an instrument in the pilot's cockpit which will indicate Mach number directly. In addition to its uses for experimental purposes, an instrument of this kind is also very useful in high-speed aircraft being used for normal service purposes, because on many aircraft there is a maximum safe Mach number which should not be exceeded in service.

The design of a Machmeter, for giving a direct reading of Mach number to the pilot, is considered by Smelt in Ref. 94. The operation of the instrument depends on the fact that the Mach number is a function of the ratio

$$\left(\frac{H_0 - P_0}{P_0}\right)$$

where H_0 is the total head and P_0 is static pressure. To show this, put

$$M^2 = \left(\frac{V}{V_s}\right)^2 \text{ where } V_s^2 = \frac{\gamma P_0}{\rho}$$

$$\therefore \quad M^2 = \frac{2}{\gamma} \cdot \frac{\frac{1}{2}\rho V^2}{P_0} \quad \ldots\ldots\ldots\ldots\ldots\ldots\ldots\ldots \quad (44)$$

Also, it can be shown from the usual equations of compressible flow that

$$\frac{H_0 - P_0}{\frac{1}{2}\rho V^2} = 1 + \tfrac{1}{4}M^2 + \tfrac{1}{40}M^4 + \ldots \quad \ldots\ldots\ldots\ldots \quad (45)$$

(assuming $\gamma = 1{\cdot}4$)

and therefore $$\frac{H_0 - P_0}{P_0} = \frac{\gamma M^2}{2}\left[1 + \tfrac{1}{4}M^2 + \tfrac{1}{40}M^4 + \ldots\right] \quad \ldots\ldots\ldots\ldots \quad (46)$$

Hence all that is required in a Machmeter is an ordinary A.S.I. pressure capsule whose deflection is proportional to $(H_0 - P_0)$, and an altimeter capsule having a deflection proportional to P_0, with a suitable linkage for deriving the ratio between the two movements. The movement of the pointer then depends on the ratio $(H_0 - P_0)/P_0$, and if the scale is calibrated in accordance with equation (46) a direct reading of Mach number is obtained.

Fig. 121 shows the principle of operation of the type of Machmeter which has been used at the R.A.E., and Fig. 122 shows a photograph of the instrument. The photograph shows an early instrument with a scale which is only calibrated up to a Mach number of 0·8; later experience showed that this Mach number could easily be exceeded in flight, and the instruments now in use have scales calibrated up to a Mach number of 1·0.

In flight research at high Mach numbers, considerable difficulty has sometimes been experienced in measuring aircraft drag. The following three methods have been used for determining the difference between drag and thrust :—

(1) Analysis of the dive angle. This method has been found to be very inaccurate.

(2) Analysis of the total energy of the aircraft. This method has been used with fair success, but the scatter of the results is usually rather large.

(3) By direct measurement of longitudinal acceleration.[95] This method has been found to be much more satisfactory than either of the others, and is described below.

The accelerating force on an aircraft in a dive, acting along the flight path, is

$$W \sin \theta_D - (D - T_r)$$

where W is the aircraft weight, D is drag, T_r is thrust, and θ_D is the angle of dive.

Thus the acceleration of the aircraft, along the flight path, is

$$\left[\sin \theta_D - \left(\frac{D - T_r}{W}\right)\right]g$$

and the reading (R_a) of a longitudinal accelerometer, placed in the aircraft and directed along the line of flight, will be given by

$$R_a = g \sin \theta_D - (\text{aircraft acceleration}).$$

Thus if R_a is calibrated in terms of g,

$$R_a = \frac{D - T_r}{W} \quad \ldots\ldots\ldots\ldots\ldots\ldots\ldots\ldots \quad (47)$$

Thus the expression $(D - T_r)$ can be obtained directly from the reading of a longitudinal accelerometer with its axis along the flight path.

In practice there is usually a small angle ϕ_a between the axis of the accelerometer and the flight path, and the accelerometer readings must be corrected for the effect of this. It can be shown that, if ϕ_a is measured in the positive direction when the accelerometer axis is at a positive incidence relative to the flight path,

$$\frac{D - T_r}{W} = R_a + n\phi_a + \frac{R_a\phi_a^2}{2} \text{ (approximately)} \quad .. \quad .. \quad .. \quad .. \quad (48)$$

where ϕ is measured in radians and n is the reading of a normal accelerometer in units of g ($n = 1$ in level flight).

In order to reduce the correction depending on ϕ_a to as small a value as possible, every effort should be made to set the longitudinal accelerometer in the aircraft with its axis parallel to the important part of the flight path. The incidence of the aircraft must be measured during the tests, in order to determine the value of ϕ_a and apply the correction.

The first longitudinal accelerometer to be developed at the R.A.E., for use in measuring aircraft drag at high speeds, is shown in Figs. 123 and 124. The mechanism consists of a spring-restrained weight, sliding between rotating rollers, as in the Barnes type accelerometer. The displacement of the weight is transmitted by a simple linkage to a scale calibrated in terms of g. The instrument is accurate to about $0{\cdot}005g$, giving an accuracy of about 50 lb. in $(D - T_r)$ for an aircraft weight of 10,000 lb.

Measurements of incidence in flight are required in connection with drag measurements by the longitudinal accelerometer method, and also for investigating changes of incidence at high Mach numbers due to the formation of shock waves on the wing. For this purpose the incidence vane shown in Fig. 125 was designed.

The vane is mounted on an arm, ahead of the leading edge of the wing, so that it is free to rotate about a horizontal axis. It is exactly mass-balanced, and therefore sets itself along the line of flight, so that the incidence of the aircraft is given by the angle between the fixed arm and the freely mounted vane. A spindle, which rotates with the vane when the incidence changes, is connected to a wiper which forms part of the transmitter unit of a micro-desynn. A desynn receiver, installed in an automatic observer, indicates the angular setting of the spindle and hence gives the incidence of the aircraft.

It is important that the bearings of the spindle should be as free from friction as possible and that the arm on which the vane is mounted should be rigid. Also, the vane should be far enough in front of the leading edge of the wing to make the effect of upwash very small. The distance which has usually been adopted is 60 per cent. of the local chord in front of the leading edge. When all these precautions are observed, the error in the incidence measurements is probably about $\pm \frac{1}{4}$ deg. or $\pm \frac{1}{2}$ deg. This accuracy is quite good enough for drag measurements by the longitudinal accelerometer method, but it is not always satisfactory for investigations of incidence changes at high Mach numbers.

For measuring the profile drag of a wing section at high Mach numbers, the pitot-traverse method[96] has been used. The theory of this method for high-speed flow is given in Ref. 46, and in Ref. 47 a convenient simplified method of computation is described. This simplified method has been used for all the high-speed flight measurements made at the R.A.E. during the last few years.

Figs. 126 and 127 show a typical comb, as used for measuring profile drag at high Mach numbers on a wing of about 7 ft. chord. In an attempt to include the whole of the wake from a shock-stalled wing, the width of the comb has been made considerably greater than that normally used for drag measurements at low speeds. It is now realised, however, that it is not practicable to use a comb which is wide enough to include the whole of the shock wave wake at high Mach numbers. Thus the profile drag of a wing can only be measured by the pitot-traverse method

up to a Mach number slightly above that at which the drag coefficient begins to rise. The limitations of the pitot-traverse method at high Mach numbers, and a possible alternative method of measuring drag, will be discussed later.

In a comb for measuring drag at high speeds, $\frac{1}{8}$-in. i.d. copper tubes are normally used. The spacing of the tubes is usually about $\frac{1}{2}$ in. near the centre of the comb, increasing to about 1 or $1\frac{1}{2}$ in. at the ends. The central tube usually measures both pitot and static pressure. $\frac{5}{16}$-in. o.d. tubing is used whenever practicable for connecting the pitot tubes to the instruments in the fuselage, the length of the small diameter ($\frac{1}{8}$-in. i.d.) tubing being kept as short as possible in order to reduce the lag. The comb is attached to the wing with the ends of the pitot tubes about 10 per cent. of the local wing chord behind the trailing edge.

Fig. 128 shows a typical pressure orifice as used for measuring static pressure distributions in flight, *e.g.* on a section of a wing. The fitting consists of three parts, the screw A, the barrel B, and a rubber ring C. The screw A is made of brass and is drilled with a $\frac{1}{16}$ in. hole which serves as the actual pressure orifice. This screw has a countersunk, slotted head, which when fitted through the wing skin into the barrel can be cut down flush with the wing surface. A rubber ring C fits into a groove in the barrel B in order to ensure a leakproof joint. Before assembly, the screw thread is smeared with jointing compound in order to prevent leakage and also to avoid loosening of the screw. A short length of $\frac{1}{8}$-in. i.d. tubing is connected to the barrel but, in order to reduce lag, $\frac{5}{16}$-in. o.d. tubing is used to connect this small diameter tube to the instruments in the fuselage.

Wool tufts have sometimes been used in flight tests at high Mach numbers, for investigating breakaway of flow. The results obtained with these tufts are described later in this report.

6. *Compressibility Phenomena Experienced in Flight.*—Flight tests at high Mach numbers have been made at the R.A.E. on seven different types of aircraft. These aircraft, and the results of the tests, are described below.

6.1. *Description of Aircraft.*—Brief details of the aircraft on which tests have been made are given in Table 3.

TABLE 3

Details of aircraft

Aircraft	Wing			Type of Engine	Propellers
	Type of Section	Root t_ω/c	Tip t_ω/c		
Spitfire XI	N.A.C.A.22XX	0·13	0·07	1 Merlin 70	4-blade
Spitfire XXI	N.A.C.A.22XX	0·13	0·07	1 Griffon 61	5-blade
Mustang I	Semi-low drag	0·15	0·11	1 Allison V.1710	3-blade
Gloster E.28/39	ECXX40/0640	0·125	0·10	1 W.2/700 Jet Unit	None
Meteor I	ECXX40/0640	0·12	0·10	2 W.2B/23 or W.2/700 Jet units.	None
Welkin	N.A.C.A.230XX	0·21	0·15	2 Merlin 72	4-blade
Thunderbolt	N.A.C.A. Conventional	0·16	0·09	1 P. & W.R. 2800	4-blade
Lightning	N.A.C.A. Conventional	0·16	0·12	2 Allison V.1710	4-blade

On all these aircraft, measurements of overall drag at high Mach numbers have been made, and on all except the last three in Table 3, measurements of elevator angle to trim at high Mach numbers have also been made. Pressure distribution and profile drag at a section of the wing have been measured on the Spitfire XI, Mustang I, and Gloster E.28/39. On the Thunderbolt and Lightning, tests on dive recovery flaps were made. On the Welkin, tests were made to investigate pitching oscillations at high Mach numbers.

Fig. 129 shows the general arrangement of the Spitfire XI. This is a photographic reconnaissance type with no guns, and the external finish is better than on Spitfire fighter aircraft such as the Mark IX or XXI. During the dive tests on the Spitfire XI the all-up weight was about 6,500 lb., giving a wing loading of about 27 lb. per sq. ft. The position of the wing test section, at which measurements of pressure distribution and profile drag were made, is shown in Fig. 129.

The Spitfire XXI resembles the Mark XI fairly closely in external shape, but on the Mark XXI the wing area is about 2 per cent. greater, the radiators are larger, the front of the fuselage is larger to accommodate the Griffon engine, and there are fairly large ammunition blisters on the wing at the position of the guns. The photographs in Fig. 130 show these blisters on the Spitfire XXI. The all-up weight of the Spitfire XXI is about 9,100 lb., and the wing loading is about 36 lb. per sq ft.

Fig. 131 shows the general arrangement of the Mustang I used for the dive tests. The position of the wing test section, at which measurements of pressure distribution and profile drag were made, is also shown. The ceiling of the Mustang I (with Allison V.1710 engine) is not very high, but this was increased as much as possible for the dive tests by removing guns, radio, armour plating, and all accessory equipment which was not essential. The all-up weight was then 7,400 lb. and the dives could be started at 28,000 ft. The wing loading was about 31 lb. per sq. ft.

The Gloster E.28/39, shown in Fig. 132, was the first jet-propelled aircraft to be flown in this country, and was designed for engine test bed purposes. The aircraft is considerably smaller than the others which have been used for high-speed flight research ; the all-up weight is only about 4,500 lb. and the wing area is 140 sq. ft. The wing loading is about 30 lb. per sq. ft.

The Meteor I is a single-seat fighter powered by two Rolls Royce W2B/23 jet propulsion engines. For some of the high-speed flight tests made at the R.A.E., the engines were replaced by W.2/700 units in order to give better performance at high altitudes. Tests on this aircraft have been made with three alternative types of nacelle. The short nacelles, which are fitted on standard Meteor I aircraft, gave buffeting and high drag at Mach numbers above about 0·74. To reduce the buffeting and the drag the nacelles were modified, first by extending the nose, and later by extending both the nose and the tail. Fig. 133 shows the aircraft with extended nose and tail nacelles. In this form the external shape of the aircraft is very nearly the same as that of the Meteor IV, and the Meteor I with extended nose and tail nacelles will sometimes be referred to as the Meteor IV in this report.

The Meteor which was used for high-speed flight tests was not fitted with cannon, but appropriate ballast was installed to compensate for this. The aircraft was fitted with specially strengthened wings and metal covered ailerons. For the earlier tests the rudder and elevator were both fabric covered, but in later tests the fabric covered elevator was replaced by a metal covered one in order to reduce the stick forces required at high Mach numbers.

Fig. 134 shows the general arrangement of the Welkin I. This aircraft was designed as a high-altitude fighter and the aspect ratio of the wing is unusually large for a single-seat fighter. In order to give a reasonably low structure weight with this high aspect ratio, the thickness ratio of the wing was made rather large (21 per cent. at the nacelles). Because of the thick wing, the Mach number at which serious compressibility effects are experienced is lower on the Welkin than on most other fighter aircraft.

Figs. 135 and 136 show the general arrangements of the Thunderbolt and Lightning respectively. On these two aircraft only short tests were made, to investigate the effects of the dive recovery flaps and to measure the overall drag of the aircraft at high Mach numbers. Both aircraft were tested in standard service condition.

6.2. *Drag of Complete Aircraft.*—Fig. 137 shows the variation of profile drag coefficient with Mach number, for several complete aircraft.[63, 85, 97, 98, 99, 100, 101] On all the aircraft except the Mustang I and the Meteor I (with short nacelles), the drag was measured by the longitudinal accelerometer method which has already been described. The drag measurements on the Mustang I and the

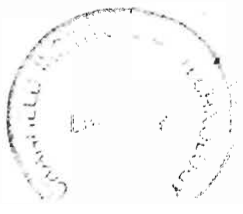

Meteor I were made by the energy method and these results are therefore less reliable than the others. In all cases the calculated induced drag has been subtracted from the measured total drag, but this correction for induced drag is usually very small.

For the Spitfire XXI[97], two curves are given. One of these refers to the aircraft in standard service condition, with guns and blisters on the wing (Fig. 130). The other curve gives the results of measurements made after removing the guns and ammunition blisters and fairing the leading edge of the wing. The undercarriage blisters, shown on the left of the photographs in Fig. 130, were present in all the tests. Fig. 137 shows that removal of the guns and blisters increased the Mach number for a given drag coefficient by about 0·04, a surprisingly large amount for such a small alteration to the aircraft.

A Spitfire XI has been dived to a Mach number of about 0·90 (Ref. 98). This is probably the highest Mach number which has yet been recorded in flight on any aircraft in the world. During these tests on a Spitfire XI, drag measurements were made by the energy method, but these were not considered very reliable and they have therefore not been included in Fig. 137. The highest Mach number reached during the tests on the Spitfire XXI (without guns and blisters) was about 0·88. This value is lower than the highest Mach number reached by the Spitfire XI, although the wing loading of the Mark XXI is considerably higher than that of the Mark XI. However, the external finish of the Mark XXI was not as clean as that of the Mark XI, even after removing the guns and blisters, and this probably explains the higher diving Mach number of the Spitfire XI.

It should be noted that the highest Mach number shown in Fig. 137 for a particular aircraft is sometimes less than the highest Mach number reached in the dives. For example, a Mach number of 0·88 was reached in the tests on the Spitfire XXI (without guns and blisters), but no drag results can be given for Mach numbers above 0·86. The reason for this is that there are sometimes not enough experimental points at the highest Mach numbers to give a reliable measurement of the drag coefficient.

The curve in Fig. 137 marked " Meteor IV " gives the results of drag measurements made on a Meteor I which had been modified by fitting lengthened nacelles.[63] The external shape of the modified aircraft was very nearly the same as that of a Meteor IV. Fig. 137 shows that the Mach number for a given drag coefficient is about 0·06 higher with the long nacelles than with the short ones. The improvement due to lengthening the nacelles will be discussed in more detail later in connection with buffeting.

On the Mustang I there is a small spoiler flap under the fuselage which, when lowered, is intended to block the radiator entry to prevent over-cooling during glides. It was found that the drag at high Mach numbers was reduced by lowering this spoiler flap,[98] but the explanation of this surprising result is not known. Fig. 137 shows drag curves for the aircraft with the spoiler raised and lowered, but as only one dive was made with the spoiler raised, the results for this condition are not very accurate. The effect of the spoiler flap on trim changes at high Mach numbers will be discussed later.

On the Welkin,[101] severe pitching oscillations were sometimes experienced at high Mach numbers, and it was found that the drag coefficient at a given Mach number appeared to depend on the severity of these oscillations. Two curves for the Welkin have therefore been included in Fig. 137, showing the estimated upper and lower limits of the drag coefficient at each Mach number. The lower curve shows the drag of the aircraft in steady flight, with no oscillations, and the upper curve shows the drag when there are severe pitching oscillations.

The results given for the Lightning[100] and Thunderbolt[99] were obtained during a series of tests to investigate dive recovery flaps. In the case of the Thunderbolt, the drag at high Mach numbers was not appreciably affected by opening the dive recovery flaps, but on the Lightning the flaps caused a large increase of drag.

Apart from excrescences such as radiators, nacelles, and blisters on the wing, the most important variable affecting the drag of an aircraft at high Mach numbers is the thickness ratio of the wing. Fig. 137 and Table III show that the Mach number at which the steep rise of drag occurs usually

increases as the wing thickness ratio decreases, except in cases where excrescences cause the drag to rise at an unusually low Mach number (*e.g.* the short nacelles on the Meteor I). The flight tests have shown that the thickness ratio of the wing is much more useful than the critical Mach number, as an indication of the Mach number at which the drag of the aircraft will rise steeply. This is shown, for example, by comparing the curves for the Spitfire XXI (without guns and blisters) and the Mustang I in Fig. 137. The thickness ratio is considerably greater for the Mustang wing than for the Spitfire, but the Mustang wing has a semi-low drag type of section while the Spitfire has a conventional NACA section, so that the critical Mach number (defined as the flight Mach number at which sonic velocity is first reached locally on the wing) is slightly greater for the Mustang wing than for the Spitfire. The results show, however, that the Mach number at which the drag starts to rise steeply is considerably less for the Mustang than for the Spitfire (without guns and blisters), indicating that the greater thickness ratio of the Mustang wing has a more important effect on the drag rise than the slightly greater critical Mach number. The results of high-speed wind tunnel tests lead to similar conclusions (*see* 4.11).

In many cases it has been found that the drag of an aircraft at a given high Mach number is greater in the later part of the dive, when the Mach number is decreasing, than in the early part of the dive, when the Mach number is increasing. As this effect is still under investigation, and may possibly be due to faulty experimental technique, most of the curves shown in Fig. 137 give mean values for increasing and decreasing Mach number. In the case of the Welkin the first part of the dive, up to the highest Mach number, was usually fairly steady, but severe pitching oscillations occurred in the later part of the dive with decreasing Mach number. It was considered that in this case a mean curve would not have much significance, and two drag curves for the Welkin have therefore been included in Fig. 137.

For an aircraft which can only reach high Mach numbers by diving, it is very difficult to investigate this apparent hysteresis effect on drag, because in the later part of the dive, when the Mach number is decreasing, the lift coefficient is usually greater than in the earlier part of the dive. The increase of lift coefficient may partly explain the higher drag observed in the later part of the dive. This point will be discussed later in connection with wing profile drag measurements. A further difficulty in dive tests at high Mach numbers is caused by the reduced rate of descent in the later part of the dive. If the results were wrongly corrected for lag, the change of rate of descent might introduce an apparent hysteresis effect. However, the method of determining the lag corrections which has already been described is considered fairly satisfactory, and it is unlikely that the apparent hysteresis effect can be explained in this way.

With the greatly increased thrusts now available from jet-propulsion units, it will be possible in the future to measure drag at high Mach numbers in level flight. The difficulties mentioned above will then disappear, and it is hoped that the explanation of the hysteresis effect which has been observed in dives will be found.

6.3. *Buffeting and its Removal by Better Fairing.*—During flight tests at high Mach numbers, buffeting of the aircraft has often been experienced. This buffeting is probably caused by the formation of shock waves on the main wing, which may lead to partial separation of the flow. In some cases the disturbed wake from the wing causes buffeting of the tail plane. In other cases the buffeting occurs first on the wing, and is then often accompanied by irregular rolling and yawing of the aircraft. Any buffeting which is caused by disturbed flow on the wing, or at junctions of the wing with nacelles or fuselage, can be investigated by the use of wool tufts. This method has been applied successfully in flight tests on the improvement of the Meteor nacelles.[63]

During early flight tests on Meteor aircraft, a severe wing-aileron flutter was experienced at a Mach number of about 0·74. This was cured by over mass-balance of the ailerons, but subsequent flights showed that the flutter had been initiated by a breakaway of the flow in the outboard nacelle-wing junction at Mach numbers above about 0·74. High-speed wind tunnel tests had shown that the breakaway could be considerably improved by extending the nacelles fore and aft. (*see* §4.35 and Ref. 60). Flight tests were made first on the aircraft with standard (short nacelles), then with extended nose nacelles, and finally with extended nose and tail nacelles.

Fig. 133 shows the aircraft with extended nose and tail nacelles ; the differences between these nacelles and the earlier ones are shown in Figs. 138 to 143 and in Fig. 69. The maximum Mach numbers reached during the tests were 0·78 with short nacelles, 0·80 with extended nose nacelles, and 0·84 with extended nose and tail nacelles.

During the flight tests, raised wool tufts on the port wing and nacelle were photographed by a camera mounted in the tail of the aircraft. Simultaneous photographs of an instrument panel in the fuselage were taken, in order to record the air speed, altitude, and normal acceleration. Photographs of the tufts at various Mach numbers and normal accelerations are given in Figs. 138 to 143. With short nacelles, the flow begins to break down on the inboard nacelle-wing junction at $M = 0{\cdot}72$ and $1g$, followed by a breakaway on the outboard side at $M = 0{\cdot}76$ and $1g$. With extended nose nacelles there is no appreciable breakaway up to $M = 0{\cdot}79$ and $2g$, although higher normal accelerations at this Mach number cause a breakaway on both sides of the nacelle. With extended nose and tail nacelles, no serious breakdown of flow occurs below $M = 0{\cdot}84$ and $3g$. The breakaway then seems to be mainly on the outboard side of the nacelle, and from pilots' reports this seems to be accompanied by a general shock-stalling of the whole wing. With the extended nacelles, tests at the higher Mach numbers could not be made at normal accelerations as low as $1g$, because the aircraft developed a considerable nose-up change of trim at high Mach numbers. This trim change is discussed below.

These tuft observations have shown that the Mach number at which buffeting occurs can be considerably increased by extending the nacelles. The extended nacelles also gave an increase in the Mach number at which the aircraft drag started to rise steeply (Fig. 137). Both these conclusions are in agreement with the results of the tunnel tests (*see* § 4·35).

Using the pilot's reports of buffeting under various conditions, curves have been drawn showing the buffeting limit as a function of Mach number and normal acceleration (Fig. 144). For level flight conditions ($1g$), the buffeting Mach number is 0·74 with short nacelles, 0·81 with extended nose nacelles, and 0·85 with extended nose and tail nacelles. The highest Mach number reached in the flight tests was only 0·84 because, as already explained, flight at $1g$ at the highest Mach numbers was not possible on account of the nose-up trim change.

The raised tuft technique has also been used to investigate buffeting on the Gloster E.28/39[85]. On this aircraft buffeting was experienced at a Mach number of about 0·81, accompanied by irregular yawing, pitching, and rolling. At this Mach number the drag of the aircraft appeared to be rising fairly steeply, and as the wing thickness ratio is fairly small (*see* Table 3), it was suggested that the buffeting and the steep drag rise might be caused by a breakaway of flow at the wing root fillet. Accordingly, raised tufts were fitted on the upper surface of the wing at the junction with the fuselage, and these were photographed by a camera mounted in a streamline fairing at the wing tip. However, the results of these tests showed no appreciable signs of breakaway at the wing root at any Mach number up to 0·80, except for a small disturbed region behind an undercarriage blister on the upper surface of the wing. (This blister can be seen in Fig. 132.) It was considered that the small breakaway behind the blister was insufficient to account for the violent buffeting which had been reported by the pilot. It was intended to use tufts to explore the flow on other parts of the aircraft, but at this stage the tests had to be discontinued because the aircraft was required for other purposes.

6.4. *Changes of Longitudinal Trim at High Mach Numbers.*—On most of the aircraft which have been tested at high Mach numbers, there has been a nose-down change of trim with increasing Mach number. Because of this trim change, the pilot has to exert a very large pull on the stick in order to recover from a dive at high Mach numbers, or even to prevent the Mach number from increasing still further.

Figs. 145 to 147 show the change of elevator angle required to counteract the nose-down trim change on several different aircraft.[63, 85, 97, 98] In these diagrams, the change of elevator angle is measured relative to the elevator angle to trim in level flight ($1g$), at the same E.A.S. and at a low Mach number. The curves for the Mustang I (Fig. 146) show that the trim change at high

Mach numbers is reduced by lowering the spoiler flap in front of the radiator entry. Lowering this flap also reduces the drag at high Mach numbers (Fig. 137), but the explanation of these effects is not known.

Fig. 147 shows the change of elevator angle with Mach number, for the Meteor with the original short nacelles, and also for the aircraft with extended nose and tail nacelles[63]. With the short nacelles the beginning of the usual nose-down trim change can be seen, but with the extended nacelles the behaviour of the aircraft is unusual, the trim change being in the nose-up direction. The curves in Fig. 147 for the short nacelles refer to the aircraft with fabric-covered elevators at an altitude of 20,000 ft., whereas the results for the extended nacelles are for the aircraft with metal-covered elevators at 30,000 ft. However, some other tests at 20,000 ft. on the aircraft with extended nose and tail nacelles and fabric-covered elevators, showed that the differences between the two sets of curves in Fig. 147 were mainly due to the change of nacelle shape, and not to the changes of altitude and elevator construction.

Figs. 148 and 149 show the stick forces required at high Mach numbers on the Spitfire XI and XXI, reduced to a constant E.A.S. of 400 m.p.h. These results show that, if the aircraft is trimmed for this E.A.S. at a low Mach number (*i.e.*, at low altitude), a pull of more than 50 lb. is required to recover from a dive at a Mach number of 0·85. At slightly higher Mach numbers the required pull on the stick is considerably greater, and it has been estimated that, with this trimmer setting, the pilot would be unable to recover from a dive at a Mach number greater than about 0·91. Tests made on a Spitfire XI have shown that the elevator trimming tab is still quite effective at a Mach number of about 0·9, but if the tab is moved in order to reduce the pull required on the stick at high Mach numbers, there is a danger that a very high normal acceleration may develop suddenly at a lower altitude, when the Mach number has decreased. Pilots are therefore advised not to use the trimmer to reduce the pull required on the stick at high Mach numbers. The procedure which has been adopted for all the high Mach number dive tests at the R.A.E. is to make the tests at as high an altitude as possible and to keep the trimmer setting constant throughout the dive. By pulling hard on the stick the pilot has been able to prevent the dive from becoming steeper, and if this can be done the Mach number decreases slightly with altitude, because of the change of air density, thus making recovery from the dive possible at a lower altitude. With increase of aircraft wing loading, however, the altitude at which a recovery can be made by this method tends to decrease, and with future aircraft having very high wing loadings it may be essential to use the trimming tab, or some other device, to assist recovery from the dive.

The causes of the usual nose-down trim change at high Mach numbers have already been considered (*see* 4.32). It was shown that a fairly large trim change in passing from subsonic to supersonic speeds is inevitable with aircraft of conventional lay-out. This trim change, especially the part that occurs at Mach numbers up to about 0·85, can be reduced considerably by using a symmetrical wing.

Fig. 150 shows a comparison between the flight measurements of elevator angle to trim, on the Spitfire and Mustang, and the supersonic values as estimated roughly by Smelt[58]. The dotted lines show possible transition curves for the transonic speed range, but the correct shapes of these curves are not known, and the ones given in Fig. 150 should only be regarded as tentative suggestions. The results suggest that for aircraft of conventional design most of the change of trim, in passing from subsonic to supersonic speeds, probably occurs at Mach numbers below about 0·9.

As already mentioned, the behaviour at high Mach numbers of the Meteor with extended nacelles is unusual, because in this case the trim change with increasing Mach number is in the nose-up direction. Although this agrees with the results of wind tunnel tests (*see* 4.32), the complete explanation is not yet clear, because later flight tests have shown that the trim change is affected by altering the tail plane setting, suggesting that aero-elastic distortion may be having an important effect.

On nearly all the aircraft which have been used for tests at high Mach numbers, a vane for measuring incidence has been fitted. In most cases the accuracy of the results has not been good enough to show the sudden change of incidence at high Mach numbers which is the principal cause of the change of trim. In the tests on the Gloster E.28/39[85], however, a change of this kind was recorded, as shown in Fig. 151. During these tests aileron angles were also recorded, and it was found that the aileron down-float increased slightly with Mach number. This change of aileron down-float may partly explain the gradual decrease of incidence with increasing Mach number up to $M = 0{\cdot}775$. The sudden increase of incidence at higher Mach numbers is probably not much affected by aileron float and is one of the principal causes of the nose-down trim change shown in Fig. 145.

In Ref. 58 it is shown that, in passing from subsonic to supersonic speeds on an aircraft of conventional design, a considerable increase of longitudinal stability is to be expected, in addition to the nose-down trim change discussed above. An increase of longitudinal stability at high subsonic speeds has also been found in high-speed wind tunnel tests on complete aircraft models (*see* § 4.33). No direct measurements of longitudinal stability have been made in flight at very high Mach numbers, but the curves given in Figs. 145 and 146 for different normal accelerations give an indication of the changes of stability at high Mach numbers. These curves show that the change of elevator angle required to produce a given normal acceleration, as shown by the spacing of the curves for different values of g, usually increases with Mach number. It has already been shown that the nose-down trim change makes recovery from a dive very difficult at high Mach numbers, and this increase of stability, or reduction of manœuvrability, increases still further the difficulty of recovering from a dive.

The use of dive recovery flaps to counteract the nose-down trim change at high Mach numbers has already been explained (*see* §4.32). Flight tests to investigate the effects of these dive recovery flaps have been made on two aircraft—Thunderbolt[99] and Lightning[100]. On the Thunderbolt the flaps were fitted on the inboard part of the wing at 30 per cent. of the local chord (Fig. 135) ; the flap chord was 6 in. and the span was 40 in. on each side. The maximum flap deflection was 20 deg. At a Mach number of $0{\cdot}7$, the flaps gave a normal acceleration of about $2g$ at 25,000 ft., but the pilot moved the elevator about $\frac{1}{2}$ deg. to 1 deg. during the recovery, in such a direction as to reduce the acceleration. Thus the normal acceleration produced by the flaps would have been greater than $2g$ if the elevator had not been moved. No tests were made at Mach numbers greater than $0{\cdot}7$.

On the Lightning[100], the dive recovery flaps were placed outboard of the nacelles at about 30 per cent. of the local wing chord (Fig. 136). Each flap had a span of 58 ins. and a chord of $8{\cdot}5$ ins., and the maximum flap angle was 35 deg. It was found that the normal acceleration produced was about $1{\cdot}2g$. Thus, although the area of the dive recovery flaps on the Lightning was about twice that on the Thunderbolt, the normal acceleration produced by the flaps was much greater on the Thunderbolt than on the Lightning. The greater flap effectiveness on the Thunderbolt is probably due to the inboard position of the flaps on that aircraft, giving an increase of downwash at the tail when the flaps are opened. On the Lightning, the flaps are outboard of the nacelles and booms (Fig. 136), and there is probably no increase of downwash at the tail when the flaps are opened.

On the Thunderbolt, the total area of the dive recovery flaps is about 1 per cent. of the wing area. The flight test results show that this is a suitable size for flaps placed on the inboard part of the wing, in front of the tail plane. From the results of the Lightning tests, it appears that a flap area about three or four times as great is required, if the flaps are outboard of the tail plane so that they give no increase of downwash at the tail. For a given Mach number, the normal acceleration produced by a dive recovery flap is proportional to the atmospheric pressure, and thus the acceleration at 10,000 ft. will be about three times that at 35,000 ft. This means that the flap size must be chosen very carefully in order to avoid giving either too great an acceleration at low altitudes or too small an acceleration at high altitudes.

6.5. *Control Characteristics.*—In the flight tests which have been made at high Mach numbers, there have been no definite indications of any loss of control effectiveness. Since the tests have

been mainly concerned with changes of longitudinal trim and stability, the movements of the ailerons and rudder have always been fairly small, but the pilots have never complained of ineffectiveness of these controls. The curves given in Figs. 145 and 146, showing elevator angles required for different normal accelerations at high Mach numbers, indicate that there is no very serious loss of elevator effectiveness up to the highest Mach numbers which have been reached in the tests. As already mentioned, the curves show that the elevator movement required to produce a given normal acceleration increases at high Mach numbers, but this could be due either to loss of elevator effectiveness (a_2) or to increase of stick fixed manœuvre margin[67]. The results of wind tunnel tests (*see* 4.33) show that the effect is more likely to be due to an increase of manœuvre margin than to a loss of elevator effectiveness (a_2). Wind tunnel tests have also shown that, on conventional aircraft at high flight Mach numbers, the local Mach number in the region of the tail plane is considerably less than the flight Mach number, because of the effects of the wing and body wakes (*see* 4.34 and Ref. 69). This reduced Mach number in the region of the tail plane explains the satisfactory elevator effectiveness found in flight at high Mach numbers. With a high tail plane position, the wing and body wakes have less effect on the local Mach number in the region of the tail plane, and some loss of elevator effectiveness at high Mach numbers may then be expected. Flight tests on a Meteor, the only aircraft with the tail plane in a high position which has yet been flown at high Mach numbers, have not yet given any definite information on the variation of elevator effectiveness (a_2) with Mach number.

It may be noted that the phenomenon which is sometimes described by pilots as " loss of elevator control " or " elevator freezing " in dives at high Mach numbers, is really only the nose-down trim change which has already been discussed. When this trim change occurs, the pilot has to exert a large pull on the stick in order to maintain a positive wing lift. At lower Mach numbers, fairly large normal accelerations are usually experienced when the stick is pulled hard, and thus at a high Mach number, when only a small normal acceleration is produced, the elevator appears to be ineffective. In most cases, however, the elevator effectiveness, defined as the change of pitching moment for unit elevator deflection, probably has nearly the same value as at low Mach numbers, and the apparent ineffectiveness of the elevator is due to the nose-down change of trim on the aircraft. As already mentioned, the difficulty of recovery from a dive, *i.e.*, the apparent loss of elevator effectiveness, may often be augmented by an increase of manœuvre margin at high Mach numbers.

There is only a little information on trimming tab effectiveness at high Mach numbers because, as already explained in discussing trim changes, most of the tests have been made at a constant setting of the elevator trimming tab. In one dive on a Spitfire XI, up to a Mach number of about 0·9, the elevator tab setting was different from that used in the previous dives on the same aircraft, and it was found that the pull required on the stick at high Mach numbers was considerably reduced by this change of tab setting. No quantitative results are available, but it appears that the elevator trimming tab on the Spitfire is still reasonably effective at a Mach number of about 0·9.

Tests at two different settings of the elevator trimming tab have also been made on a Meteor with extended nacelles[63]. In this case quantitative measurements were made, and it was found that when the tab angle was changed by 2 deg. the stick force (at 400 m.p.h. E.A.S.) was changed by about 25 lb. at $M = 0{\cdot}75$ and by about 30 lb. at $M = 0{\cdot}81$. It may be concluded that, within the accuracy of the measurements, the effectiveness of the elevator trimming tab on the Meteor is independent of Mach number up to $M = 0{\cdot}81$.

Although the tests mentioned above have shown that elevator tabs remain effective up to Mach numbers of 0·8 or 0·9, loss of tab effectiveness is to be expected at still higher Mach numbers. It is therefore recommended that, on aircraft which are expected to fly at Mach numbers approaching 1, an all-moving tail plane should be provided. This may either be adjustable in flight for trimming purposes, retaining the conventional elevator control, or the movable tail plane may be power operated and used as the only longitudinal control. The latter alternative is preferable for very high Mach numbers, because it can be shown theoretically[102] that the effectiveness of a conventional flap control is considerably less at supersonic than at subsonic speeds, whereas the effectiveness of an all-moving tail plane as a control is of the same order

at supersonic speeds as at subsonic speeds. Thus the effectiveness of an elevator control may be expected to fall off at some Mach number in the transonic range, even with the relief due to wing and body wakes mentioned above, but with an all-moving tail plane used as a control the loss of effectiveness would be less serious.

Most of the compressibility effects discussed in this report have occurred at Mach numbers above about 0·7. However, at points on an aircraft where the suction coefficients are high, it is possible for quite serious compressibility effects to appear at much lower Mach numbers.

An interesting example of a compressibility effect occurring at a comparatively low Mach number is the vibration which was experienced on the ailerons of the Spitfire[103]. During flight tests on a Spitfire II for the measurement of aileron characteristics, vibration was reported at large aileron angles. The tests were made at an altitude of about 5,000 ft., and at 200 m.p.h. E.A.S. ($M = 0{\cdot}3$) vibration occurred at an aileron angle of about 15 deg. The critical aileron angle for vibration was found to decrease steadily with increasing speed. Fig. 152 shows the variation with Mach number (or speed) of the aileron angle at which the vibration started. Tests in the 24 ft. wind tunnel at the R.A.E.[104] showed that very high suctions occurred on the protruding nose of the up-going aileron at large aileron angles, and it was therefore concluded that the aileron vibration experienced in flight was probably caused by compressibility effects on the up-going aileron. Further tests made in the high speed wind tunnel[51] showed that the compressibility effects at large negative aileron angles were due to separation of flow just behind the nose of the aileron, caused by the steep adverse pressure gradient. It was found that shock waves were not present at Mach numbers below about 0·6 at any aileron angle, because the separation mentioned above caused the peak suction coefficient on the aileron at large negative angles to decrease with increasing Mach number.

In some of the dive tests which have been made to investigate drag and longitudinal trim at high Mach numbers, aileron angles have also been measured. The results of these measurements have been used to determine the aileron float and the aileron angle applied by the pilot to prevent roll. Figs. 153 and 154 show the results for the Gloster E.28/39[85]. In both these diagrams the aileron angles shown are measured relative to the position at the same E.A.S. at a Mach number of 0·4, so that the variations shown are entirely due to changes of Mach number.

Fig. 153 shows that the aileron down-float tends to increase with Mach number for a constant E.A.S. The aileron angle applied the by pilot to prevent roll (Fig. 154) has little significance, except to indicate that the effects of varying Mach number on the wing characteristics are not quite the same on the port wing as on the starboard one. This may be due to a slight difference in the rigging of the two wings, or to a difference of surface finish.

6.6. *Longitudinal Oscillations.*—At present, there are two known types of longitudinal oscillation which may appear in flight at high Mach numbers on an aircraft which exhibits no oscillations at lower Mach numbers. The first of these types is caused by changes of elevator hinge-moment characteristics with Mach number, and the second is caused by shock stalling of the wing. The longitudinal oscillations which have been experienced on Vampire aircraft have not yet been explained and may not belong to either of these two classes.

The first type of oscillation, depending on changes of elevator hinge-moment characteristics with Mach number, was found during flight tests on the E.28/39[85]. In preliminary flights on an aircraft with a fabric-covered elevator, no oscillations were reported at any Mach number up to about 0·78. With a metal-covered elevator, however, longitudinal pitching oscillations of about one second period developed at a Mach number of about 0·72 and could not be stopped by the pilot. No oscillations were noticed at Mach numbers below about 0·72.

The pilot reported uncontrollable motion of the elevator during the oscillations. This, together with the fact that the oscillations had not been reported in previous flights with a fabric-covered elevator, suggested the elevator as a possible cause of the trouble. The elevator is convex in form, following the EC 1240 section of the tail plane with a trailing edge angle of 20 deg. It was suggested that the elevator characteristics, although satisfactory at low Mach numbers, might change with Mach number in such a manner as to give a longitudinal hunting

essentially similar to the directional " snaking " associated with convex or horn balanced rudders with positive b_1. Accordingly, the remedy usually applied for directional " snaking " was tried ; one foot of $\frac{3}{16}$-in. cord was attached to each side of the trailing edge of the elevator on top and bottom surfaces. This cured the oscillations up to $M = 0{\cdot}80$, where the pilot again reported incipient oscillations. The amount of cord was then doubled and no further longitudinal oscillations were reported, but at a Mach number of $0{\cdot}816$ buffeting and irregular rolling, yawing and pitching of the aircraft occurred. The cord on the elevator increased the stick forces considerably, but since the elevator control was normally very light this increase of stick force was not troublesome.

Longitudinal oscillations, similar to those found on the E.28/39, were observed on a Meteor (with lengthened nacelles) when the tail setting was increased by 1 deg. to make the elevator angle to trim approximately zero at high speeds. In this case the oscillations were cured by reducing the tail setting by $\frac{1}{2}$ deg.

The second type of longitudinal oscillation, caused by shock stalling of the wing, has been experienced on the Welkin[101] at a Mach number of about $0{\cdot}68$. Fig. 155 shows a typical record of the oscillations. There is apparently little or no correlation between the fluctuations of normal acceleration, elevator angle, and incidence. In particular, the fluctuations of incidence are much too small to account for the large fluctuations of normal acceleration, and the peak normal accelerations which are reached momentarily are greater than the maximum attainable steady values as found in other tests[32] at the same air speed and altitude. The probable explanation of these phenomena is that the wing is shock stalled during the oscillations, and that in this condition large fluctuations of lift coefficient can occur without any corresponding changes of incidence or elevator angle. The low Mach number at which the wing shock stalls is due to the large thickness ratio (21 per cent. at the nacelles). Attempts were made to reduce the oscillations by lowering the inboard flaps slightly, so as to increase the maximum lift coefficient at high Mach numbers. This only gave a small improvement, the Mach number at which the oscillations started, for a given normal acceleration, being increased by about $0{\cdot}03$ when the inboard flaps were lowered 15 deg. It is probable that a greater improvement than this could only be obtained by reducing the thickness ratio of the wing.

6.7. *Maximum Lift Coefficients at High Speeds.*—The maximum lift coefficient which can be obtained on an aircraft at a high Mach number is important, because it limits the normal acceleration which is possible in a turn at high altitude, and in some cases it may even limit the ceiling of the aircraft. Comparatively few measurements of maximum lift coefficient have been made in flight at high Mach numbers, mainly because a high altitude is required for the tests in order to reduce the normal accelerations required, and only a few aircraft are available which can reach the necessary high speeds at a high enough altitude. In some cases the quantity which is measured in flight is not the true maximum lift coefficient, but the highest lift coefficient which is possible without severe buffeting. This may be considerably less than the true maximum lift coefficient, but in these cases the latter cannot be reached in flight and has no practical significance.

Measurements of maximum lift coefficient at high Mach numbers have been made at the A. & A.E.E. on a Welkin[32]. In these tests, the maximum normal acceleration which could be reached in recovery from a dive at a high altitude was measured over a range of Mach numbers. The results are shown in Fig. 40, and have already been discussed (*see* 4.12). As mentioned above, the low maximum lift coefficient on the Welkin at high Mach numbers is associated with severe longitudinal pitching oscillations of the aircraft, caused by irregular fluctuations of lift on the shock stalled wing.

Tests have also been made at the A. & A.E.E. on a Spitfire IX[105], to determine the greatest normal acceleration which could be reached in recovery from a dive at a high altitude, over a range of Mach numbers. In this case the normal acceleration which could be obtained was limited by buffeting, and this occurred at a lift coefficient which was probably below the true maximum value. Fig 156 shows the variation with Mach number of the lift coefficient at which

buffeting starts. Comparison of Figs. 40 and 156 shows that, at high Mach numbers, considerably greater lift coefficients are possible on the Spitfire than on the Welkin, probably because of the smaller wing thickness ratio on the Spitfire.

At the R.A.E. no specific measurements of maximum lift coefficient have been made at high Mach numbers, but during diving tests for the investigation of drag and longitudinal trim, pull-outs have been made at fairly high normal accelerations. For example on a Meteor with long nacelles a pull-out has been made at $3g$ ($C_L = 0{\cdot}33$) at an altitude of 30,000 ft. and a Mach number of $0{\cdot}84$. In this case there was some buffeting, but there were no indications that the maximum lift coefficient had been reached.

6.8. *Wing Pressure Distributions.*—Measurements of pressure distribution at a section of the wing have been made in flight at high speeds on three aircraft, each having a different type of wing section. The aircraft used for these measurements were the Mustang[106], Spitfire XI[16], and Gloster E.28/39[85]. The Mustang wing had an early type of low-drag section. This differed in some respects from more recently designed sections, but no other high-speed aircraft with a low-drag wing section was available at the time. The Spitfire wing had a conventional section (NACA 2211). This section was designed many years ago[107], but the unusually good behaviour of the Spitfire at high speeds[98] had aroused considerable interest in the pressure distribution on this section at high Mach numbers. The third aircraft to be tested, the Gloster E.28/39, was fitted with a wing of EC 1240/0640 section. This section was designed with an elliptical fairing over the first 40 per cent. of the chord, in order to give a low peak suction coefficient and hence a high theoretical critical Mach number.

The tests on the Mustang I were completed and results were obtained up to the highest Mach number attainable on that aircraft. The tests on the Spitfire XI were in progress when, owing to a failure of the supercharger caused by propeller overspeeding, a forced landing was made and the aircraft caught fire, with the result that the tests had to be abandoned. On the E.28/39 only one pressure-plotting flight could be made before the aircraft was required for other purposes. Thus on both the latter aircraft the tests were not finished.

6.81. *Mustang I—results.*—Fig. 157 shows the section of the Mustang wing where the pressure measurements were made, with ordinates of the theoretical NA73 section and of the actual section on the aircraft. The test section was on the starboard wing, 114 inches from the aircraft centre line, and was in a position which was inboard of the aileron and yet outside the slipstream (Fig. 131). The landing flap extended across the test section, but this was kept at zero setting throughout the tests, and probably had little effect on the pressure distribution, except for a slight irregularity near the flap shrouds. The maximum thickness and camber of the wing test section were $14{\cdot}5$ per cent. and $1{\cdot}2$ per cent. of the chord respectively, and the maximum thickness occurred at abut 40 per cent. of the chord.

Fig. 158 shows pressure distributions on the Mustang wing section at low speeds, as obtained from tests in level flight. These results show that, at $C_L = 0{\cdot}2$ (roughly the design lift coefficient), there is a slight favourable pressure gradient on both surfaces over the first 50 per cent. of the chord. Thus the pressure distribution is of the type required for a low-drag wing section, but during the tests the transition point was probably near the leading edge because of waviness and roughness of the wing surface. The sudden increase of suction at about 70 per cent. of the chord is due to irregularities in the section profile near the flap shrouds.

Fig. 159 shows the variation of pressure coefficient with Mach number, for a constant mean (aircraft) lift coefficient of $0{\cdot}07$, at several points on the wing test section. At most points on the section, $(-C_P)$ increases gradually with Mach number until the local speed of sound is exceeded, then rises rapidly with further increase of Mach number. This rapid increase of suction coefficient occurs at a slightly lower Mach number on the upper surface than on the lower surface, even at this low value of C_L.

In Fig. 160, the full lines show the wing section pressure distributions at several Mach numbers, as obtained from the flight measurements. At Mach numbers above about $0{\cdot}7$, a high peak suction develops at about 50 per cent. of the chord on the upper surface, and at the same time

a peculiar kink appears in the pressure distribution at about 30 per cent. of the chord. Similar effects can be seen in the lower surface pressure distribution at the highest Mach number ($M = 0{\cdot}78$). The dotted curves in Fig. 160 show the results of wind tunnel tests on the same wing section, and are discussed below (*See* §7.1).

It was suspected that the high peak suctions observed on both upper and lower surfaces at high Mach numbers might be caused partly by bulging of the wing surface in flight. Loading tests[108] were therefore made on another Mustang I wing in order to determine the distortion of the upper surface caused by a uniform external suction. It was found that the suctions which occurred in flight at high speeds would cause deflections of the order of $\frac{3}{8}$ in. on the ammunition bay door. This door extends from 35 per cent. to 56 per cent. of the chord on the upper surface (Fig. 157). It was considered that distortions of this order would probably explain the unusually high peak suctions observed on the upper surface of the wing at high Mach numbers, and also the peculiar kink in the pressure distribution curve at about 30 per cent. of the chord. Although there is no door in the corresponding position on the lower surface, it is quite possible for distortions of the same order to occur there, thus explaining the high peak suctions observed on the lower surface at high speeds.

It may be noted that all the curves given in Fig. 160 show a return to a positive pressure coefficient at the trailing edge, indicating that there is probably no serious separation of the boundary layer at any Mach number up to $0{\cdot}78$.

Figs. 161 and 162 show the variation with Mach number of the section lift- and pitching-moment coefficients, as determined from the measured pressure distributions, for constant values of the aircraft lift coefficient. At a Mach number of about $0{\cdot}7$ the high suction which develops on the upper surface at about 50 per cent. of the chord causes an increase of section lift coefficient and a reduction of pitching-moment coefficient. At higher Mach numbers these effects are counteracted by the high suction on the lower surface at about 45 per cent. of the chord. However, since the high suctions observed on both upper and lower surfaces are probably caused partly by distortion of the wing in flight, the results given in Figs. 161 and 162 are also probably affected by distortion.

6.82. *Spitfire XI—results.*—Fig. 163 shows the wing test section on the Spitfire XI, together with the theoretical section NACA 2211_4. The test section was 98 inches from the aircraft centre line, inboard of the aileron and outside the slipstream (Fig. 129). The maximum thickness of this section is $11{\cdot}4$ per cent. chord, occurring at 30 per cent. of the chord.

No pressure measurements were made in front of the main spar (27 per cent. chord), because this part of the wing was occupied by a fuel tank. At the time of the tests it was thought that the absence of pressure measurements on the front part of the wing would not be important, but it is now realised that no satisfactory comparison with wind tunnel tests can be made unless the pressures are measured over the whole length of the chord, so that the section lift coefficients can be found. In an attempt to indicate the probable form of the curves in front of the spar, the theoretical pressure distributions for the wing section were calculated, for low Mach numbers, for several values of the section lift coefficient. However, it was not found possible to relate these theoretical curves to the experimental results, because the section lift coefficients for the latter were not known.

Fig. 164 shows the pressure distributions on the test section of the Spitfire wing, aft of the 27 per cent. chord point, for several Mach numbers at a constant aircraft lift coefficient of $0{\cdot}10$. With increasing Mach number the shock wave on the upper surface moves steadily back, until at a Mach number of $0{\cdot}85$ the local supersonic region extends over about half the chord. The formation of the lower surface shock wave cannot be seen in Fig. 164, because on this aerofoil section at low lift coefficients there is a high suction peak on the lower surface near the leading edge, so that the lower surface shock wave is first formed in front of the 27 per cent. chord point. The shock wave on the lower surface probably moves back at very high Mach numbers, and in Fig. 164 it can just be seen at a Mach number of $0{\cdot}85$ at about 30 per cent. chord.

The shock wave on the upper surface appears in Fig. 164 as a gradual rise of pressure spread over about 0·1 chord. Possible explanations of this gradual pressure rise have already been discussed (*See* § 4.11).

As in the tests on the Mustang wing, the pressure distributions shown in Fig. 164 all return to a positive pressure coefficient at the trailing edge, indicating that there is no serious separation of the boundary layer at any Mach number up to 0·85.

The curves in Fig. 159, showing the variation of pressure coefficient on the Spitfire wing with Mach number, differ in one respect from the corresponding curves for the Mustang wing. On the Spitfire wing the pressure coefficient at a given point is very nearly independent of Mach number, up to the Mach number at which a sudden increase of suction occurs, while on the Mustang wing there is a gradual increase of $(-C_p)$ with Mach number. However, the curves given in Fig. 159 refer to a constant mean (aircraft) lift coefficient, so that the incidence probably changes with Mach number, and hence the constancy of C_p shown for the Spitfire wing is not necessarily inconsistent with the Karman law.[15] The sudden increase of suction shown for the Spitfire wing at high Mach numbers is similar to that found on the Mustang wing, except that the change occurs at a considerably higher Mach number on the Spitfire than on the Mustang.

6.83. *E.28/39—results.*—Fig. 165 shows the test section of the wing on the Gloster E.28/39. This section is of the EC 1240/0640 series, with maximum thickness and camber of 11·7 per cent. and 0·6 per cent. of the chord respectively. The position of the maximum thickness is at 40 per cent. of the chord. The test section was 81 in. from the aircraft centre line, inboard of the aileron on the starboard wing.

As only one pressure-plotting flight could be made on this aircraft, results were only obtained for a limited range of Mach numbers (from 0·68 to 0·82).

Fig. 159 shows the variation of pressure coefficient with Mach number at several points on the test section, for a constant section lift coefficient of 0·11. The interesting point about these curves is that, over a large part of the wing, the pressure coefficient at a given point is lower when the Mach number is decreasing than when it is increasing. This hysteresis effect is particularly noticeable on the lower surface of the wing at 63 per cent. of the chord. No such hysteresis effect could be detected in the drag measurements on the same aircraft, or in measurements of pressure distribution on other aircraft. The effect is not yet understood, but it seems unlikely that it could be entirely due to faulty experimental technique.

Fig. 166 shows the chordwise pressure distributions on the wing test section at different Mach numbers and lift coefficients, arranged so that a direct comparison can be made between the distributions for increasing and decreasing Mach number at roughly the same Mach number and lift coefficient. For a given Mach number the upper surface shock wave is more intense when the Mach number is decreasing than when it is increasing. On the lower surface, with increasing Mach number, a weak shock wave appears at about 40 per cent. chord at a Mach number of about 0·78, the shock wave moving back and becoming stronger as the Mach number increases up to 0·82. When the Mach number decreases, the lower surface shock wave appears to divide into two parts, one staying at 65 per cent. chord and the other moving forward to 45 per cent. chord. These shock waves persist until a Mach number is reached which is lower than that at which a shock wave is first formed on the lower surface when the Mach number is increasing.

It might be expected that these hysteresis effects on pressure distributions would cause the profile drag coefficient of the test section to be greater, for a given Mach number, when the Mach number is decreasing than when it is increasing. In the profile drag measurements on the E.28/39 wing, no such effect could be detected, but in similar profile drag measurements on a Spitfire, a hysteresis effect of this kind was found (*See* § 6.9).

6.9. *Wing Profile Drag.*—Several attempts have been made to measure the profile drag of a wing section in flight at high speeds by the wake traverse method. These attempts have not been very successful at high Mach numbers, for the following reasons :—

(*a*) It is not practicable to make a pitot comb wide enough to include the whole of the wake

from the shock stalled wing. Hence with a comb of moderate size the profile drag can only be measured up to a Mach number a little above that at which shock waves are first formed.

(*b*) Even if the comb could be made wide enough to include the whole of the shock wave wake, the accuracy which would be required in the measurement of the small total head loss due to the shock waves would be greater than is possible with the instruments in use at present. This difficulty arises from the fact that the drag due to direct shock wave loss is measured as a small pressure difference extending over a large area, so that a small error in total pressure causes a comparatively large error in the drag.

(*c*) In several cases, the supports used for attaching the comb to the wing have caused serious interference effects on the total head measurements at the comb.

Profile drag measurements by the wake traverse method have been made on the Spitfire XI[17], Mustang I[109] and E.28/39[85], the test sections on the wings being the same as those used for the measurements of pressure distribution (Figs. 157, 163 and 165). In the case of the Spitfire XI, different aircraft were used for the measurements of profile drag and pressure distribution, but the position of the test section on the wing was the same in each case, and there were only slight differences in the shape of the test section. On the Mustang I and E.28/39, the measurements of profile drag and pressure distribution were made on the same aircraft.

Figs. 167, 168 and 169 show the results of the measurements on the Mustang I, Spitfire XI, and E.28/39. On the Mustang and Spitfire, the comb supports caused serious interference effects on the total head measurements near the ends of the comb, so that it was impossible to make even a rough estimate of the shock wave drag from the wake measurements. The highest Mach number reached in the Mustang tests (0·75) was so low that there may have been no appreciable drag due to direct shock wave losses. The curve given in Fig. 167, which does not include any direct shock wave drag, would then be correct. However, if there were appreciable shock waves formed at Mach numbers below 0·75, the true drag at high Mach numbers would be greater than is shown in Fig. 167, making the flight results agree better with the wind tunnel tests.[11]

On the Spitfire, there was certainly a considerable drag due to direct shock wave losses at the higher Mach numbers. Since this could not be measured directly by the wake traverse method, an attempt was made to calculate roughly the order of the upper surface shock wave drag, from the pressure distribution as measured at the same position on the wing of another Spitfire[16], and this very rough estimate is shown as the dotted curve in Fig. 168. No such estimate could be made for the lower surface shock wave drag, because the pressure distribution was not measured far enough forward on the wing to include the lower surface shock wave.

The full lines in Fig. 168 show the profile drag coefficient, excluding the drag due to direct shock wave losses. This part of the drag, which may be called the " basic " drag, includes the extra drag due to the effect of the shock waves on the boundary layer, but it does not include the direct effect of the shock waves on the drag. In wake traverse measurements, the basic drag is given by the area of the central part of the wake, not including the wake due to loss of total head at the shock waves.

For the Spitfire wing, the basic drag at a given Mach number was greater when the Mach number was decreasing than when it was increasing, as shown in Fig. 168. The explanation of this difference of basic drag is not yet known, but comparison of the wakes for increasing and decreasing Mach number shows that the extra drag when the Mach number is decreasing occurs mostly at the upper surface of the wing (Fig. 170). Thus some of the difference may be due to the greater lift coefficient in the later part of the dive, when the Mach number is decreasing, but it is unlikely that this could account for the whole of the difference shown in Fig. 168. The effect is similar to the hysteresis which has been observed in measurements of overall aircraft drag and in measurements of pressure distribution on the E.28/39 wing. It is not yet certain that these hysteresis effects are not caused by faulty experimental technique.

The results given in Fig. 168 show that the basic drag coefficient of the Spitfire wing section (excluding direct shock wave drag) is fairly small even at very high Mach numbers. For example,

the basic drag coefficient at a Mach number of 0·85 is only about 70 per cent. above the low-speed value, whereas at the same Mach number the rough estimate of the shock wave drag due to the upper surface alone is greater than the total profile drag coefficient at low speeds. Remembering that there is probably also a considerable shock wave drag due to the lower surface, it may be concluded that at a Mach number of 0·85 the greater part of the drag increase on this wing is probably caused by direct shock wave losses, and not by separation or thickening of the boundary layer. At higher Mach numbers, the proportion of the total drag increase which is due to direct shock wave losses is probably even greater. High-speed wind tunnel tests on the same section of a Spitfire wing have also shown that, at a low incidence, the drag due to direct shock wave losses is more important than the increase of basic drag (*See* § 4.14 and Ref. 42).

The results of the profile drag measurements on the E.28/39 wing are shown in Fig. 169. In this case there was no appreciable interference from the comb supports, and the shock wave drag could be measured up to a Mach number of 0·78. At higher Mach numbers the wake extended beyond the edges of the comb and the direct shock wave drag could not be determined. Even at Mach numbers below 0·78, however, the accuracy in determining the direct shock wave drag was poor, for the reasons already explained.

Because of the difficulties outlined above, no further measurements of profile drag in flight at high speeds will be made by the wake traverse method. In future, it is hoped that it will be possible to use measurements of pressure distribution to determine the form drag of a wing section in flight at high speeds.

7. *Comparisons between Wind Tunnel and Flight Results at High Speeds.*—Comparison of the results of high-speed wind tunnel tests with full scale flight measurements is a useful method of checking the validity of the tunnel results, and a number of flight and tunnel tests have been made for this purpose. In come cases, however, it has proved difficult to ensure that the conditions were strictly comparable in flight and in the tunnel, so that satisfactory comparisons cannot always be made. Some cases in which comparisons are valid are discussed below.

7.1. *Pressure Distributions.*—Fig. 160 shows a comparison between measurements of pressure distribution on a Mustang wing section in flight[106] and in the R.A.E. and N.P.L. High Speed Tunnels.[11] At Mach numbers up to about 0·6 there is fairly good agreement between the flight and tunnel results. At higher Mach numbers the flight results show considerably greater peak suctions than the tunnel results, but at least part of this discrepancy may be caused by distortion of the wing in flight (*See* § 6.81). In other respects the discrepancy between the flight and tunnel results is no greater than that between the results of the tests in the two different tunnels.

In comparing flight and wind tunnel results at high Mach numbers it should be remembered that the coefficients C_p, C_L, C_D, etc. vary rapidly with Mach number, and hence a comparatively small error in the measurement of Mach number may cause a fairly large change in the force or pressure coefficient. Thus some of the discrepancies shown in Fig. 160 for the higher Mach numbers may be caused partly by fairly small errors in the measurement of Mach number, either in flight or in the tunnel.

7.2. *Drag.*—Fig. 171 shows a comparison between tunnel and flight measurements of the drag of a Mustang I.[52, 98] The flight curve refers to the aircraft with radiator spoiler up, as represented in the model tests. The agreement at high Mach numbers is very good, but it should be noted that these flight results (with radiator spoiler up) were obtained from only one dive.

In Ref. 98 it is suggested that at high Mach numbers there is a large difference between the drag of a Spitfire as measured in flight and the drag measured in the High Speed Tunnel. However, the methods of determining the tunnel blockage and strut corrections have been considerably improved since the Spitfire tunnel tests[36] were made. The Mustang results were corrected by these improved methods, and since these show good agreement with flight tests it seems possible that a fairly large part of the discrepancy originally found on the Spitfire may have been due to wrong corrections to the tunnel results.

A further difficulty in comparing flight and tunnel measurements of drag at high Mach numbers is caused by the large effect on drag of comparatively small excrescences on the wing. On the Spitfire XXI, the Mach number for a given drag coefficient was increased by about 0·04 when the guns and blisters were removed (Figs. 130 and 137). This suggests that small differences in shape between the model and the full-scale aircraft might have appreciable effects on drag at high Mach numbers.

As already explained, the difficulties experienced in attempting to measure wing profile drag in flight at high speeds have made it impossible to obtain any satisfactory results for comparison with wind tunnel measurements.

7.3. *Trim changes at High Mach Numbers.*—Figs. 172 and 173 show the change of elevator angle to trim at high Mach numbers, for the Mustang and Spitfire, as determined from flight[98] and tunnel tests.[36, 52] The flight test results have been reduced to zero normal acceleration (1*g*), and the tunnel results are given for the corresponding lift coefficient. Most of the flight tests on the Mustang, described in Ref. 98, were made with the radiator spoiler down, a condition which was not represented in the tunnel tests. The flight results with radiator spoiler up, given in Fig. 172, were all obtained from one dive, and hence the accuracy of these results is not good. This may partly explain the differences between the flight and tunnel results, shown in Fig. 172.

The results given for the Spitfire in Fig. 173 show good agreement between flight and tunnel results, but the tunnel tests do not include high enough Mach numbers to show much of the trim change. The flight and tunnel tests were made on different " Marks " of Spitfire, but the effect of this difference on the trim change is probably not important. In Fig. 173, the tunnel results have been corrected for blockage, although this correction was not included in the results as originally given in Ref. 36. The uncertainties in the strut corrections for the Spitfire, mentioned above, are known to have much less serious effects on lift and pitching moment than on drag, so that the curve in Fig. 173 would probably not be affected much by revision of the strut corrections.

7.4. *Longitudinal Stability.*—It has already been shown that on most of the complete models tested in the High Speed Tunnel there has been a slight loss of manœuvre margin with increasing Mach number up to the shock stalling speed. Some tests were made on a Spitfire XXI (with guns and blisters removed) in order to investigate this effect in flight. Since only the stick-fixed manœuvre margin can be investigated in the tunnel, the quantity of importance in comparing the flight and tunnel results is the elevator movement per *g*. The change of this quantity from the value at $M = 0{\cdot}5$ is plotted in Fig. 174. The elevator movement per *g* was also calculated from the tunnel results, using the equation given in Ref. 67. Since this diagram shows only the change with Mach number, the flight results for two different C.G. positions ought to agree. Thus the difference between the two curves gives an indication of the experimental error in the flight tests. The difference between the flight and tunnel results is of the same order as this experimental error.

The flight tests on the Spitfire XXI were made at a constant indicated air speed and various altitudes, in order to change the Mach number while keeping C_L and distortion effects approximately constant. Hence, in deriving the tunnel curve in Fig. 174, allowance has been made for the variation of the term $\frac{a_1 \bar{V}}{2\mu_1}$ with altitude.

7.5. *Conclusions—Agreement with Flight Tests.*—From the evidence available at present, it seems that the results of high-speed tunnel tests, with the possible exception of drag measurements, are fairly reliable up to a Mach number of about 0·78 or 0·80. The reliability of drag measurements at high Mach numbers, either in a wind tunnel or in flight, is still rather uncertain. It is known that the drag of a wing at high Mach numbers is very sensitive to small changes of shape, and the effect of varying Reynolds number may also be important. Further, there are some indications from flight tests that the drag coefficient of a body or wing at a given Mach number may depend partly on the previous history of the flight, *e.g.* on whether the Mach number is increasing or decreasing.

At Mach numbers above about 0·8, the corrections to be applied to high-speed tunnel results are still very uncertain. It is probable that, at these high Mach numbers, the blockage corrections which are applied at present are too low. There are also considerable uncertainties in the determination of strut interference corrections at high Mach numbers. It is hoped, however, that both these causes of uncertainty will be reduced in the future.

8. *Conclusions and Future Developments.*—The flight and tunnel tests which have already been made have given some indication of the difficulties likely to be encountered in flying near the speed of sound. Much more experimental work will be required before it is possible to design an aircraft to fly satisfactorily at these high speeds, without any serious handling troubles, but a few important facts are now known which will help to minimise troubles due to compressibility effects at high speeds. It is known that reduction of the wing thickness-chord ratio is a most important and useful method of increasing the Mach number at which serious compressibility effects occur. Also, the nose-down trim change which probably occurs on all aircraft of conventional layout at high Mach numbers is considerably less severe with a symmetrical wing section than with a cambered one. Information obtained recently from Germany has shown that compressibility effects can be delayed to considerably higher Mach numbers by the use of a wing with a large angle of sweepback or with a very small aspect ratio. Other difficulties, such as tip stalling at low speeds and severe aero-elastic distortion effects, are associated with the use of highly swept-back wings, but it may be possible to overcome these in the future. On a wing with a very small aspect ratio, aero-elastic distortion is usually not important, but there may be difficulties caused by the large induced drag and low lift-curve slope.

The High Speed Tunnel work described in this report has been concerned entirely with subsonic Mach numbers, up to about 0·8. This Mach number has often been exceeded by diving aircraft during the last few years, and recently it has been reached in level flight. It is expected that much higher Mach numbers will be reached in flight during the next few years, and thus there is now an urgent need for wind tunnel research at transonic and supersonic speeds.

There is no serious difficulty in designing and using a supersonic tunnel for tests on models at Mach numbers above about 1·15 or 1·2. There are at present several of these tunnels in use at the N.P.L., but the largest of them have working sections only about a foot wide, and these are too small for satisfactory tests on complete aircraft models. Several larger supersonic tunnels are now being designed, however, and these will probably be running in a few years time.

As indicated above, wind tunnel tests at Mach numbers either below about 0·8 to 0·85 or above about 1·15 to 1·2 can be made without any very serious difficulties. On the other hand, tests at Mach numbers in the intermediate range, between about 0·85 and 1·15, involve very great difficulties which become increasingly serious as the speed of sound is approached. At Mach numbers near unity, the effects of tunnel wall interference become very uncertain. In addition, the phenomenon of " choking " imposes an upper limit of Mach number in a subsonic tunnel, and a similar effect imposes a lower limit in a supersonic tunnel. These effects can be minimised by using very small models, but the Reynolds number is then reduced. In the speed range where these small models have to be used a considerable increase of tunnel pressure is required to maintain a reasonable Reynolds number. This demands additional fan power and increases the stresses in the model and its supports. Also, if the conventional strut supports are used, the problems of support interference become much more serious as the model size is reduced. In the future, it may be possible to overcome these support difficulties by using a very small model supported from behind, but it will then be necessary to adopt a new technique for the measurement of forces and moments.

Because of the above difficulties in wind tunnel tests at Mach numbers near unity, it will be necessary to use free flight experiments to obtain much of the required information at transonic speeds. Tests of the kind described in this report, using full-scale, piloted aircraft, will be very useful in the future as a means of investigating the behaviour of aircraft near the speed of sound. With the increased thrusts which will shortly be available from jet-propulsion units, it will be possible to make many of these tests in level flight. This will considerably reduce the danger

which is at present involved in these experiments, but even in level flight the risks to the pilot are so great that other forms of free flight experiment, using pilotless models, are being considered. These models have the additional advantage that they can be constructed much more quickly and cheaply than a piloted aircraft, so that variations in the geometry of the aircraft can be investigated more easily. The simplest form of experiment, using pilotless models, consists of dropping the models from an aircraft. Measurements of pressure and acceleration are made by means of instruments in the model, and the readings of these are transmitted by radio to a ground station. This method is only suitable for drag measurements, however, because the model normally falls in a free trajectory at zero lift. A more useful, but more elaborate, method is to use radio-controlled models of complete aircraft, propelled by rocket or ram-jet. These models would be about 10 or 12 ft. in span, and in order to increase the endurance at high speeds they would be carried up to about 35,000 ft. on a conventional aircraft before releasing them. The use of rocket-powered models, driven along a straight railway track on the ground, has also been suggested as a means of investigating the forces acting on aircraft at Mach numbers near unity.

APPENDIX

Aerofoil Notation

1. *Standard N.A.C.A. System.*—In this system, four digits are used, preceded by the letters NACA. The first digit gives the percentage camber, the second gives the position of the maximum camber, and the last two give the maximum thickness, as a percentage of the chord. For example, the aerofoil NACA 2417 has 2 per cent. camber, with the maximum camber at 40 per cent. of the chord, and the maximum thickness is 17 per cent. of the chord.

2. *N.A.C.A. 5-Digit System.*—In this later system, 5 digits are used after the letters NACA. The first digit gives the percentage camber, the last two give the maximum thickness, and the second and third define the shape of the camber line. For example, the aerofoil NACA 23021 has 2 per cent camber, and a maximum thickness of 21 per cent. of the chord. The camber line shape is defined in this case by the digits 30, and is a conventional type of camber line (not reflex), with the maximum camber at 15 per cent. of the chord.

3. *British System.*—In a British system, used for early types of low-drag aerofoils, there are eight digits preceded by two or more letters. The letters give an indication of the type of algebraic expression used for calculating the thickness distribution. The first two digits give the maximum thickness, as a percentage of the chord, and the third and fourth give the position of the maximum thickness. The fifth and sixth digits give the percentage camber, and the last two give the position of the maximum camber. For example, the aerofoil EC 1240/0640 has an elliptical fairing over the front part of the aerofoil, forward of the maximum thickness, and a cubic fairing over the rear part. The maximum thickness is 12 per cent. of the chord, and the position of the maximum thickness is at 40 per cent of the chord. The percentage camber is 0·6 per cent. and the position of the maximum camber is at 40 per cent. of the chord.

LIST OF SYMBOLS

A Cross-sectional area of working section of tunnel (without model).

A_m Effective cross-sectional area of working section of tunnel, with model in position.

a Lift gradient $\frac{dC_L}{d\alpha}$ for wing and body.

a_1 Tail plane lift gradient.

a_2 Elevator effectiveness.

B Constant in equation (26).

$b_1 = \frac{dC_H}{d\alpha_T}$ for tail plane and elevator.

C_D Drag coefficient.

C_{D0} Profile Drag coefficient.

C_D' *See* Fig. 170.

C_{DB} " Basic " drag coefficient = C_D (total) − C_{DS}.

C_{DS} Drag coefficient due to direct shock wave loss.

C_H Hinge-moment coefficient.

C_L Lift coefficient (for complete aircraft except where otherwise stated).

$C_{L\,\max}$ Maximum lift coefficient.

C_{LT} Tail plane lift coefficient.

C_m Pitching-moment coefficient.

C_{m0} Pitching-moment coefficient at zero lift, for wing or complete aircraft without tail.

C_{mT} Pitching-moment coefficient on complete aircraft due to tail plane load.

C_{mw} Pitching-moment coefficient of wing and body.

C_p Pressure coefficient $= \frac{P - P_0}{\frac{1}{2}\rho V^2}$.

C_R Resultant force coefficient $= \sqrt{(C_L^2 + C_D^2)}$.

c Chord (of wing).

$\bar{c}$ Mean chord (of wing).

D Drag of aircraft.

D_a Distance between two aircraft (in position error measurements).

d Internal diameter of tube (in lag calculations).

$d_1\ d_2\ d_3$ Diameters of individual tubes (in lag calculations).

E *See* equation (15).

$F(h_c)$ Height lag function (*see* equation (34)).

f Focal length of camera lens (in photographic method of determining height).

$f(M)$ Compressibility function $= 1 + \frac{1}{4}M^2 + \frac{1}{40}M^2 + \ \ldots$

$G(h_c)$ Pressure lag function (*see* equation (33)).

g Acceleration due to gravity.

H Total head in wake of wing.

H_0 Total head in free stream at position of model (in tunnel), or as measured by aircraft pitot tube (in flight).

H_m Manœuvre margin (*see* equation (7)).

H_T " Tape measure " height.

$h = \frac{1}{\bar{c}}$ (Distance of aircraft C.G. behind L.E. mean chord).

$h_0 = \frac{1}{\bar{c}}$ (Distance of aerodynamic centre of wing and body behind L.E. mean chord).

h_1 Height of Spitfire above camera axis (in position error measurements).

h_2 True difference of height between two aircraft (in position error measurements).

h_c Corrected altitude.

Δh_c Altitude correction (for position error or lag).

K Theoretical lag factor (*see* equation (29)).

K_1 Experimental lag factor (*see* equation (38)).

K_{12} K_{13} K_{24} etc. Theoretical lag factors for individual tubes or instruments.

K_n Static margin $= -\frac{dC_m}{dC_R}$ (*see* equation (4)).

l Tail arm (distance from aircraft C.G. to tail plane $\frac{1}{4}$-chord point).

l_T Length of tube (in lag calculations).

l_{T1} l_{T2} l_{T3} Lengths of individual tubes (in lag calculations).

M Mach number (fully corrected unless otherwise stated).

M_0 Mach number corresponding to speed V_i and standard sea level.

M_c Mach number corresponding to speed V_c and height h_c.

M_r Mach number corresponding to speed V_r and indicated height.

M_{r0} Mach number corresponding to speed V_r and standard sea level.

$\frac{dm}{dt}$ = Rate of mass flow from tube into instrument (in lag calculations).

N Constant in equation (26).

n Reading of normal accelerometer in units of g ($n = 1$ in level flight).

P Local static pressure at any given point.

P_0 Static pressure in free stream (at position of model in empty tunnel) or in undisturbed air (in flight).

P_s Static pressure at aircraft static head.

ΔP Pressure change due to lag in tube.

p Relative pressure $= \frac{P_0 \text{ at given altitude}}{P_0 \text{ at standard sea level}}$.

p_1 Static pressure at reference hole in settling chamber.

p_2 Static pressure at reference hole at upstream end of working section.

} *See* Fig. 19.

Q	Volume of altimeter or other instrument.
$Q_1\ Q_2\ Q_3$	Volumes of individual instruments (in lag calculations).
R	Reynolds number.
R_a	Reading of longitudinal accelerometer.
S	Wing area.
S'	Tail plane area.
S_c	Pressure coefficient at aircraft static head $= \frac{P_s - P_0}{\frac{1}{2}\rho V^2}$
S_R	Slant range (in measurements of height and speed).
S_T	Internal cross-sectional area of tube (in lag calculations).
T	Temperature in working section of tunnel.
T_0	Stagnation temperature (as measured in settling chamber of tunnel).
T_r	Thrust.
t	Time.
$\frac{t_w}{c}$	$\frac{\text{Maximum thickness}}{\text{chord}}$ for wing.
V	Wind speed (in tunnel) or true air speed (in flight).
$\overline{V}$	Tail volume coefficient $= \frac{S'l}{S\bar{c}}$
V_c	Indicated air speed, corrected for calibration compressibility error.
V_E	Resultant true speed relative to earth (*i.e.* neglecting effect of wind on air speed).
V_i	Equivalent air speed $= V\sqrt{\sigma}$.
V_r	A.S.I. reading, corrected for instrument error only.
V_s	Speed of sound in undisturbed air at any given altitude.
V_{s0}	Speed of sound in undisturbed air at standard sea level (15° C.).
$\Delta_1 V$	Correction to air speed for calibration compressibility error $= V_c - V_r$.
$\Delta_2 V$	Correction to air speed for position error and compressibility error $= V_i - V_c$.
ΔV_i	Lag correction to indicated air speed.
v	Mean velocity in tube (in lag calculations).
v_2	$\frac{\Delta_2 V}{V_c}$ (*see* equation (19)).
v_d	Rate of descent of aircraft.
W	Aircraft weight.
w	Wing loading $= W/S$.
$\begin{pmatrix} X_1 & Y_1 \\ X_2 & Y_2 \end{pmatrix}$	Co-ordinates of two points on ground (in photographic method of determining height).
$\begin{pmatrix} x_1 & y_1 \\ x_2 & y_2 \end{pmatrix}$	Co-ordinates of two points on camera film, corresponding to points (X_1Y_1) and (X_2Y_2) on ground.

$(x_p\ y_p)$ Co-ordinates giving plan position of aircraft (in Radar measurement of speed and height).

x Distance along chord of wing from leading edge.

y Distance above or below wing chord line.

Z Constant in equation (10).

z Distance from closed end of tube (in lag calculations).

α Incidence.

α_T Tail plane incidence.

α_w Wing incidence.

β Compressibility factor $= (1 - M^2)^{1/2}$

γ Ratio of specific heats of air.

ε Mean downwash angle at tail plane.

η Elevator angle

$\eta_{P\,\max}$ Maximum propeller efficiency (in Fig 79).

η_T Tail plane setting, relative to wing chord.

θ Elevation (in Radar method of measuring speed and height).

θ' Angle measured in the pitching plane (in photographic method of determining height).

θ_c Angle between camera axis and horizontal (in position error measurements).

θ_D Angle of dive.

ξ Aileron angle.

μ Coefficient of viscosity of air.

μ_1 $\dfrac{w}{\rho l}$ (*see* equation (8)).

ρ Density of air in free stream (in tunnel) or of undisturbed air (in flight). Also density of air at a given point in tube (in lag calculations).

ρ' $= \dfrac{d\rho}{d\,t}$ (in lag calculations).

ρ_0 Density of air at sea level in standard atmosphere. Also value of ρ for $z = 0$ (in lag calculations).

ρ_l Value of ρ for $z = l$ (in lag calculations).

σ Relative air density $= \dfrac{\rho}{\rho_0}$.

ϕ Azimuth (in Radar method of measuring speed and height).

ϕ' Angle measured in the rolling plane (in photographic method of determining height).

ϕ_a Angle between axis of accelerometer and flight path.

N.P.L. National Physical Laboratory.

R.A.E. Royal Aircraft Establishment.

REFERENCES

No.	*Author*	*Title, etc.*
1	L. J. Briggs, G. F. Hull and H. L. Dryden	Aerodynamic Characteristics of Airfoils at High Speeds. N.A.C.A. Technical Report No. 207. 1924.
2	A. Bailey and S. A. Wood	Development of a High-speed Induced Wind Tunnel. R. & M. 1468. May, 1932.
3	A. Thom, J. S. Thompson and W. Port ..	Velocity Fluctuations in the R.A.E. High Speed Tunnel and in the 1/16 Scale Model. R.A.E. Report No. Aero. 2008. A.R.C. 8409. January, 1945. (Unpublished.)
4	J. S. Thompson and M. Marcowicz ..	Measurements of Turbulence in the R.A.E. High Speed Tunnel. R.A.E. Tech. Note No. Aero. 1232. A.R.C. 6966. July, 1943. (Unpublished.)
5	D. Adamson	Further Measurements of Turbulence in the R.A.E. High Speed Tunnel. R.A.E. Technical Note No. Aero. 1527. A.R.C. 8188. October, 1944. (Unpublished.)
6	J. Seddon	The Technique of Model Tests of Duct Systems in Aircraft, as used in the Small Wind Tunnels of the R.A.E. R.A.E. Report No. Aero. 2100. A.R.C. 9479. December, 1945. (Unpublished.)
7	H. Glauert	Wind Tunnel Interference on Wings, Bodies and Airscrews. R. & M. 1566. 1933.
8	S. Goldstein and A. D. Young	The Linear Perturbation Theory of Compressible Flow, with Applications to Wind-tunnel Interference. R. & M. 1909. July, 1943.
9	A. Thom	Blockage Corrections and Choking in a Closed High-speed Tunnel. R. & M. 2033. November, 1943.
10	A. Thom and M. Jones	Tunnel Blockage near the Choking Condition. R.A.E. Report No. Aero. 2056. A.R.C. 8878. June, 1945. (Unpublished.)
11	J. S. Thompson, M. Markowicz, J. A. Beavan and R. G. Fowler.	Pressure distributions and wake traverses on models of Mustang wing section in the R.A.E. and N.P.L. High Speed Tunnels. R. & M. 2251. August, 1944.
12	J. S. Thompson and D. Adamson ..	High Speed Wind Tunnel Measurements of Pressure Distribution on an Aerofoil of N.A.C.A. 23021 Section. R.A.E. Report No. Aero. 1985. A.R.C. 8350. November, 1944. (Unpublished.)
13	J. A. Beavan and G. A. M. Hyde ..	Examples of Pressure Distributions at Compressibility Speeds on EC 1250. R. & M. 2056. September, 1942.
14	G. Temple and J. Yarwood	The Approximate Solution of the Hodograph Equations for Compressible Flow. R.A.E. Report No. S.M.E. 3201. A.R.C. 6107. June, 1942. (To be published.)
15	Th. von Kármán	Compressibility Effects in Aerodynamics. *Journal of the Aeronautical Sciences.* Vol. 8. No. 9. July, 1941.
16	W. J. Charnley and W. A. Mair.. ..	Measurements of Pressure Distribution on a Spitfire Wing in Flight at High Speeds. R. & M. 2160. August, 1945.
17	W. A. Mair and W. J. Charnley ..	Profile Drag Measurements on a Spitfire Wing in Flight at High Speeds. R. & M. 2159. June, 1945.

REFERENCES—(*contd.*)

No.	*Author*	*Title, etc.*
18	W. A. Mair	German High Speed Wind Tunnel Tests on Four Aerofoils of Different Camber, with Comments. R.A.E. Technical Note No. Aero. 1685. A.R.C. 9058. September, 1945. (Unpublished.)
19	B. Göthert (comments by W. A. Mair) ..	German High Speed Wind Tunnel Results. R.A.E. Technical Note No. Aero, 1684. A.R.C. 9064. August, 1945. (Unpublished.)
20	W. A. Mair	Note on Critical Mach Numbers. R.A.E. Report No. Aero. 1961. A.R.C. 8093. August, 1944. (Unpublished.)
21	R. Smelt	Note on the Relation between High-speed Drag and Critical Mach Number—German Information. R.A.E. Technical Note No. Aero. 1663. A.R.C. 8908. July, 1945. (Unpublished.)
22	B. Göthert	Hochgeschwindigkeitsmessungen an einem Flügel sehr Kleiner Streckung im D.V.L. Hochgeschwindigkeitswindkanal. L.G.L. 156, 118. (Translated as M.A.P. Volkenröde R. & T. No. 370.)
23	H. Glauert	The Effect of Compressibility on the Lift of an Aerofoil. R. & M. 1135. September, 1927.
24	A. D. Young	Note on the Effect of Compressibility on the Lift-curve Slope of a Wing of Finite Span. R.A.E. Technical Note No. Aero. 1250. A.R.C. 7046. August, 1943. (Unpublished.)
25	W. F. Hilton	An Experimental Analysis of the Forces of Eighteen Aerofoils at High Speeds. R. & M. 2058. August, 1942.
26	A. Anscombe	High Speed Tunnel Tests on Aerofoils H.S.1 and H.S.2. R.A.E. Report No. Aero. 1811. A.R.C. 6740. March, 1943. (Unpublished.)
27	J. Caldwell and J. Y. G. Evans	High Speed Tunnel Tests on a Model of Typhoon I. R.A.E. Report No. Aero. 1815. A.R.C. 6741. April, 1943. (Unpublished.)
28	J. Caldwell, J. Y. G. Evans and F. W. Jackson.	High Speed Tunnel Tests on the Tempest V with Nose Radiator. R.A.E. Report No. Aero. 1828. A.R.C. 6934. June, 1943. (Unpublished.)
29	W. A. Mair, S. P. Hutton and H. E. Gamble.	High Speed Wind Tunnel Tests on the Supermarine F.1/43. R.A.E. Report No. Aero. 1908. A.R.C. 7596. January, 1944. (Unpublished.)
30	W. A. Mair, S. P. Hutton and H. E. Gamble.	High Speed Wind Tunnel Tests on a Twin-engined Naval Aircraft (Short S.11/43). R.A.E. Report No. Aero. 2062. A.R.C. 9040. August, 1945. (Unpublished.)
31	W. A. Mair, S. P. Hutton and H. E. Gamble.	High Speed Wind Tunnel Tests on the Welkin. R.A.E. Report No. Aero. 1888. A.R.C. 7388. November, 1943. (Unpublished.)
32	D. R. H. Dickinson	Welkin F., Mk. I. D.X.279. Effect of Mach Number on Dive and Recovery Characteristics. 14th Part of Report No. A. & A.E.E./808. A.R.C. 7854. March, 1944. (Unpublished.)
33	J. Caldwell, J. Y. G. Evans and F. W. Jackson.	High Speed Wind Tunnel Tests on a Twin Boom Jet-propelled Fighter (Vampire). R.A.E. Report No. Aero. 2026. A.R.C. 8711. March, 1945. (To be published.)
34	W. A. Mair, S. P. Hutton and H. E. Gamble.	High Speed Wind Tunnel Tests on the Meteor I. R.A.E. Report No. Aero. 1833. A.R.C. 7013. July, 1943. (To be published.)

REFERENCES—(*contd.*)

No.	*Author*	*Title, etc.*
35	W. A. Mair, S. P. Hutton and H. E. Gamble.	High Speed Wind Tunnel Tests on a Twin-engined Fighter (Hornet). R.A.E. Report No. Aero. 1971. August, 1944. (Unpublished.)
36	W. A. Mair, S. P. Hutton and H. E. Gamble.	High Speed Wind Tunnel Tests on the Spitfire I. R.A.E. Report No. Aero. 1810. A.R.C. 6739. March, 1943. (To be published.)
37	W. A. Mair	Note on the Effect of Compressibility on C_{m0}. R.A.E. Technical Note No. Aero. 1293. A.R.C. 7236. October, 1943. (Unpublished.)
38	W. F. Hilton	Empirical Laws for the Effect of Compressibility on Quarter Chord Moment Coefficient, and for the Choice of an Aerofoil with Small Compressibility Effects on C.P. R. & M. 2195. March, 1943.
39	J. Y. G. Evans	High Speed Wind Tunnel Tests on an Aerofoil suitable for Tailless Aircraft. R.A.E. Report No. Aero. 1899. A.R.C. 7515. December, 1943. (Unpublished.)
40	W. A. Mair	Note on Trim Changes at High Mach Numbers. R.A.E. Report No. Aero. 1918. A.R.C. 7721. March, 1944. (Unpublished.)
41	G. I. Taylor	Applications to Aeronautics of Ackeret's Theory of Aerofoils moving at Speeds Greater than that of Sound. R. & M. 1467. April, 1932.
42	J. S. Thompson and W. Port	High-speed Wake Traverse Drag Measurements on a Model Spitfire Half-wing. R. & M. 2152. May, 1945.
43	J. A. Beavan	Note on Rise of Drag above the Critical Mach Number—Results in the N.P.L. High Speed Tunnels. A.R.C. 8682. May, 1945. (Unpublished.)
44	B. Göthert	Profilmessungen im Hochgeschwindigkeitskanal 2·7m.Φ. F.B. 1490. 1941. (M.O.S. Völkenrode Reports and Translations No. 410.)
45	W. A. Mair and H. E. Gamble ..	The Effect of Model Size on Measurements in the High Speed Tunnel. Part I.—Drag of Two-dimensional Symmetrical Aerofoils at Zero Incidence. R.A.E. Report No. Aero. 1998. A.R.C. 8372. December, 1944. (To be published.)
46	C. N. H. Lock, W. F. Hilton and S. Goldstein.	Determination of Profile Drag at High Speeds by a Pitot-traverse Method. R. & M. 1971. September, 1940.
47	J. S. Thompson	A Simple Method of Computing C_D from Wake Traverses at High Speeds. R.A.E. Report No. Aero. 2005. A.R.C. 8462. December, 1944. (Unpublished.)
48	J. Caldwell, J. Y. G. Evans and F. W. Jackson.	High Speed Tunnel Tests of an EC1540 Aerofoil with 20 per cent. Plain Flap fitted with Balance Tabs. R.A.E. Report No. Aero. 1923. A.R.C. 7888. March, 1944. (Unpublished.)
49	J. Caldwell, B. D. Hills and F. W. Jackson.	High Speed Tunnel Tests of a 0·4 Scale Model of the Typhoon I Tail Plane and Elevator. R.A.E. Report No. Aero. 1836. A.R.C. 7072. July, 1943. (Unpublished.)
50	J. Caldwell, B. D. Hills and F. W. Jackson.	High Speed Tunnel Tests of a Tail Plane Elevator of EC1240 Section. R.A.E. Report No. Aero. 1839. A.R.C. 7139. July, 1943. (Unpublished.)
51	W. A. Mair, J. S. Thompson and S. P. Hutton.	High Speed Wind Tunnel Tests on a Spitfire Type Wing and Aileron. R.A.E. Report No. Aero. 1848. A.R.C. 7169. August, 1943. (Unpublished.)

REFERENCES—(*contd.*)

No.	*Author*	*Title, etc.*
52	J. Y. G. Evans, J. Caldwell and C. M. Britland.	High Speed Wind Tunnel Tests on a Single-engined Fighter (Mustang I). R.A.E. Report No. Aero. 2038. A.R.C. 8707. April, 1945. (To be published.)
53	W. A. Mair, S. P. Hutton and H. E. Gamble.	High Speed Wind Tunnel Tests on the Mosquito (Twin-engined Fighter). R.A.E. Report No. Aero. 2000. A.R.C. 8525. December, 1944. (Unpublished.)
54	S. P. Hutton and H. E. Gamble	High Speed Wind Tunnel Tests on an Aircraft designed for Supersonic Speeds (Miles E.24/43). R.A.E. Report No. Aero. 2057. A.R.C. 8904. July, 1945. (To be published.)
55	J. Y. G. Evans and C. M. Britland ..	High Speed Tunnel Tests on a Tailless Aircraft (AW52G). R.A.E. Report No. Aero. 2048. A.R.C. 8773. May, 1945. (Unpublished.)
56	C. M. Britland	High Speed Wind Tunnel Tests on a suggested Vampire Development (DH 107). R.A.E. Technical Note No. Aero. 1726. A.R.C. 9456. November, 1945. (Unpublished.)
57	S. P. Hutton, D. A. Clarke and D. J. Tremlett.	High Speed Wind Tunnel Tests on a Jet-propelled Fighter (Supermarine E.10/44). R.A.E. Report No. Aero. 2112. A.R.C. 9559. January, 1946. (To be published.)
58	R. Smelt	Note on Longitudinal Stability and Trim Changes at Speeds near the Speed of Sound. R.A.E. Report No. Aero. 1911. A.R.C. 7551. February, 1944. (Unpublished.)
59	B. S. Benson and J. St. L. Philpot ..	An Aerofoil System whose Subsonic Centre of Pressure is at or behind its Supersonic Centre of Pressure. R. A. E. Technical Memorandum No. Inst. 122.
60	W. A. Mair and S. P. Hutton	High Speed Wind Tunnel Tests on Extended Nacelles for the Meteor I. R.A.E. Technical Note No. Aero. 1474. A.R.C. 8241. July, 1944. (To be published.)
61	W. A. Mair and S. P. Hutton	Further High Speed Wind Tunnel Tests on Extended Nacelles for the Meteor (F.9/40). R.A.E. Technical Note No. Aero. 1631. April, 1945. (Unpublished.)
62	G. F. Hughes and C. M. Britland ..	High Speed Tunnel Measurements of the Effect of Tailplane Height on the Stability and Trim of the Meteor and Vampire. R.A.E. Technical Note No. Aero. 1696. A.R.C. 9183. October, 1945. (To be published.)
63	F. Smith and A. W. Thom	Flight Tests on Meteor I. E.E.211 (Twin-engined Jet-propelled Fighter), with Lengthened Nacelles. R.A.E. Report No. Aero. 2064. A.R.C. 8998. July, 1945. (Unpublished.)
64	E. P. Bridgland	A Collection of Data on Dive Recovery Flaps. R.A.E. Technical Note No. Aero. 1710. A.R.C. 9252. October, 1945. (Unpublished.)
65	S. Neumark and A. D. Young	A Simplified Approach to the Problem of the Recovery of an Aeroplane from a High-speed Dive with Constant Elevator Angle. R.A.E. Report No. Aero. 1905. A.R.C. 7423. January, 1944. (Unpublished.)
66	C. M. Britland	High Speed Wind Tunnel Tests on Dive Recovery Flaps for a Single-engined Fighter (Tempest V). R.A.E. Technical Note No. Aero. 1683. A.R.C. 9253. September, 1945. (Unpublished.)

REFERENCES—(*contd.*)

No.	*Author*	*Title, etc.*
67	S. B. Gates and H. M. Lyon	A Continuation of Longitudinal Stability and Control Analysis. Part I. General Theory. R. & M. 2027. February, 1944.
68	P. R. Owen..	The Effect of Compressibility on Longitudinal Stability below the Shock Stall. R.A.E. Report No. Aero. 1829. A.R.C. 7803. March, 1944. (To be published.)
69	J. Y. G. Evans	High Speed Tunnel Investigation of the Velocity Distribution in the Tailplane Regions of Typical High-speed Aircraft. R.A.E. Report No. Aero. 2004. A.R.C. 8450. December, 1944. (Unpublished.)
70	W. Port	High Speed Wind Tunnel Measurements of Pressure Distribution on Extended Nacelles for the Meteor I. R.A.E. Technical Note No. Aero. 1588. A.R.C. 8566. January, 1945. (Unpublished.)
71	W. A. Mair and S. P. Hutton	High Speed Wind Tunnel Tests on Nacelles for a Twin-engined Fighter (Hornet). R.A.E. Technical Note No. Aero. 1521. A.R.C. 8226. October, 1944. (Unpublished.)
72	G. S. Hislop and J. Caldwell	Tests of Model Propellers in the High Speed Tunnel ; Thrust and Torque Measurements on a 2-blade, 6 per cent. thick, Clark Y Section Propeller. R.A.E. Report No. Aero. 2096. A.R.C. 9408. November, 1945. (Unpublished.)
73	J. Caldwell, J. Y. G. Evans and F. W. Jackson.	High Speed Tunnel Measurements of the Effect of a Propeller at Zero Torque on the Pitching and Yawing Moments of a Single-engine Fighter (Typhoon I). R.A.E. Report No. Aero. 1958. A.R.C. 8058. July, 1944. (Unpublished.)
74	P. R. Owen	Note on the Scale Effect on Stick-fixed Static Longitudinal Stability in the Glide. R.A.E. Technical Note No. Aero. 1104. A.R.C. 6394. December, 1942. (Unpublished.)
75	S. P. Hutton	High Speed Tunnel Tests on a Mock-up 20 m.m. cannon. R.A.E. Technical Note No. Aero. 1215. June, 1943. (Unpublished.)
76	S. P. Hutton	Tests on External Stores on a 1/7·5 Scale Model Meteor I in the High Speed Wind Tunnel. R.A.E. Technical Note No. Aero. 1498. A.R.C. 8158. September, 1944. (Unpublished.)
77	S. P. Hutton	High Speed Wind Tunnel Tests on Airship Type Drop Tanks for the Meteor I. R.A.E. Technical Note No. Aero. 1575. January, 1945. (Unpublished.)
78	W. A. Mair and S. P. Hutton	High Speed Wind Tunnel Tests on Cabins for the Supermarine F.1/43. R.A.E. Technical Note No. Aero. 1247. A.R.C. 7045. July, 1943. (Unpublished.)
79	W. Stewart	Effect of Conical Windscreen on Performance of a Spitfire IX. R.A.E. Technical Note No. Aero. 1284. September, 1943. (Unpublished.)
80	S. P. Hutton	Underwing Pressure Head and Static Vent on Model Typhoon at High Speed. R.A.E. Technical Note No. Aero. 1195. A.R.C. 6754. May, 1943. (Unpublished.)
81	A. D. Young, G. L. Green and E. Young	High Speed Wind Tunnel Tests of the Effect of Camouflage Paint Roughness on Drag. R.A.E. Report No. Aero. 1977. A.R.C. 8152. October, 1944. (To be published.)

REFERENCES—(*contd.*)

No.	*Author*	*Title, etc.*
82	D. Cameron	Note on the Effect of Position Error on the Compressibili Correction. A. & A.E.E. Report No. Res. 147. A.R.C. 574 May, 1941. (Also addendum dated September, 1941. A.R.(5748). (Unpublished.)
83	H. B. Squire and E. Milford	Table of Compressibility Corrections. R.A.E. Technical Note N. Aero. 971. A.R.C. 5957. June, 1942. (Unpublished.)
84	W. J. D. Annand and M. G. V. Paine ..	Compressibility Corrections in the Presence of Position Error– Revised Formulae. A. & A.E.E. Report No. Res. 208. A.R.(7879. May, 1944. (Unpublished.)
85	A. W. Thom, F. Smith and J. Brotherton	Flight Tests at High Mach Number on E.28/39 W.4041 (Singl(engined Jet-propelled Aircraft). R. & M. 2264. October, 194!
86	D. J. Lyons and J. G. Walker	A Review of Pitot-static Systems in High-speed Aircraft. R.A.E Technical Note No. Aero. 1659. A.R.C. 8885. July, 194! (Unpublished.)
87	W. J. Charnley	A Note on a Method of Correcting for Lag in Aircraft Pitot-stati Systems. R.A.E. Report No. 2156. A.R.C. 10,118. Septembei 1946. (To be published.)
88	S. Goldstein (Editor)	Modern Developments in Fluid Dynamics. Vol. I. Oxford, 193!
89	W. A. Wildhack	Pressure Drop in Tubing in Aircraft Instrument Installations N.A.C.A. Technical Note No. 593. February, 1937.
90	R. M. Head	Lag Determination of Altimeter Systems. *Journal of the Aeronautica Sciences*. January, 1945.
91	D. W. Lang and W. J. Charnley ..	Measurement of Aircraft Tape Measure Height and Speed in Hig speed Dives by a Photographic Method and by Radar Tracking R.A.E. Report No. Aero. 2109. A.R.C. 9558. January, 1946 (To be published.)
92	H. L. Stevens and A. E. Woodward Nutt	Charts for Aircraft Performance Reduction. R. & M. 1316. April 1930.
93	G. S. Hislop, A. K. Weaver and P. H. Blundell.	Further Measurements of Aircraft Speed by Radar, using G.L. Mk. III and S.C.R.584. A. & A.E.E. Report Res. 219. A.R.C. 9312. June, 1945. (To be published.)
94	R. Smelt	Direct Indication of Mach Number in Flight. R.A.E. Technical Note No. Aero. 1112. A.R.C. 6855. January, 1943. (Unpublished.)
95	F. Smith and A. W. Thom	Note on the use of a Longitudinal Accelerometer for measuring Aircraft Drag in Flight in the Dive. R.A.E. Technical Note No. Aero. 1649. June, 1945. (Unpublished.)
96	Cambridge University Aeronautics Laboratory.	The Measurement of Profile Drag by the Pitot-traverse Method. R. & M. 1688. January, 1936.
97	W. J. Charnley and R. Rose	Measurements of Overall Drag and Trim Change on Spitfires XI and XXI in Flight at High Mach Numbers. R.A.E. Report (not yet issued).
98	R. Smelt, W. J. Charnley and R. Rose..	Drag and Trim Changes on Spitfire, Mustang and Thunderbolt in Flight at High Mach Numbers. R.A.E. Report No. Aero. 1906. A.R.C. 7424. January, 1944. (Unpublished.)

REFERENCES—(*contd.*)

No.	*Author*	*Title, etc.*
99	E. P. Bridgland and R. Rose	Flight Tests of Dive Recovery Flaps on a Single-engine Low-wing Monoplane (Thunderbolt). R.A.E. Technical Note No. Aero. 1704. October, 1945. (Unpublished.)
100	E. P. Bridgland	Flight Tests of Dive Recovery Flaps on a Twin-engine Fighter Aircraft (Lightning). R.A.E. Technical Note No. Aero. 1702. A.R.C. 9251. October, 1945. (Unpublished.)
101	W. A. Mair, E. P. Bridgland and R. Rose	Flight Tests on a Welkin I to investigate Pitching Oscillations at High Mach Numbers. R.A.E. Report No. Aero. 2114. A.R.C. 9568. February, 1946. (Unpublished.)
102	A. R. Collar	Theoretical Forces and Moments on a Thin Aerofoil with Hinged Flap at Supersonic Speeds. R. & M. 2004. November, 1943.
103	D. J. Lyons, J. H. Martin and C. H. Naylor.	Flight Measurements of the Hinge Moments on Single Ailerons of the Spitfire. Part I. Tests on Port Aileron No. 1. R.A.E. Report No. Aero. 1801. A.R.C. 6610. February, 1943. (To be published.)
104	L. F. Nicholson, C. Roe and W. E. Gray	Spitfire Aileron Tests in the 24-ft. Wind Tunnel. Part II. Full-scale Tests. R.A.E. Report No. Aero. 1812. A.R.C. 6883. April, 1943. (Unpublished.)
105	M. G. V. Paine and D. R. H. Dickinson	Spitfire H.F. Mk. IX. B.S.310. Effect of Mach Number on Dive and Recovery Characteristics. 37th Part of Report No. A. & A.E.E./692m. A.R.C. 7923. 1944. (Unpublished.)
106	W. J. Charnley	Flight Measurements of Pressure Distribution around a Mustang Wing Section at High Speed. R.A.E. Report No. Aero. 1982. A.R.C. 8154. October, 1944. (Unpublished.)
107	E. N. Jacobs, K. E. Ward and R. M. Pinkerton.	The Characteristics of 78 Related Airfoil Sections from Tests in the Variable Density Wind Tunnel. N.A.C.A. Technical Report No. 460. 1933.
108	R. B. Coles	Wing Surface Distortion Tests on a Mustang I. R.A.E. Report No. S.M.E. 3334. A.R.C. 8837. June, 1945. (Unpublished.)
109	W. J. Charnley and W. A. Mair ..	Preliminary Profile Drag Measurements on a Mustang Wing in Flight at High Speeds. R.A.E. Technical Note No. Aero. 1604. A.R.C. 8554. February, 1945. (Unpublished.)

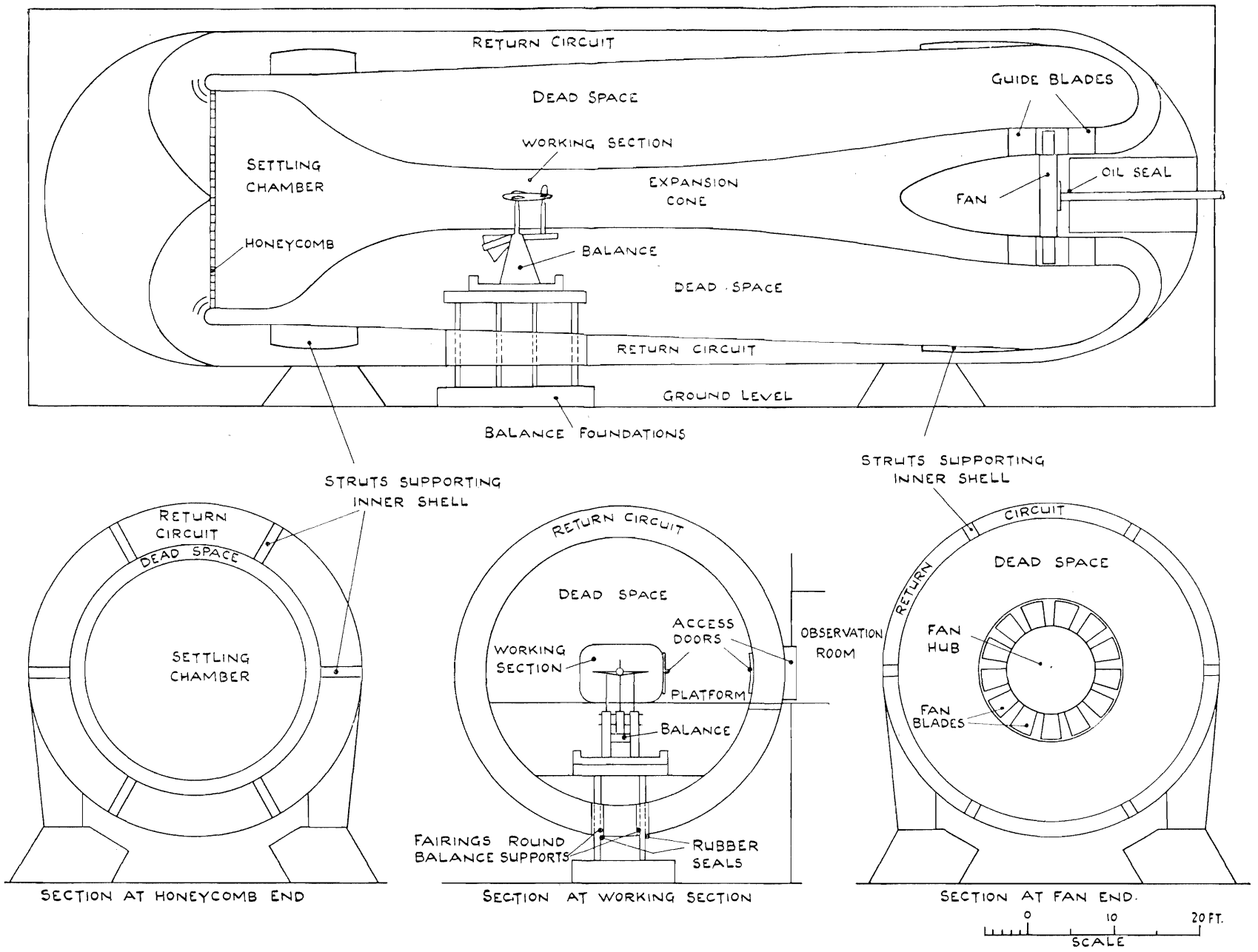

FIG. 1. General Arrangement of the High Speed Tunnel.

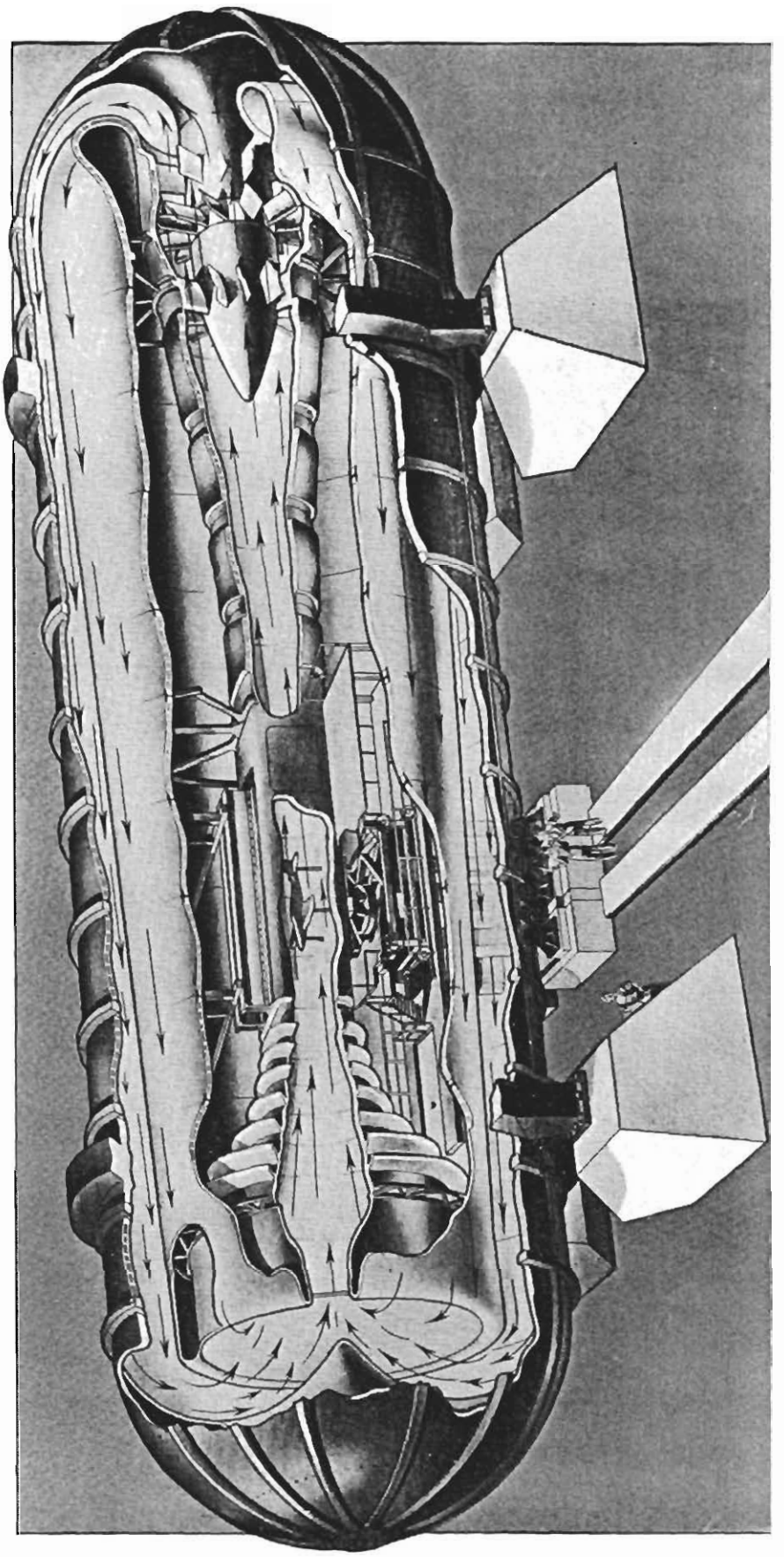

FIG. 2. Pictorial View of High Speed Tunnel.

(87158)

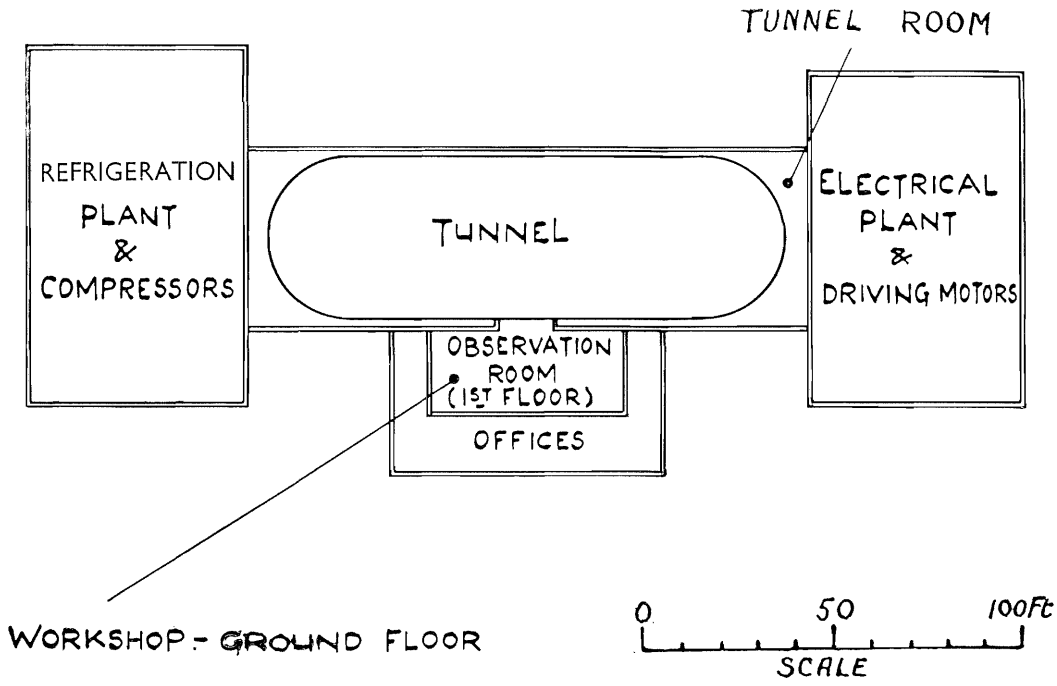

FIG. 3. Lay-out of Buildings.

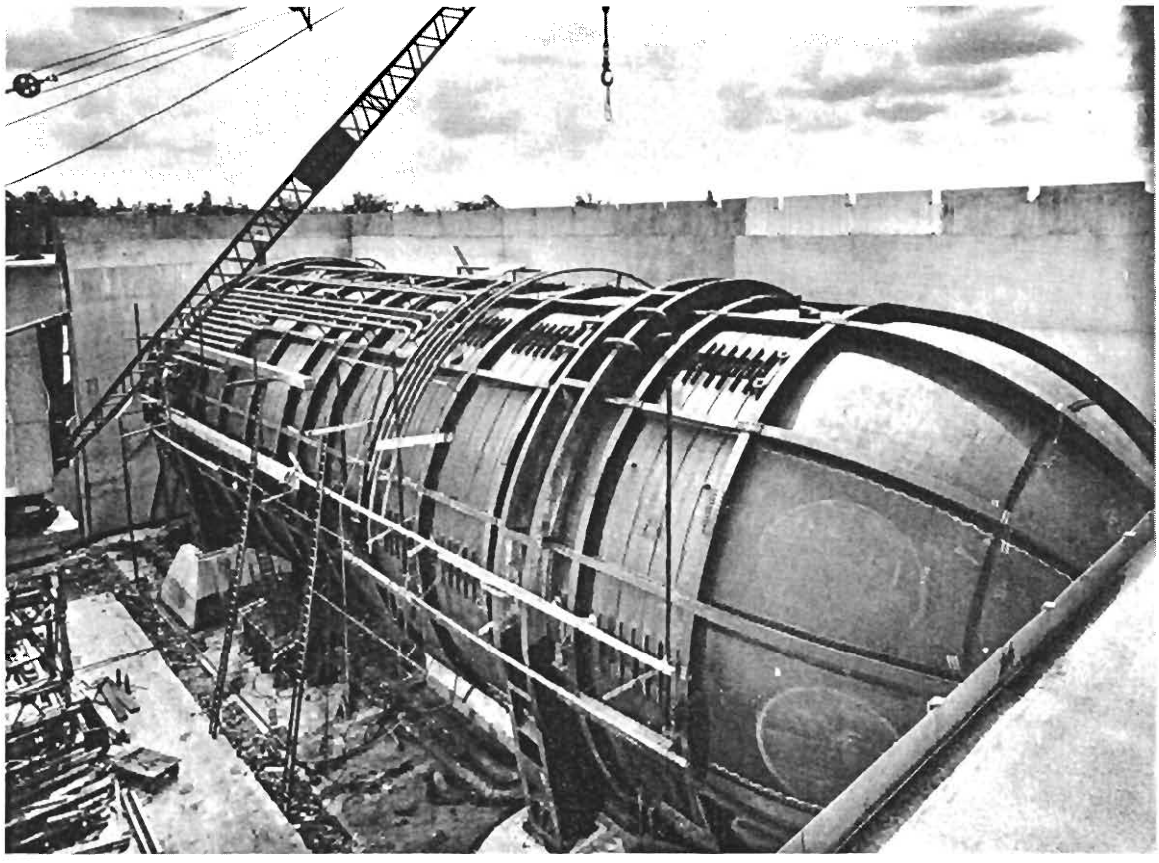

FIG. 4. Tunnel During Erection (1941).

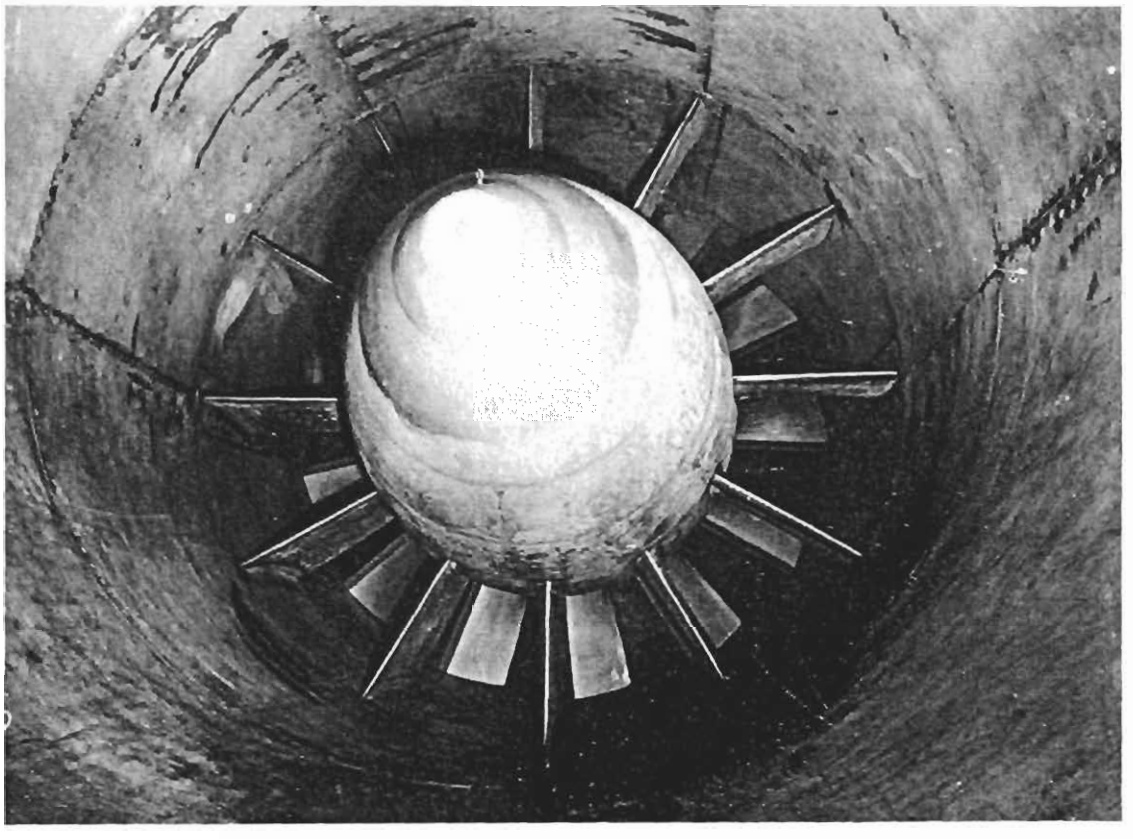

FIG. 5. Fan and Guide Blades in Tunnel.

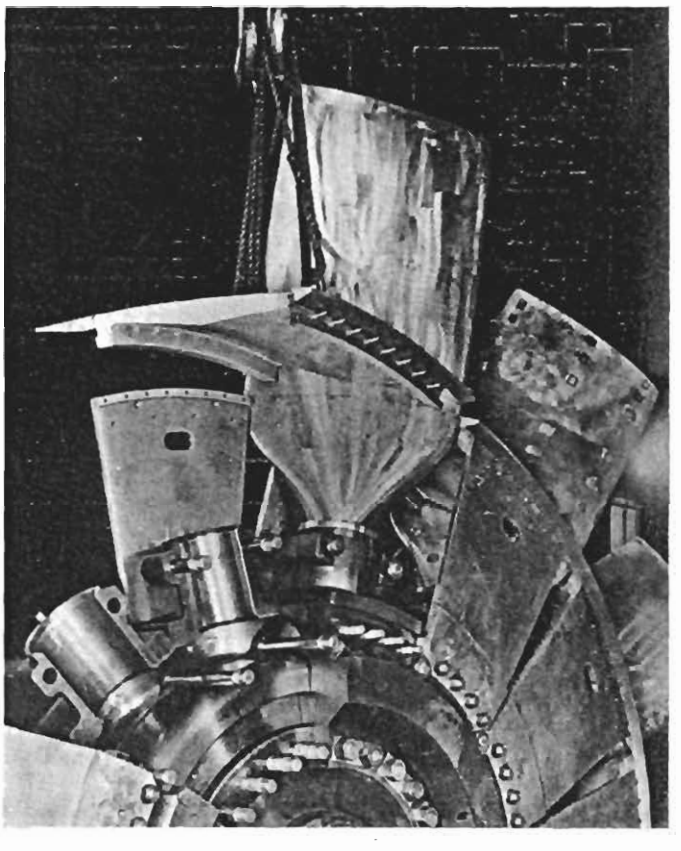

FIG. 6. High Speed Tunnel Fan During Assembly.

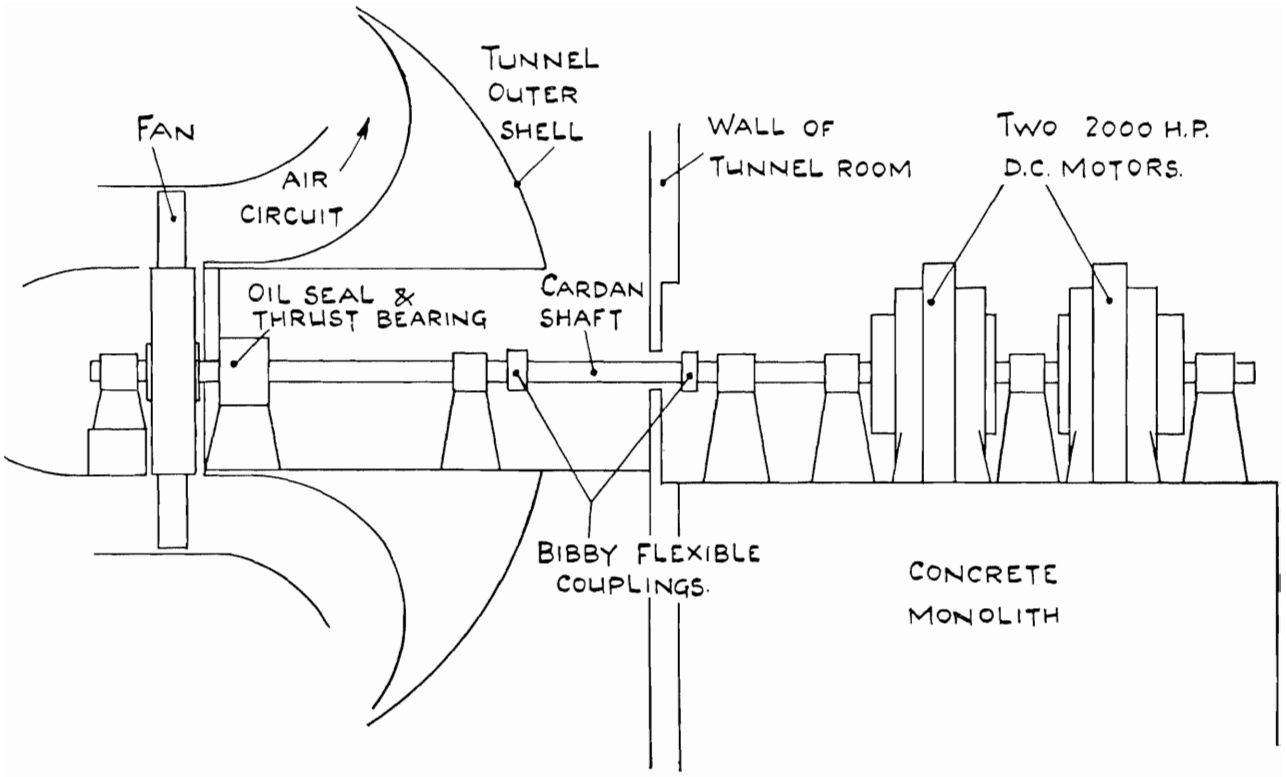

FIG. 7. Arrangement of Fan Drive and Bearings.

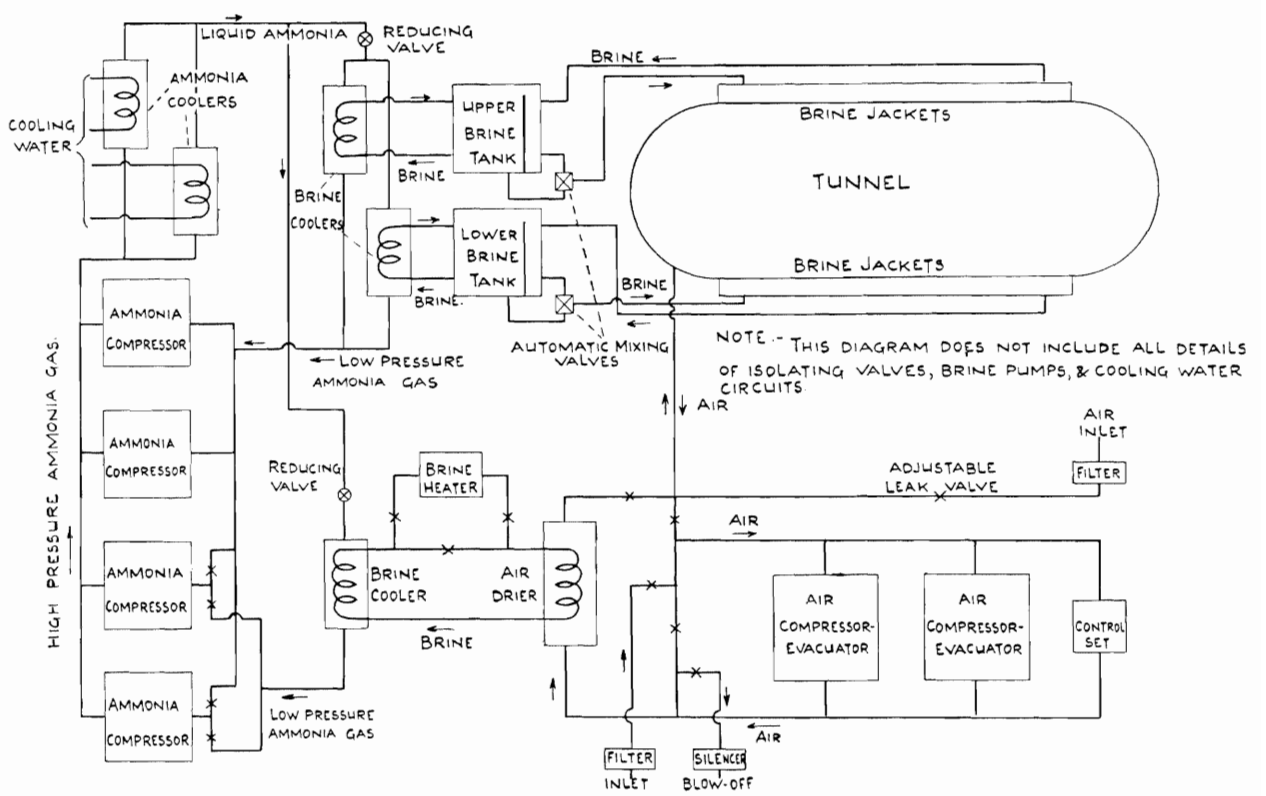

FIG. 8. Diagram of Compressor and Refrigerator Circuits.

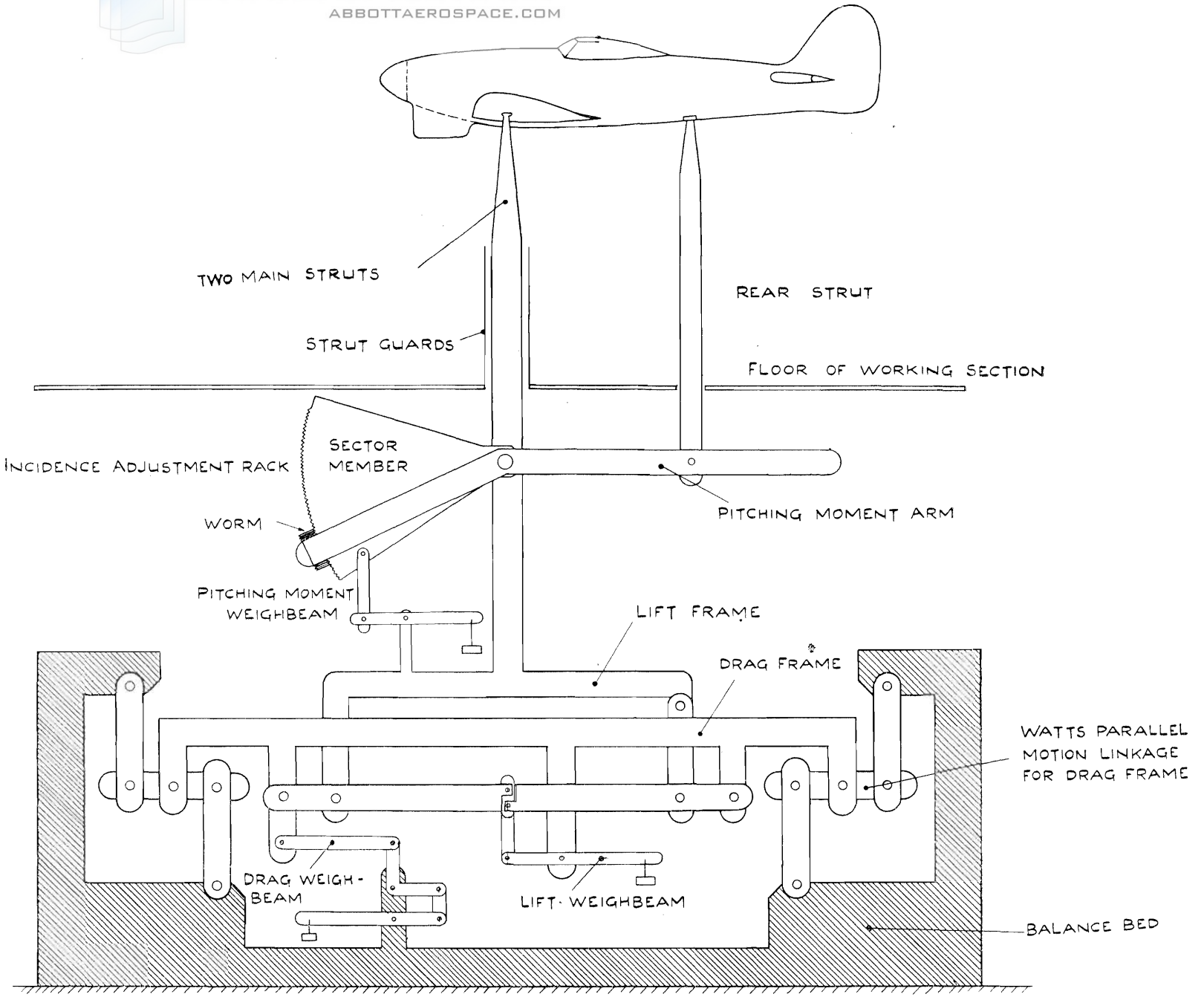

FIG. 9. Principle of Lift, Drag and Pitching-moment Balance.

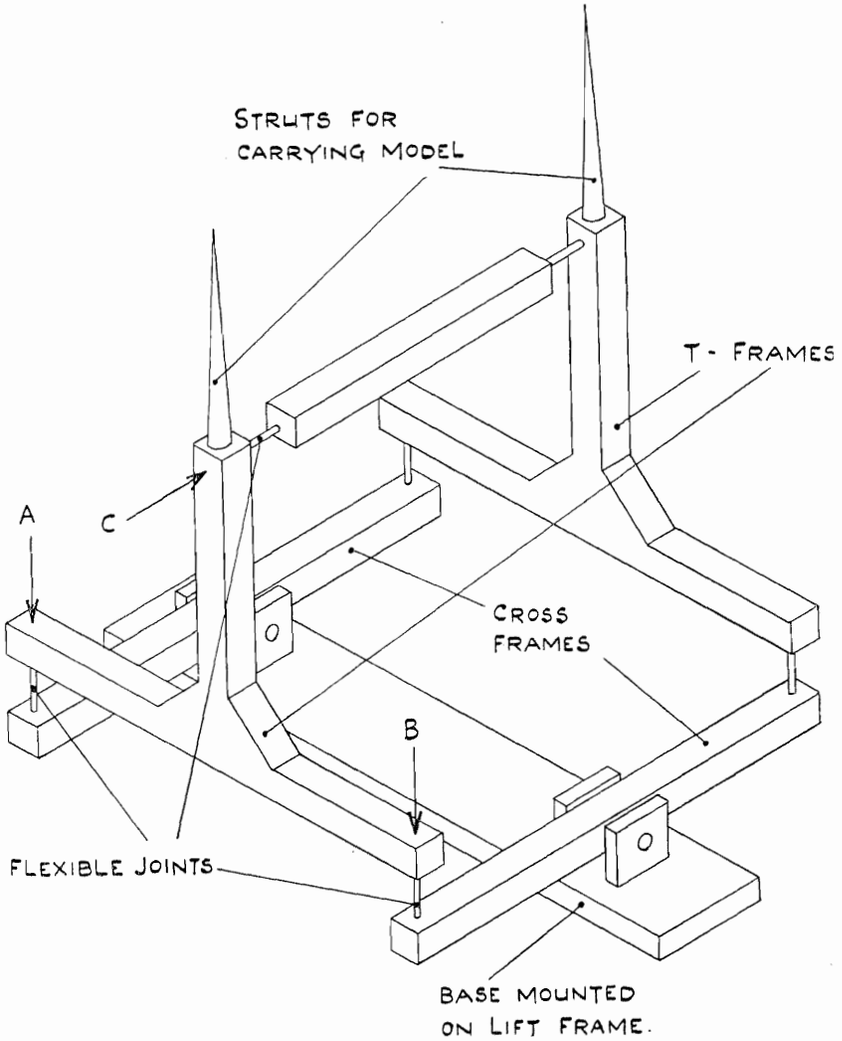

FIG. 10. Principle of Roll, Yaw, and Side-force Balance.

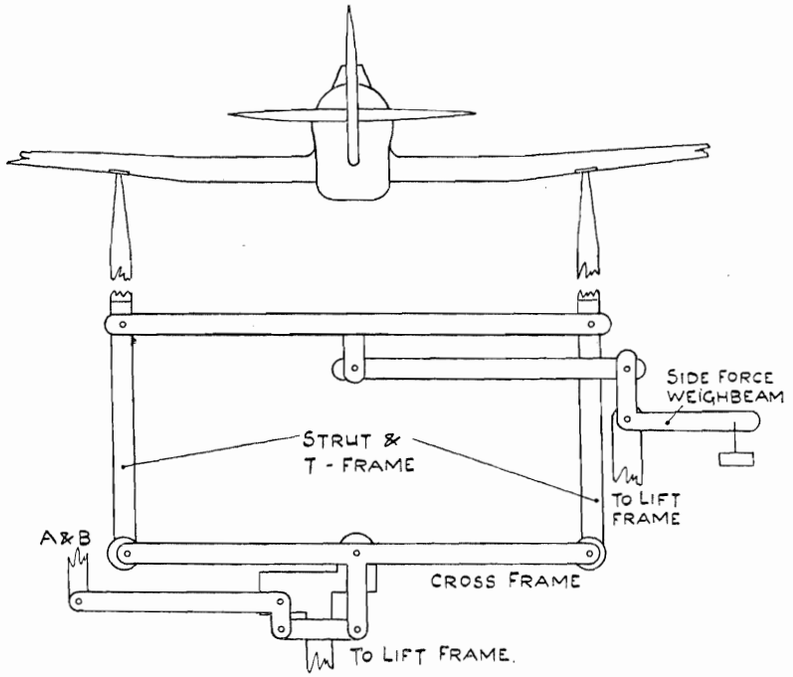

FIG. 11. Linkage for Side-force Weighbeam and Cross Frame.

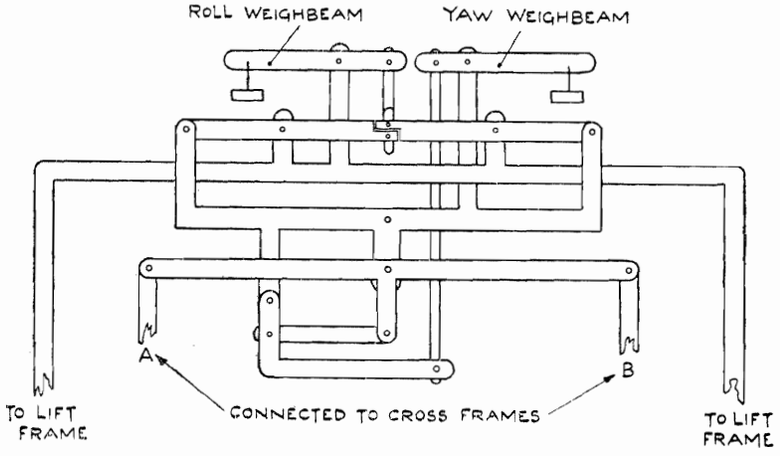

FIG. 12. Linkage for Rolling and Yawing-moment Weighbeams.

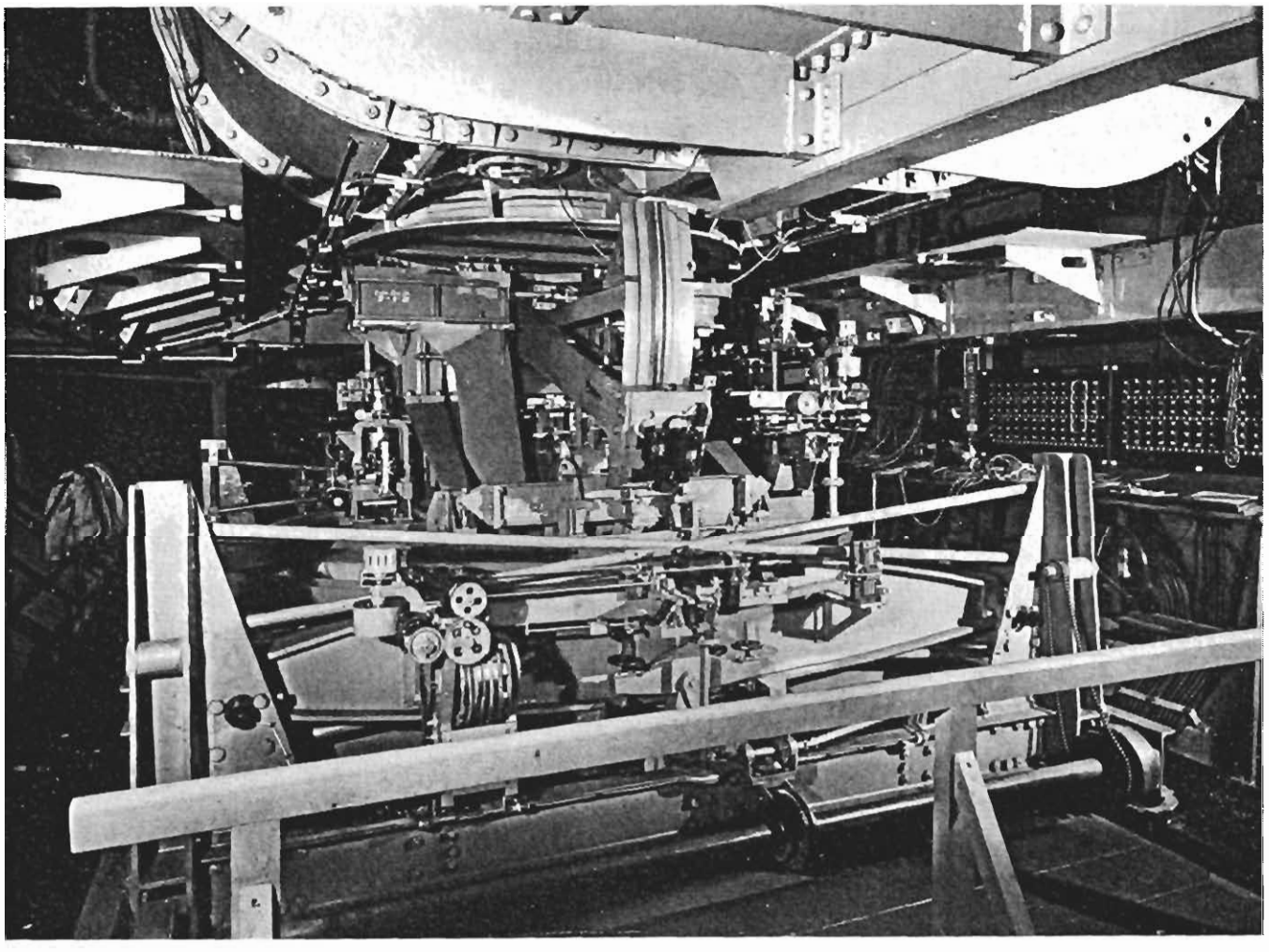

FIG. 13. General View of Six-Component Balance.

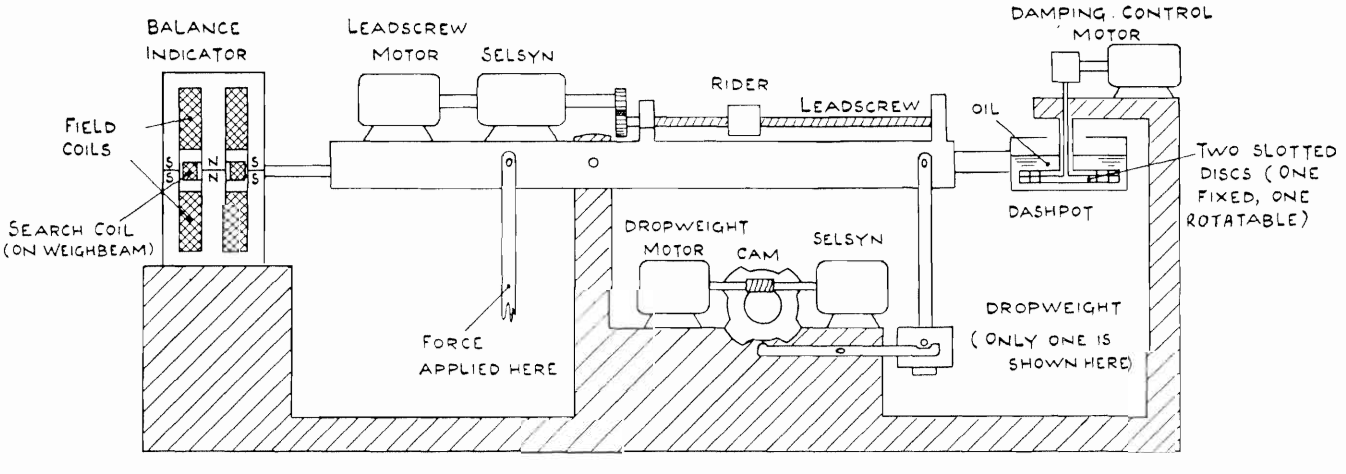

FIG. 14. Diagram of Automatic Weighbeam.

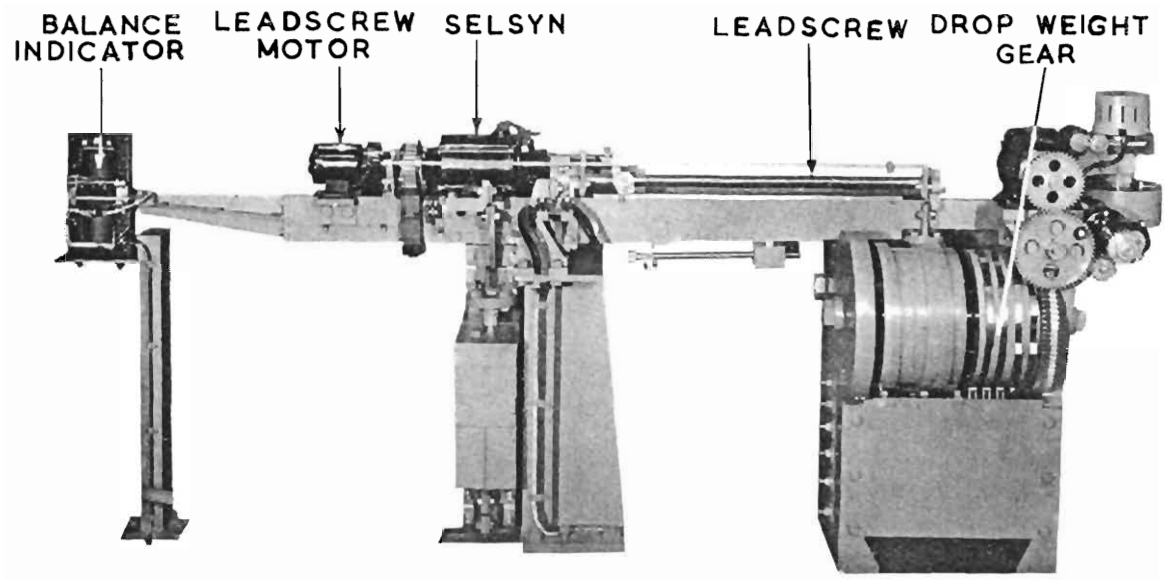

FIG. 15. Automatic Weighbeam.

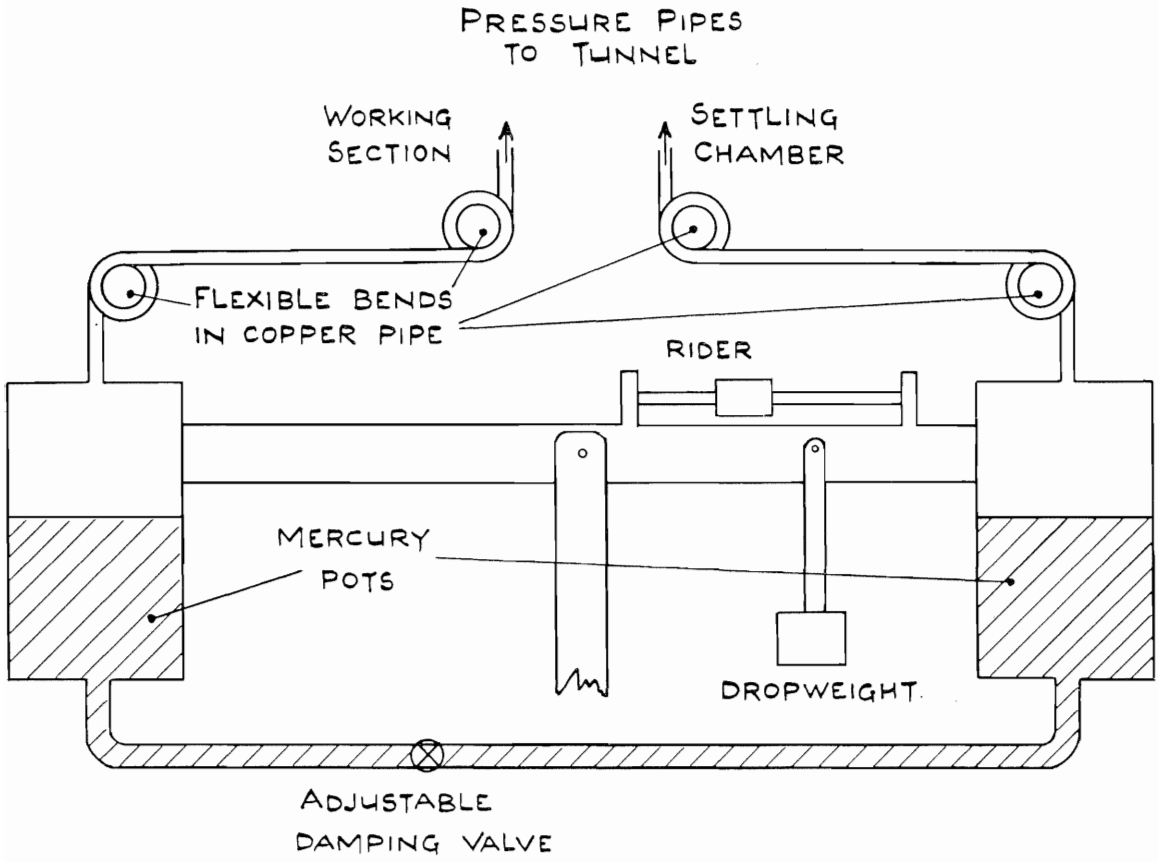

Note.—Control gear, balance indicator, and oil dash-pot, are the same as on FIG. 14.

FIG. 16. Principle of Manometric Balance.

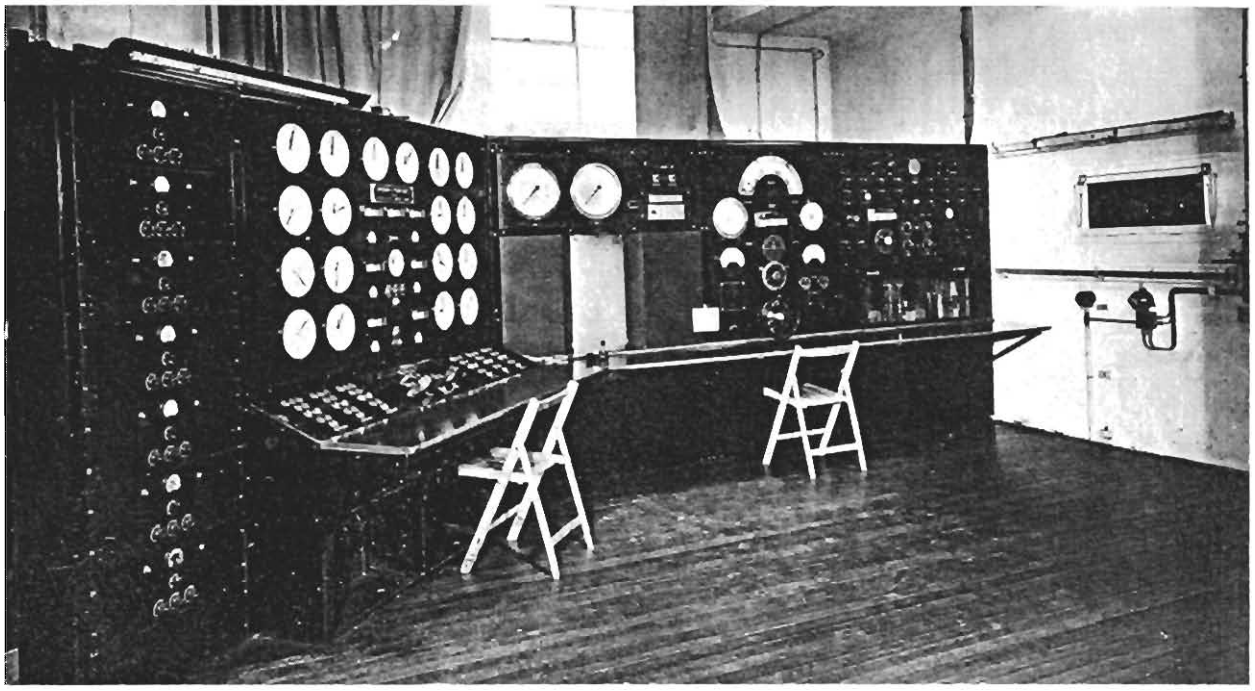

Fig. 17. Observation Room.

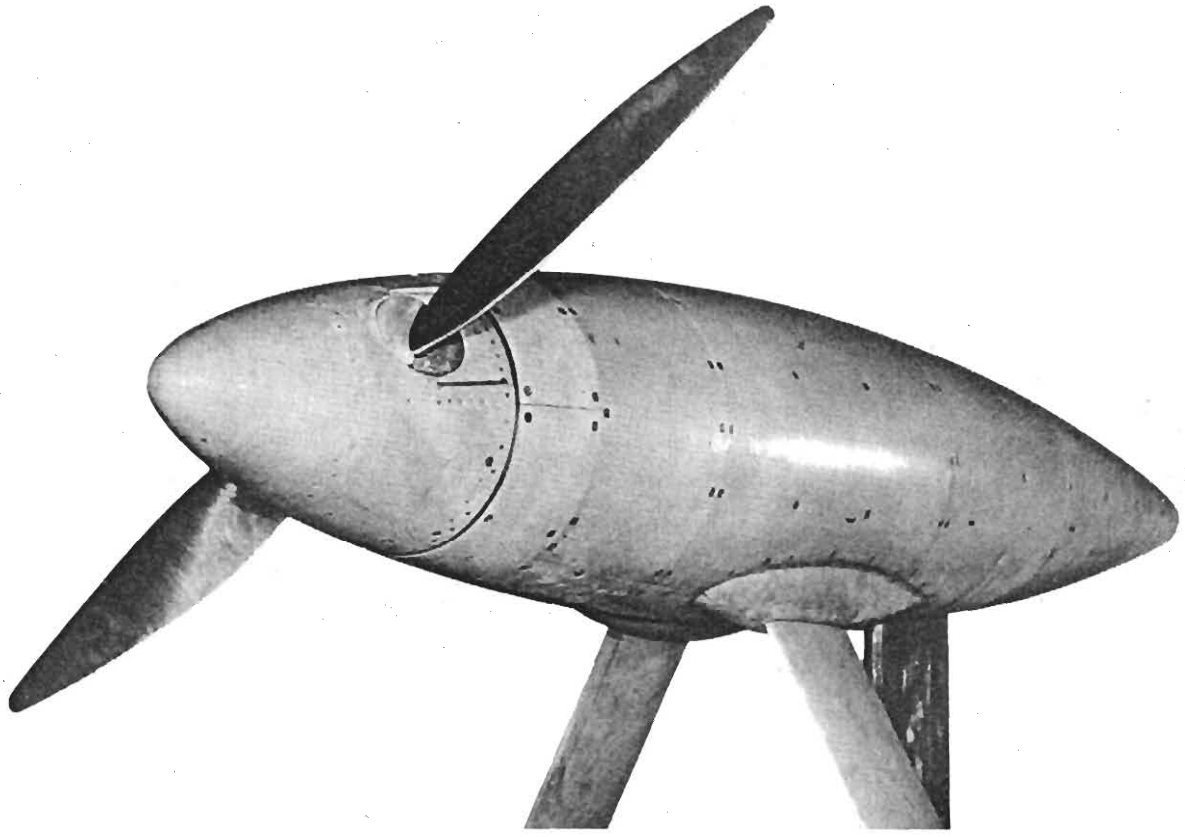

Fig. 18. Motor for Testing Propellers in the High Speed Tunnel.

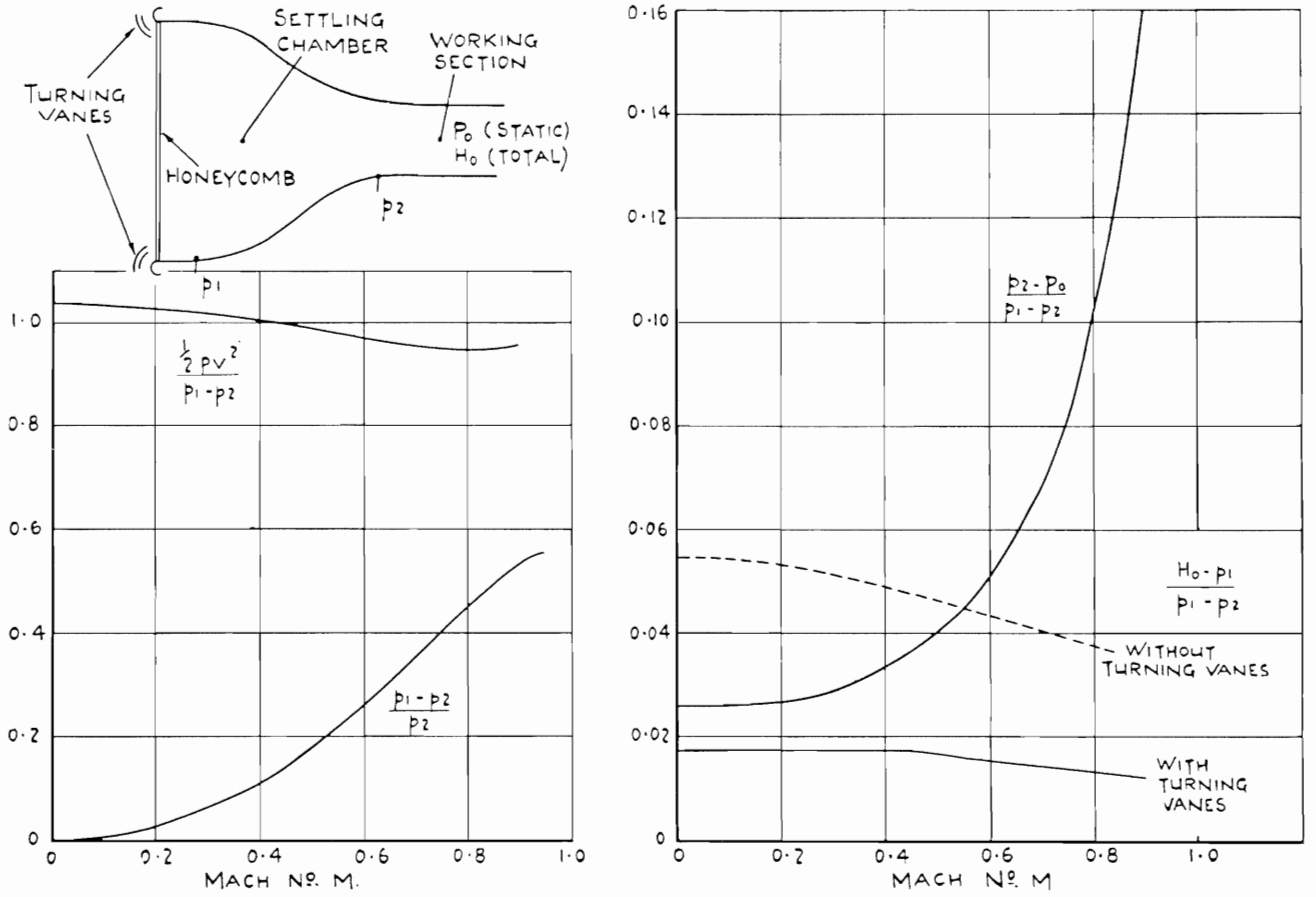

FIG. 19.—Calibration Curves of the High Speed Tunnel.

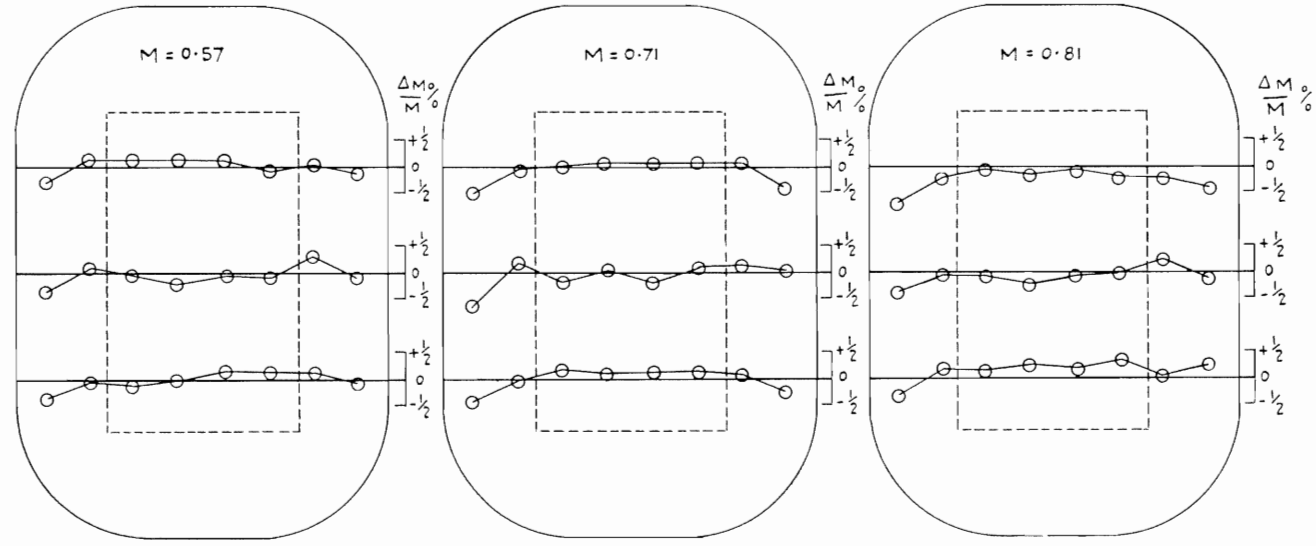

Note.—M is the mean Mach number in the area enclosed by dotted lines, and ΔM is the deviation from this mean value.

FIG. 20. Velocity Distribution Across Working Section.

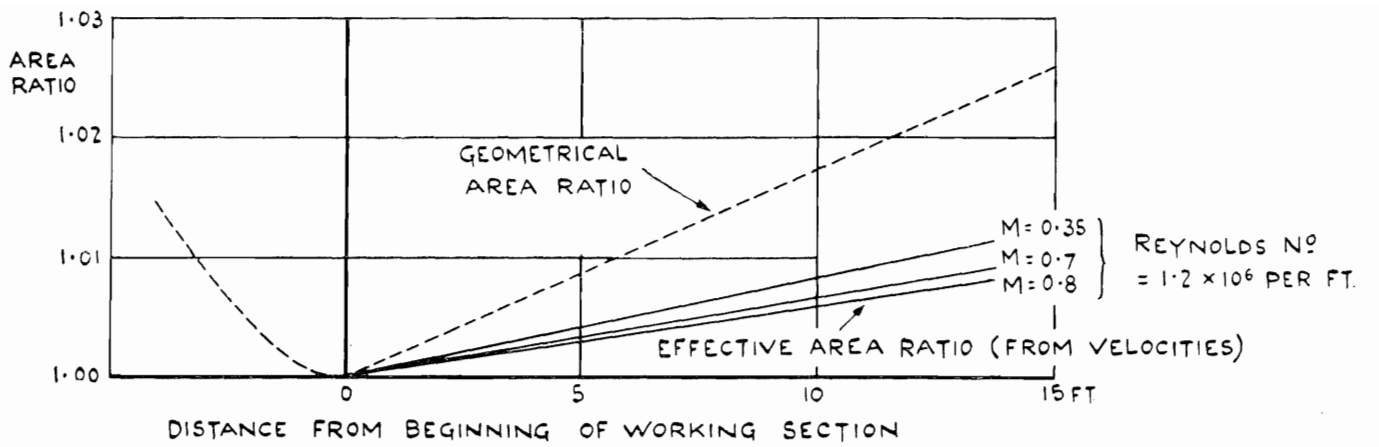

FIG. 21. Expansion in Working Section.

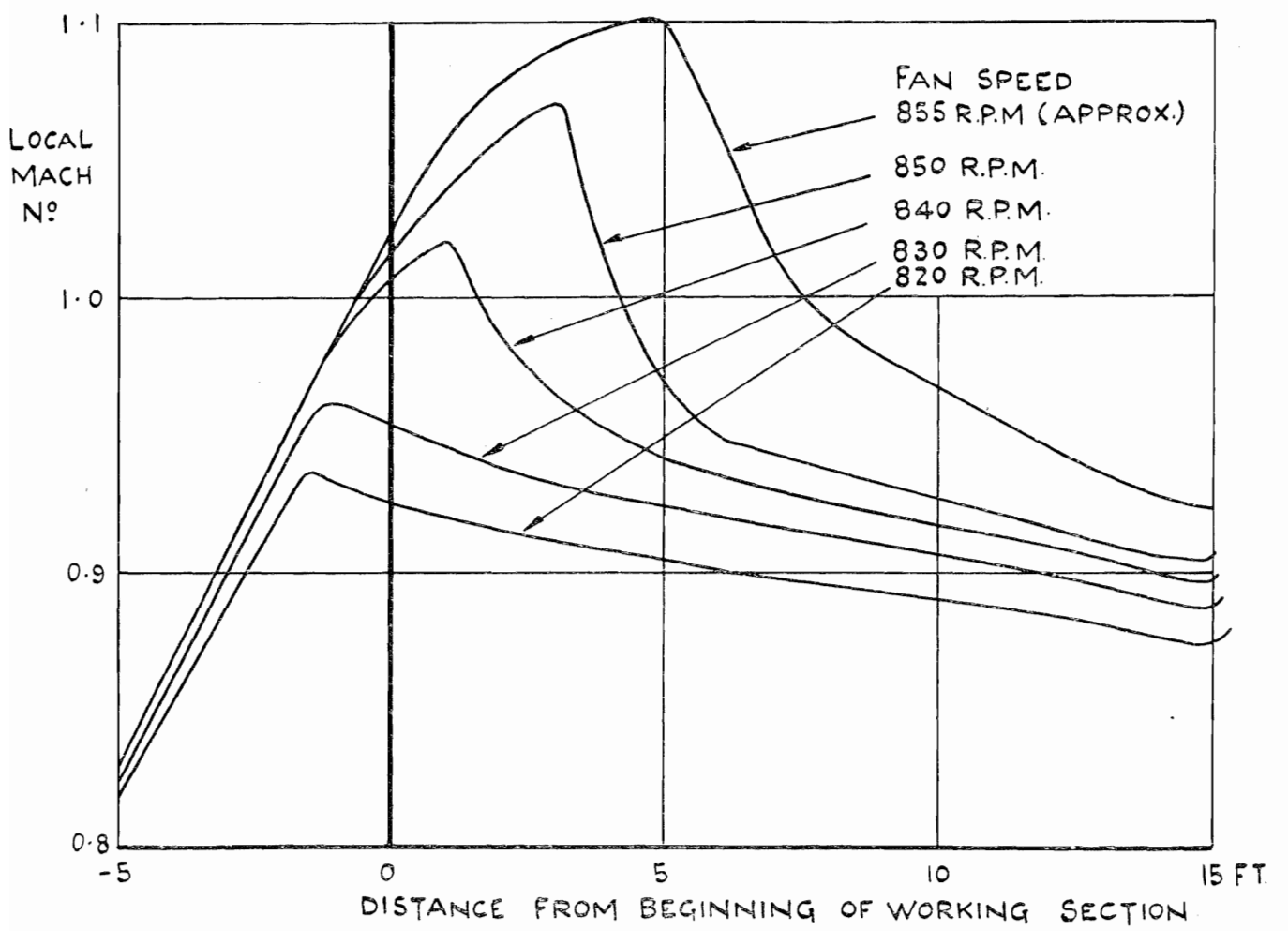

FIG. 22. Longitudinal Velocity Distributions at High Speeds.

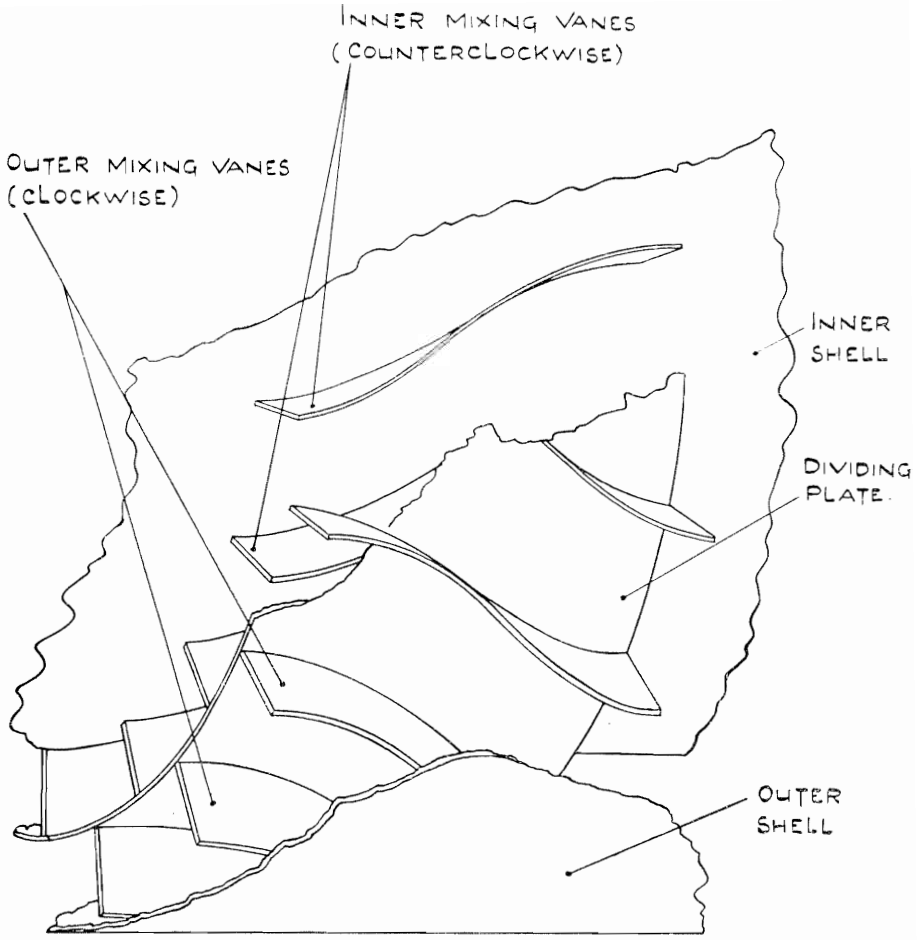

FIG. 23. Mixing Vanes in Return Circuit of Tunnel.

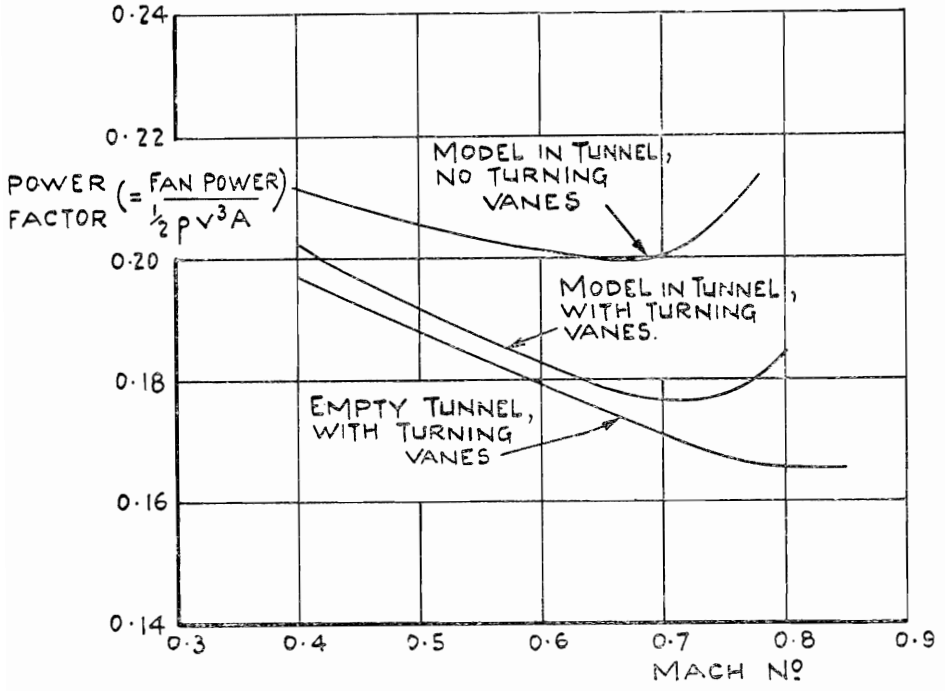

FIG. 24. Power Factor of the High Speed Tunnel.

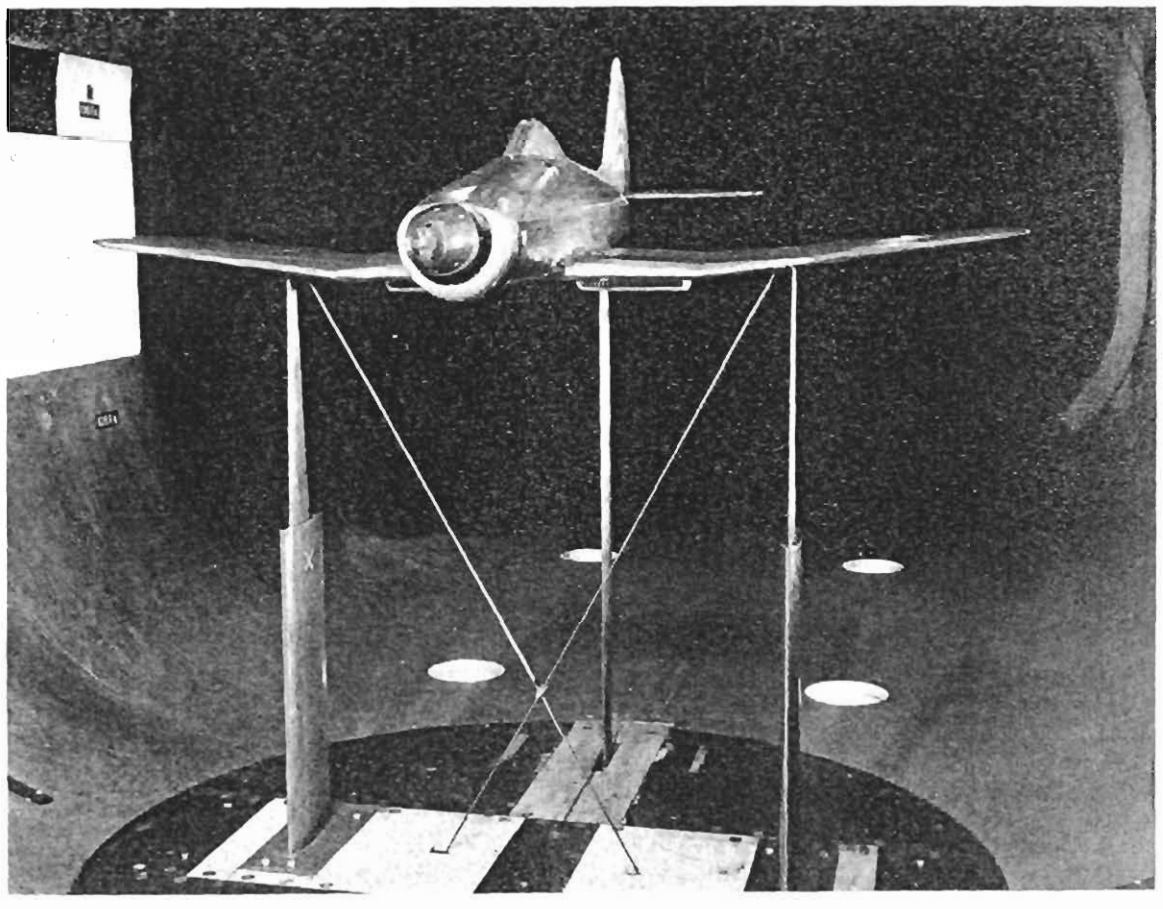

FIG. 25. Typical Model Aircraft Mounted in the Tunnel.

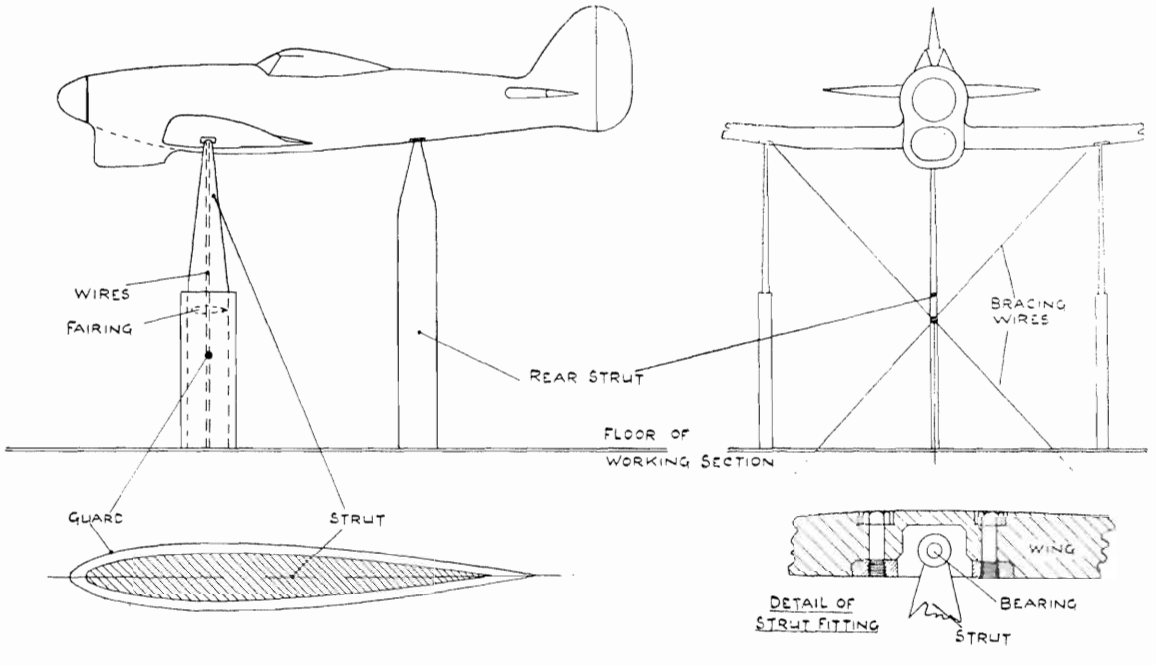

FIG. 26. Typical Rig for Complete Model.

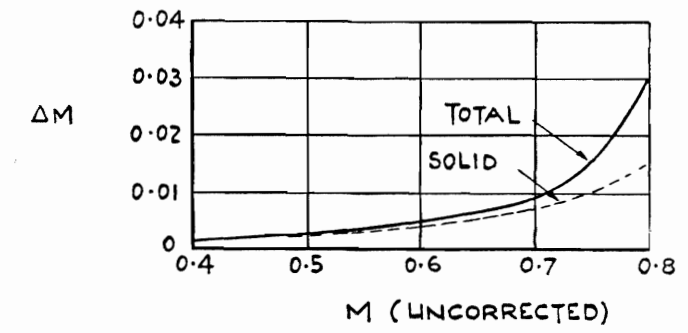

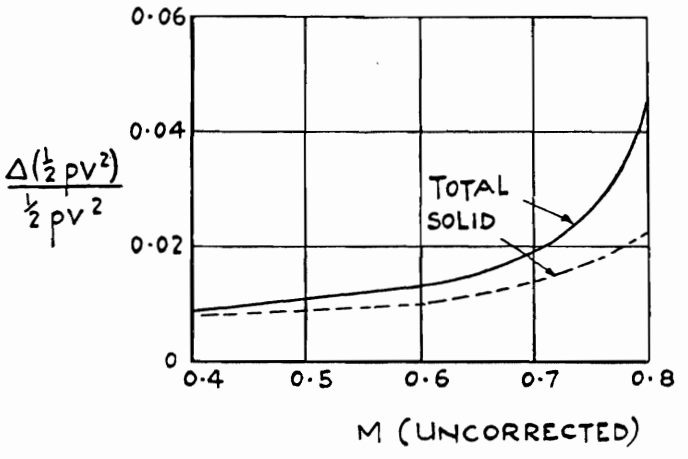

FIG. 27. Typical Blockage Corrections for a Complete Model.

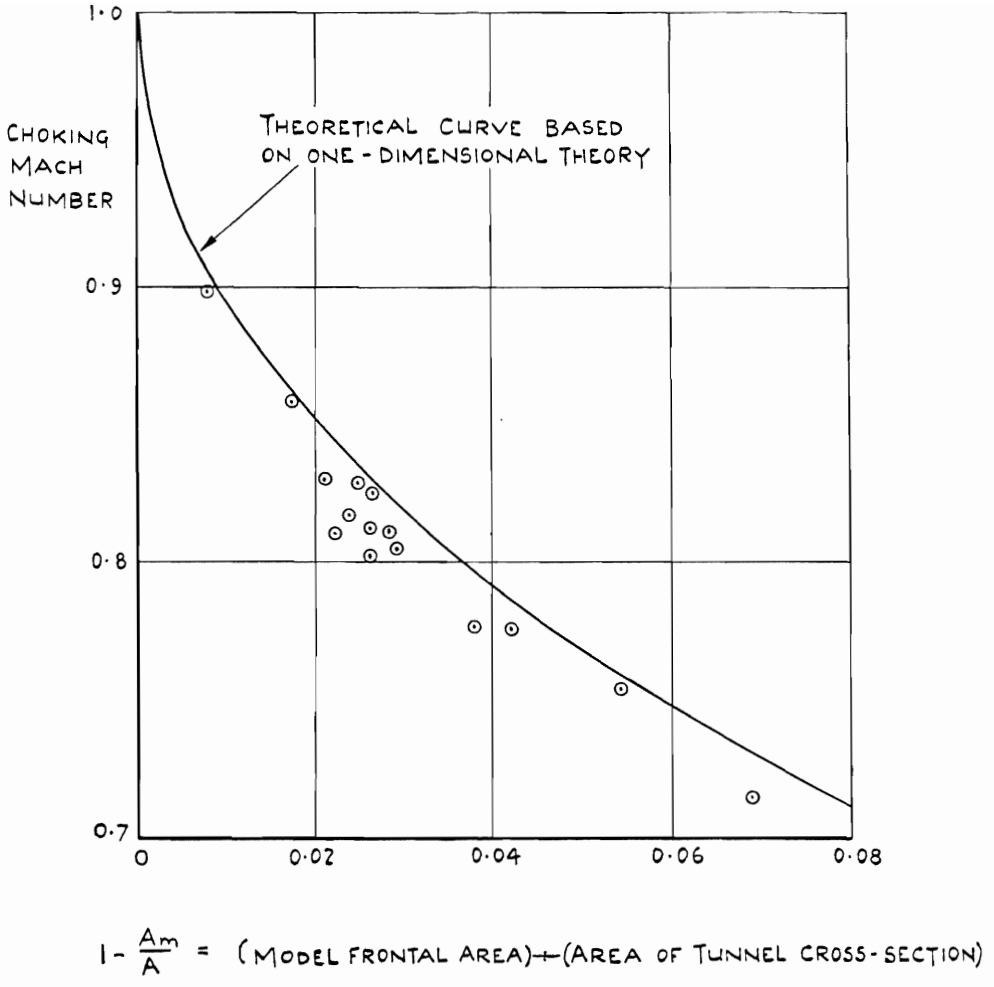

FIG. 28. Tunnel Choking Speeds.

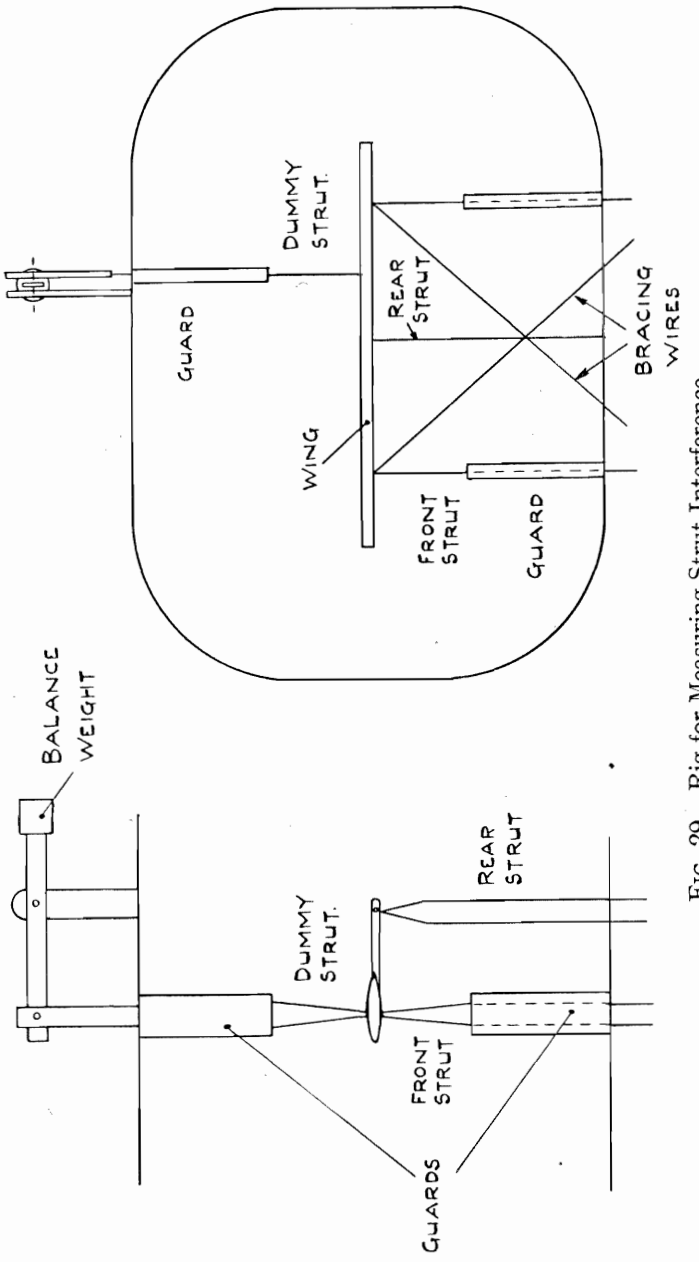

FIG. 29. Rig for Measuring Strut Interference.

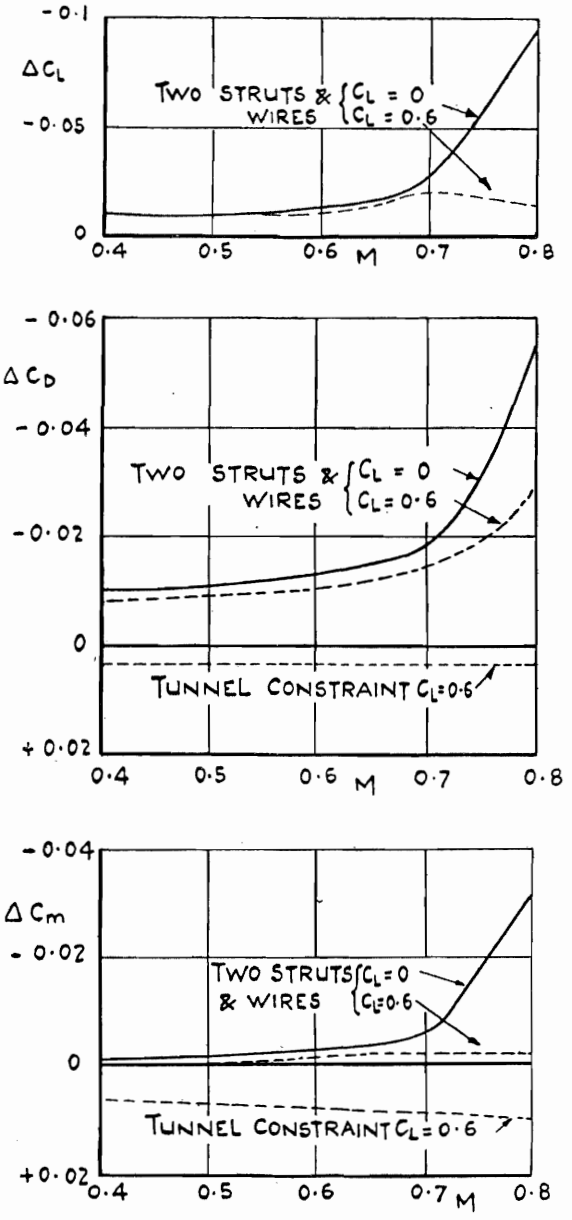

Note.—The tunnel constraint corrections shown here do not include the blockage correction applied to $\frac{1}{2}\varrho V^2$.

FIG. 30. Typical Corrections for Model Supports and Tunnel Constraint.

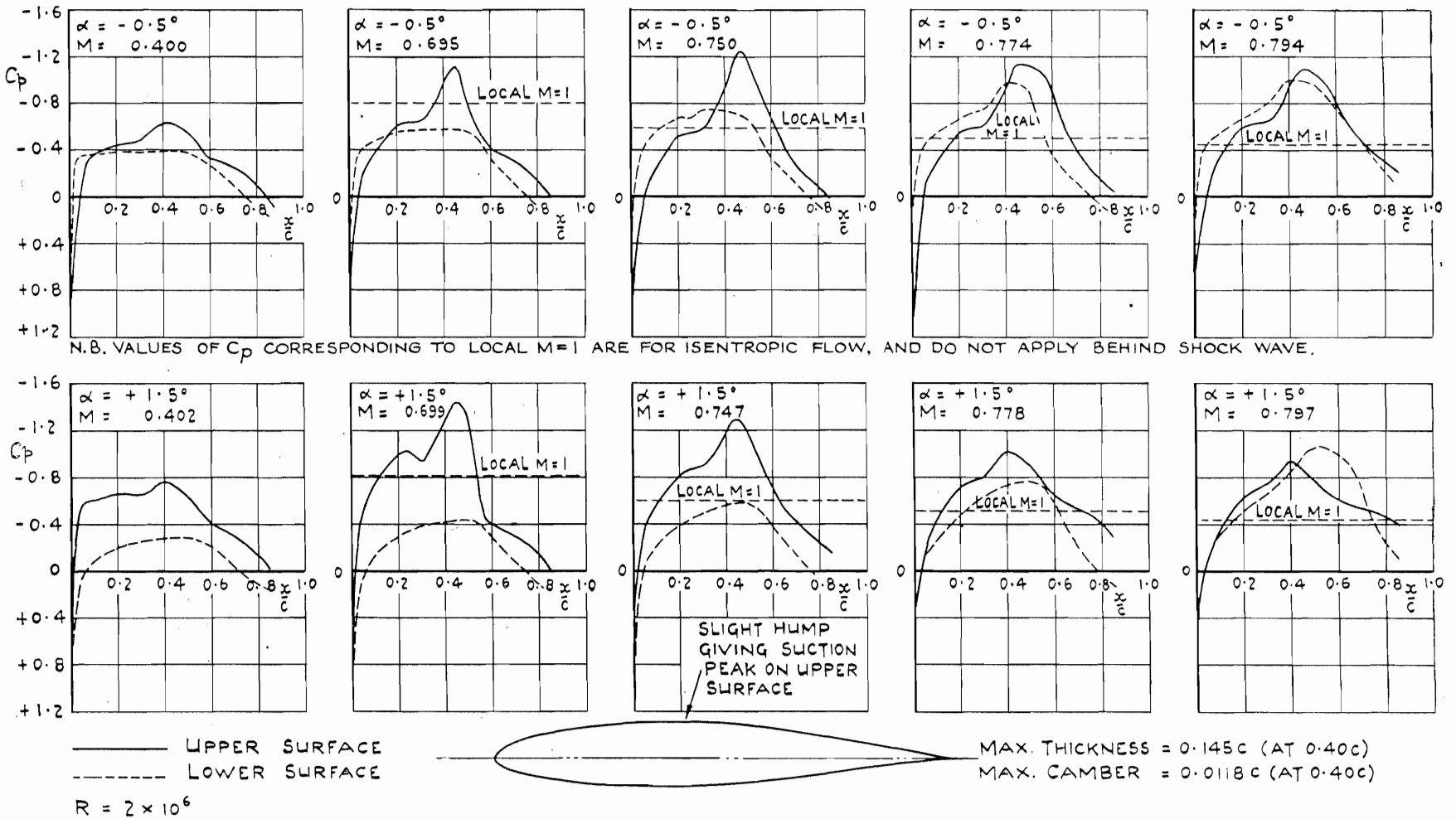

FIG. 31. Pressure Distributions on Mustang Wing Section.

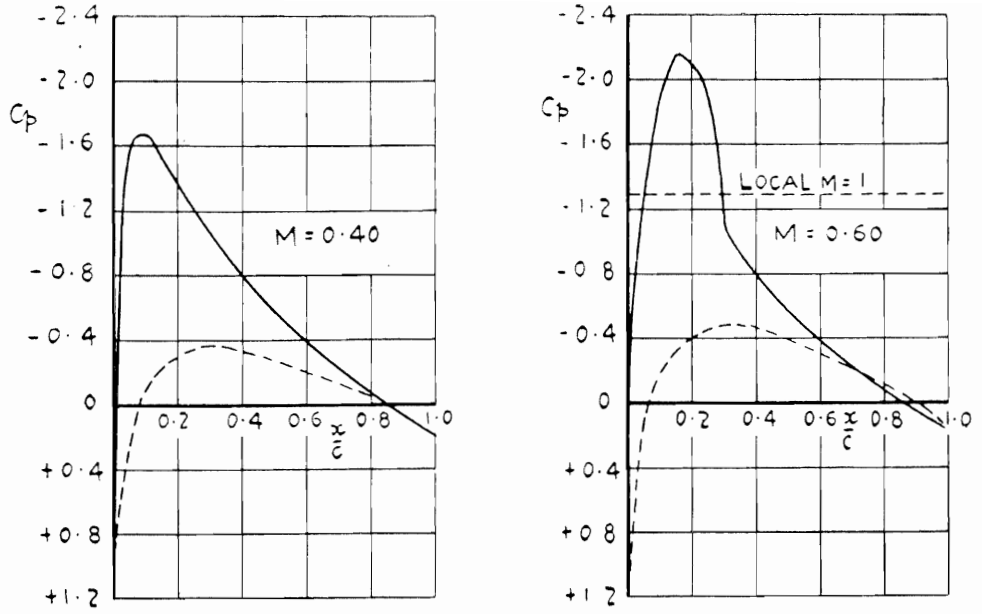

N.B VALUES OF Cp CORRESPONDING TO LOCAL M = 1 ARE FOR ISENTROPIC FLOW, & DO NOT APPLY BEHIND SHOCK WAVE

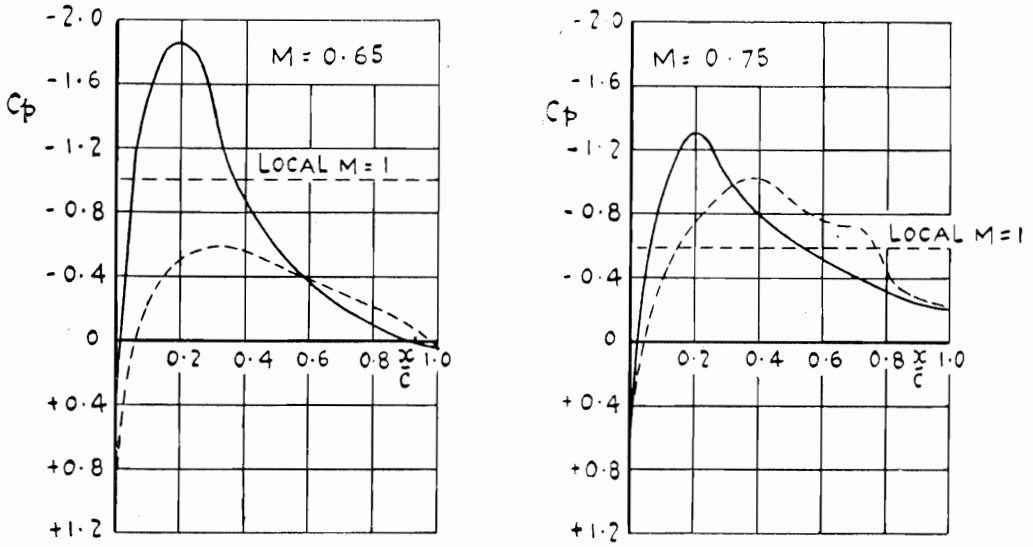

UPPER SURFACE
LOWER SURFACE

(MAX THICKNESS = 0·21 C)

FIG. 32. Pressure Distributions on NACA 23021 Aerofoil.
$R = 2 \times 10^6$ $\alpha = 5°$

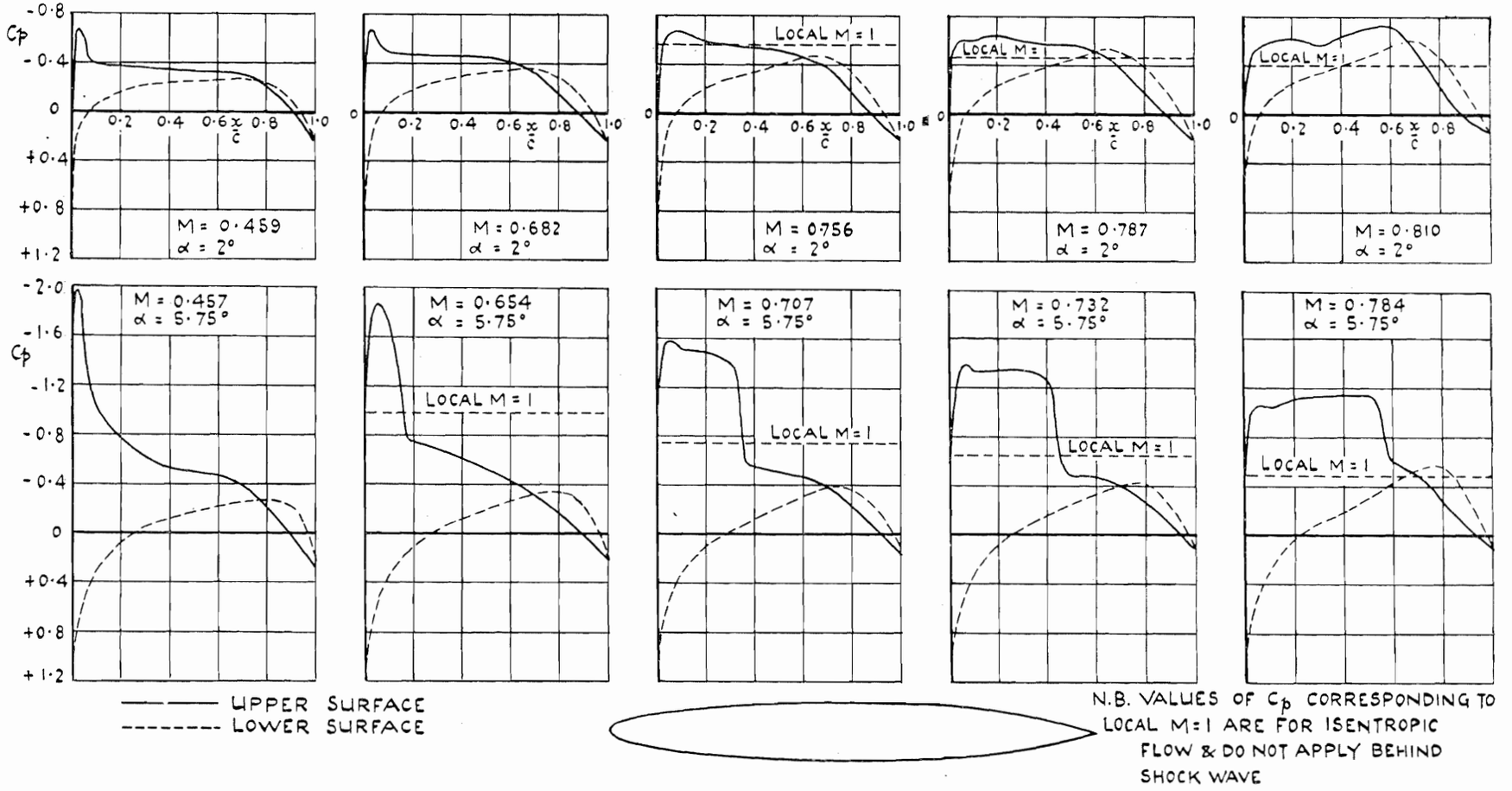

FIG. 33. Pressure Distributions on EC 1250 A rofoil (from H.S.T. tests at N.P.L.).

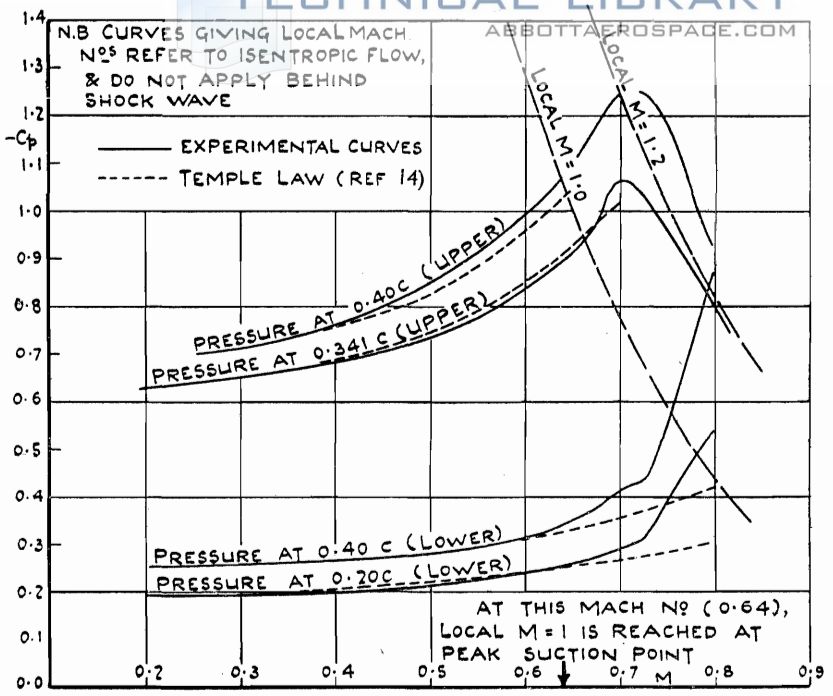

FIG. 34. Variation of Suction Coefficients with Mach Number, Mustang Wing Section, $\alpha = +1{\cdot}5°$.

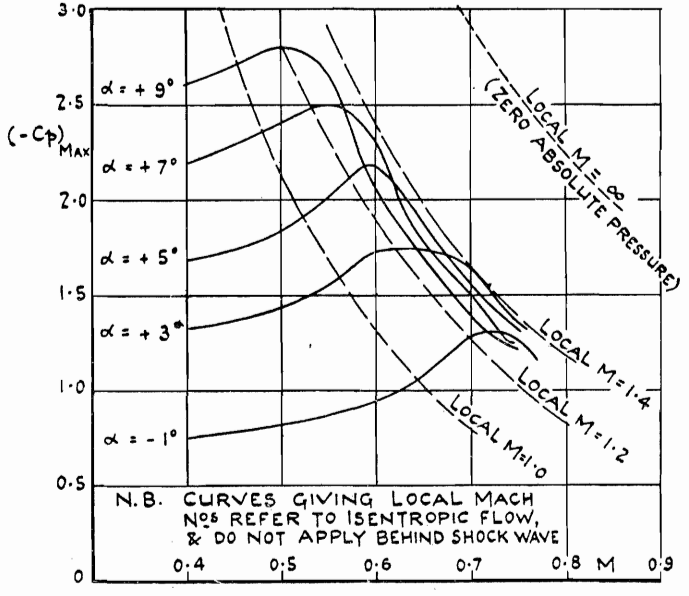

FIG. 35. Variation of Peak Suction Coefficient with Mach Number, NACA 23021 Aerofoil. (Upper surface)

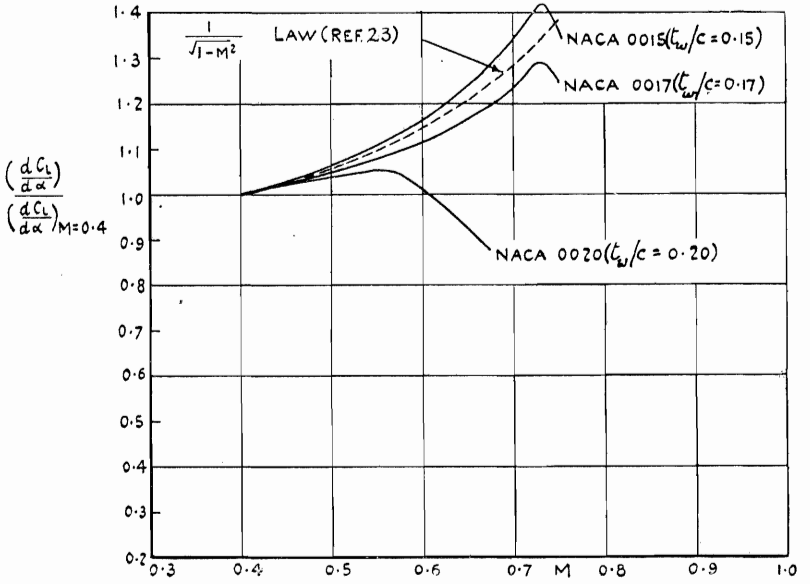

FIG. 36. Effect of Mach Number on Lift Gradient, for Symmetrical Aerofoils of Infinite Aspect Ratio (from H.S.T. tests at N.P.L.).

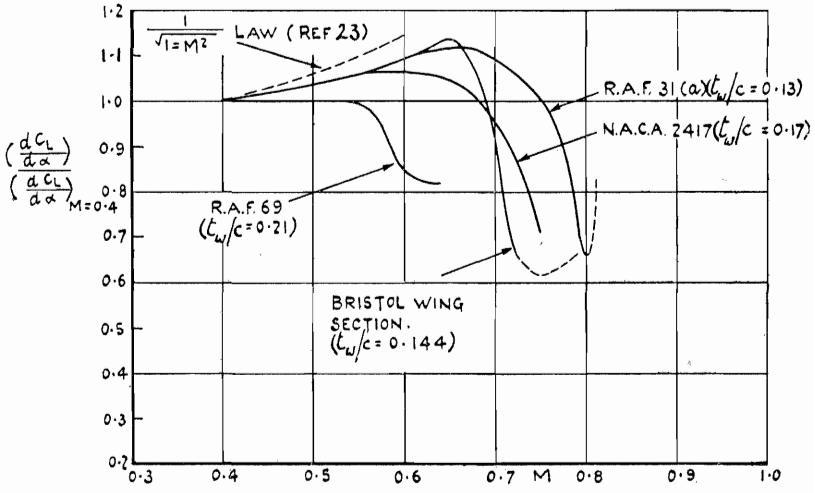

FIG. 37. Effect of Mach Number on Lift Gradient, for Cambered Aerofoils of Infinite Aspect Ratio (from H.S.T. tests at N.P.L.).

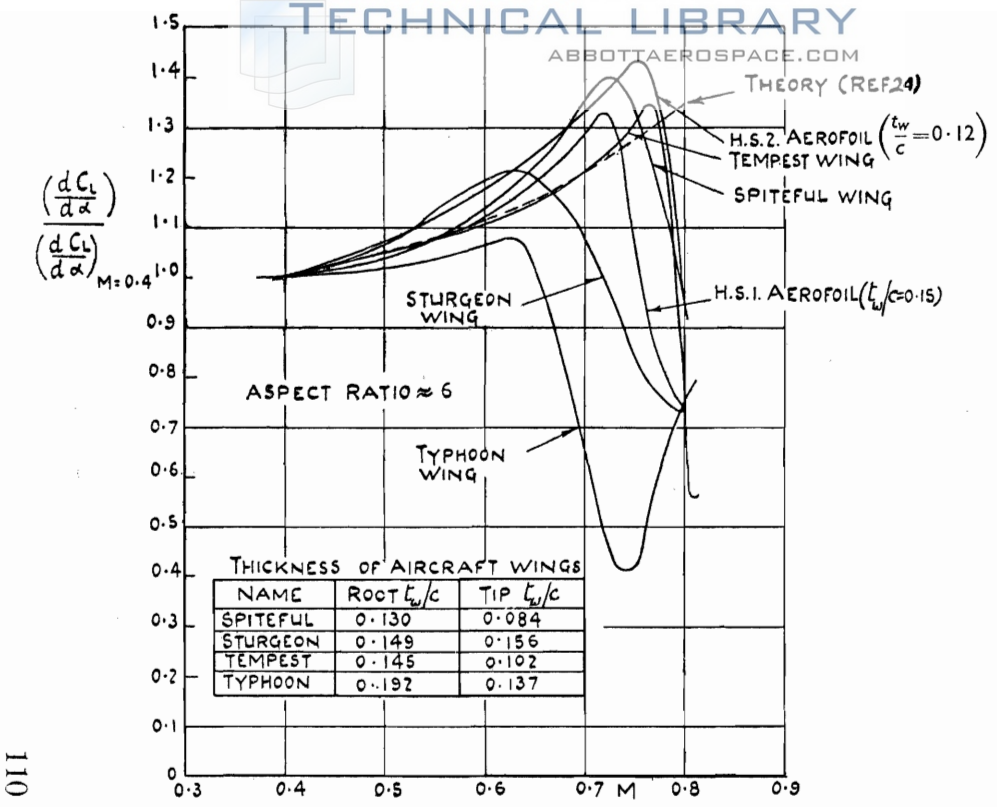

FIG. 38. Effect on Mach Number on Lift Gradient, for Cambered Wings of Finite Aspect Ratio.

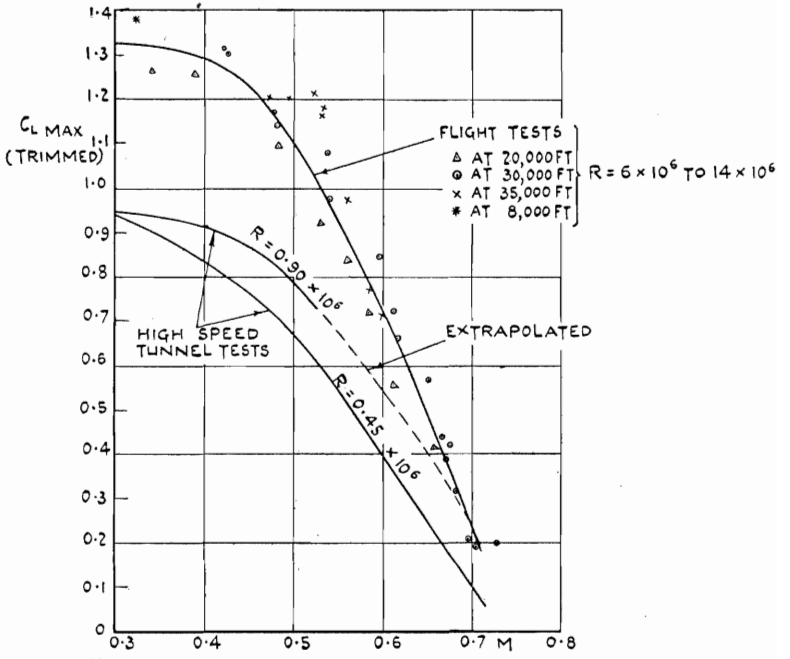

FIG. 40. Effect of Mach Number on Maximum Lift Coefficient of Welkin. (From tests in flight and tunnel.)

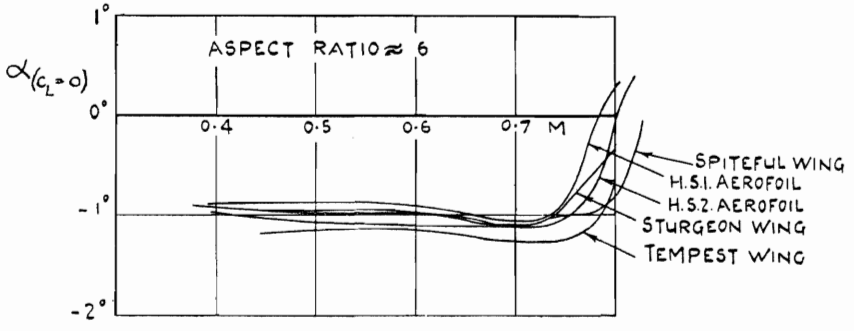

FIG. 39. Effect of Mach Number on Incidence for Zero Lift.

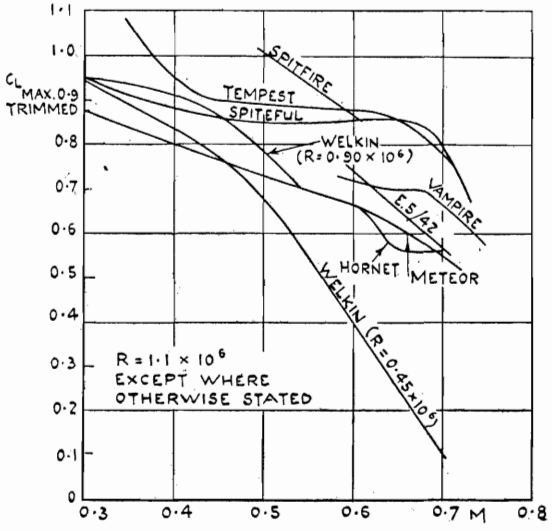

FIG. 41. Effect of Mach Number on Maximum Lift Coefficient of Several

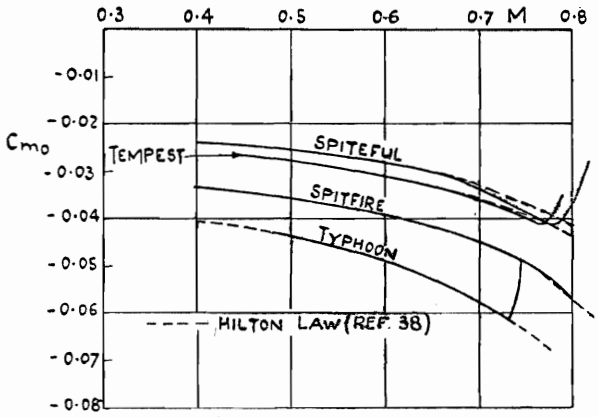

FIG. 42. Effect of Mach Number on C_{m_0}, for Cambered Wings of Finite Aspect Ratio.

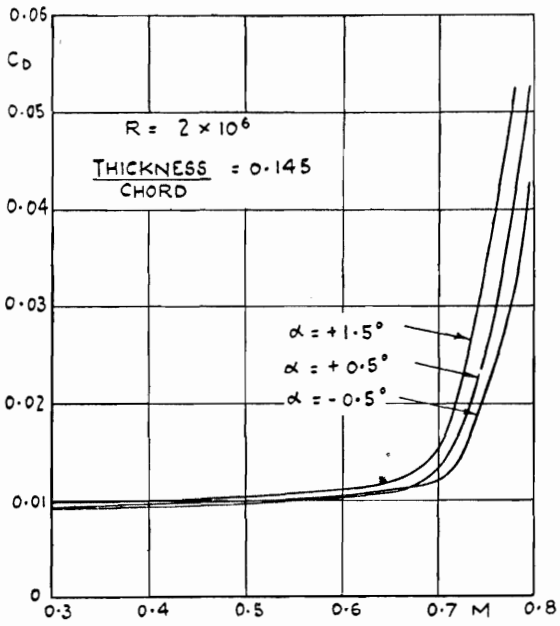

FIG. 44. Effect of Mach Number on Profile Drag. (Mustang wing section.)

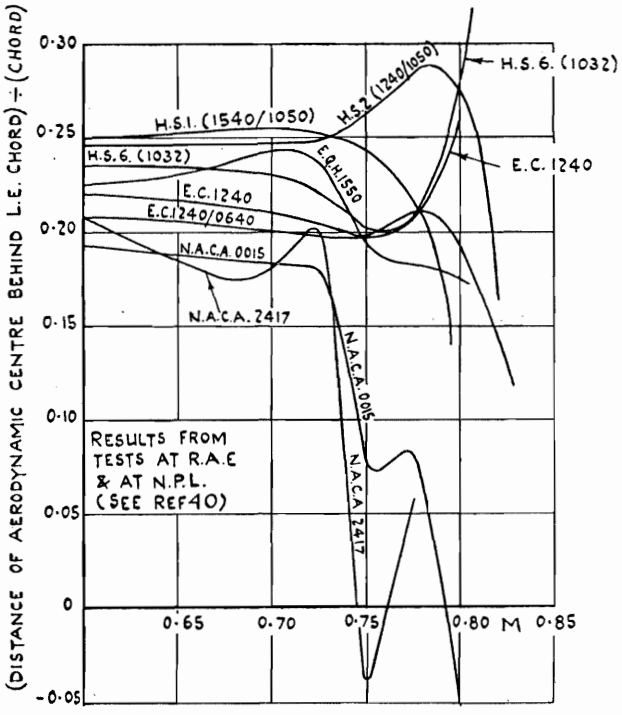

FIG. 43. Effect of Mach Number on Aerodynamic Centre of Aerofoils ($C_L = 0$ to $0 \cdot 1$).

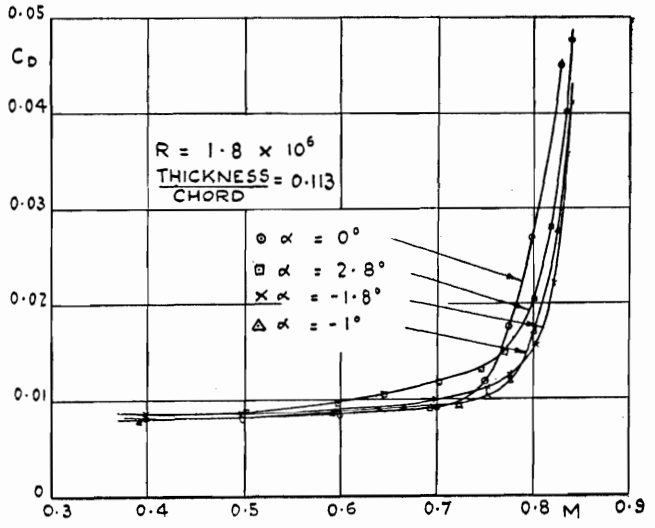

FIG. 45. Effect of Mach Number on Profile Drag of Section of Spitfire Wing.

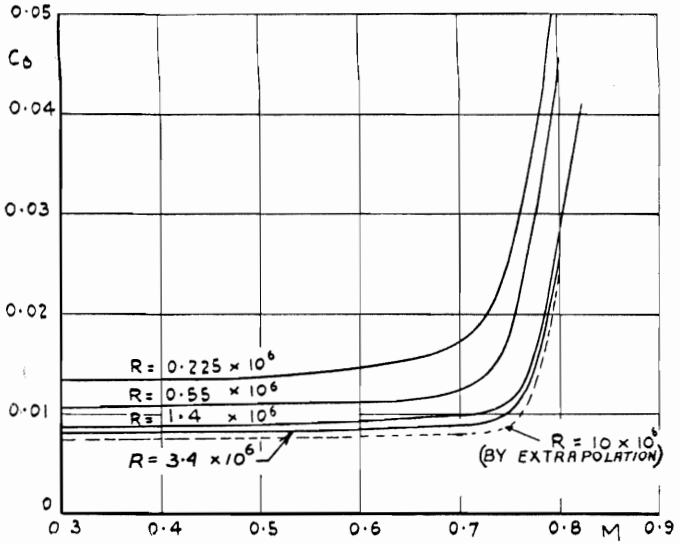

FIG. 46. Effect of Mach Number on Profile Drag at Several Reynolds Numbers (NACA. 0015 Section, $\alpha = 0°$).

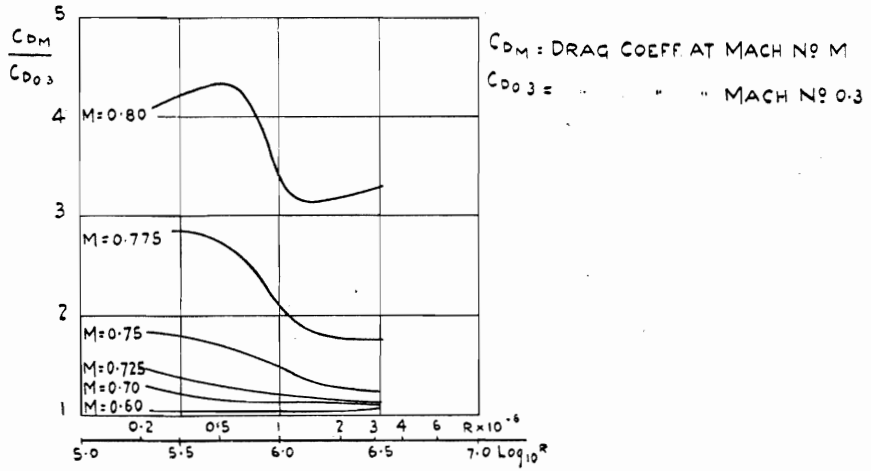

FIG. 47. Effect of Reynolds Number on Profile Drag at High Mach Numbers (NACA. 0015 Section, $\alpha = 0°$).

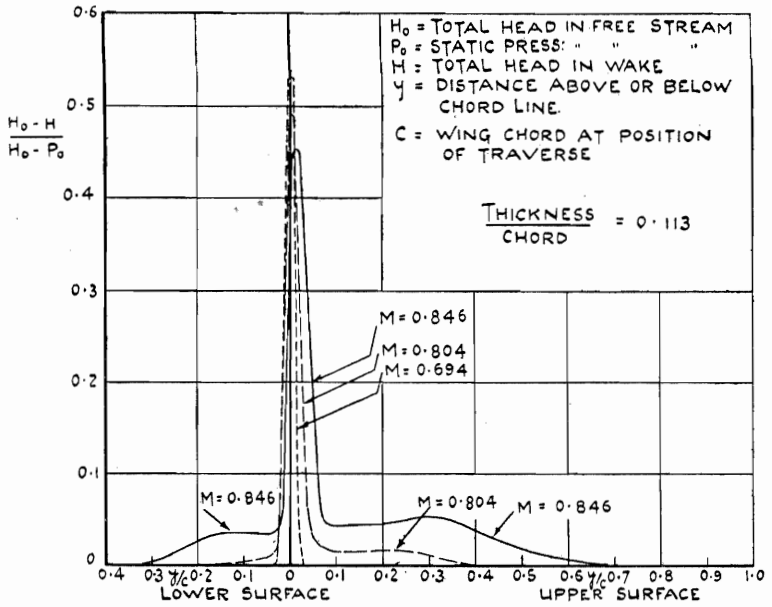

FIG. 48. Loss of Total Head behind Spitfire Wing. $R = 1{\cdot}8 \times 10^6$ $\alpha = -1°$

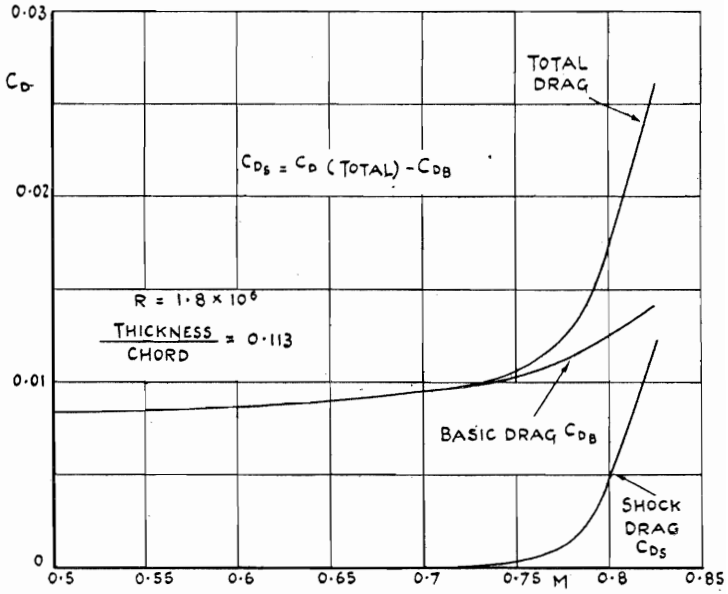

FIG. 49. Effect of Mach Number on Basic Drag and Shock Drag of Section of Spitfire Wing, $\alpha = -1°$.

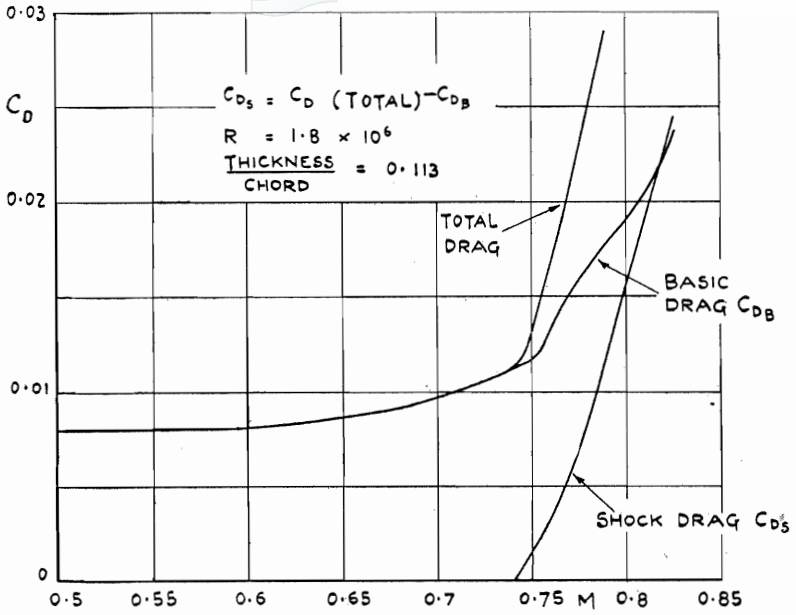

FIG. 50. Effect of Mach Number on Basic Drag and Shock Drag of Section of Spitfire Wing ($\alpha = +0{\cdot}9°$).

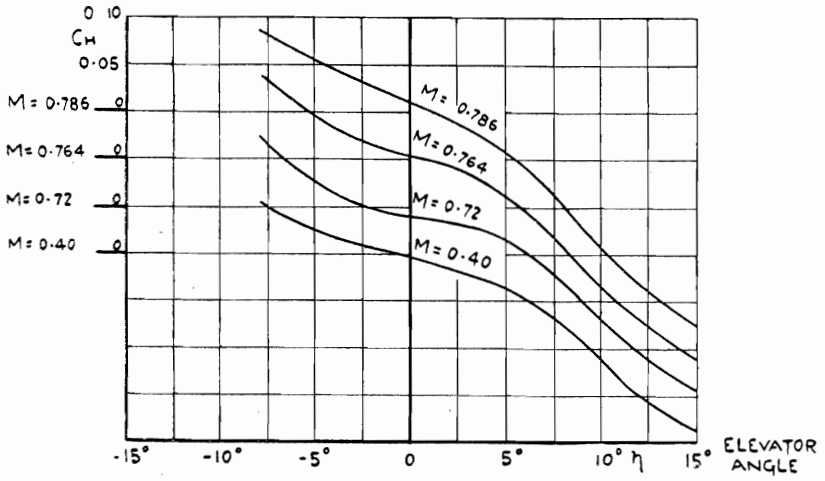

FIG. 52. Typhoon Tail Plane and Elevator: Hinge Moments (Set-back hinge, 23 per cent. balance.)

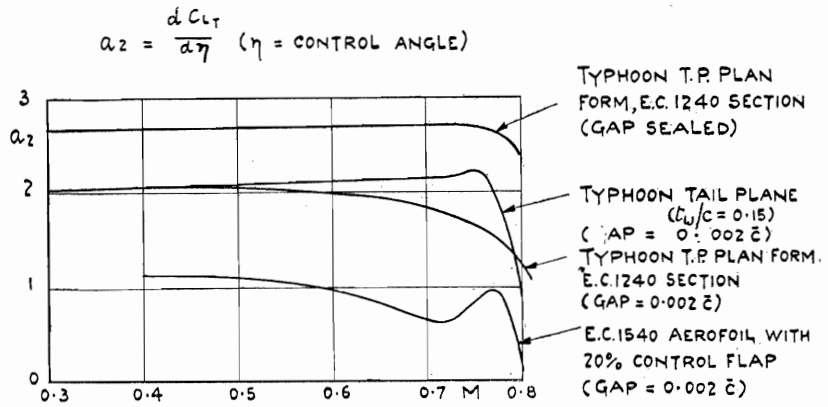

FIG. 51. Effect of Mach Number on Control Effectiveness (Incidence = 0°).

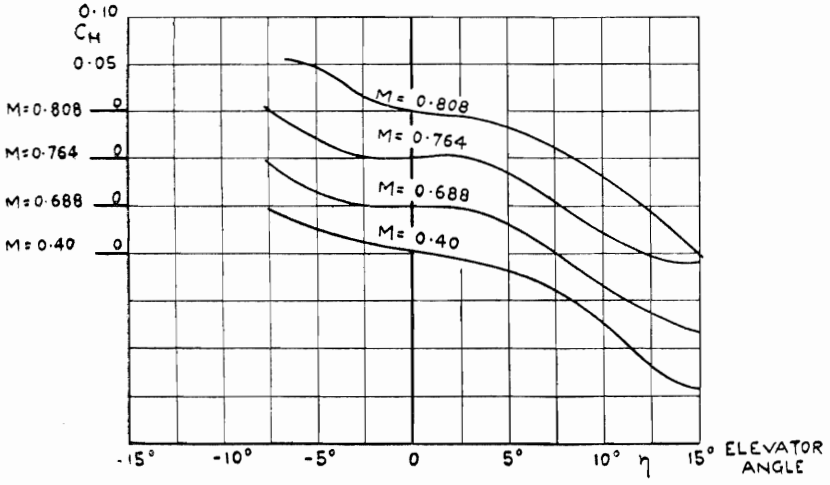

FIG. 53. Tail Plane and Elevator of Typhoon Plan Form and EC 1240 Section: Hinge Moments. (Set-back hinge, 23 per cent. balance.)

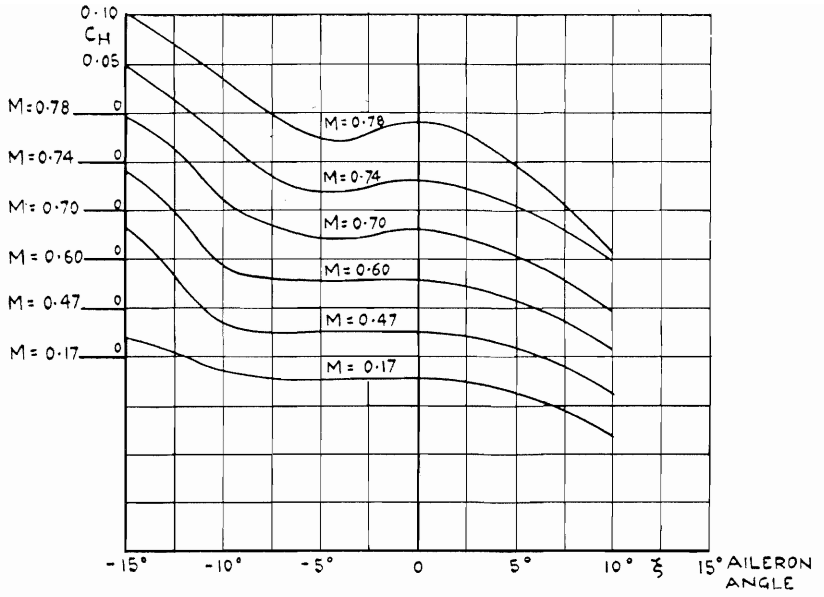

FIG. 54. Hinge Moments on Spitfire Aileron, $\alpha = 0 \cdot 1°$, Frise Type Balance.

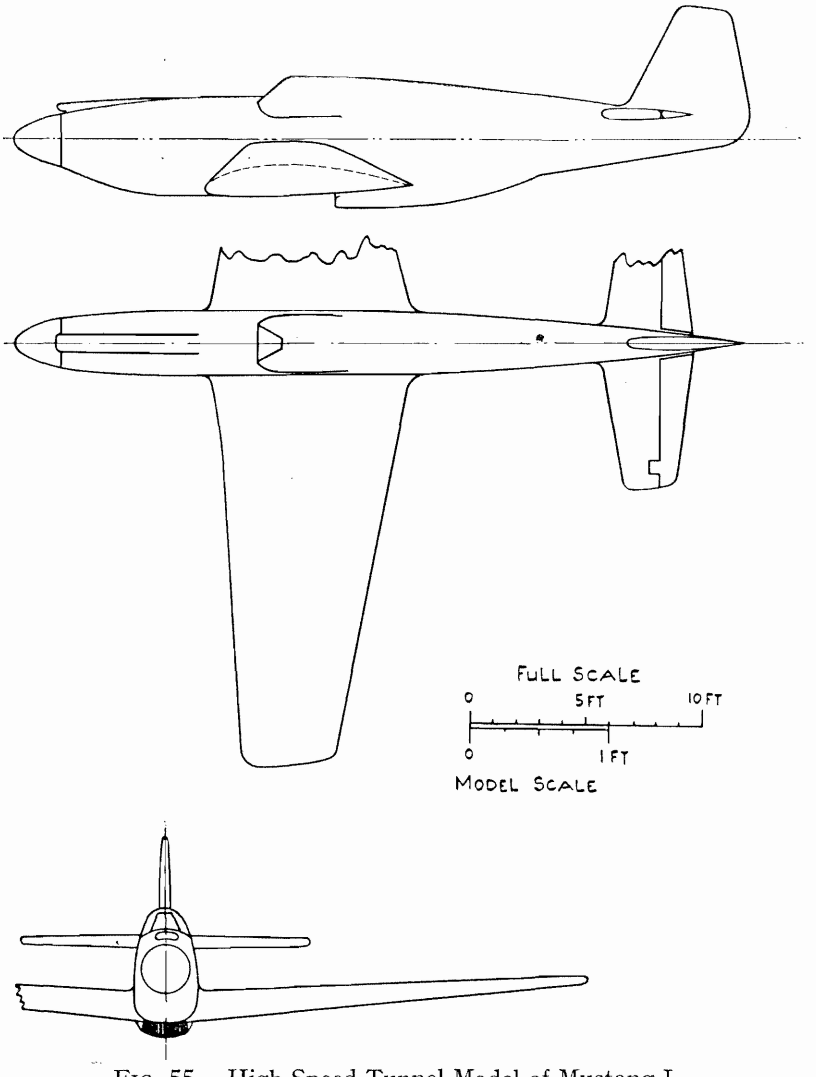

FIG. 55. High Speed Tunnel Model of Mustang I.

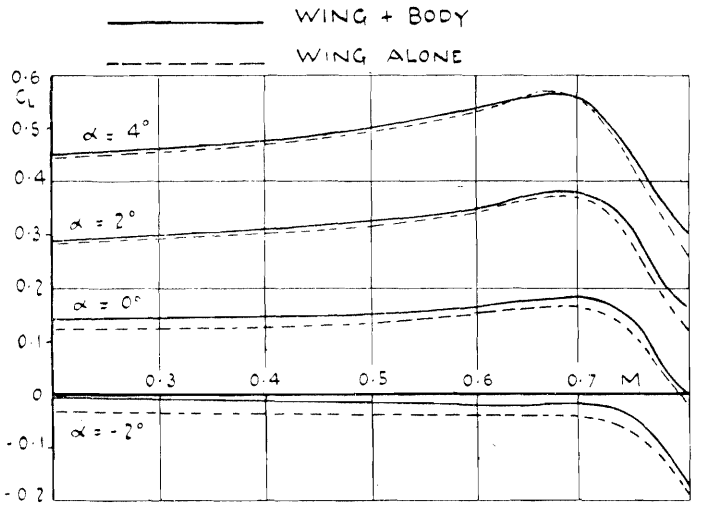

FIG. 56. Variation of C_L with Mach Number: Mustang I.

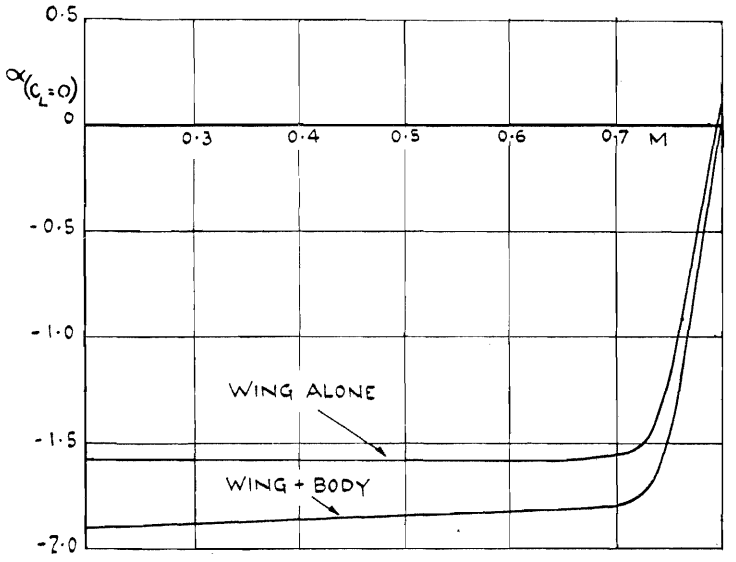

FIG. 57. Variation of No-lift Angle with Mach Number: Mustang I.

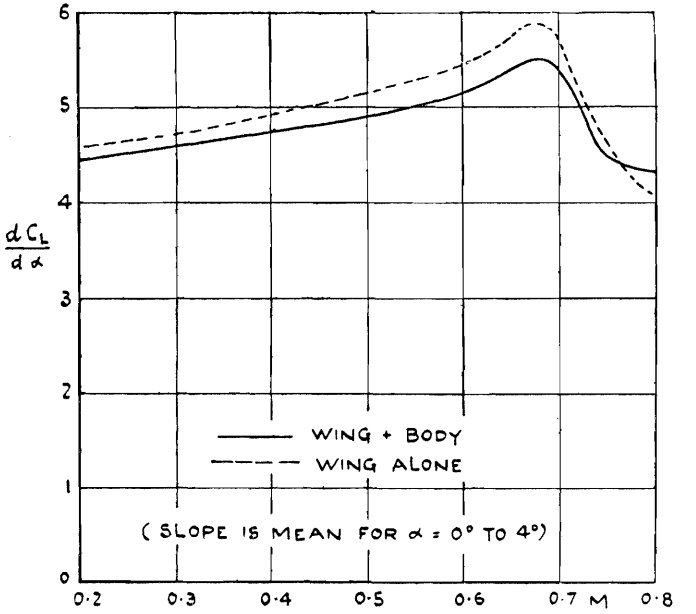

FIG. 58. Variation of Lift Gradient with Mach Number: Mustang I.

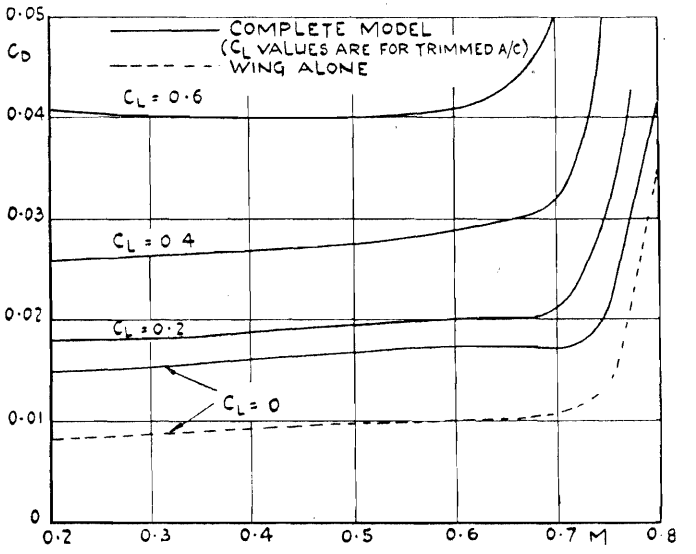

FIG. 59. Variation of Drag with Mach Number: Mustang I.

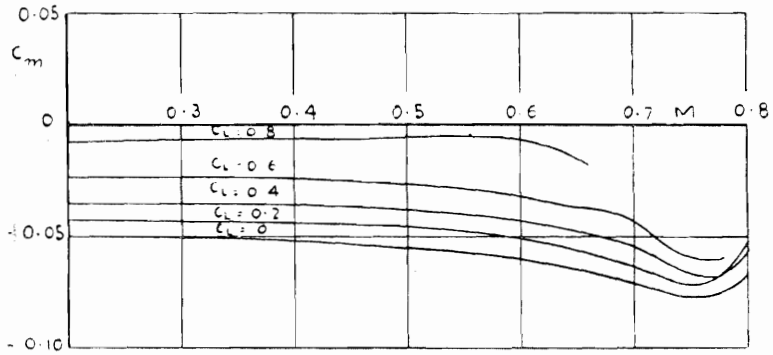

FIG. 60. Effect of Mach Number on Pitching Moment : Mustang I Wing.

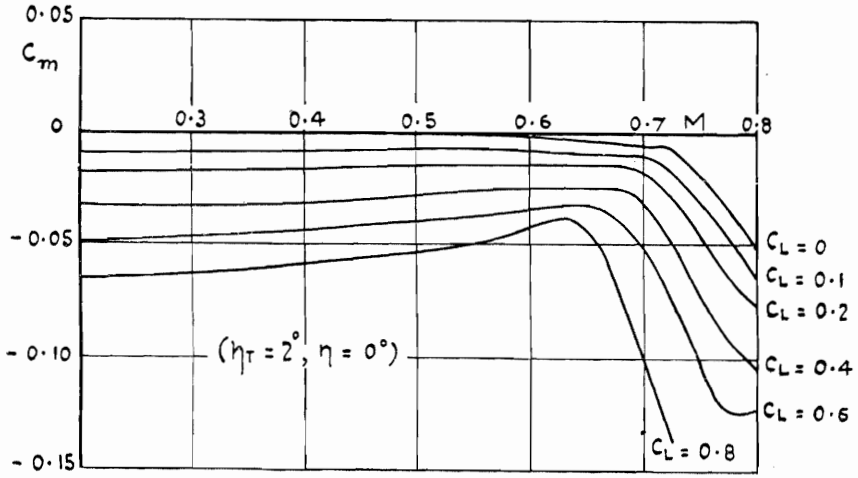

FIG. 62. Effect of Mach Number on Pitching Moment : Mustang I. (Complete model.)

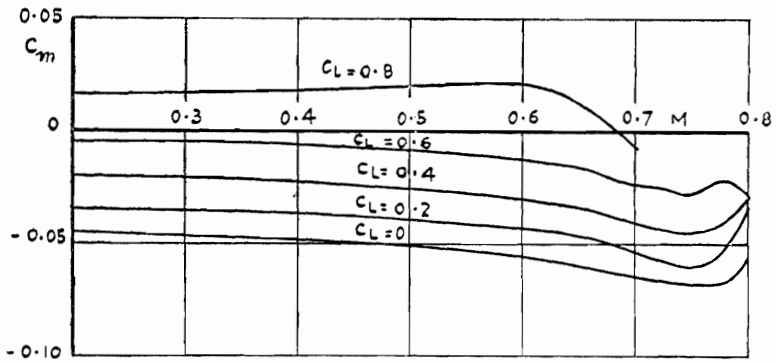

FIG. 61. Effect of Mach Number on Pitching Moment : Mustang I Wing plus Body. (No tail.)

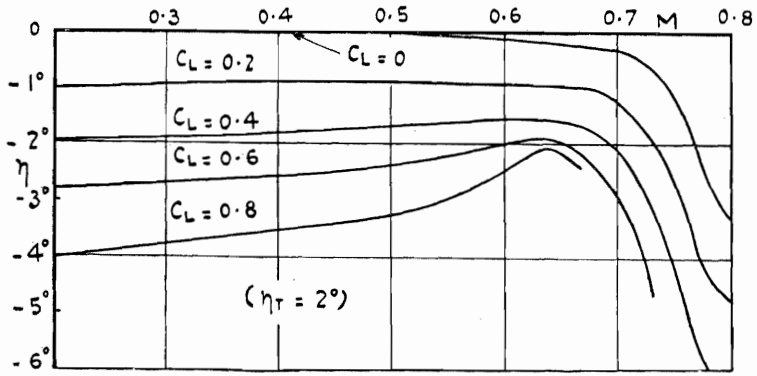

FIG. 63. Effect of Mach Number on Elevator Angle to Trim : Mustang I.

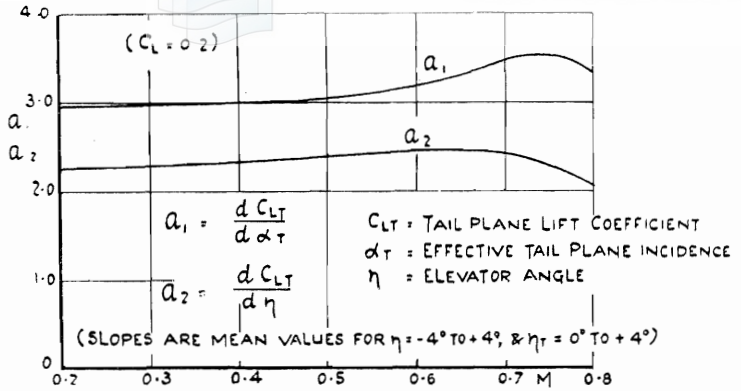

FIG. 64. Variation of a_1 and a_2 with Mach Number : Mustang I.

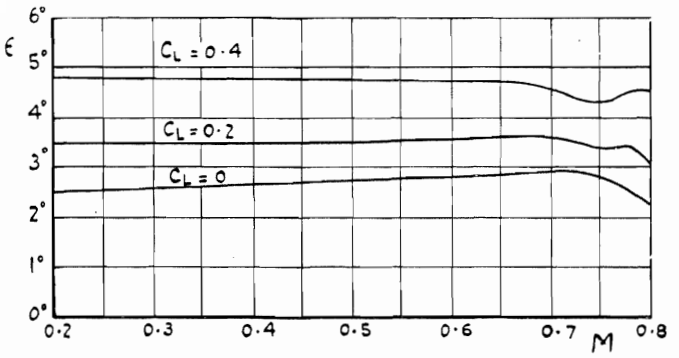

FIG. 66. Variation of Downwash at Tail with Mach Number : Mustang I.

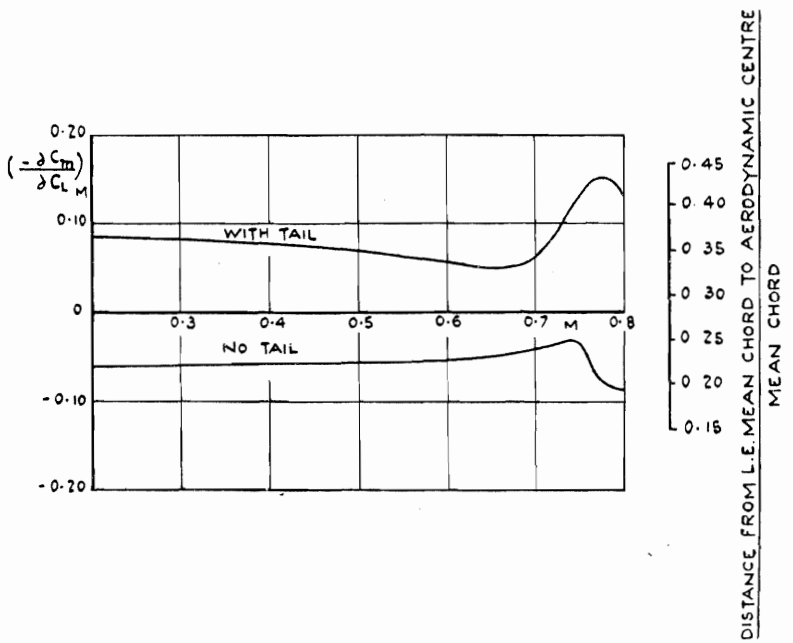

FIG. 65. Variation of $-\left(\frac{\partial C_m}{\partial C_L}\right)_M$ with Mach Number : Mustang I. $C_L = 0{\cdot}2$.

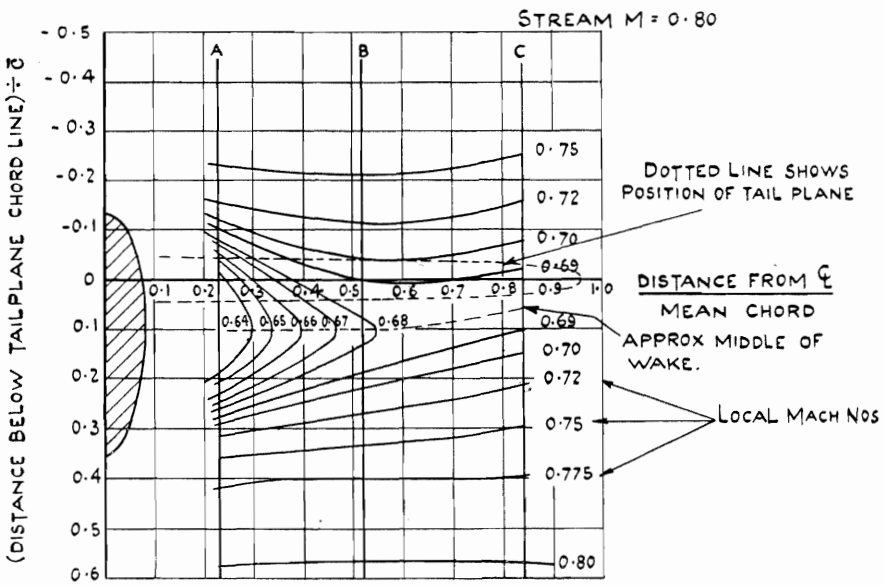

FIG. 67. Distribution of Local Mach Number at Position of Tail Plane on Typhoon.
Free stream Mach No. = 0·80
Wing incidence = 3·5°

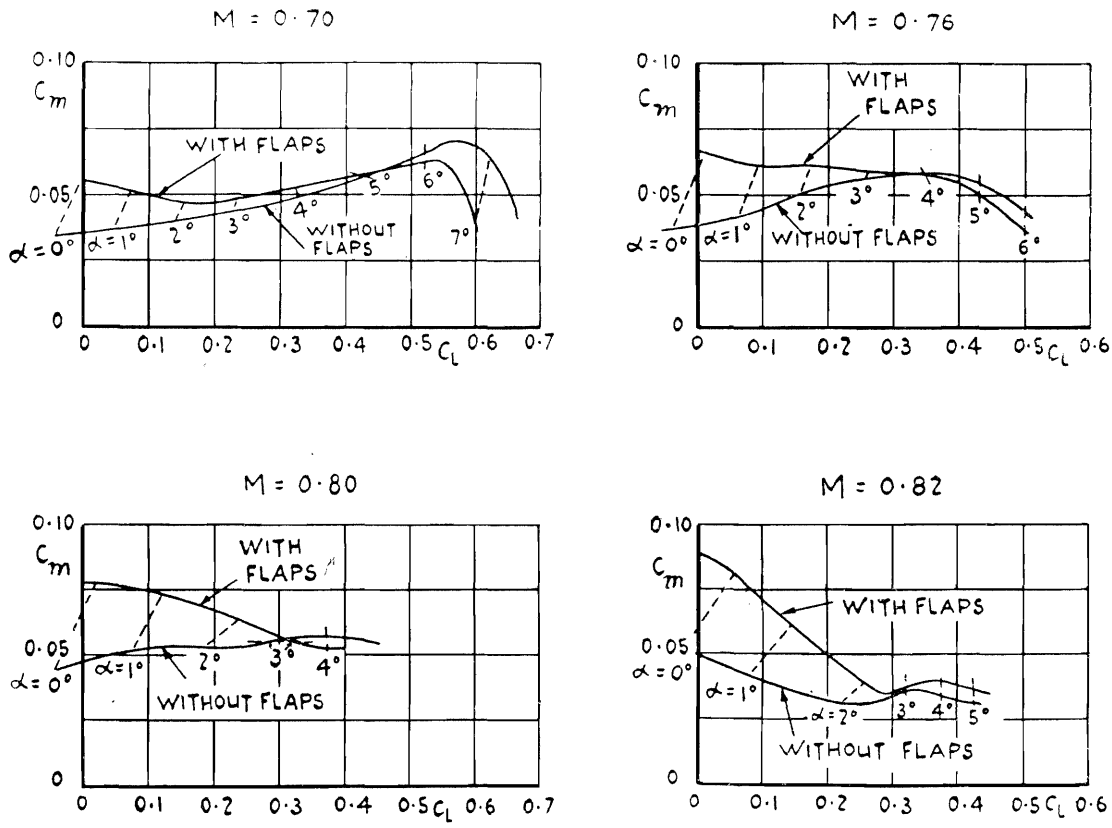

FIG. 68. Effect of Dive Recovery Flaps on a Single-engined Aircraft.
(Flaps on lower surface near wing root.)

$\frac{\text{Total Flap area}}{\text{Gross wing area}} = 0{\cdot}0066$ $\frac{\text{Flap chord}}{\text{Mean wing chord}} = 0{\cdot}059$ Flap angle = 60°

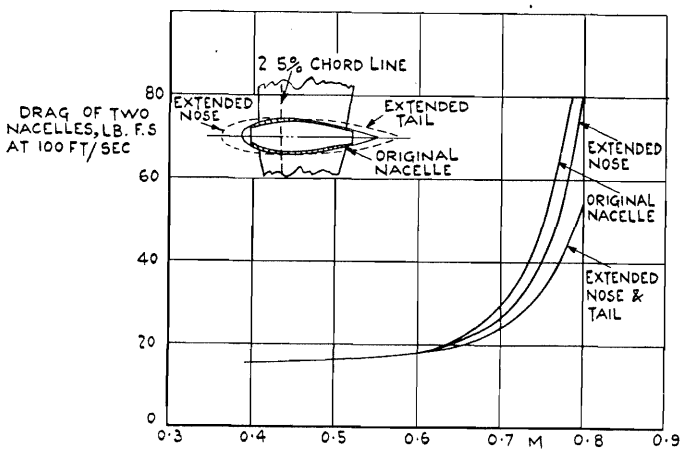

FIG. 69. Variation of Meteor Nacelle Drag with Mach Number ($C_L = 0{\cdot}1$).

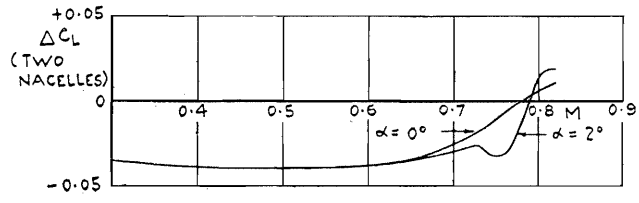

FIG. 70. Lift Increment due to Nacelles at Constant Incidence : Hornet.

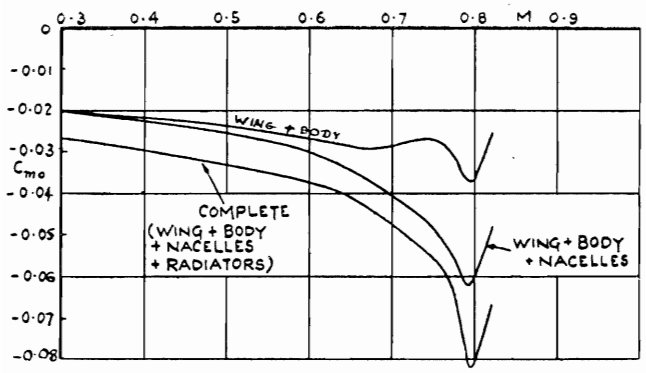

FIG. 71. Variation of $C_{m\,0}$ with Mach Number (No tail) : Hornet.

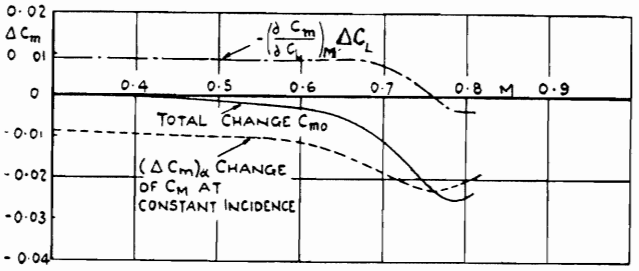

FIG. 72. Effect of Nacelles on $C_{m\,0}$ (No tail) : Hornet.

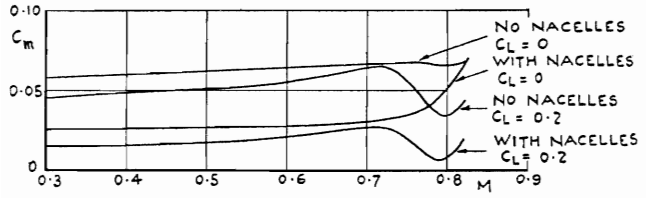

FIG. 73. Variation of C_m with Mach Number : Mosquito, with Tail, No Radiators.

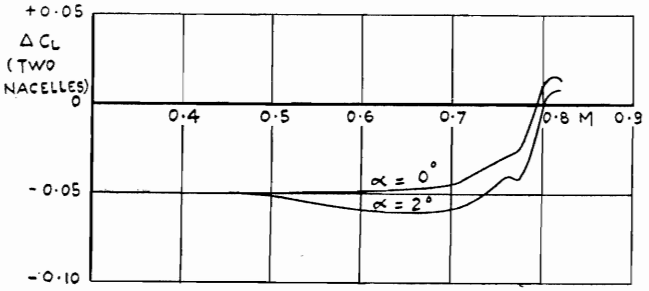

FIG. 74. Lift Increment due to Nacelles at Constant Incidence : Mosquito.

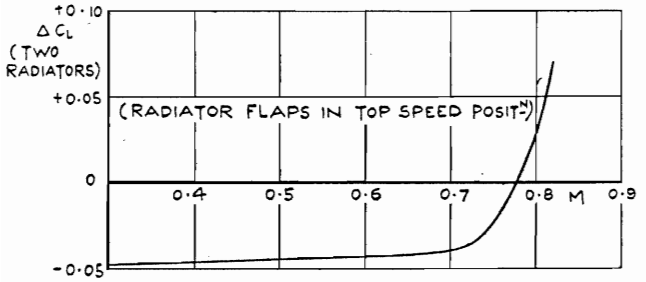

FIG. 75. Lift Increment due to Under-wing Radiators at Constant Incidence ($\alpha = +1°$) : Spiteful.

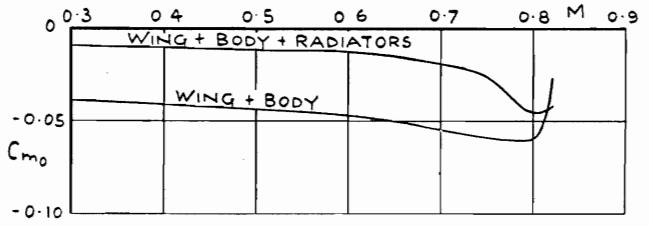

FIG. 76. Variation of $C_{m\,0}$ with Mach Number : Spiteful.

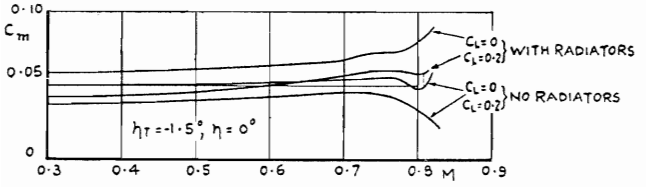

FIG. 77. Variation of C_m with Mach Number : Spiteful (With tail).

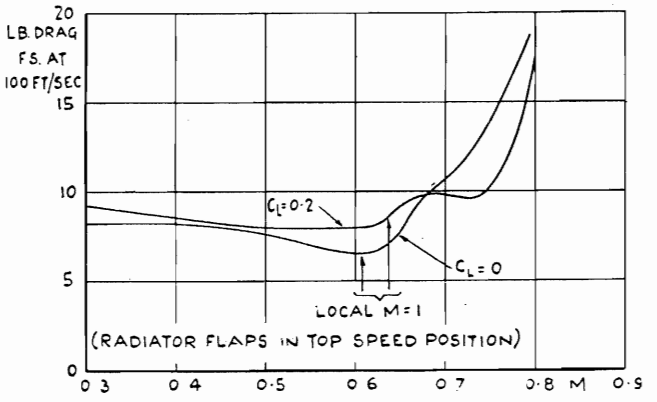

FIG. 78. Variation of Radiator Drag with Mach Number : Spiteful.

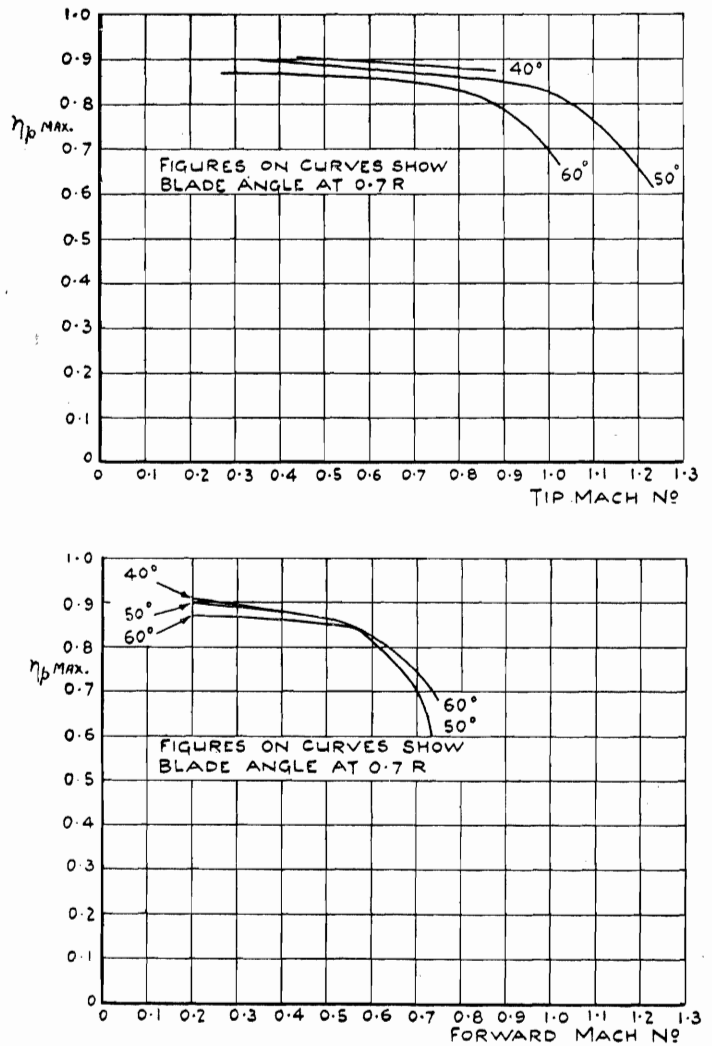

FIG. 79. Variation of Maximum Propulsive Efficiency of Propeller with Tip Mach Number and Forward Mach Number.
No. of blades = 2. Total solidity = 0·07.
Blade section : Clark Y. $t/c = 0{\cdot}06$ (from $0{\cdot}4R$ to tip)

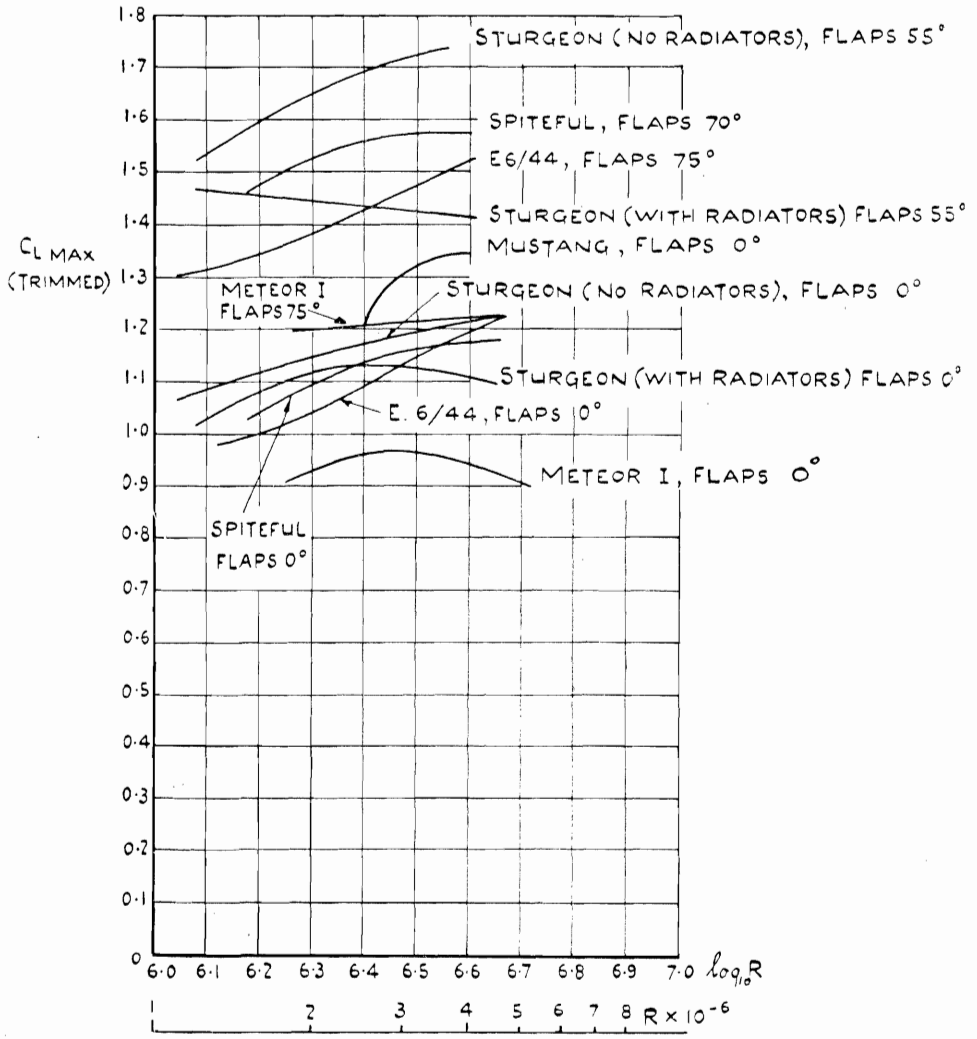

FIG. 80. Scale Effect on Maximum Lift Coefficient : (Mach Number < 0·2)

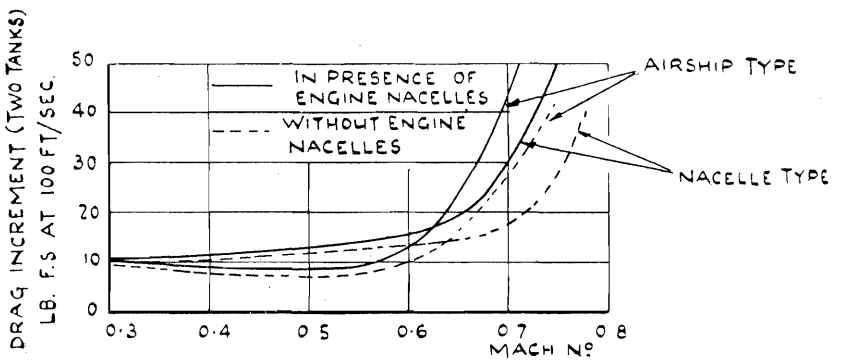

FIG. 81. Effect of Mach Number on Drag of Drop Tanks Mounted under Wing of Meteor I ($C_L = 0 \cdot 1$).

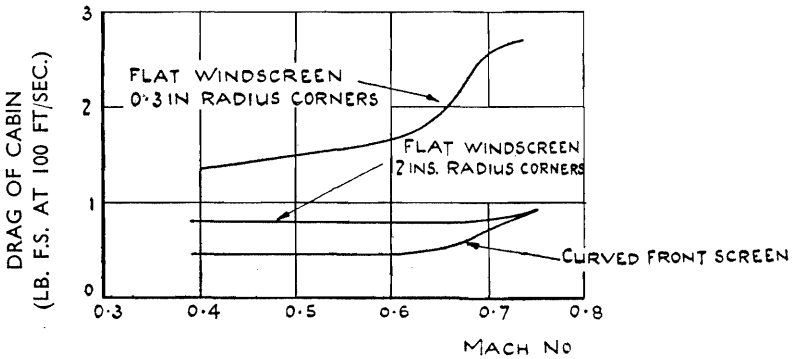

FIG. 83. Drag of Alternative Cabins on Spiteful.

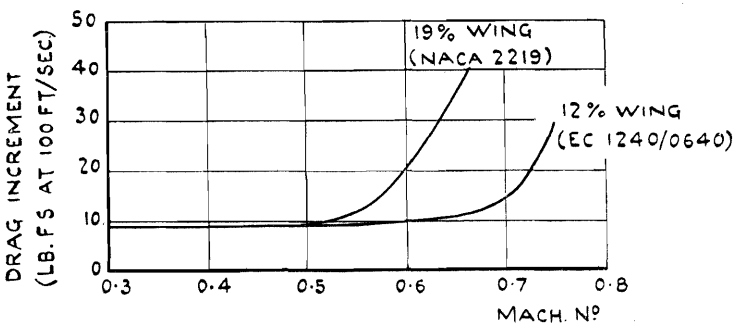

FIG. 82. Effect of Mach Number on Drag of One 1,000 lb. M.C. Bomb Mounted under Wings of Different Thickness ($C_L = 0 \cdot 1$).

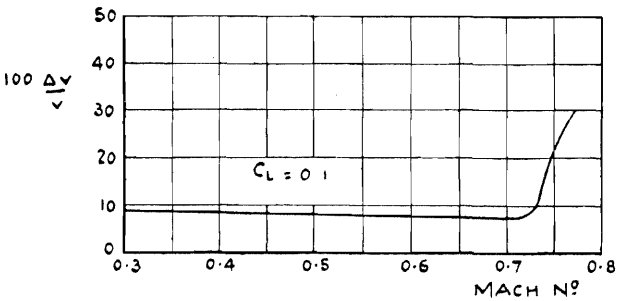

FIG. 84. Percentage Error in Speed for A.S.I. Connected to Under-wing Pitot-static Head on Typhoon.

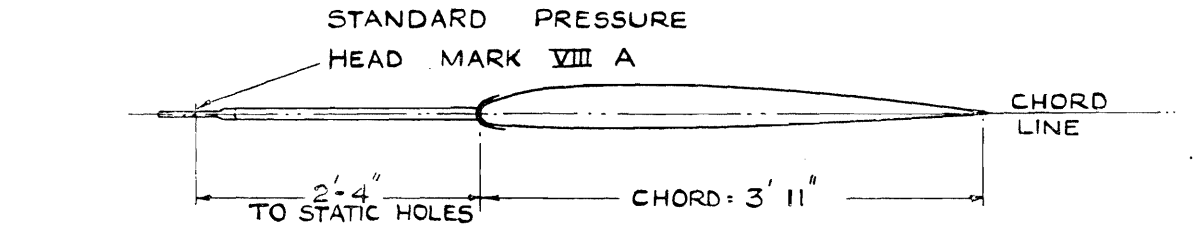

LOCAL $\frac{\text{THICKNESS}}{\text{CHORD}}$ = 0·073 HEAD IS 15' 9" OUTBOARD OF AIRCRAFT ℄.

LEADING EDGE HEAD

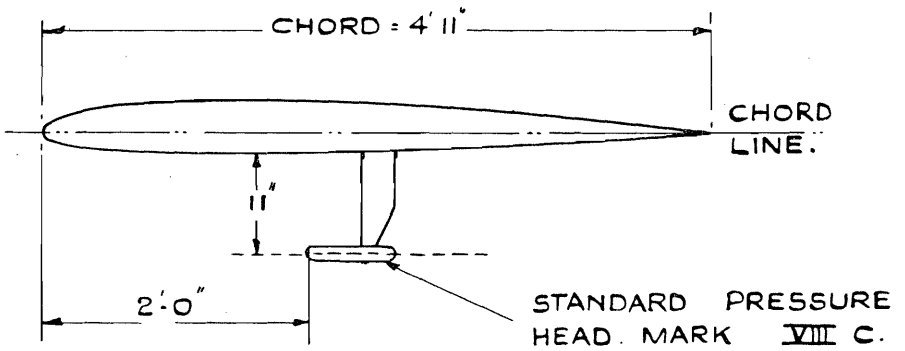

LOCAL $\frac{\text{THICKNESS}}{\text{CHORD}}$ = 0·087" HEAD IS 14' 8" OUTBOARD OF AIRCRAFT ℄.

UNDER WING HEAD.

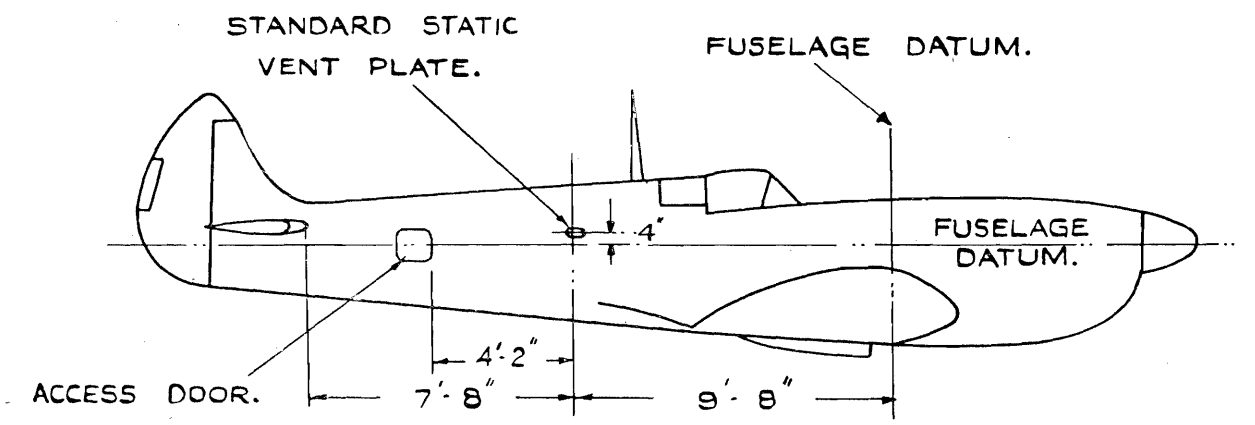

STATIC VENT.

FIG. 85. Location of Pitot-Static Heads and Static Vent for Position Error Measurements. Spitfire XI.

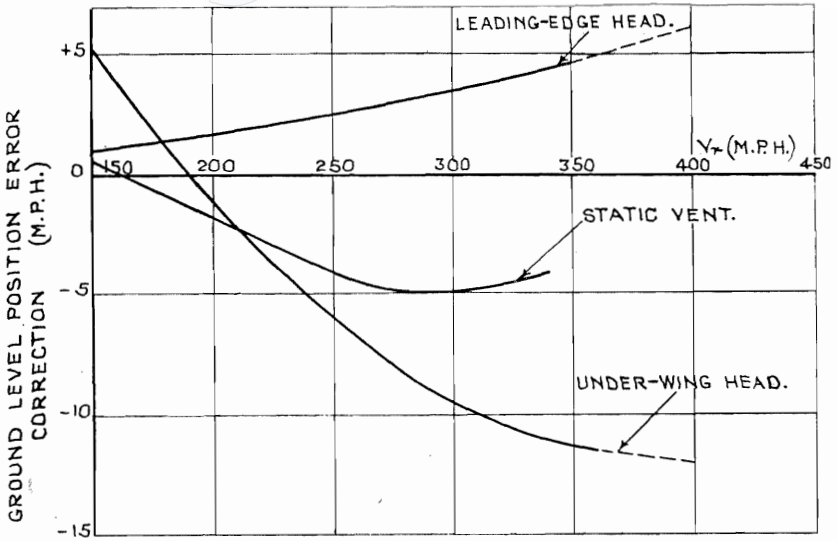

FIG. 86. Ground Level Speed Corrections for Leading-edge and Under-wing Heads and Static Vent.

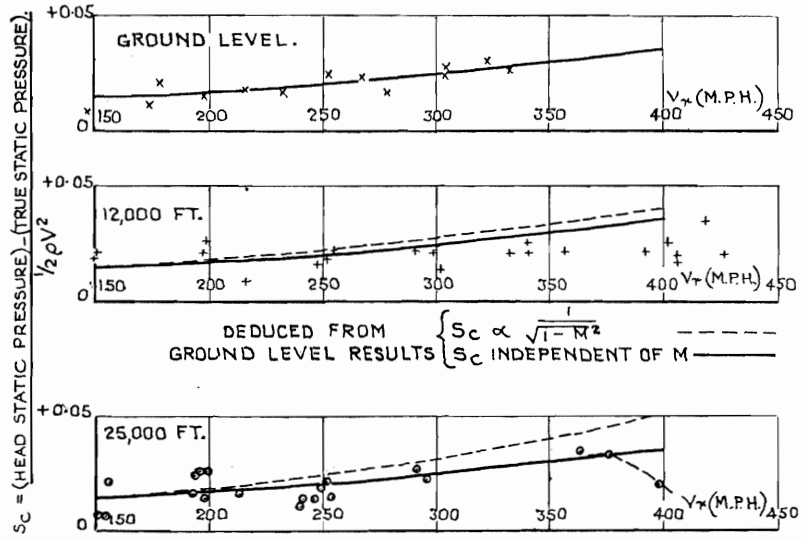

FIG. 87. Leading-edge Head—Variation of Static Pressure Correction with Altitude and Air Speed.

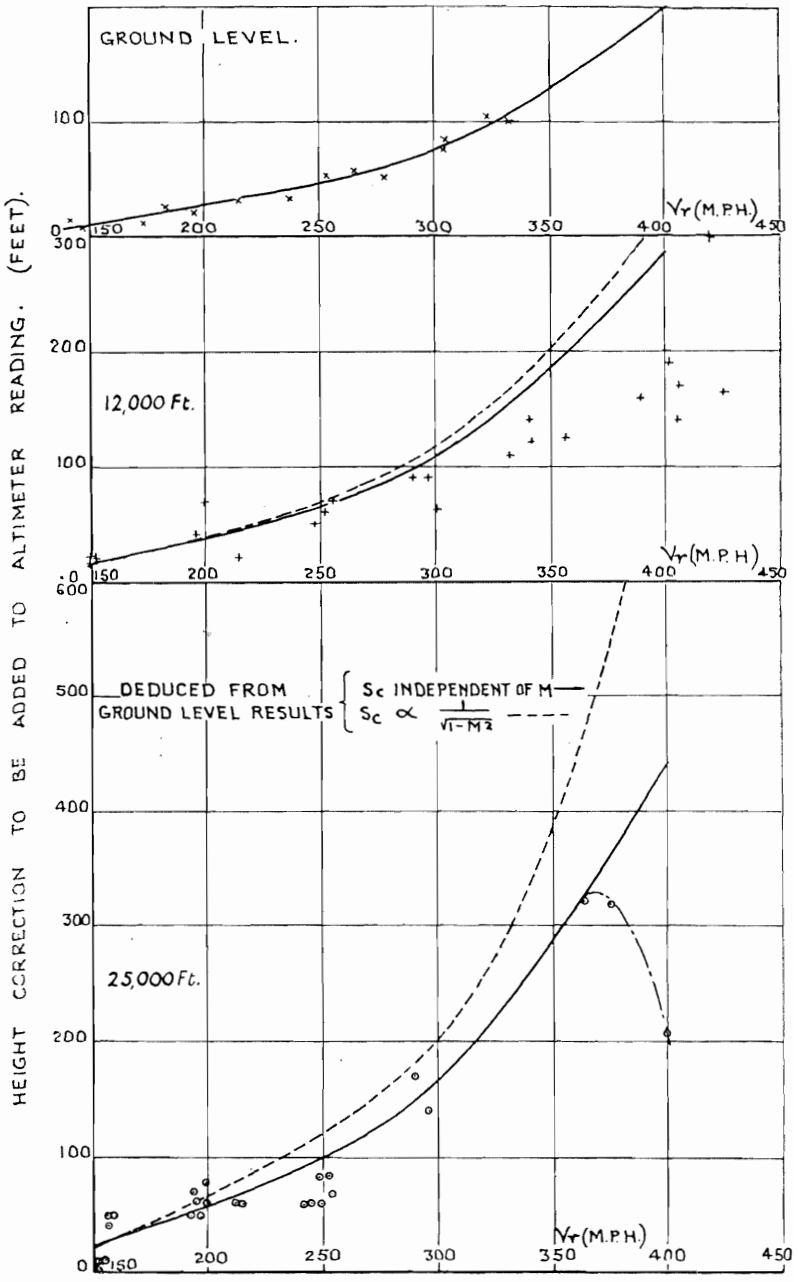

Fig. 88. Leading-edge Head—Measured Correction to Altimeter Reading.

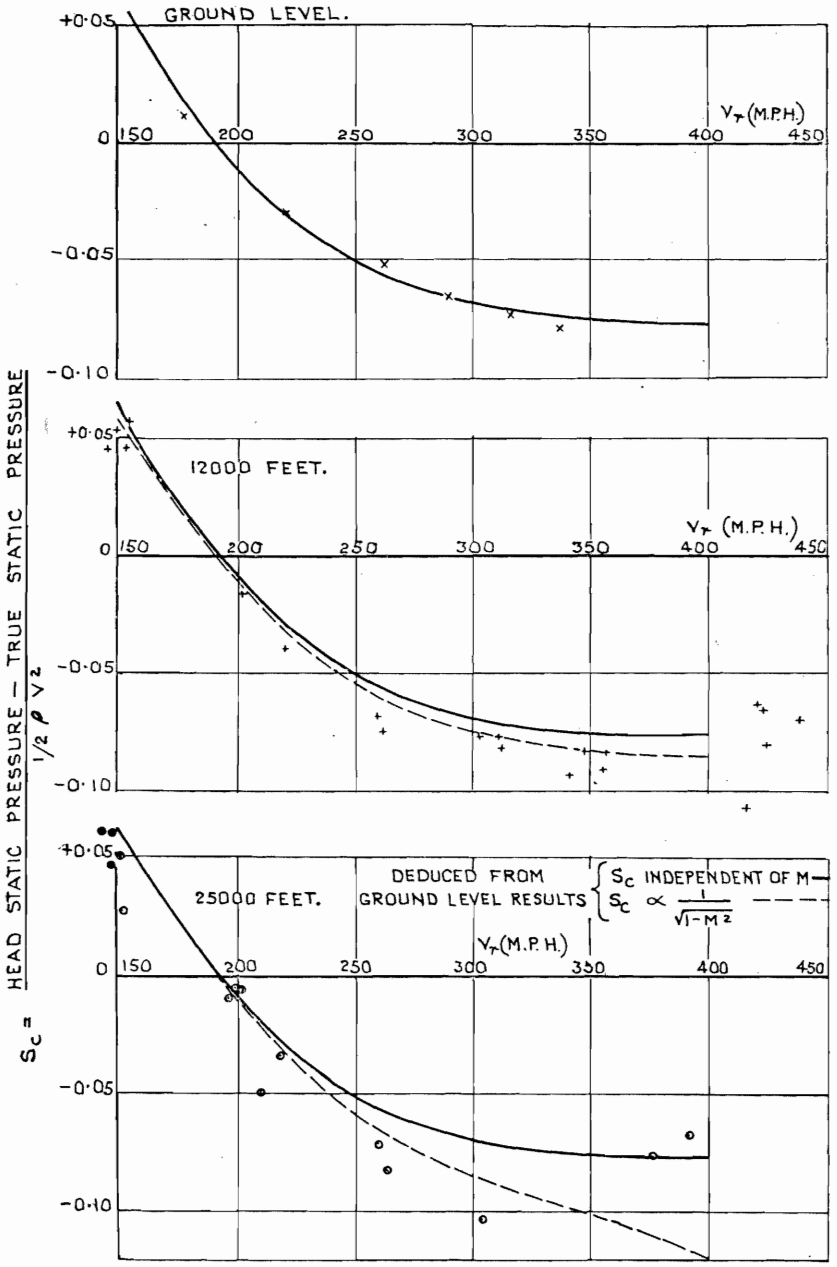

FIG. 89. Under-wing Head—Variation of Static Pressure Correction with Altitude and Air Speed.

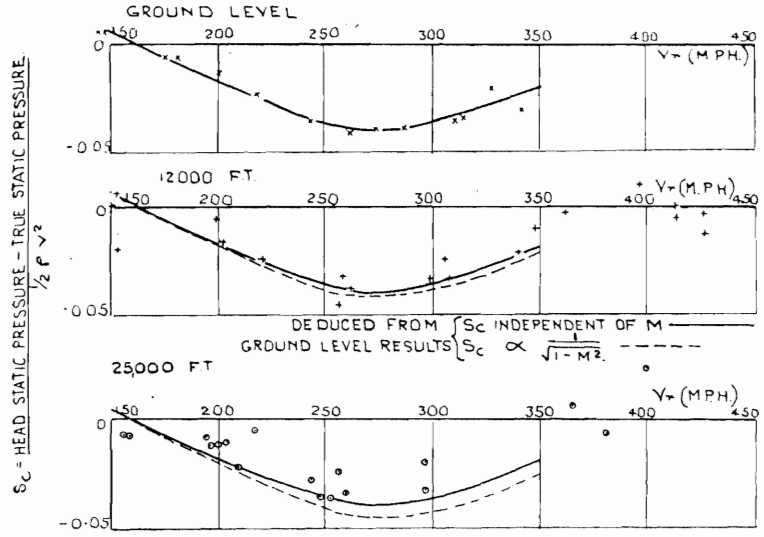

FIG. 90. Static Vent—Variation of Static Pressure Correction with Altitude and Air Speed.

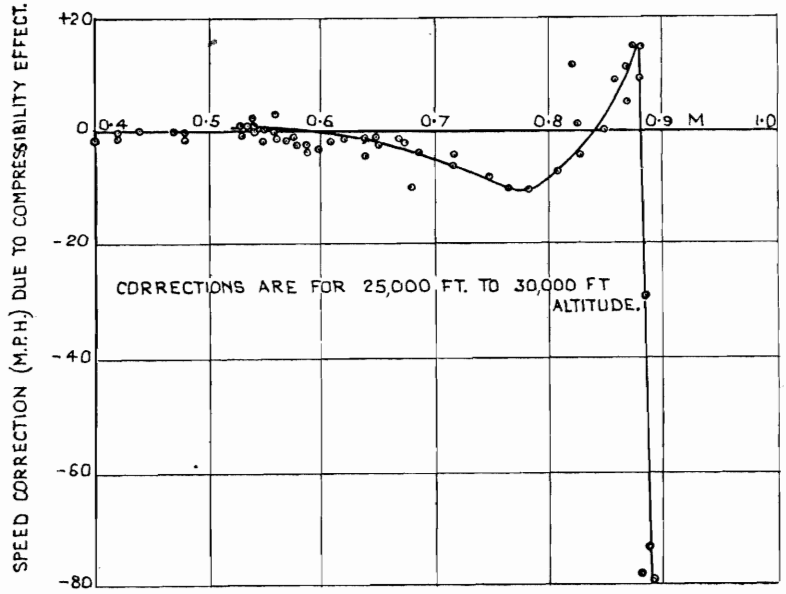

FIG. 91. Under-wing Head—Speed Correction due to Compressibility Effect on Static Pressure at Head.

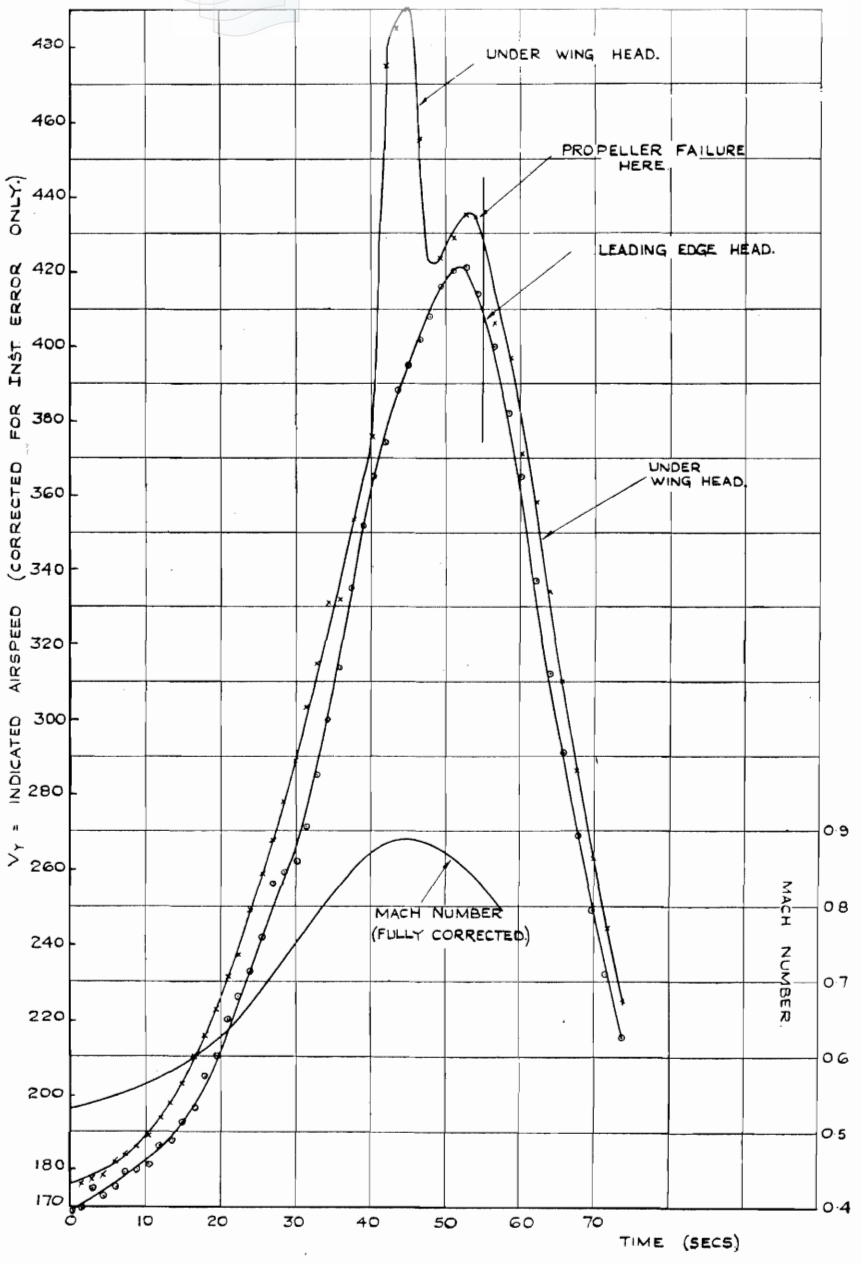

FIG. 92. Leading-edge and Under-wing Heads—Comparison of Indicated Airspeeds Recorded in a High-Speed Dive.

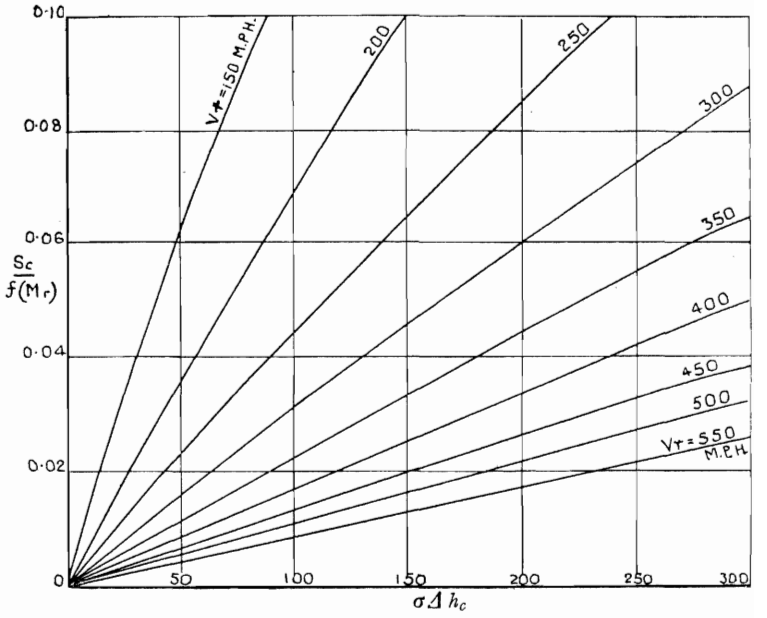

FIG. 93. Relation between Altitude Correction and Static Pressure Coefficient S_c. (Positive values of S_c)

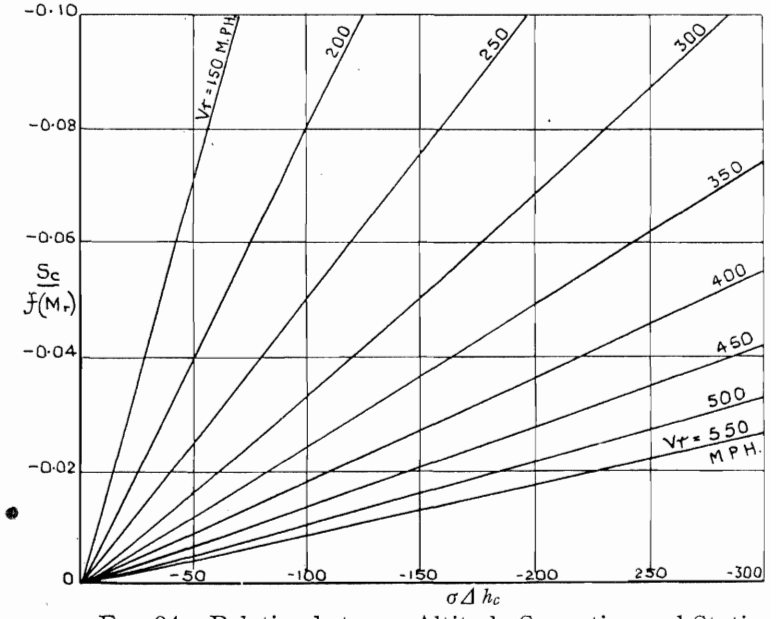

FIG. 94. Relation between Altitude Correction and Static Pressure Coefficient S_c. (Negative values of S_c)

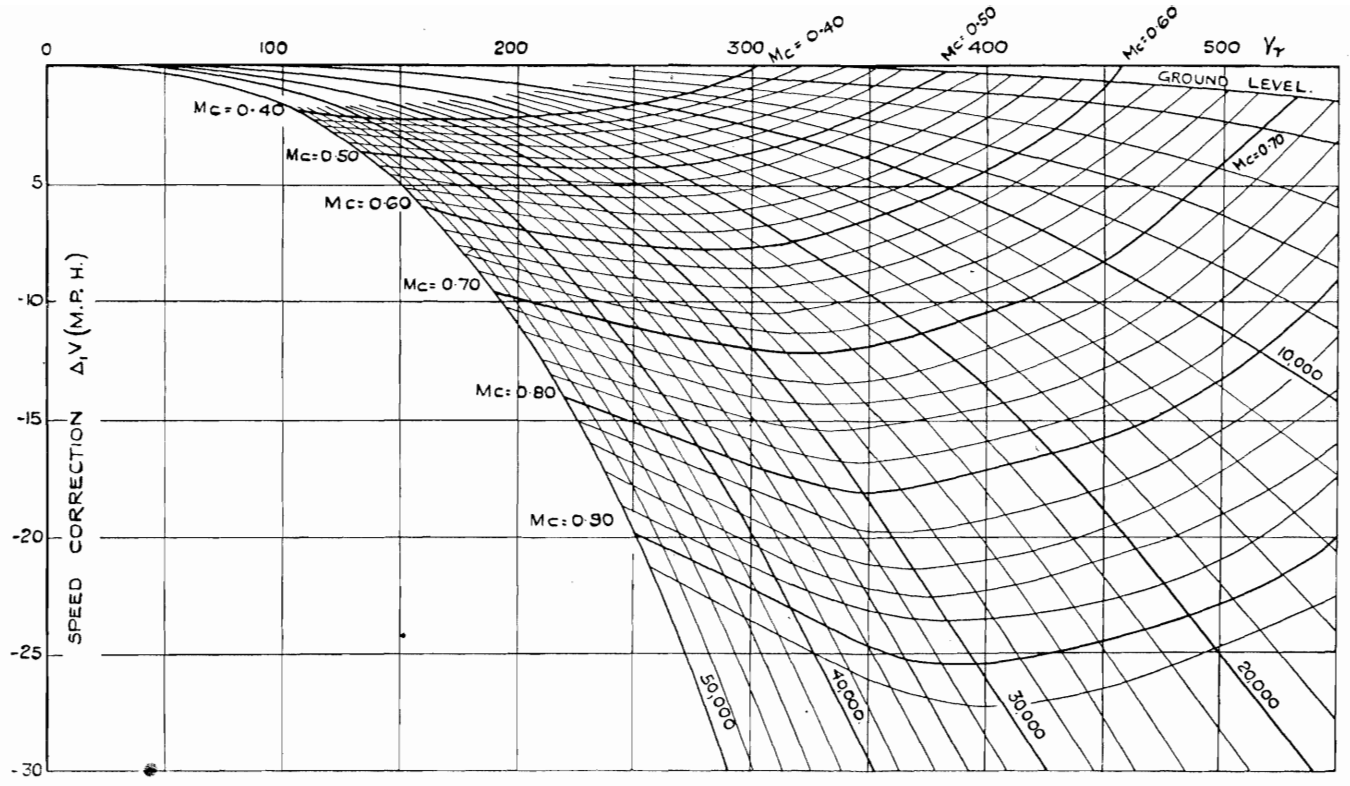

FIG. 95. Speed Correction ($\Delta_1 V$) due to Calibration Compressibility Error.

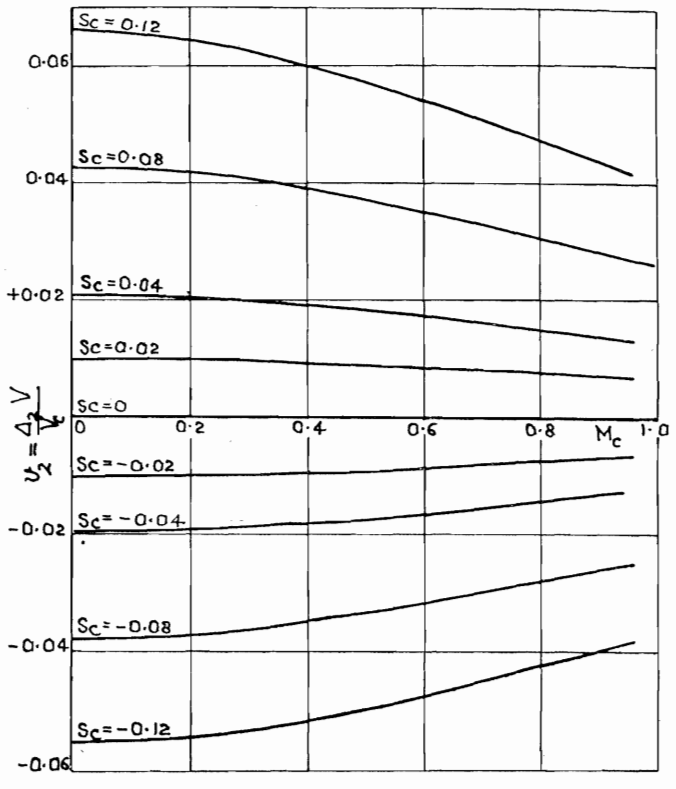

FIG. 96. Static Compressibility Error Correction to Speed.

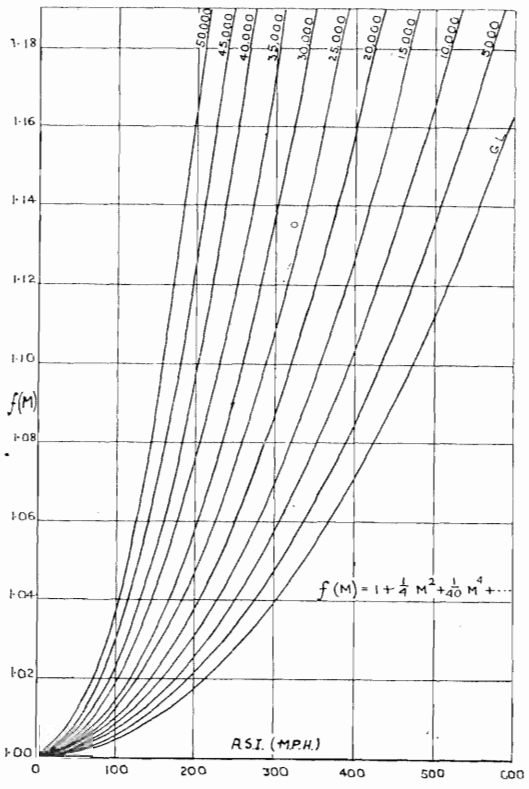

FIG. 97. Compressibility Function $f(M)$

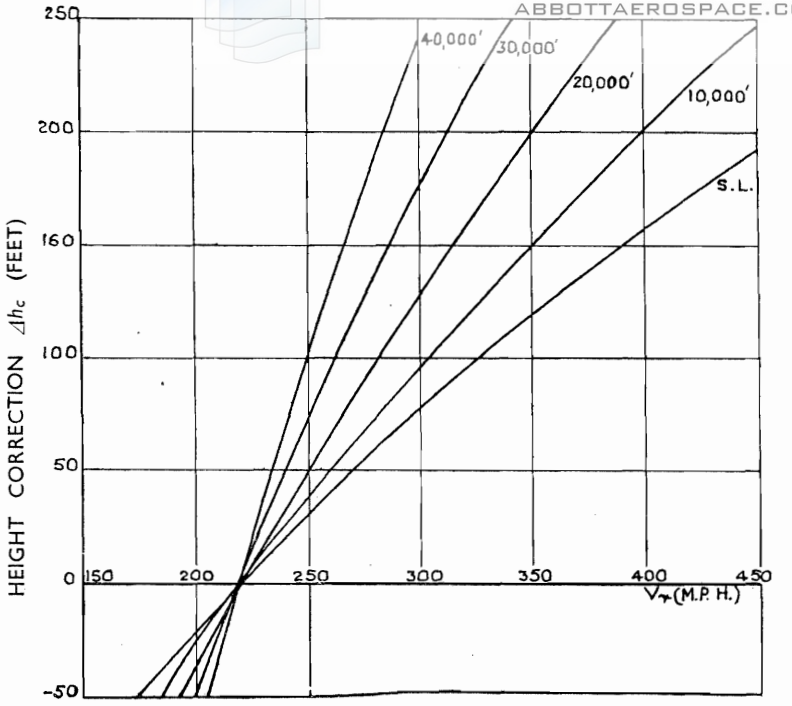

Total correction to altitude for position error and compressibility.

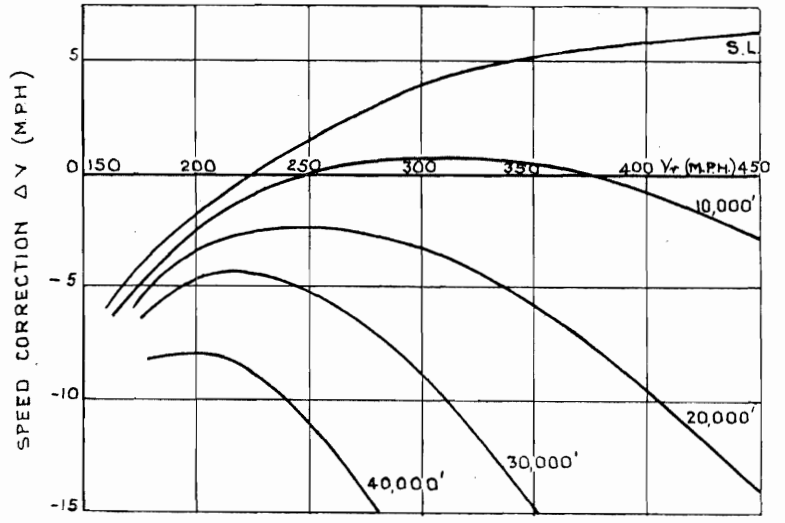

Total correction to air speed for position error and compressibility.

FIG. 98. Typical Charts for an Aircraft Fitted with a Leading-edge Pitot-Static Head.

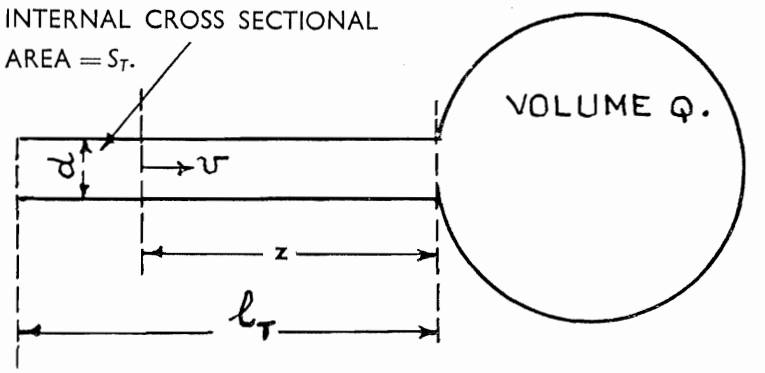

FIG. 99. Diagram of Tube from Static Head to Altimeter.

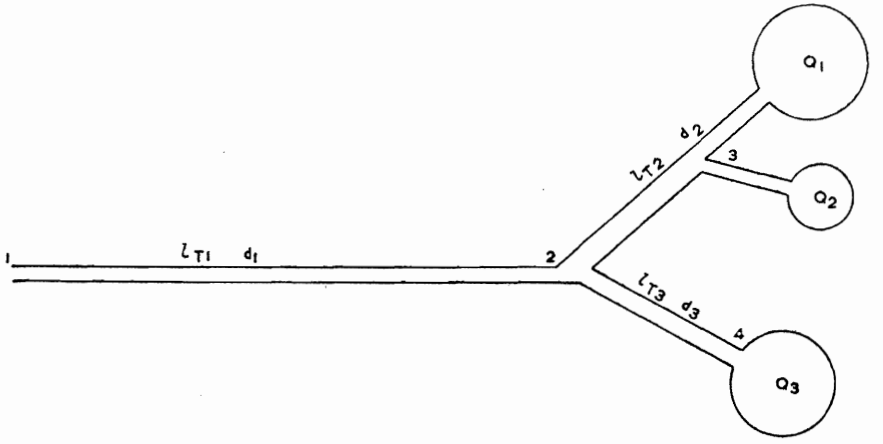

FIG. 100. Typical System of Tubes and Instruments for Lag Calculations.

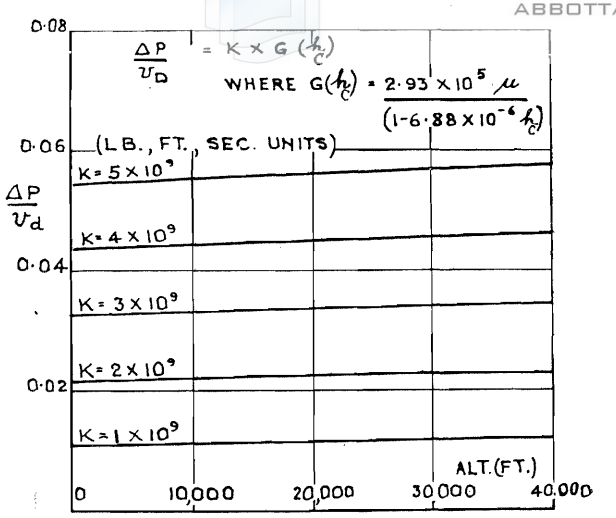

FIG. 101. Variation of Theoretical Pressure Lag with Height. (See equation (32))

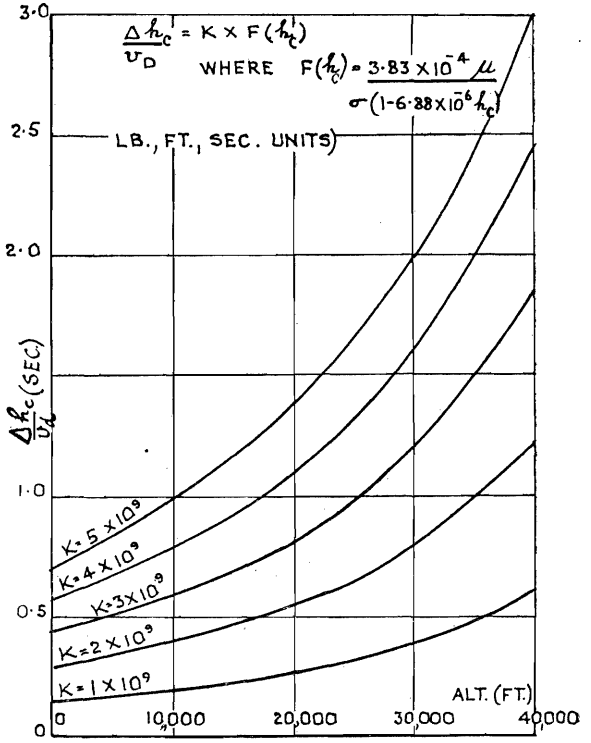

FIG. 102. Variation of Theoretical Height Lag with Height. (See equation (34))

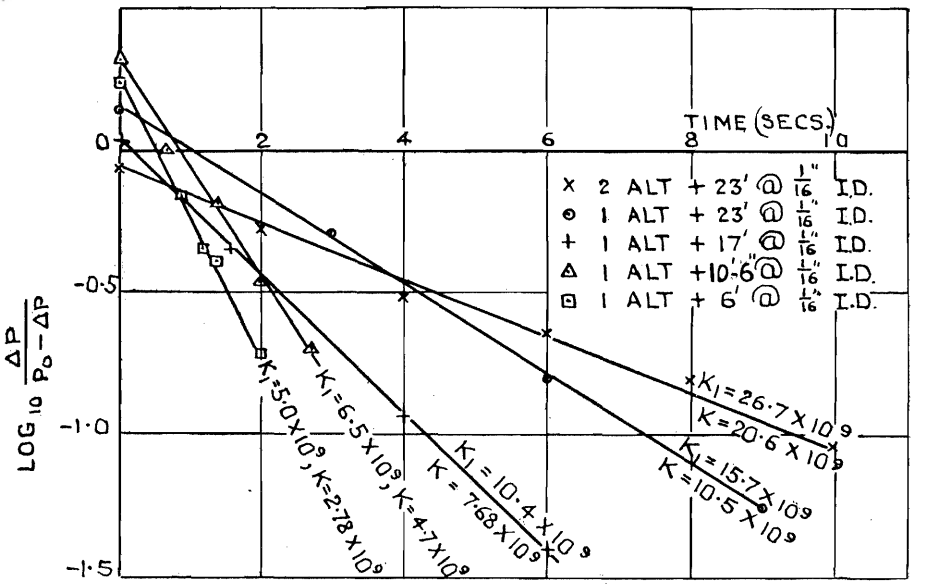

FIG. 103. Determination of Lag Factor K_1 in the Laboratory for an Altimeter and Various Tube Arrangements.

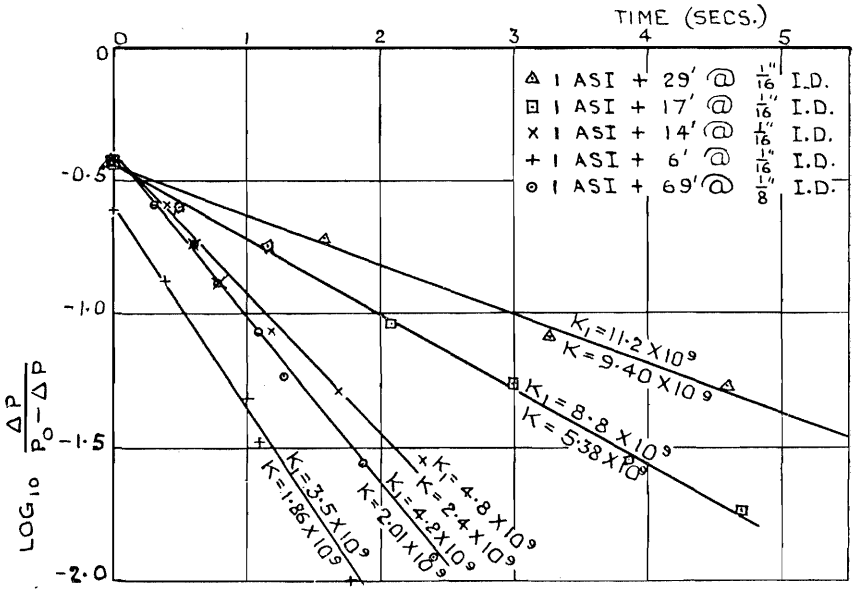

FIG. 104. Determination of Lag Factor K_1 in the Laboratory for an Air Speed Indicator and Various Tube Arrangements.

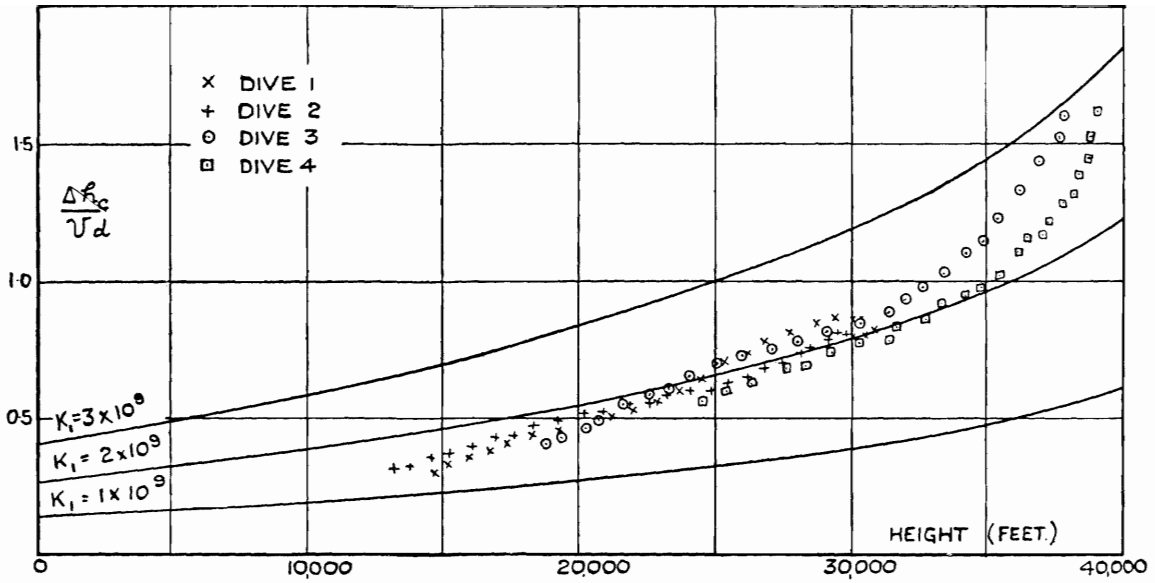

FIG. 105. Determination of Lag Factor K_1 in Flight—Spitfire XI.

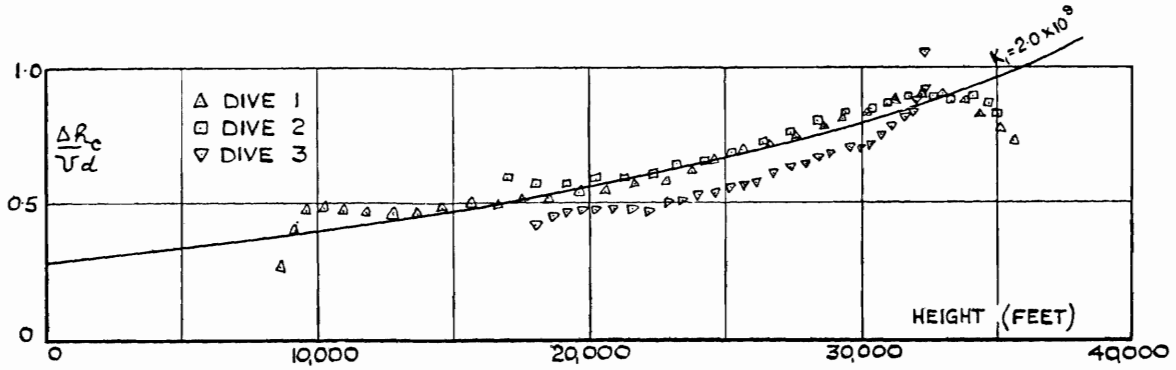

FIG. 106. Determination of Lag Factor K_1 in Flight—Spitfire XXI.

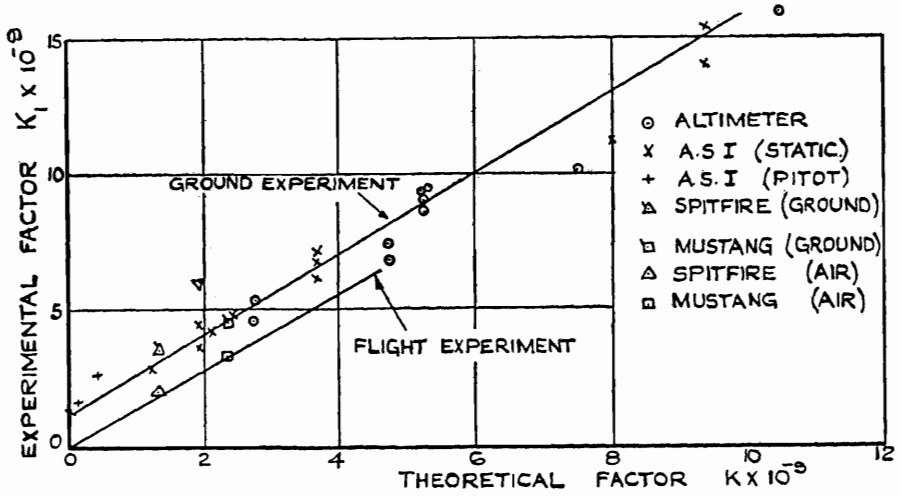

FIG. 107. Relation between Theoretical Lag Factor K and Experimental Lag Factor K_1.

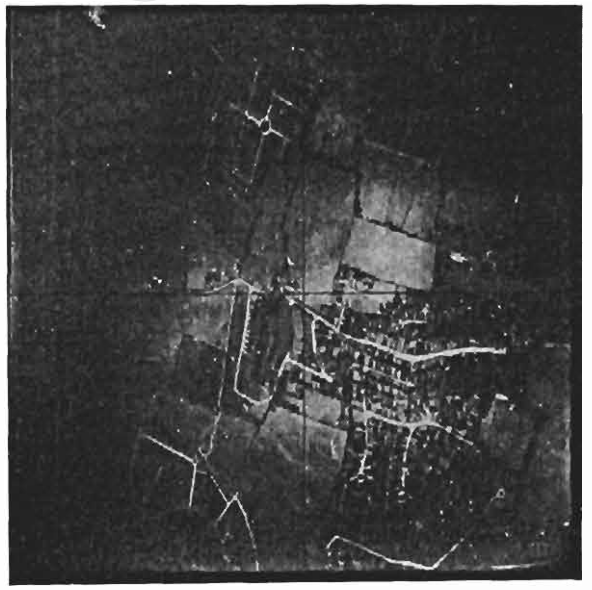

Photographic Record.

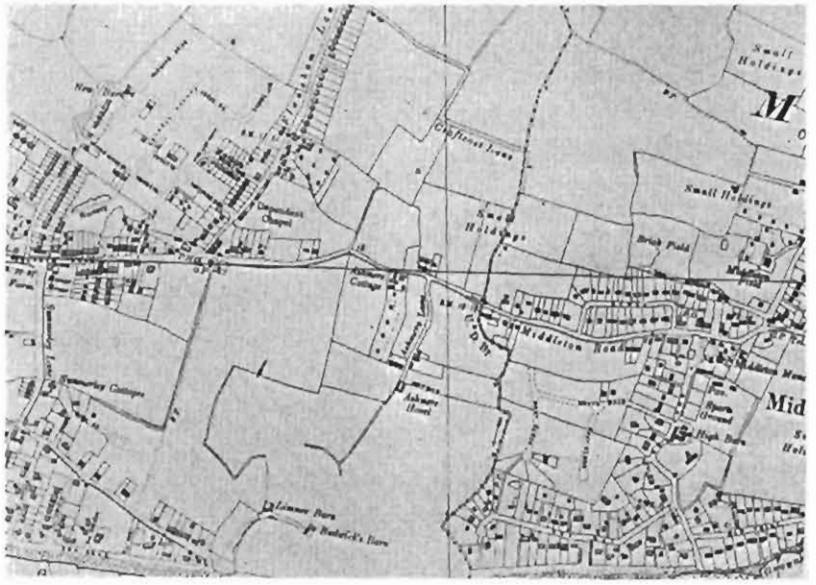

FIG. 108. Typical Aircraft Photographic Record and Ordnance Survey Map of Same Area.

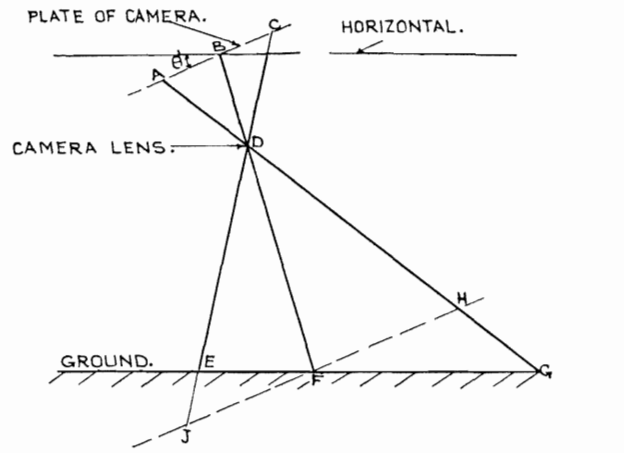

A AND C ARE TYPICAL POINTS ON FILM CORRESPONDING TO POINTS G AND E ON GROUND.

$EF = X_1$ $GF = X_2$

$BC = X_1$ $AB = X_2$

BD = FOCAL LENGTH OF CAMERA = f

$DF = S_R$

FIG. 109. Diagram of Photographic Method of Determining θ', a Pitch Angle, or φ', a Roll Angle.

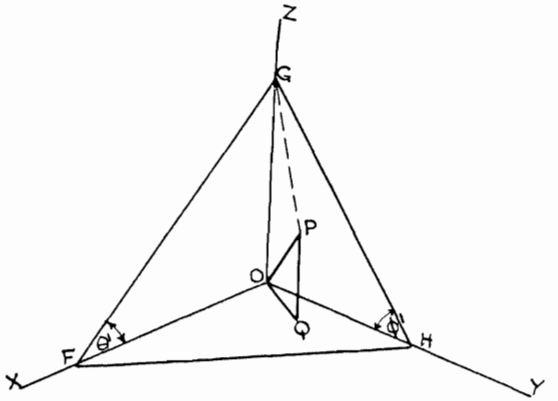

O is position of camera.

Plane OXY is plate of camera with OZ the perpendicular axis through the lens.

Plane FGH is ground plane.

OG is slant distance S_R.

OP is camera height H_T.

FIG. 110. Diagram of Photographic Method of Determining Height.

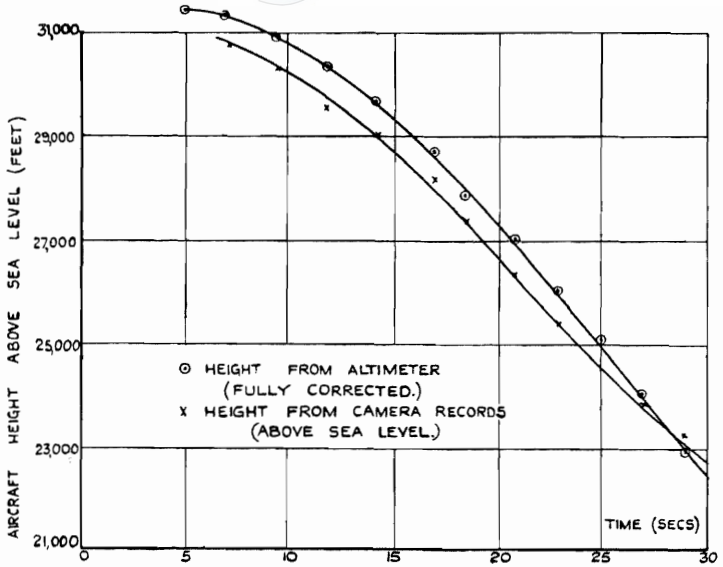

FIG. 111. Comparison of "Camera Height" and "Altimeter Height" in a Dive.

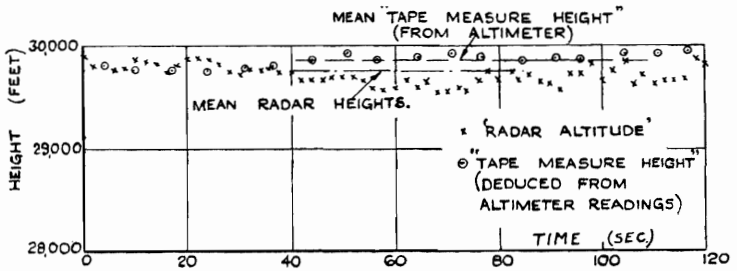

FIG. 112. Comparison of "Radar Height" and "Altimeter Height" in Level Flight (from Ref. 93).

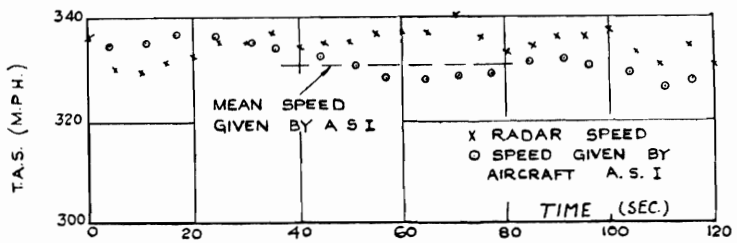

FIG. 113. Comparison of True Air Speeds Given by Radar and by Aircraft A.S.I. in Level Flight (from Ref. 93).

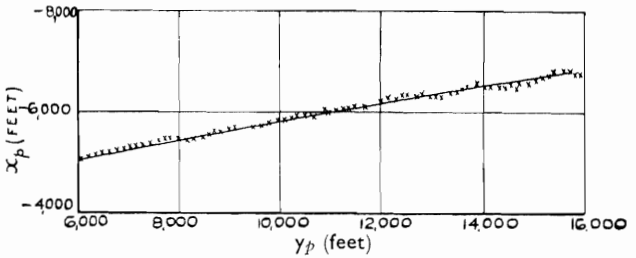

FIG. 114. Plan of Flight Path in Dive as Given by Radar Tracking.

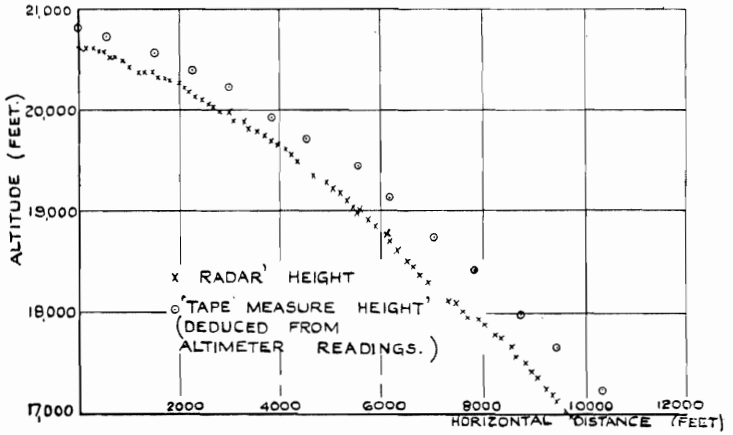

FIG. 115. Comparison of Heights Given by Radar and Altimeter in a Dive.

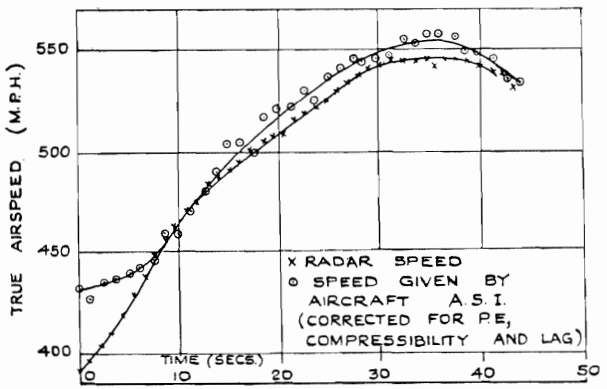

FIG. 116. Comparison of True Air Speeds Given by Radar and Aircraft A.S.I. in a Dive.

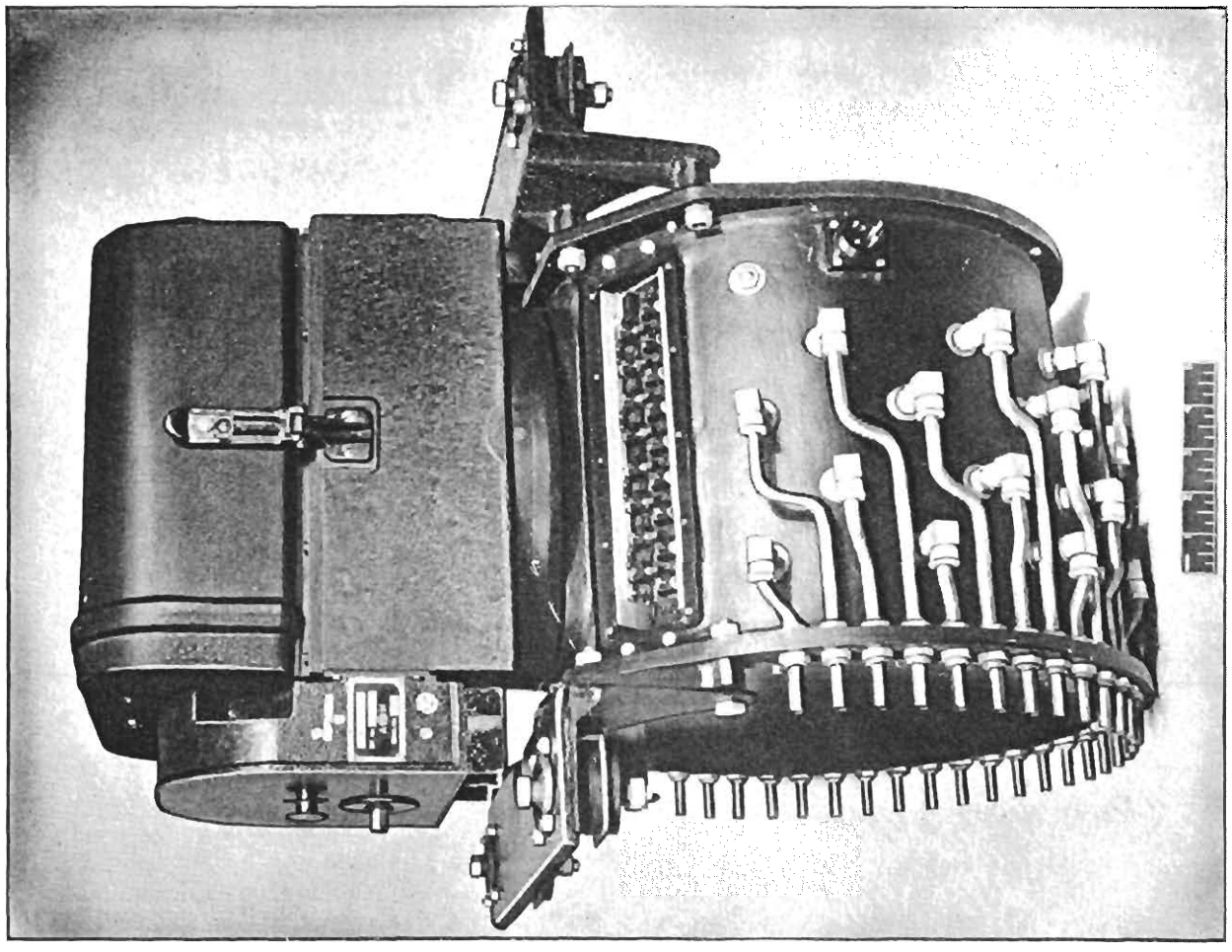

Fig. 118. Multi-capsule Manometer.

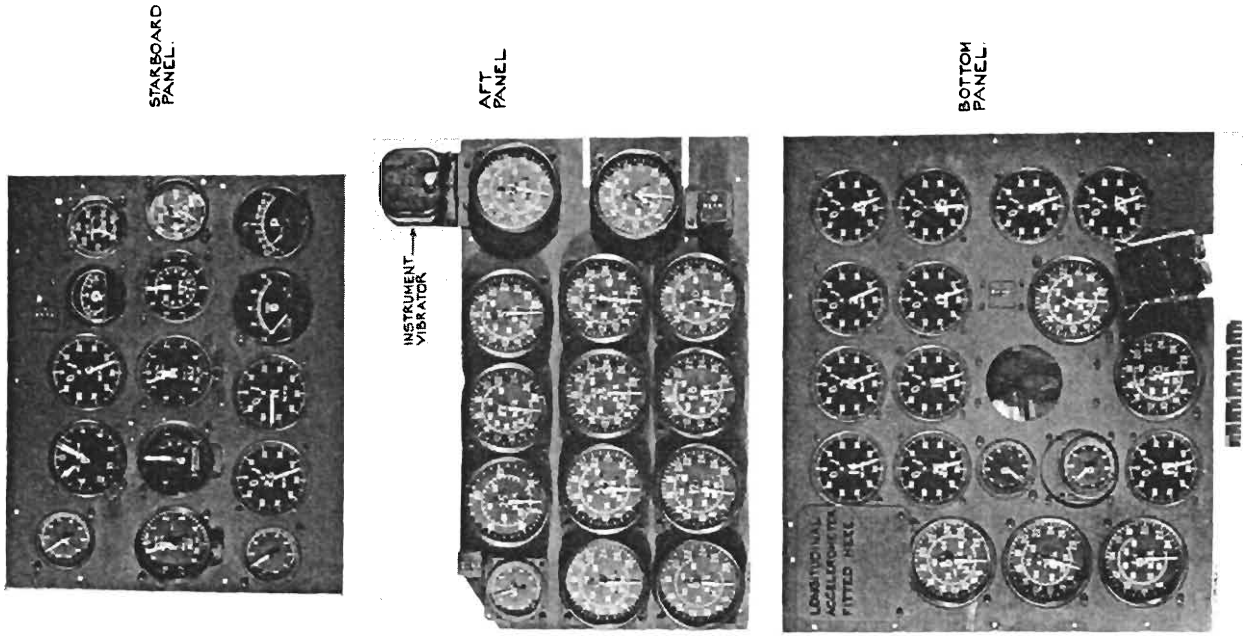

Fig. 117. Automatic Observer.

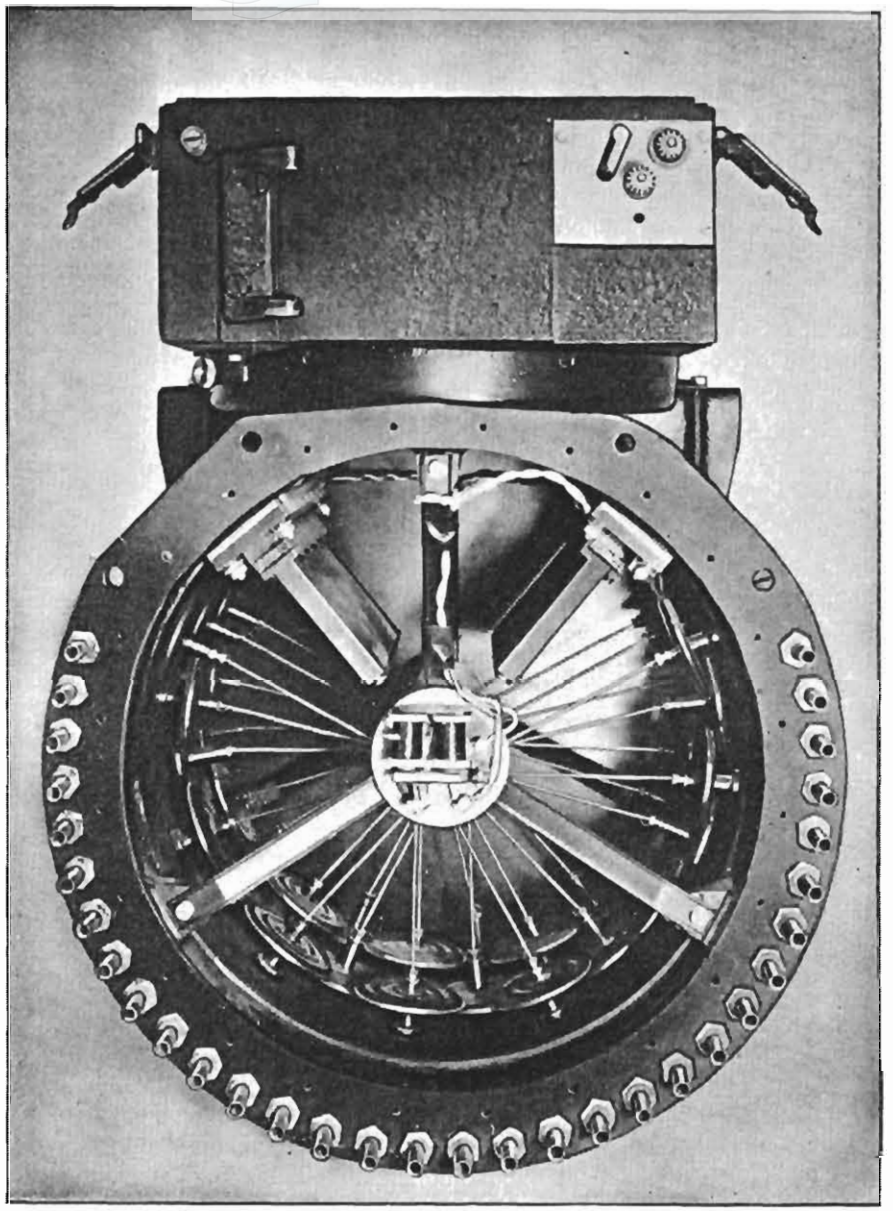

FIG. 119. Multi-capsule Manometer.

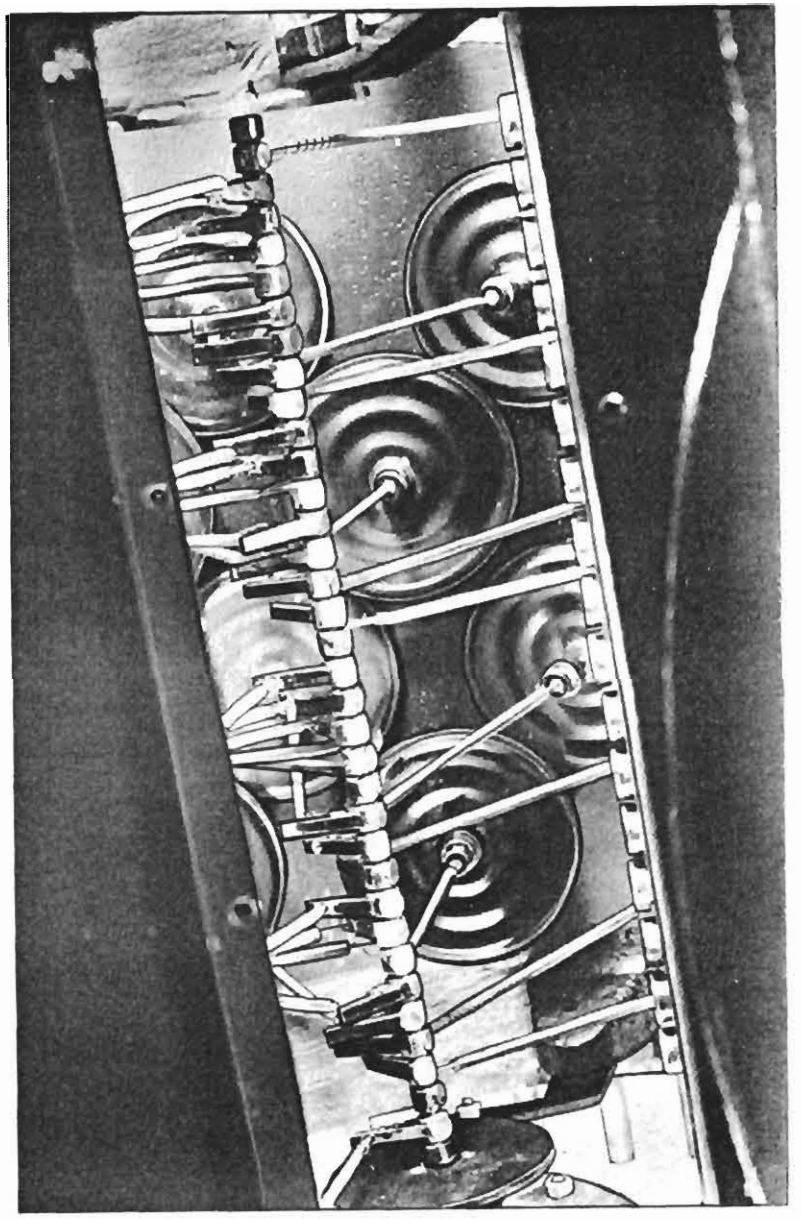

FIG. 120. Multi-capsule Manometer (showing details of capsules, linkages and mirrors).

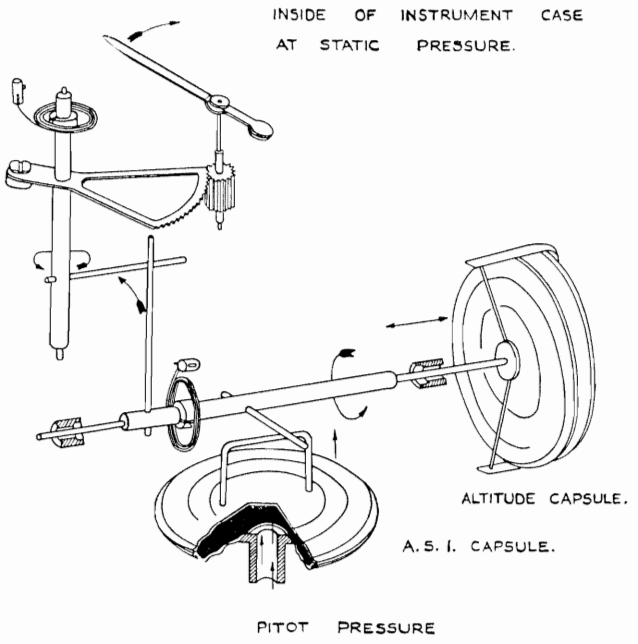

FIG. 121. Diagrammatic Arrangement of Machmeter Showing Principle of Operation.

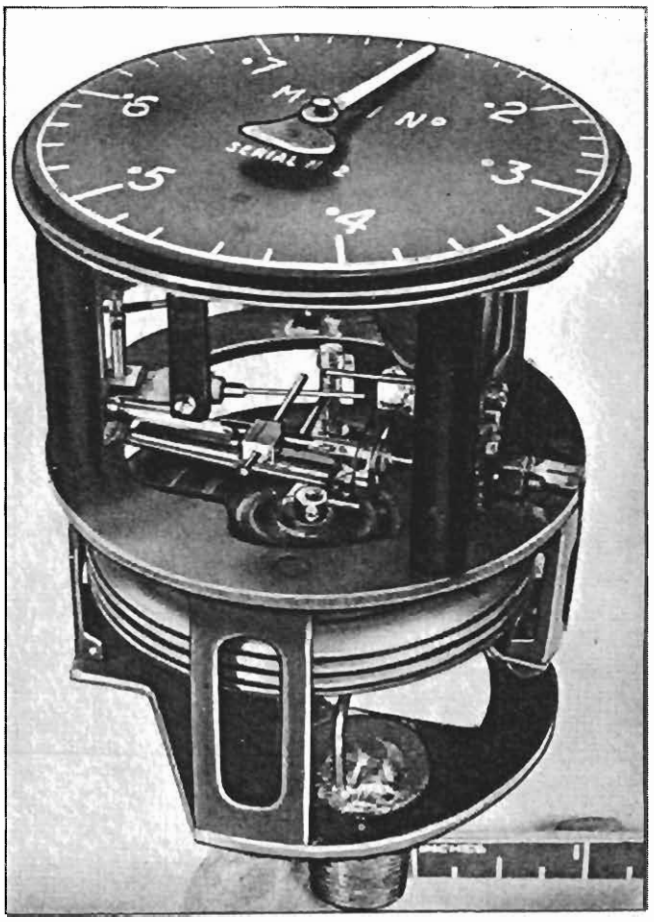

FIG. 122. Machmeter.

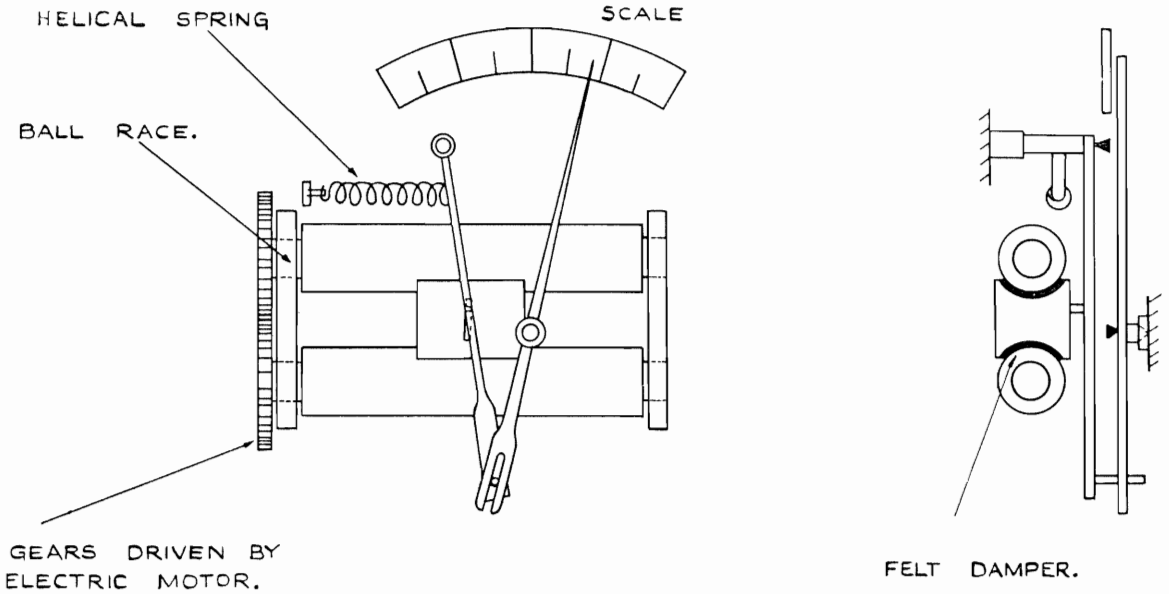

FIG. 123. Diagrammatic Sketch of Longitudinal Accelerometer (not to scale).

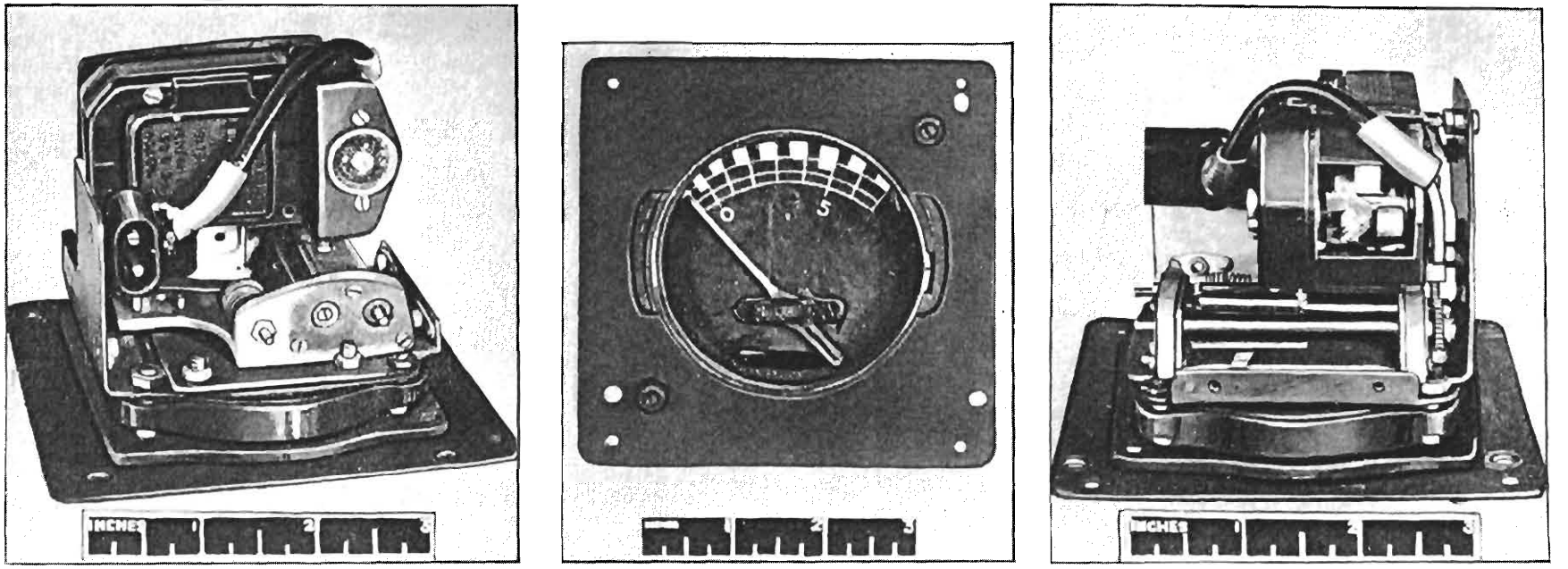

FIG. 124. The Longitudinal Accelerometer.

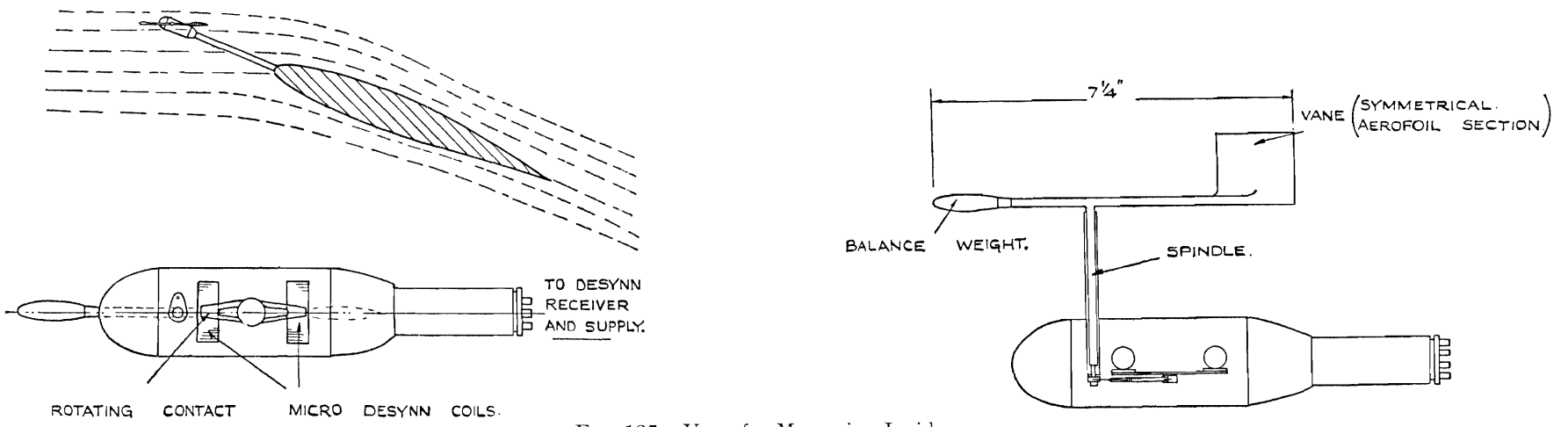

FIG. 125. Vane for Measuring Incidence.

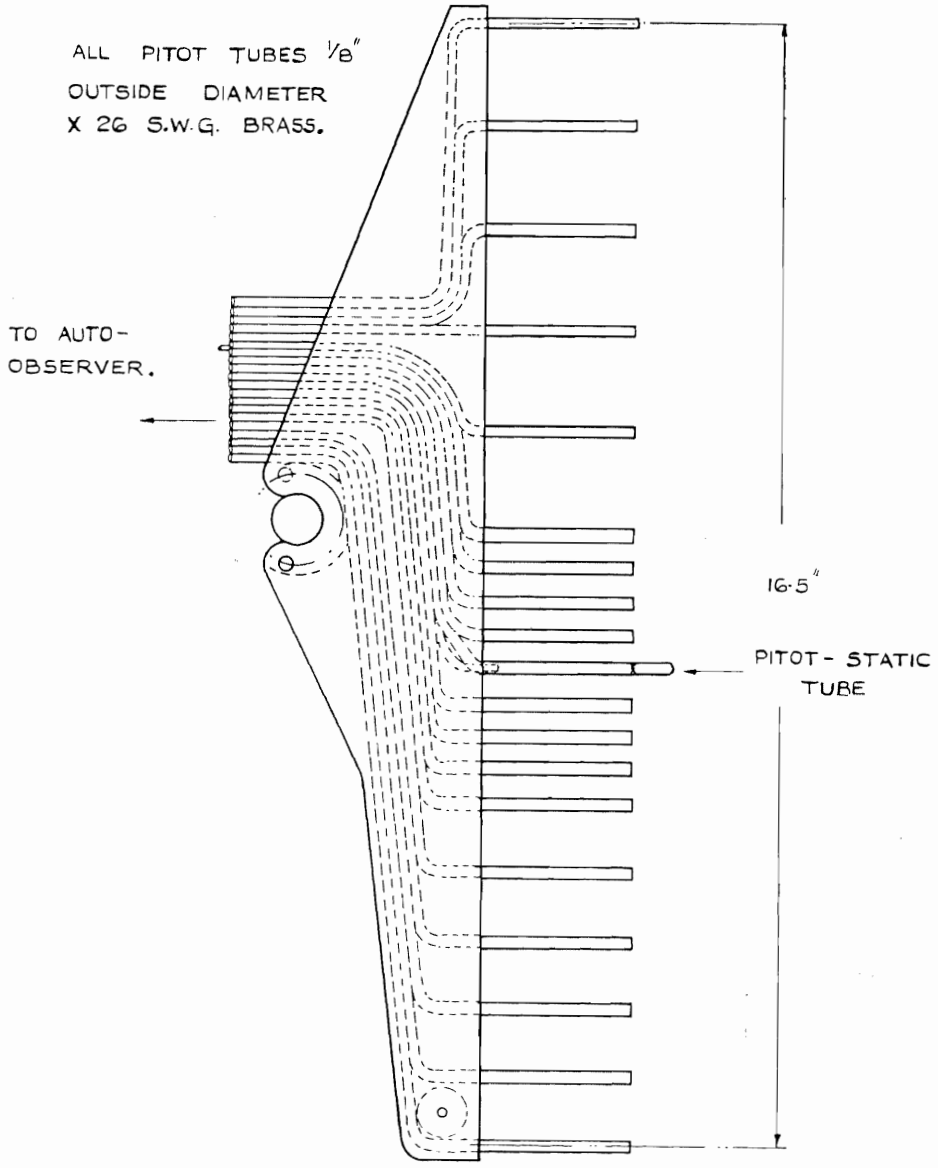

FIG. 126. Comb for Measuring Profile Drag.

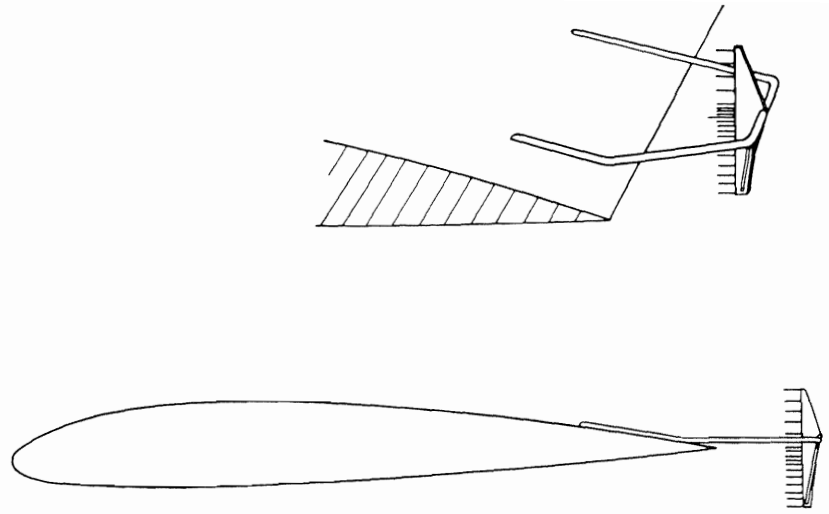

FIG. 127. Diagram Showing Typical Drag Comb Mounted Behind Wing.

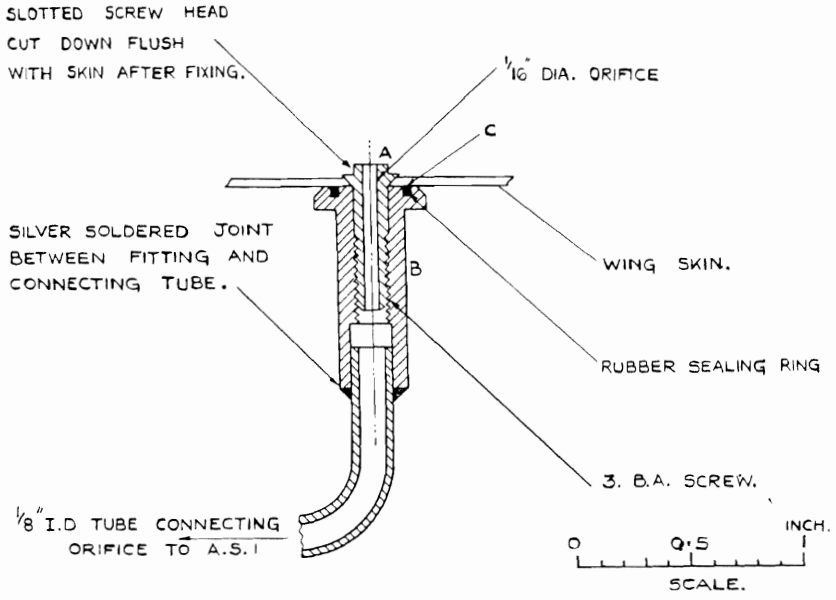

FIG. 128. Typical Pressure-Plotting Fitting.

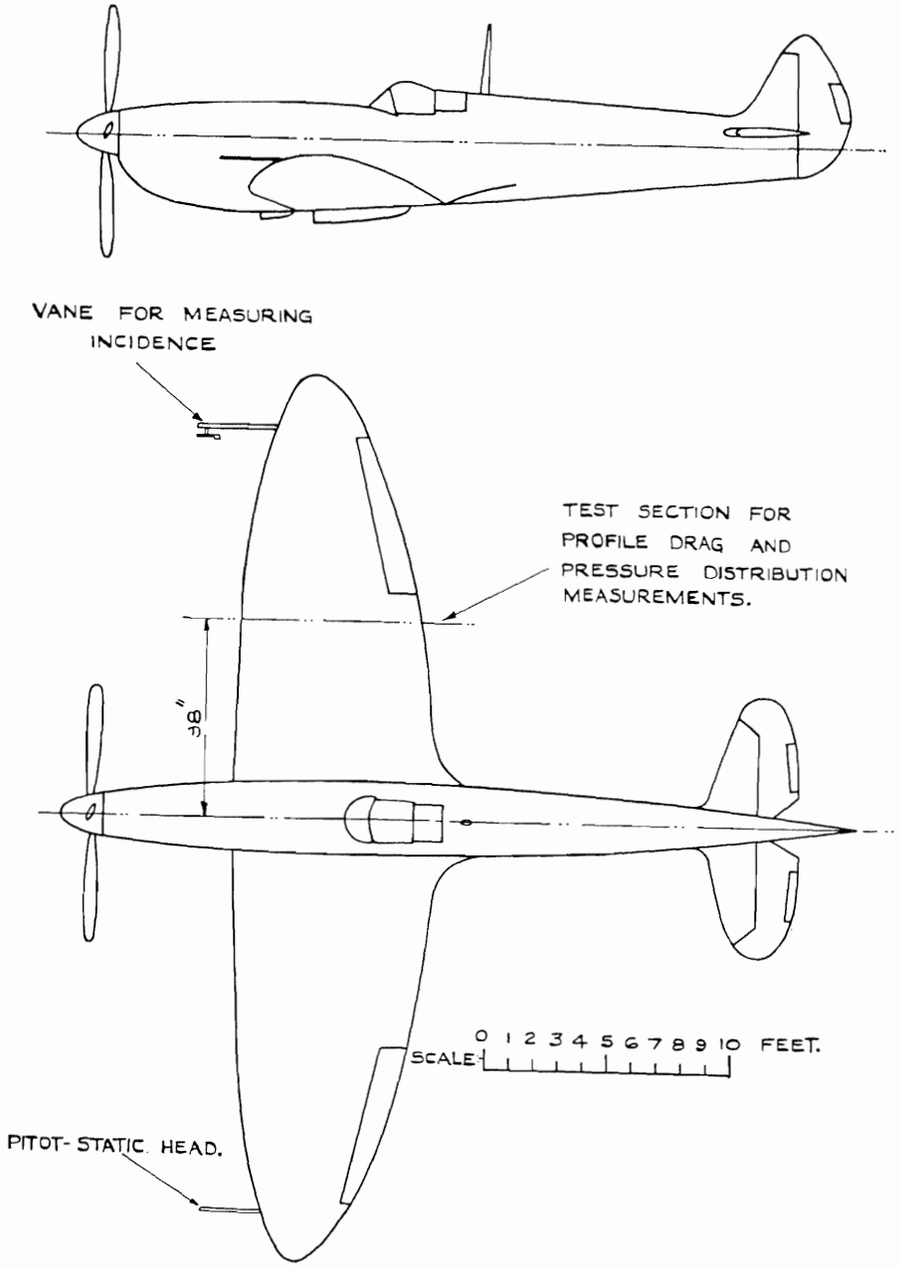

FIG. 129. Spitfire XI—General Arrangement of Aircraft.

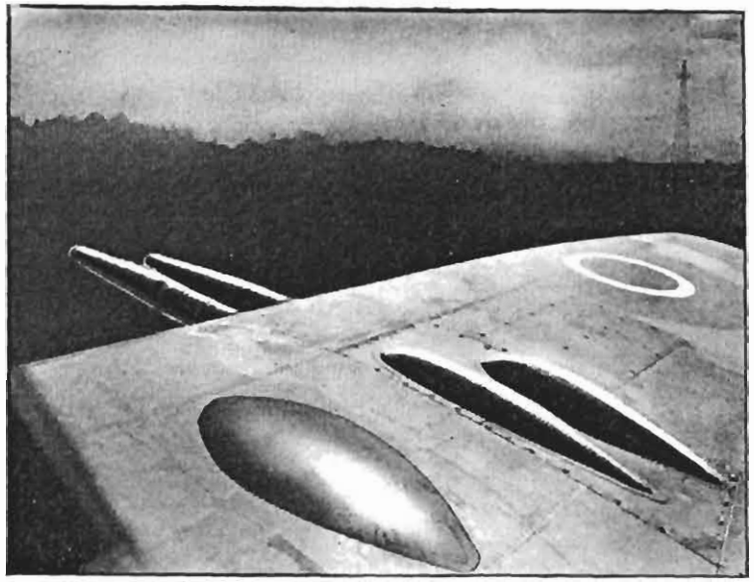

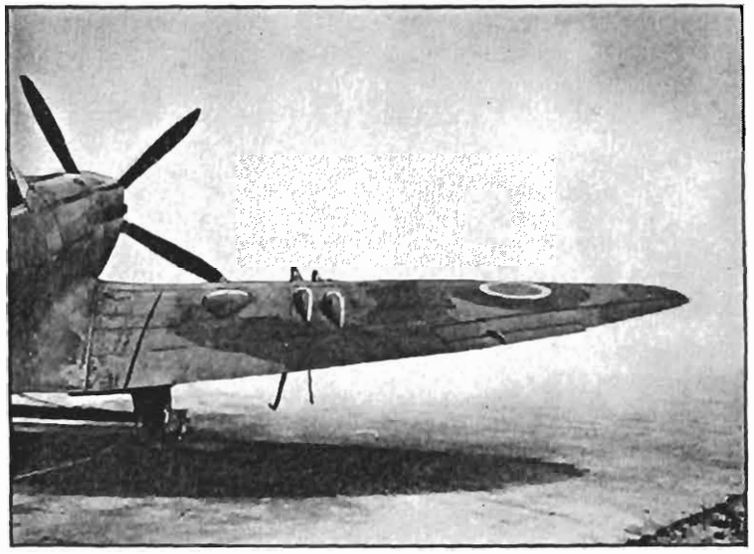

FIG. 130. Spitfire XXI with Guns and Blisters.

Fig. 132. E28/39.

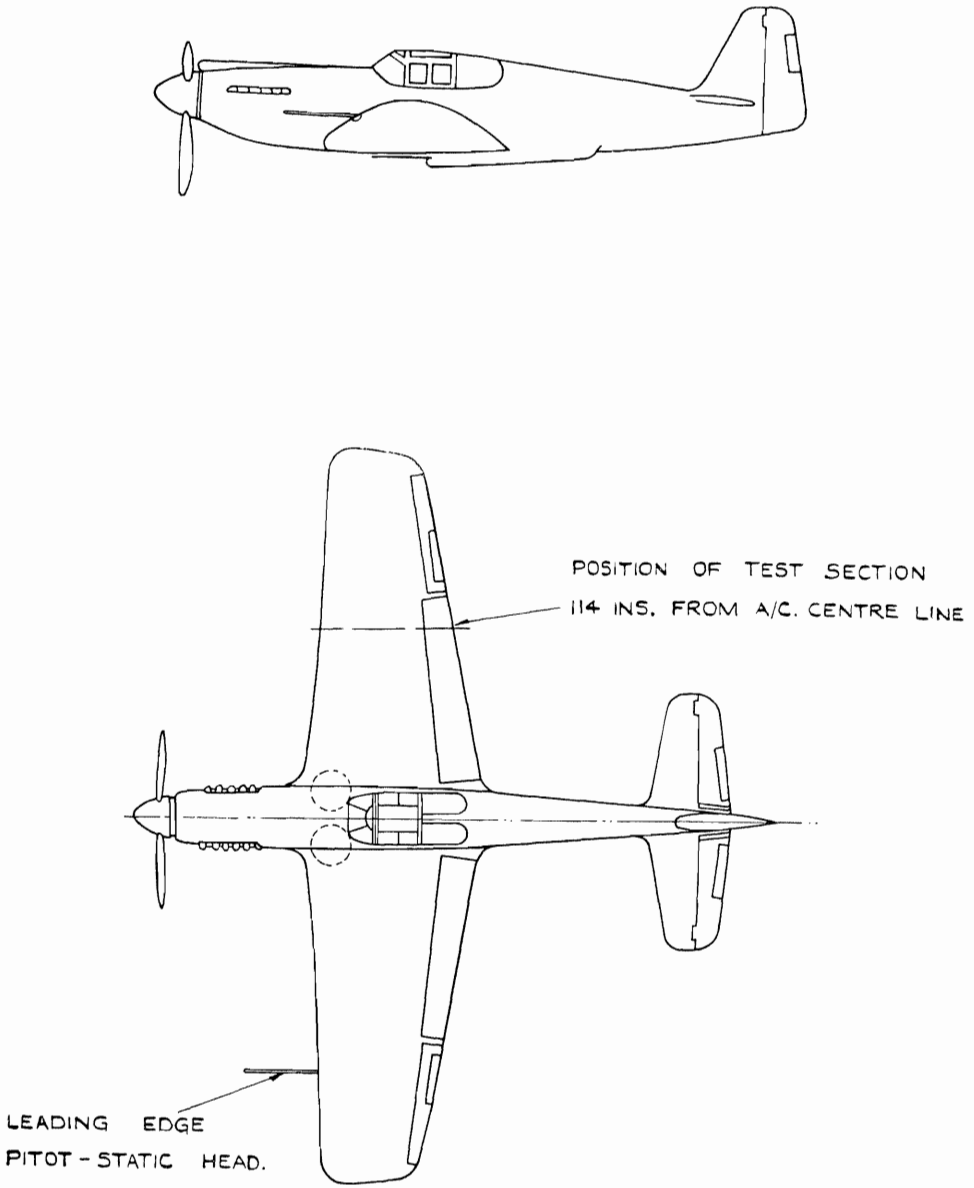

Fig. 131. Mustang I—General Arrangement of Aircraft.

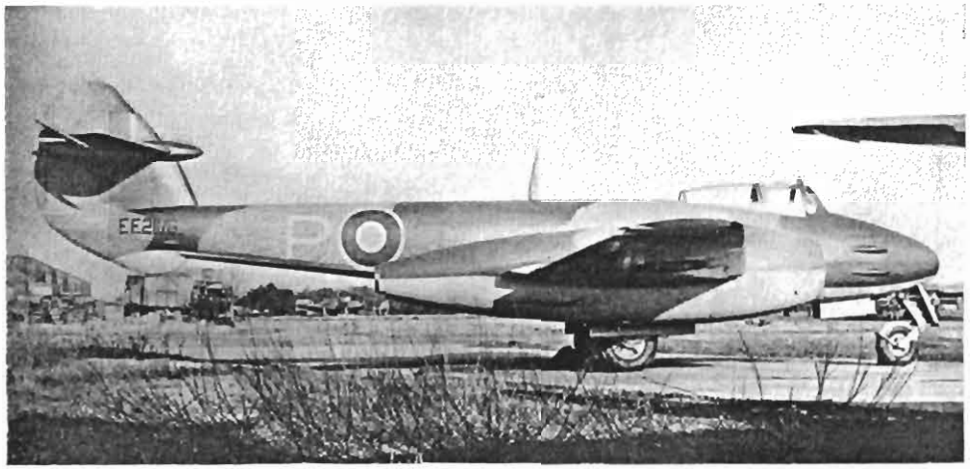

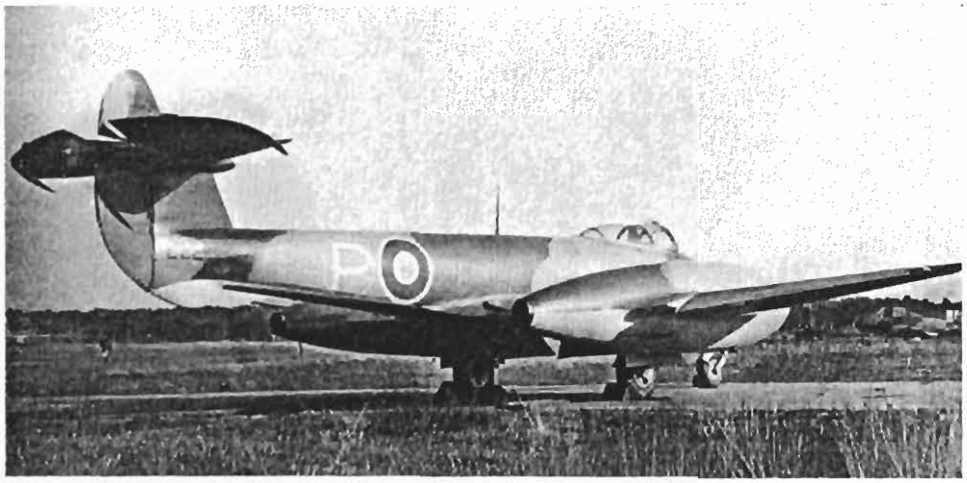

Fig. 133. Meteor I with Extended Nose and Tail Nacelles.

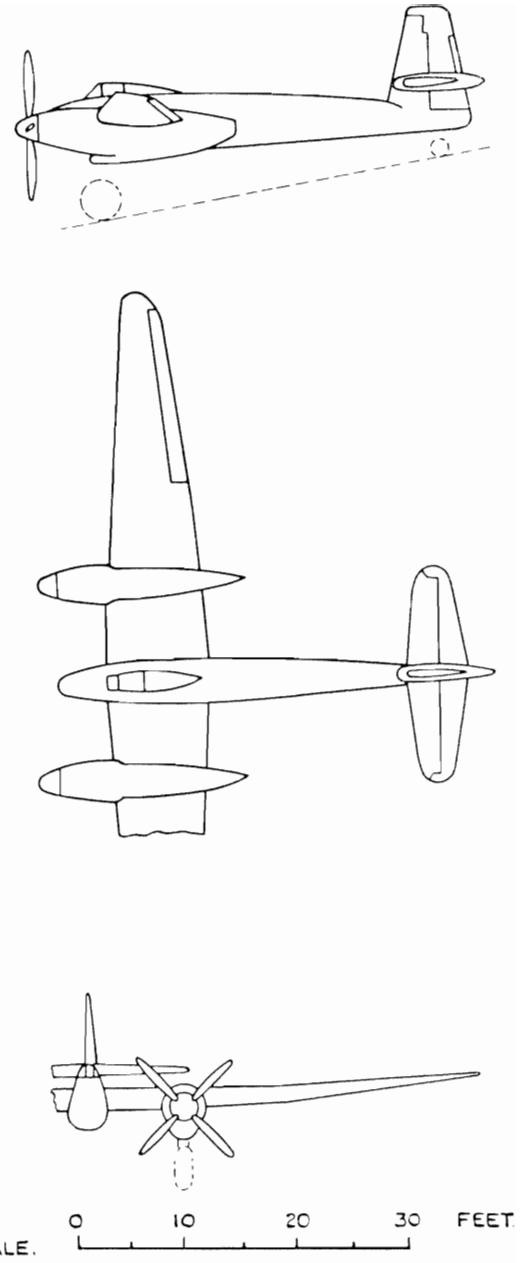

Fig. 134. Welkin Mk. I—General Arrangement.

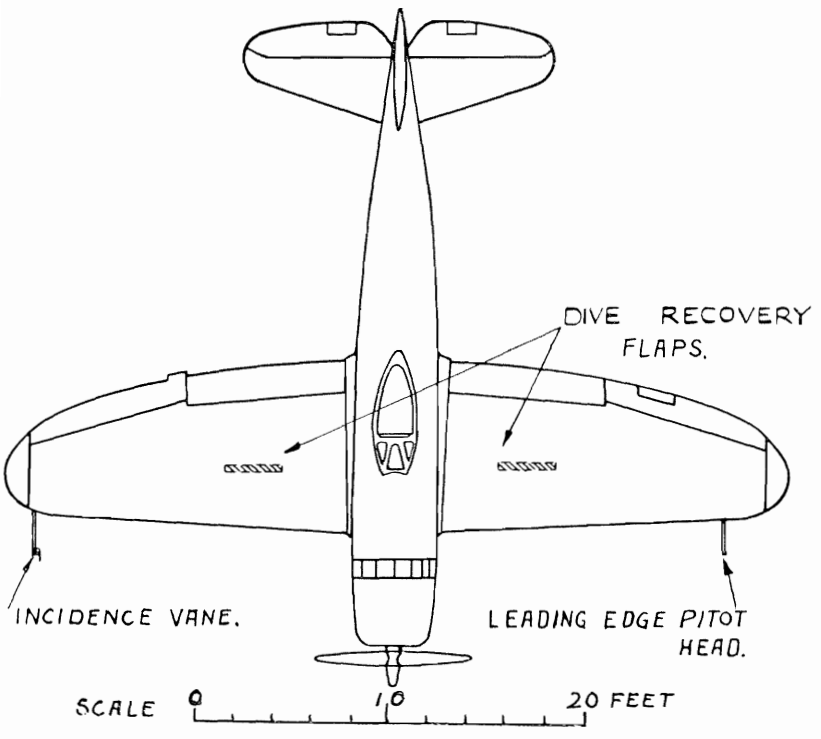

FIG. 135. Thunderbolt—Showing Position of Dive Recovery Flaps.

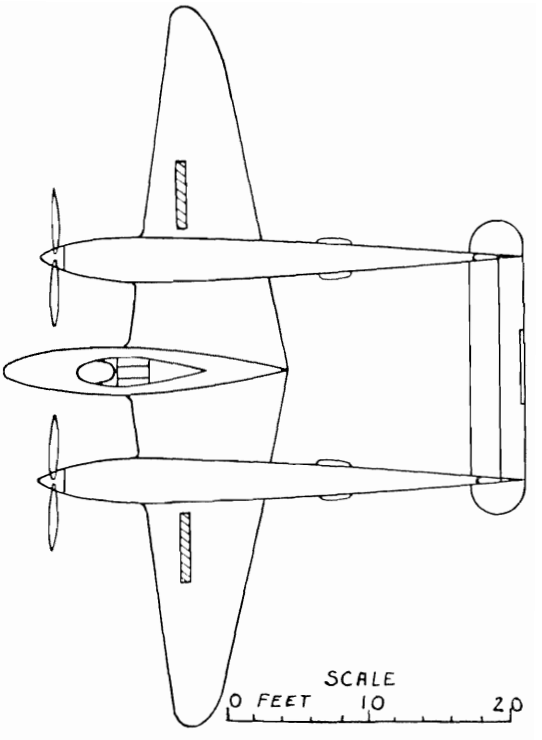

FIG. 136. Lightning—Showing Position of Dive Recovery Flaps.

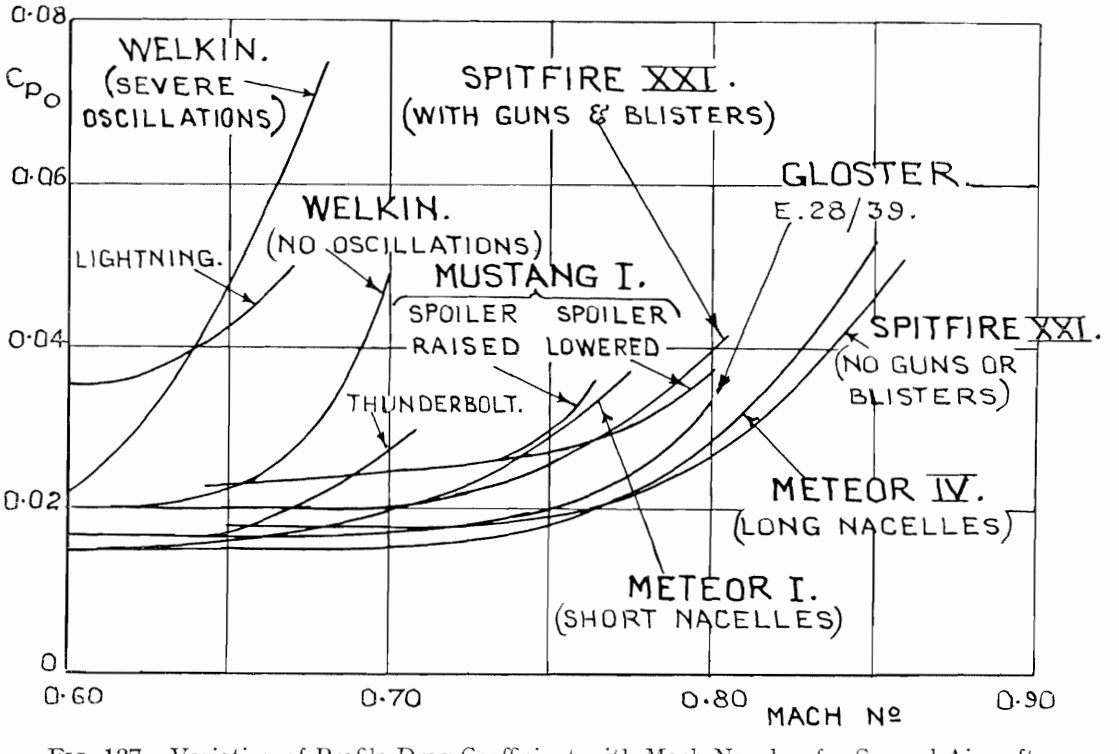

FIG. 137. Variation of Profile Drag Coefficient with Mach Number for Several Aircraft.

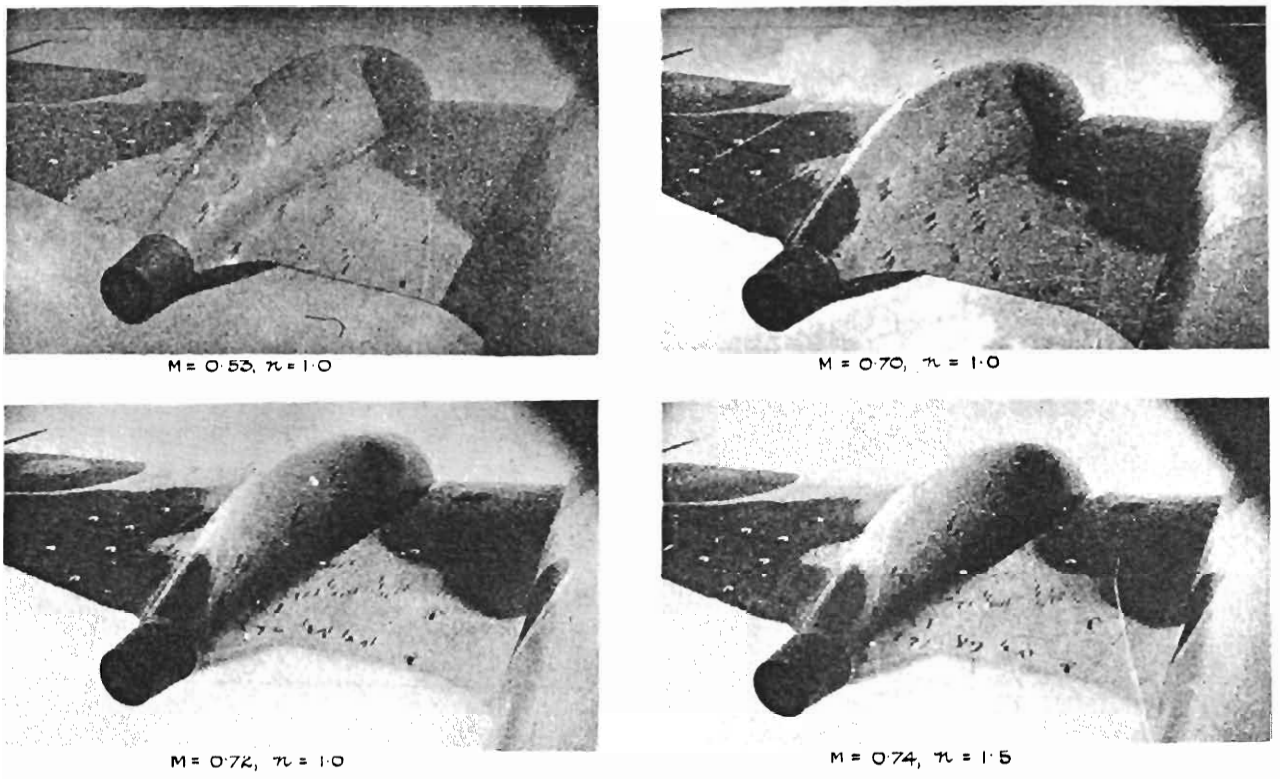

FIG. 138. Meteor I with Short Nacelles.
Nacelle Tufts at Various Values of Mach Number and Normal Acceleration ($n = 1$ in level flight).

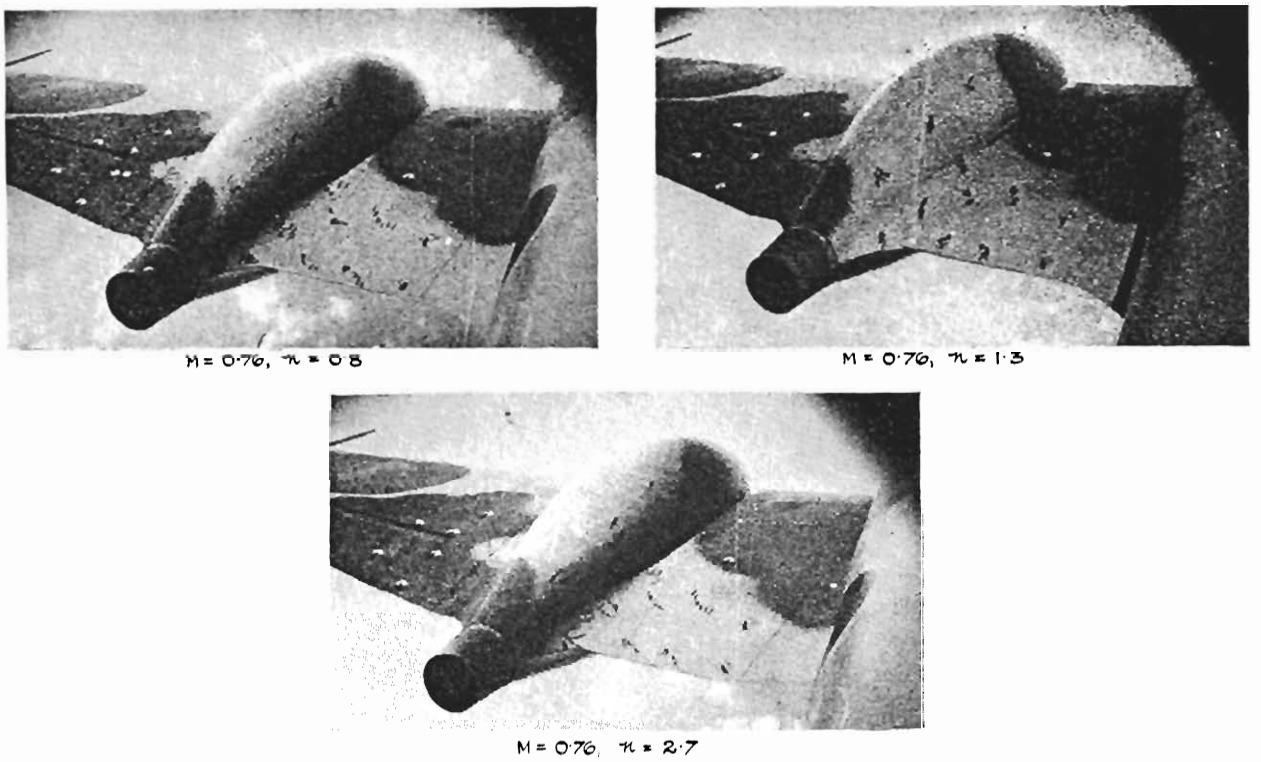

FIG. 139. Meteor I with Short Nacelles.
Nacelle Tufts at Various Values of Mach Number and Normal Acceleration ($n = 1$ in level flight).

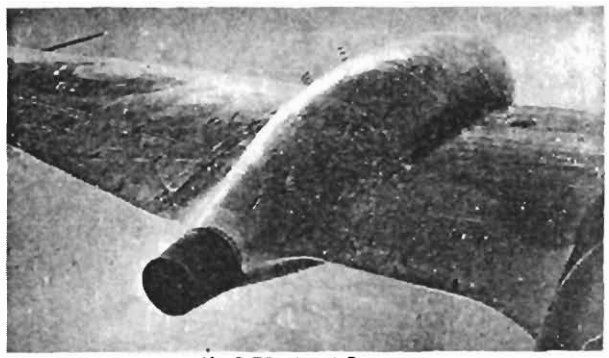

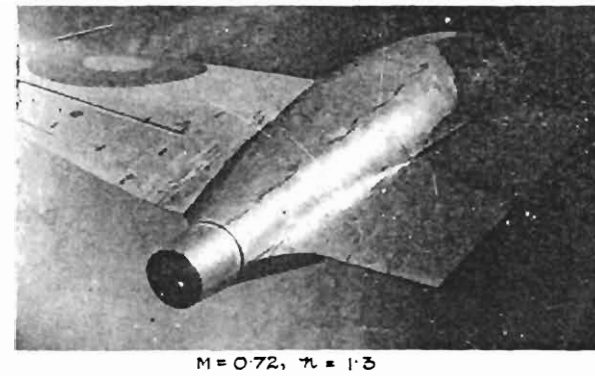

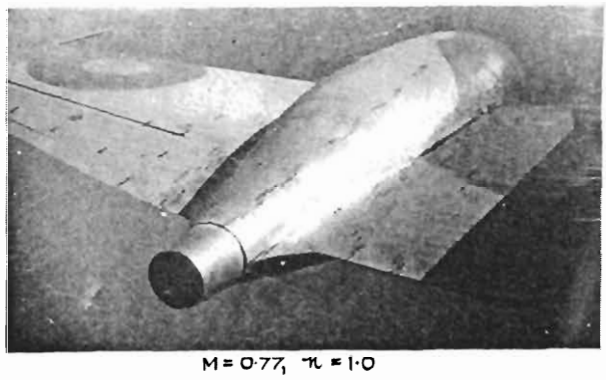

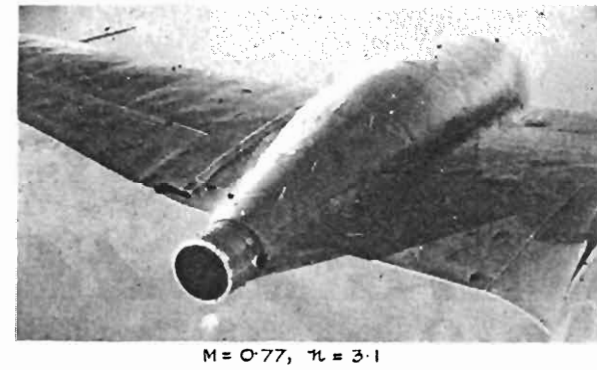

FIG. 140. Meteor I with Extended Nose Nacelles.
Nacelle Tufts at Various Values of Mach Number and Normal Acceleration ($n = 1$ in level flight).

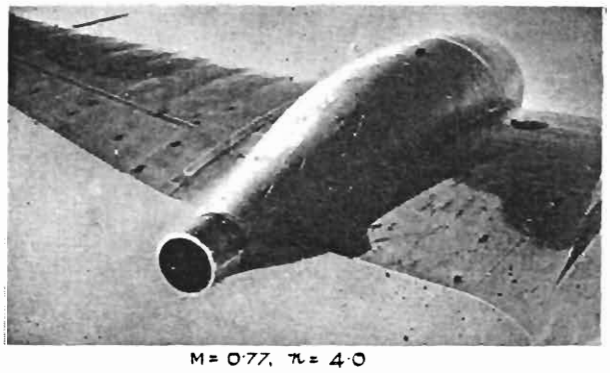

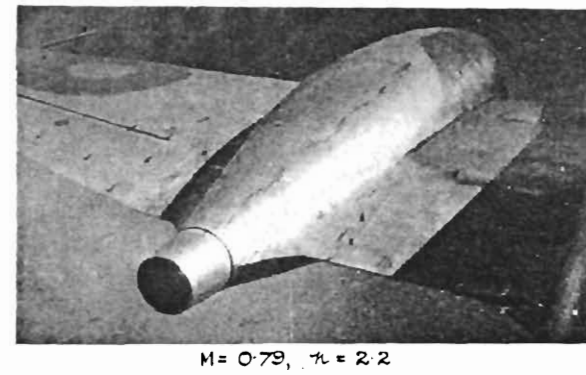

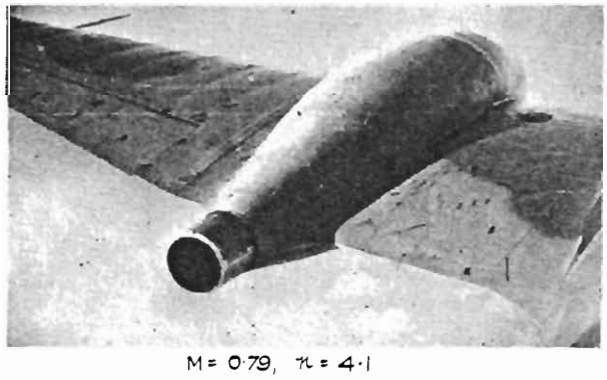

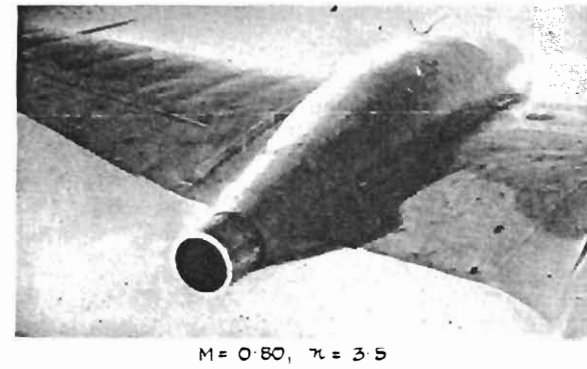

FIG. 141. Meteor I with Extended Nose Nacelles.
Nacelle Tufts at Various Values of Mach Number and Normal Acceleration ($n = 1$ in level flight).

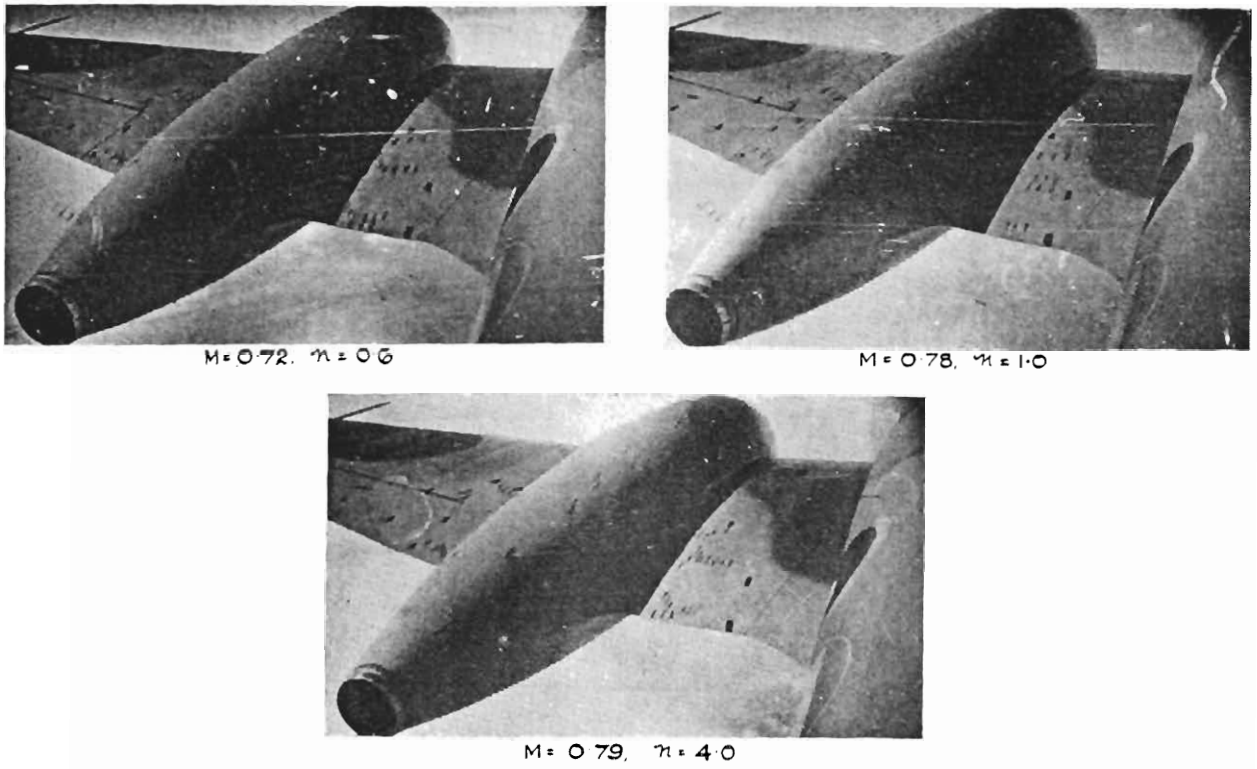

FIG. 142. Meteor I with Extended Nose and Tail Nacelles.
Nacelle Tufts at Various Values of Mach Number and Normal Acceleration (n = 1 in level flight).

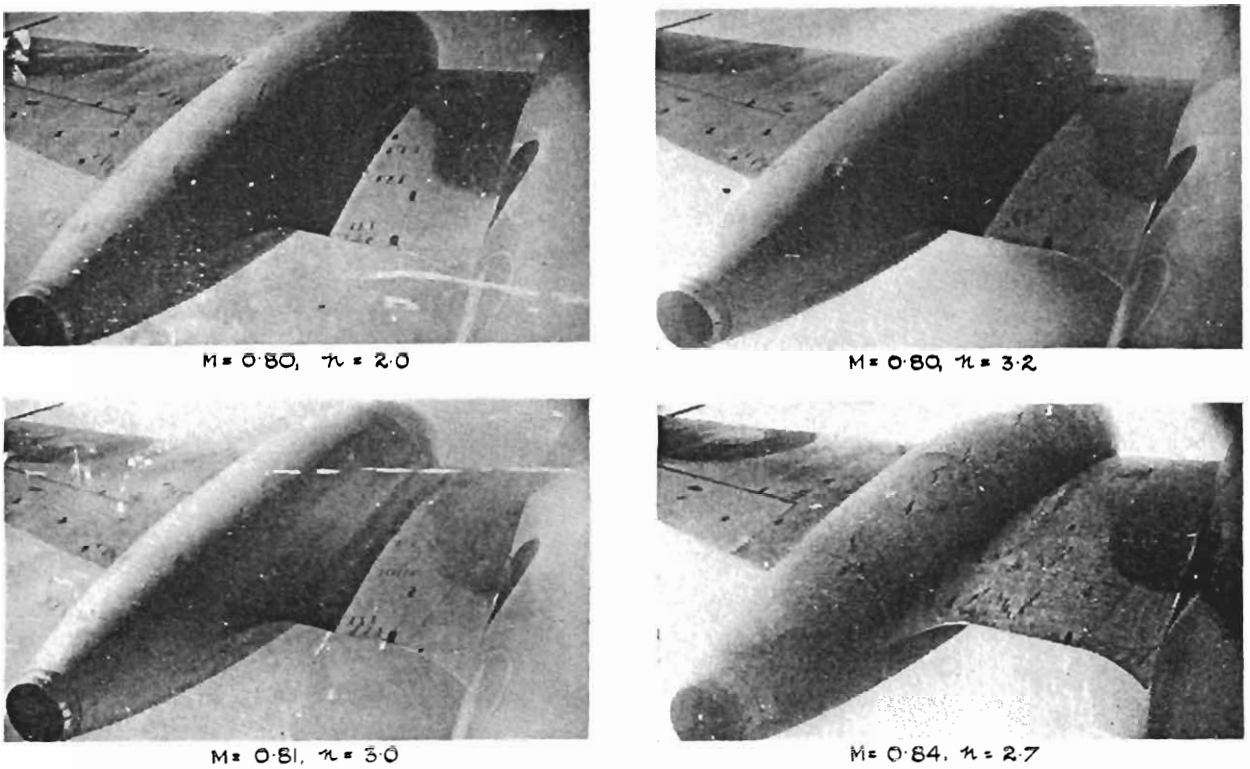

FIG. 143. Meteor I with Extended Nose and Tail Nacelles.
Nacelle Tufts at Various Values of Mach Number and Normal Acceleration (n = 1 in level flight).

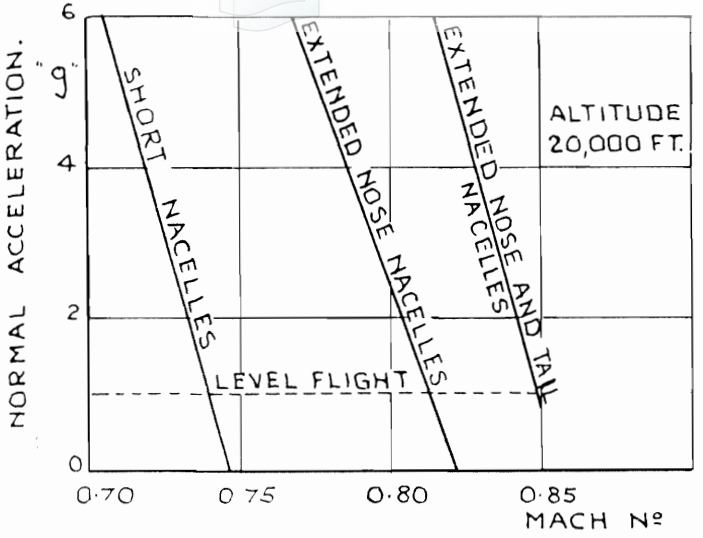

FIG. 144. Mach Number and Normal Acceleration for Onset of Buffeting with Different Nacelles—Meteor.

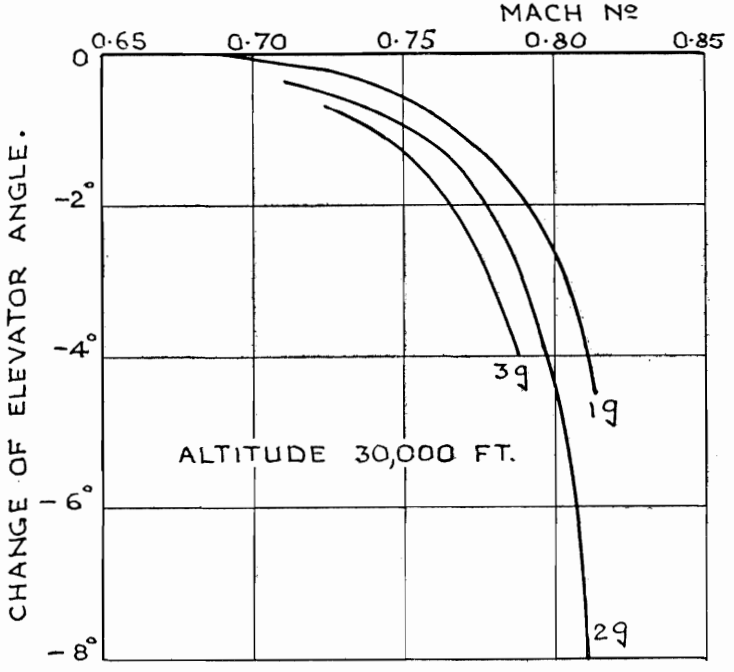

FIG. 145. Change of Elevator Angle with Mach Number—E.28/39. (Measured relative to elevator angle to trim for "1g" at same E.A.S. and low Mach number).

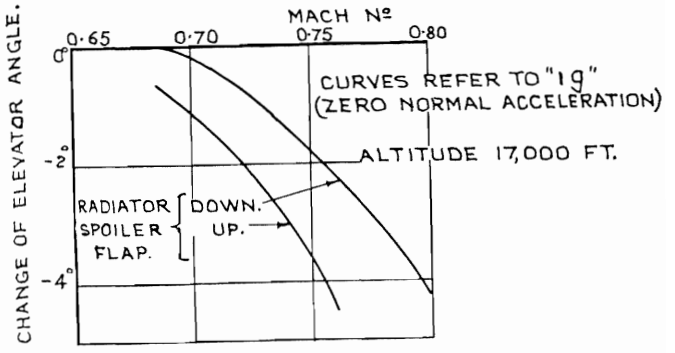

MUSTANG I.

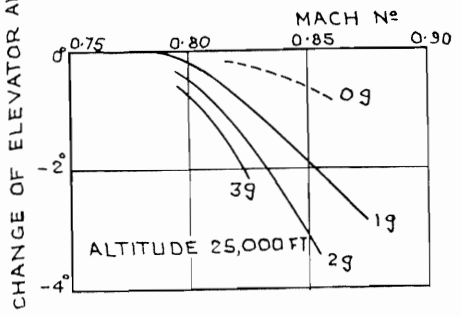

SPITFIRE XI.

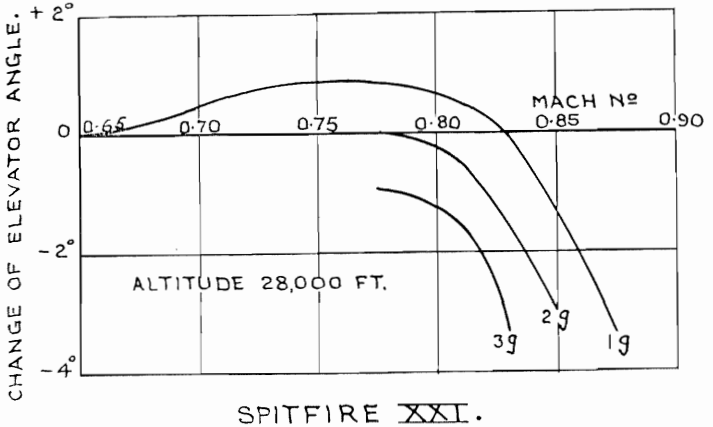

SPITFIRE XXI.
(NO GUNS OR BLISTERS).

FIG. 146. Change of Elevator Angle with Mach Number (Measured relative to elevator angle to trim for "1g" at same E.A.S. and low Mach number).

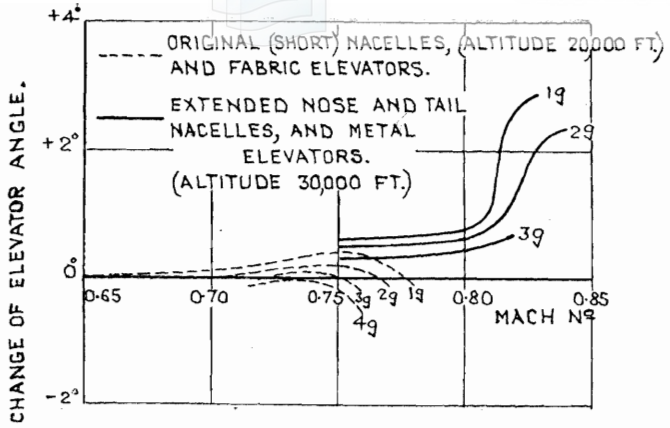

FIG. 147. Change of Elevator Angle with Mach Number—Meteor. (Measured relative to elevator angle to trim for "1g" at same E.A.S. and low Mach number).

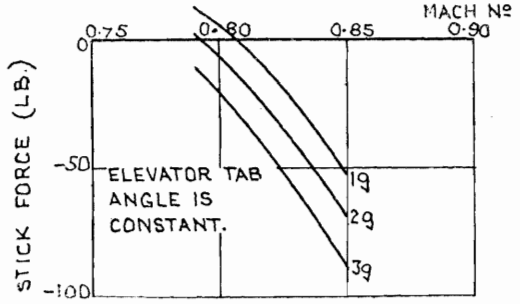

FIG. 148. Variation of Stick Force with Mach Number—Spitfire XI. (Reduced to 400 M.P.H. E.A.S.)

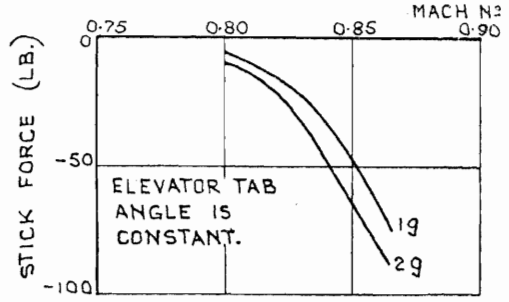

FIG. 149. Variation of Stick Force with Mach Number (Reduced to 400 M.P.H., E.A.S.)—Spitfire XXI. (No guns or blisters).

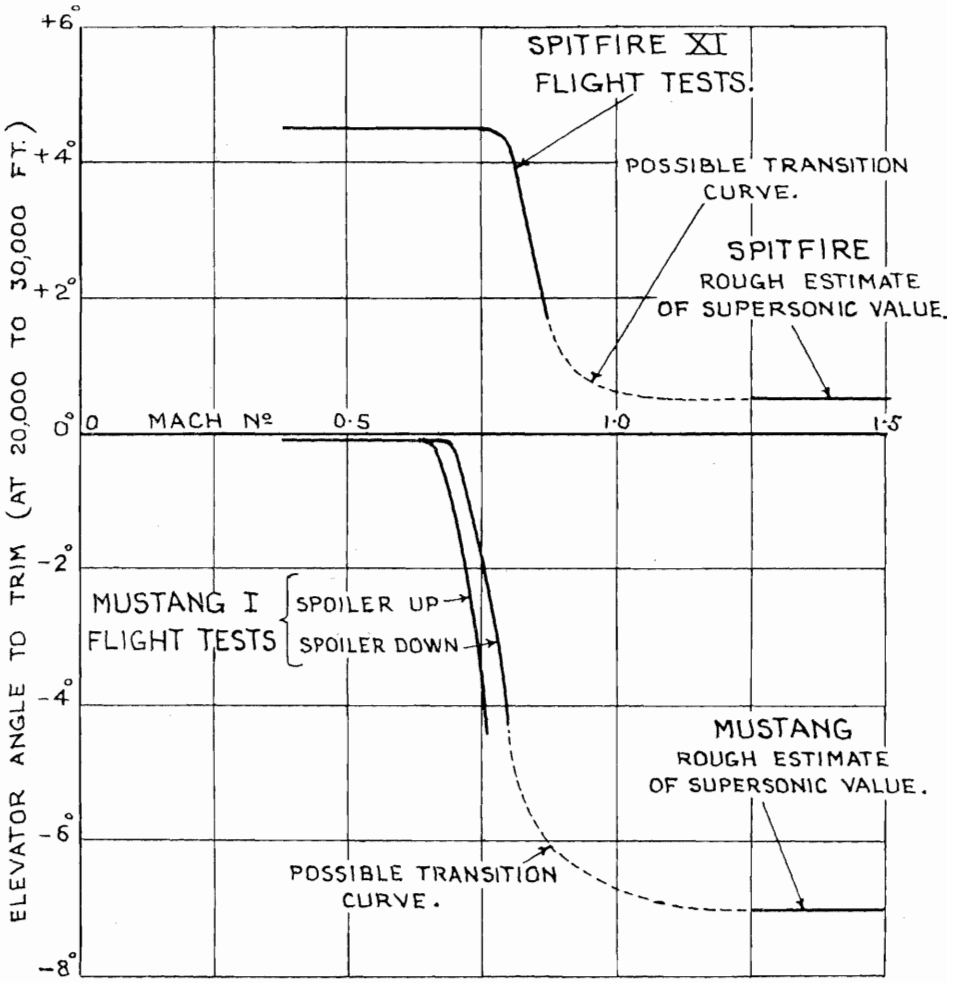

FIG. 150. Change of Elevator Angle to Trim in Level Flight at High Mach Numbers.

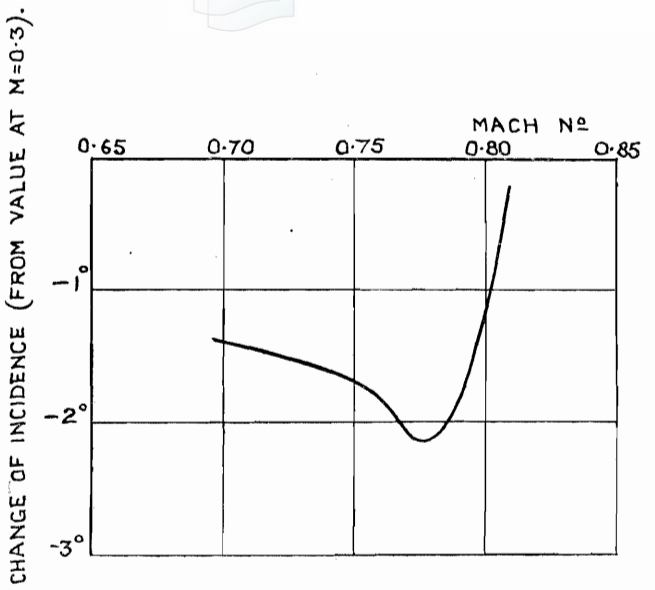

FIG. 151. Variation of Incidence with Mach Number for Constant Aircraft Lift Coefficient ($C_L = 0 \cdot 10$). E.28/39.

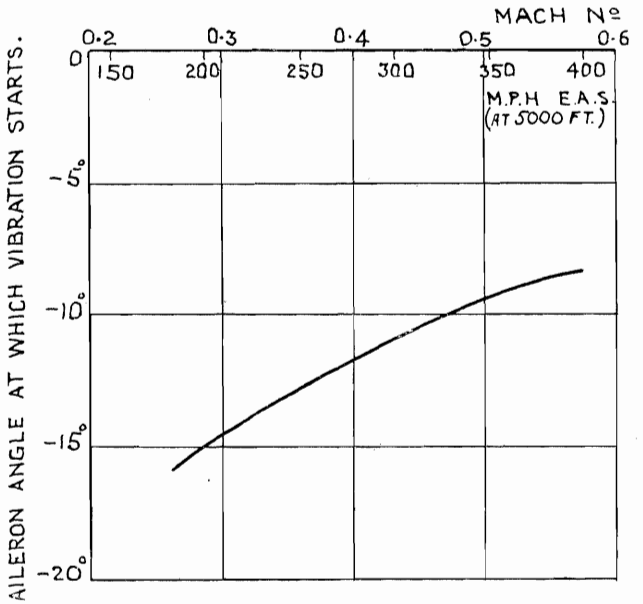

FIG. 152. Variation with Mach Number of Aileron Angle at which Vibration Starts. Spitfire II. (Frise ailerons).

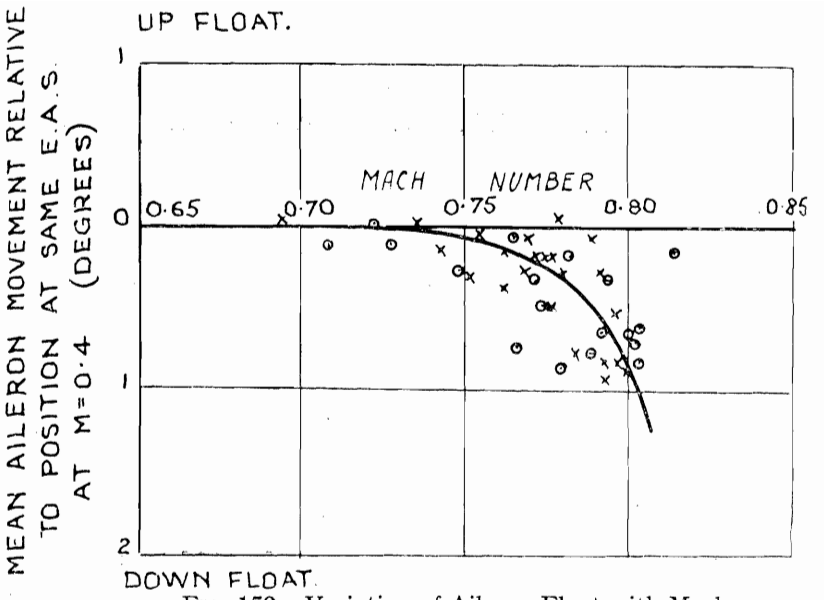

FIG. 153. Variation of Aileron Float with Mach Number—E.28/39.

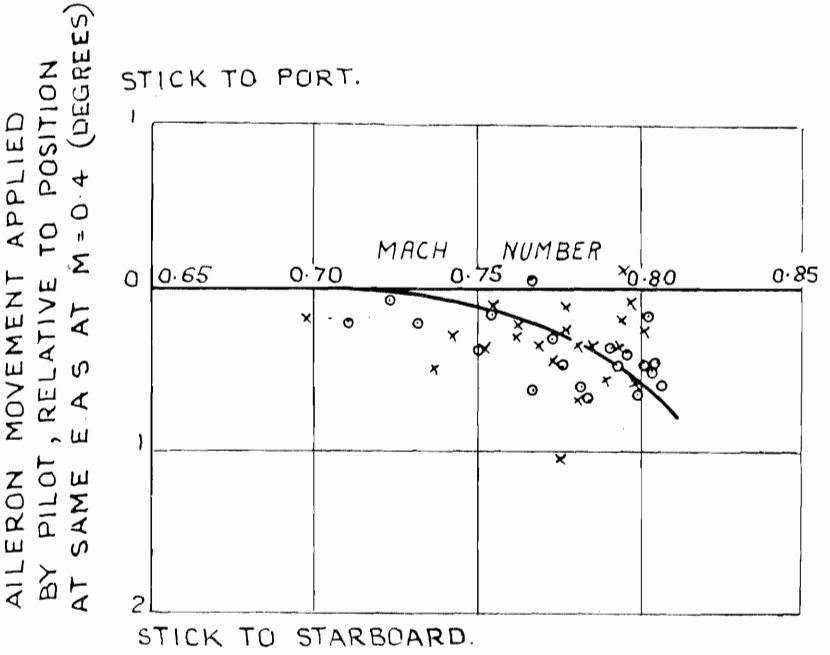

FIG. 154. Variation with Mach Number of Aileron Angle Applied by Pilot to Prevent Roll—E.28/39.

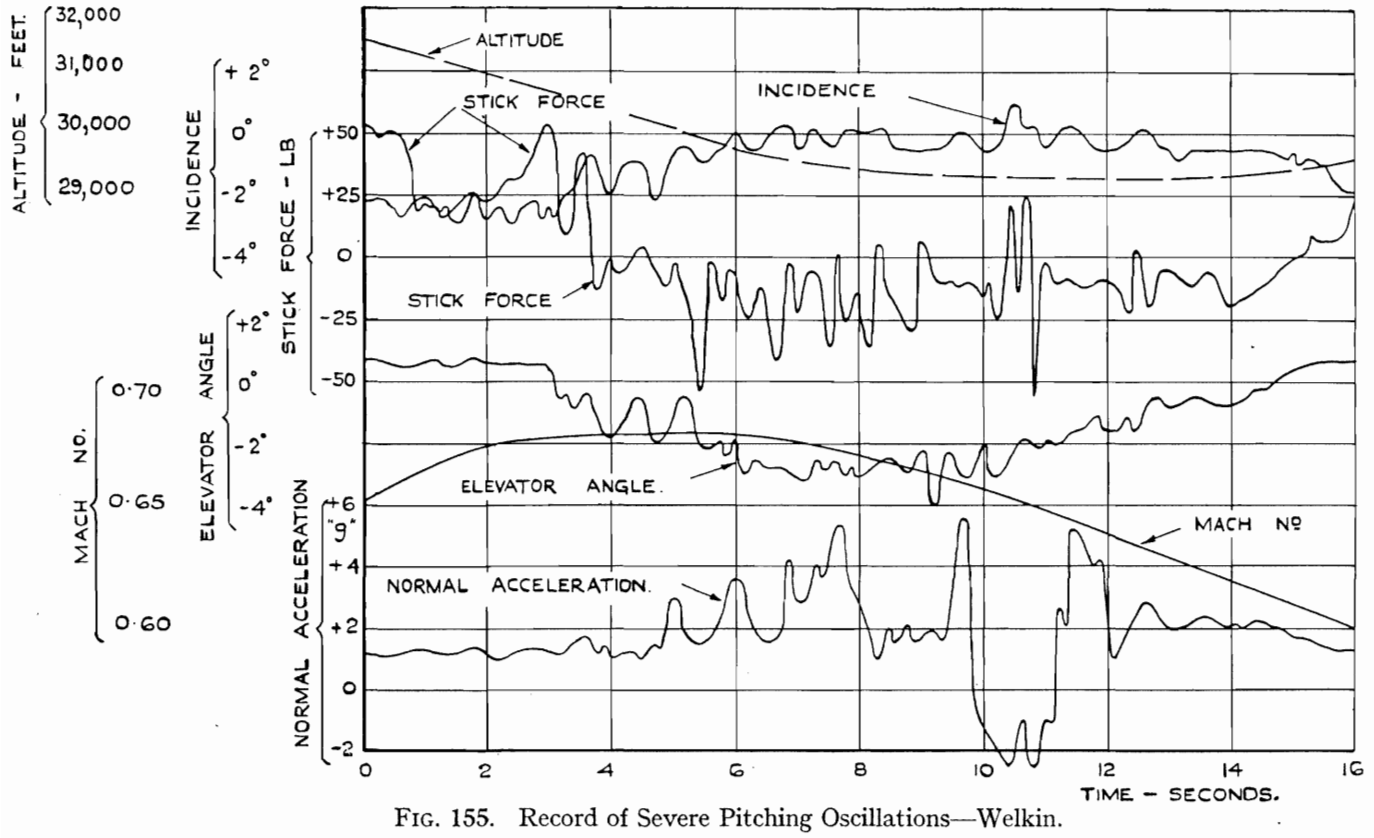

FIG. 155. Record of Severe Pitching Oscillations—Welkin.

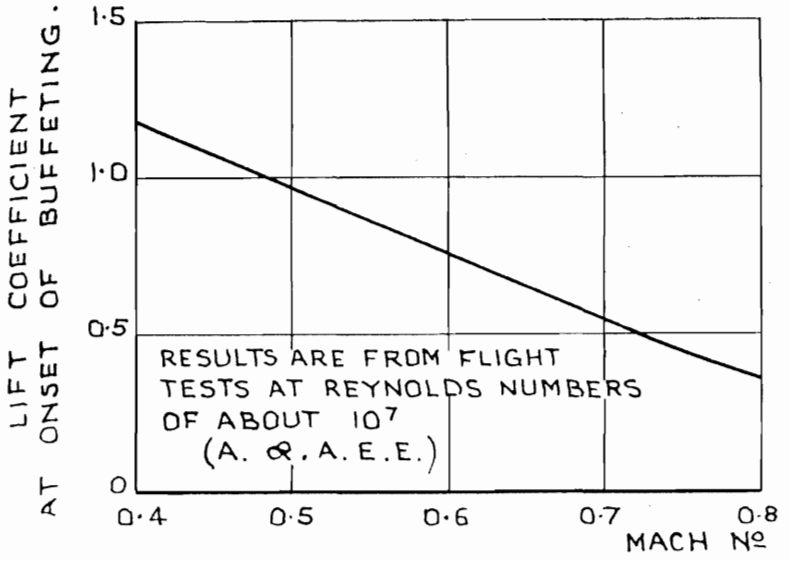

FIG. 156. Variation with Mach Number of Lift Coefficient for Onset of Buffeting—Spitfire IX.

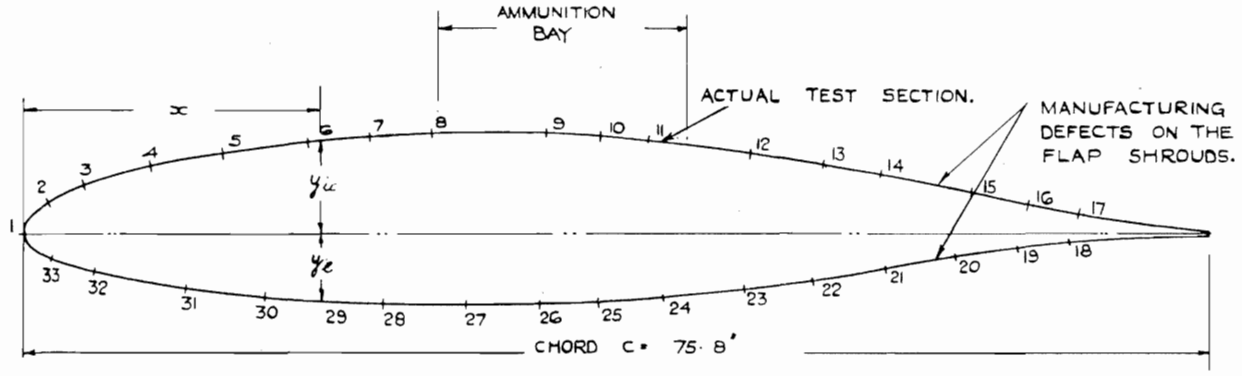

PRESSURE ORIFICES LOCATED AS NUMBERS 1–33.

ACTUAL TEST SECTION.

x/c	0·0125	0·025	0·050	0·075	0·10	0·15	0·20	0·30	0·40	0·50	0·60	0·70	0·80	0·90	0·95	1·00
y_u/c	0·0193	0·0275	0·0375	0·0455	0·0515	0·0618	0·0685	0·0793	0·0844	0·0793	0·0671	0·0531	0·0352	0·0139	0·0082	0·0007
y_l/c	0·0164	0·0218	0·0294	0·0350	0·0399	0·0487	0·0529	0·0594	0·0608	0·0577	0·0474	0·0330	0·0172	0·0061	0·0022	0·0012

THEORETICAL N.A. 73 SECTION.

x/c	0·0125	0·025	0·050	0·075	0·10	0·15	0·20	0·30	0·40	0·50	0·60	0·70	0·80	0·90	0·95	1·00
y_u/c	0·0206	0·0280	0·0399	0·0476	0·0542	0·0643	0·0719	0·0809	0·0845	0·0801	0·0687	0·0529	0·0330	0·0118	0·0030	0·0028
y_l/c	0·0145	0·0212	0·0286	0·0338	0·0386	0·0473	0·0513	0·0584	0·0598	0·0575	0·0474	0·0336	0·0193	0·0080	0·0048	0·0028

SECTION 15 114" OUTBOARD OF AIRCRAFT ℄

$\frac{\text{MAXIMUM THICKNESS}}{\text{CHORD.}} = 0·145$

FIG. 157. Wing Test Section—Mustang A.G. 393.

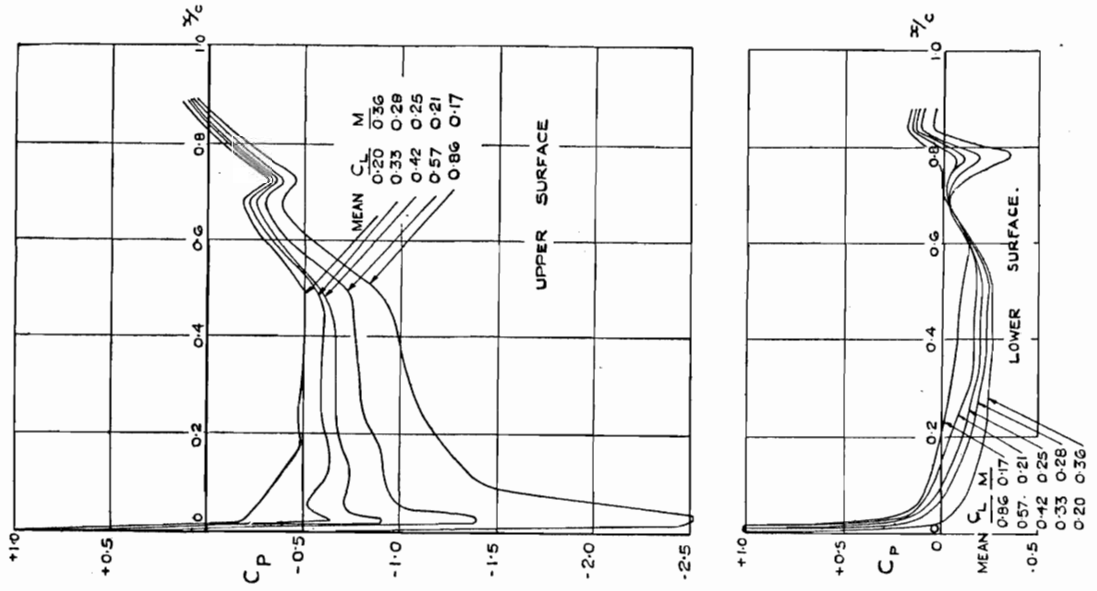

FIG. 158. Pressure Distributions at Low Mach Numbers—Mustang Wing.

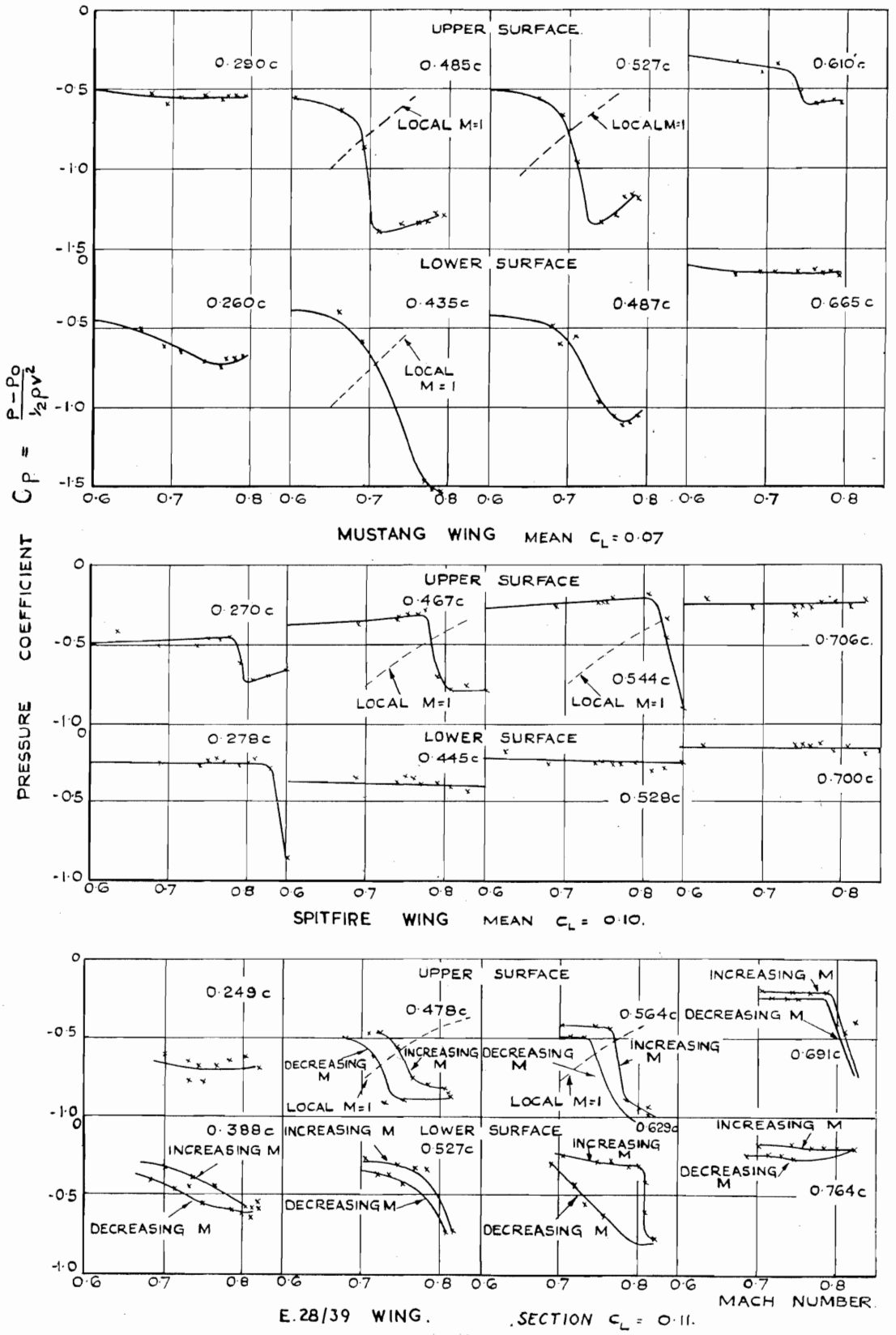

FIG. 159. Variation of Pressure Coefficients with Mach Number.

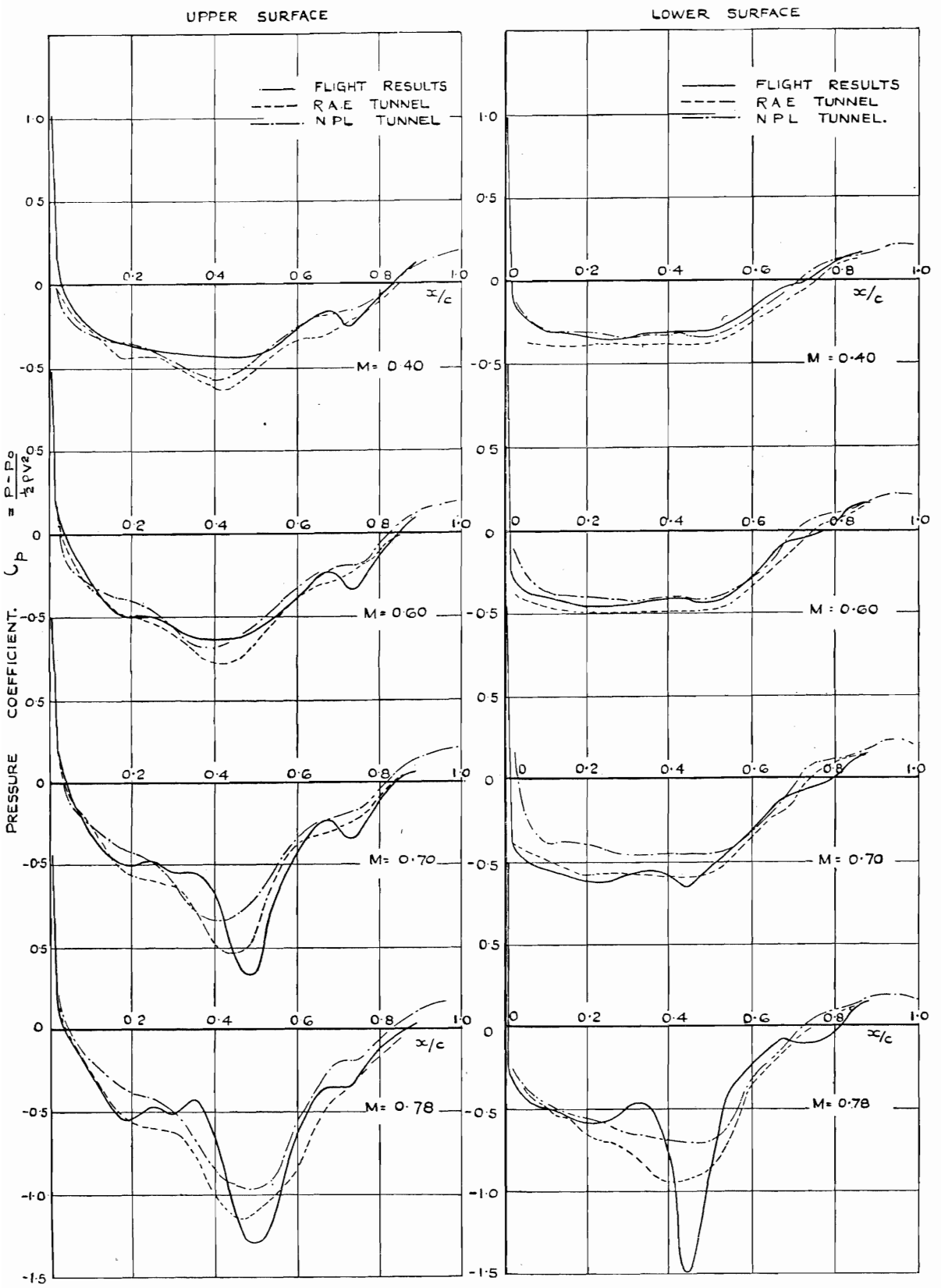

FIG. 160. Wing Pressure Distributions at High Mach Numbers. Comparison of Flight and High Speed Wind Tunnel Results—Mustang. Section $C_L = 0 \cdot 07$.

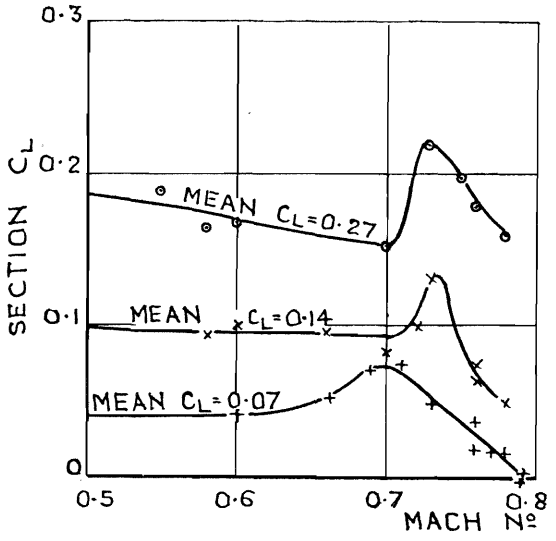

FIG. 161. Relation Between Section C_L and Mean(Aircraft) C_L at High Mach Numbers (From pressure distributions)—Mustang I.

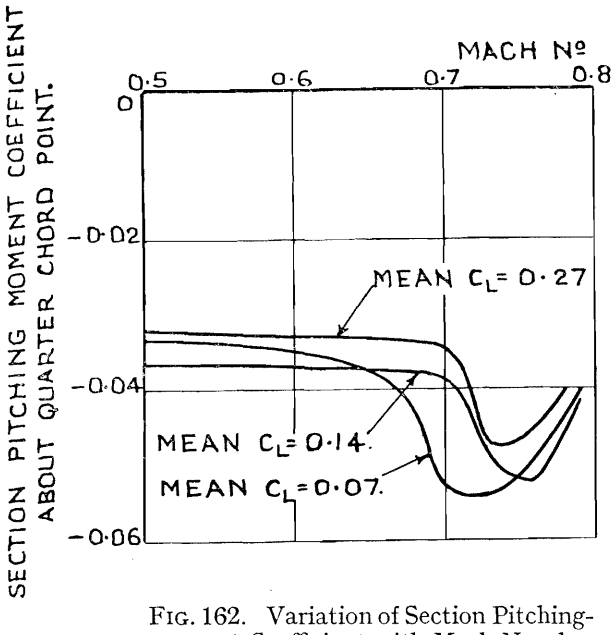

FIG. 162. Variation of Section Pitching-moment Coefficient with Mach Number for Constant Mean (Aircraft) C_L. Mustang I.

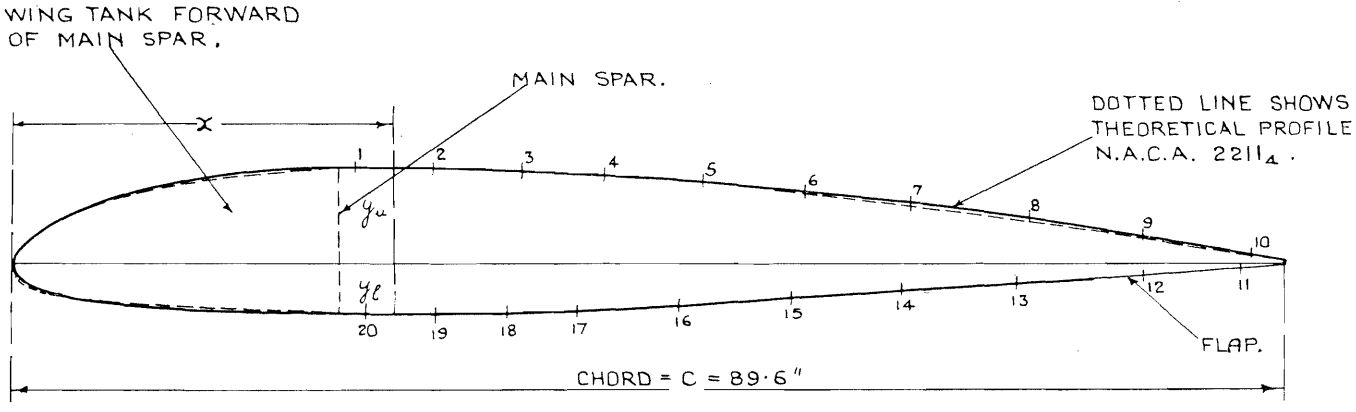

PRESSURE ORIFICES LOCATED AS NUMBERS 1-20.

x/c	0·0125	0·025	0·050	0·075	0·100	0·150	0·20	0·30	0·40	0·50	0·60	0·70	0·80	0·90	0·95	1·00
y_u/c	0·0189	0·0277	0·0400	0·0493	0·0564	0·0660	0·0715	0·0729	0·0712	0·0653	0·0572	0·0473	0·0354	0·0196	0·0116	0·002
y_l/c	0·0176	0·0226	0·0274	0·0309	0·0335	0·0372	0·0396	0·0413	0·0403	0·0362	0·0298	0·0232	0·0162	0·0099	0·0066	0·001

SECTION IS 98" OUTBOARD OF AIRCRAFT ℄ $\frac{\text{MAX. THICKNESS}}{\text{CHORD}} = 0·114$

FIG. 163. Outboard Wing Test Section—Spitfire PL.827.

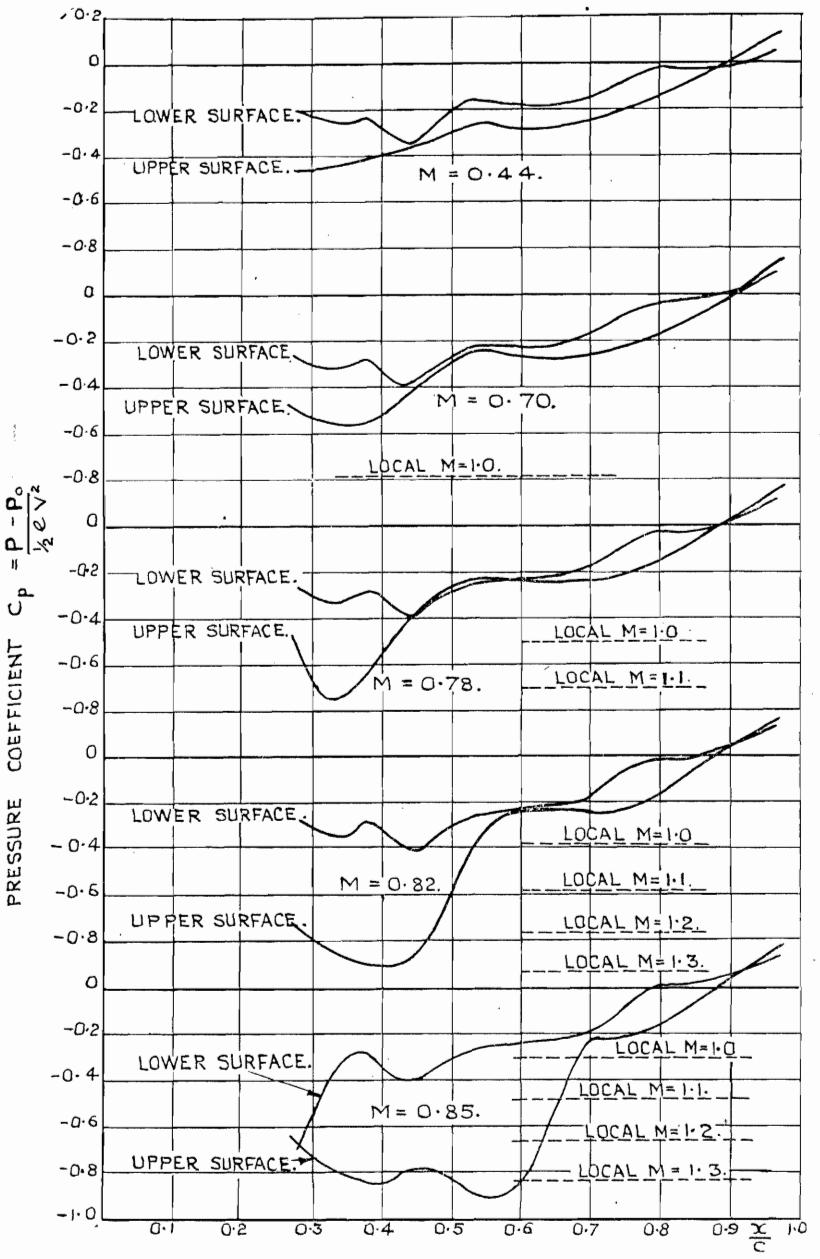

FIG. 164. Wing Pressure Distributions at High Mach Numbers (Aircraft $C_L = 0{\cdot}10$)—Spitfire.

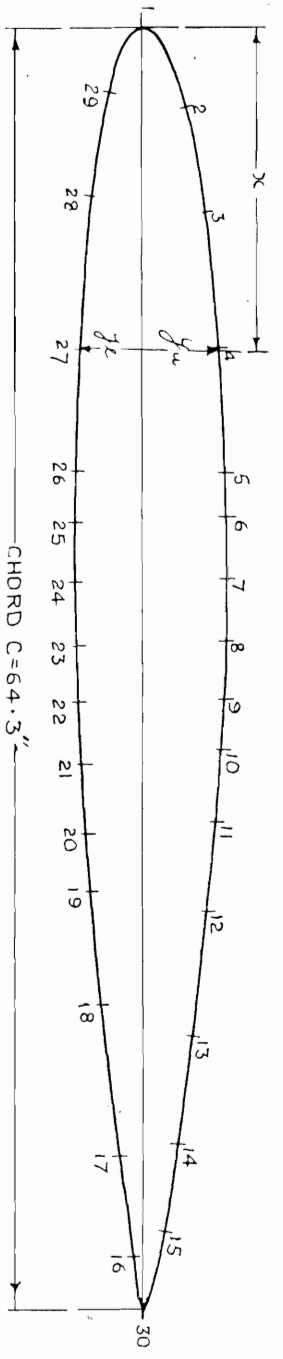

PRESSURE ORIFICES LOCATED AS NUMBER 1-30.

x/c	0·0125	0·025	0·050	0·075	0·10	0·15	0·20	0·30	0·40	0·50	0·60	0·70	0·80	0·90	0·95	1·00
y_u/c	0·0165	0·0210	0·0302	0·0375	0·0417	0·0495	0·0550	0·0624	0·0645	0·0633	0·0586	0·0482	0·0364	0·0218	0·0126	0
y_l/c	0·0112	0·0183	0·0253	0·0300	0·0353	0·0415	0·0453	0·0498	0·0521	0·0507	0·0465	0·0392	0·0288	0·0165	0·0096	0

SECTION IS 81″ OUTBOARD OF AIRCRAFT ℄.

MAXIMUM THICKNESS / CHORD = 0·117.

FIG. 165. Wing Test Section—E.28/39.

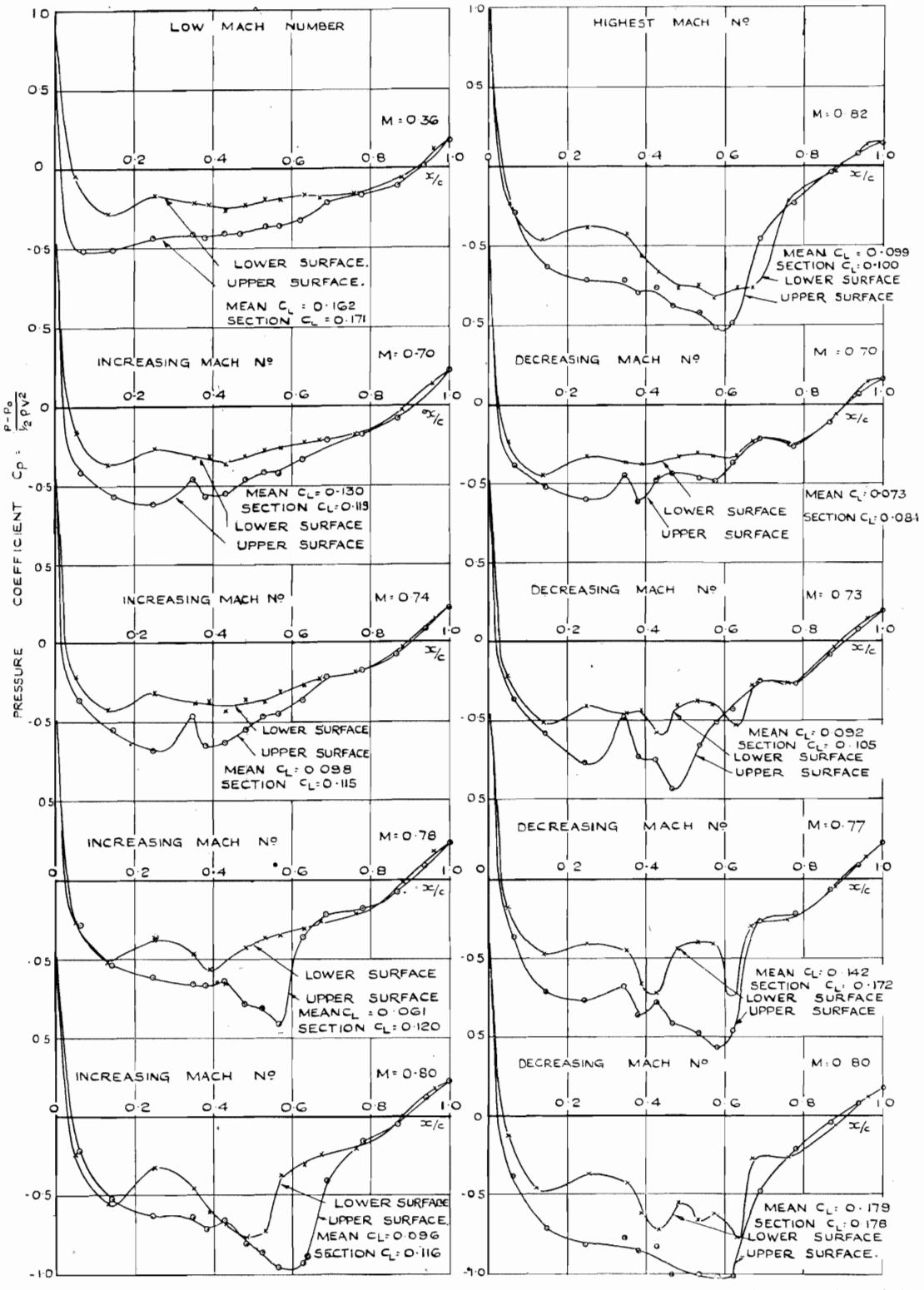

FIG. 166. Wing Pressure Distributions for Increasing and Decreasing Mach Number—E.28/39.

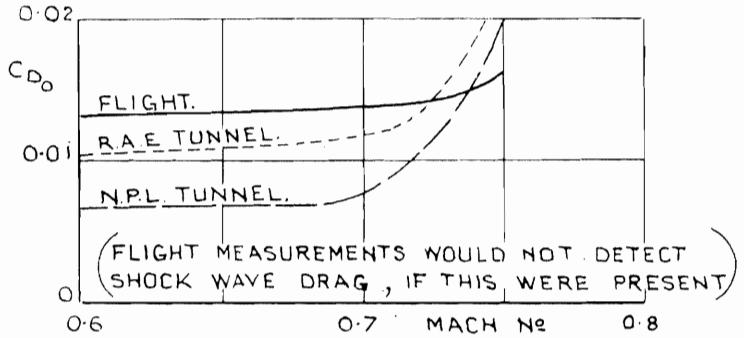

FIG. 167. Variation of Profile Drag with Mach Number—Mustang Wing Section.

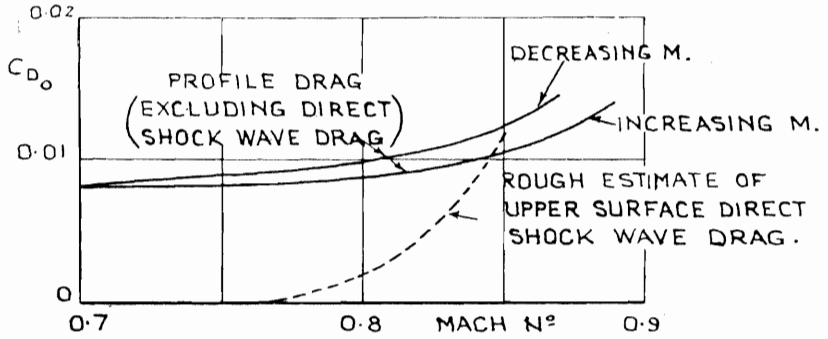

FIG. 168. Wing Section Profile Drag—Spitfire.

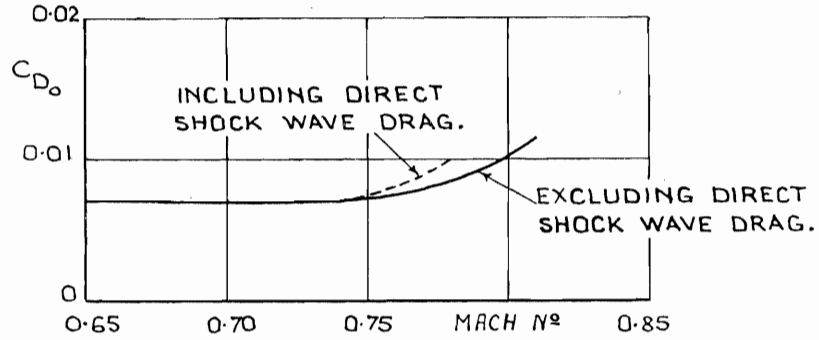

(SHOCK WAVE LOSS EXTENDED OUTSIDE PITOT COMB AT MACH Nos ABOVE 0·78.)

FIG. 169. Wing Section Profile Drag—E.28/39.

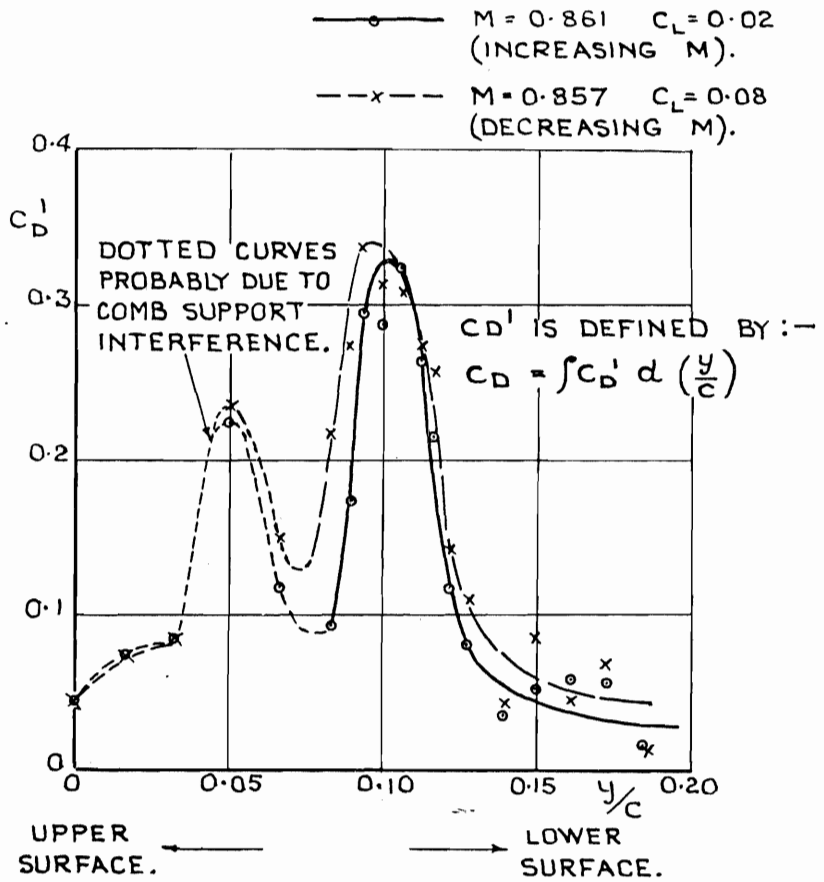

FIG. 170. Comparison of Wakes for Increasing and Decreasing Mach Number—Spitfire Wing.

(8715S) Wt. 12/818 K5 1/50 Hw.

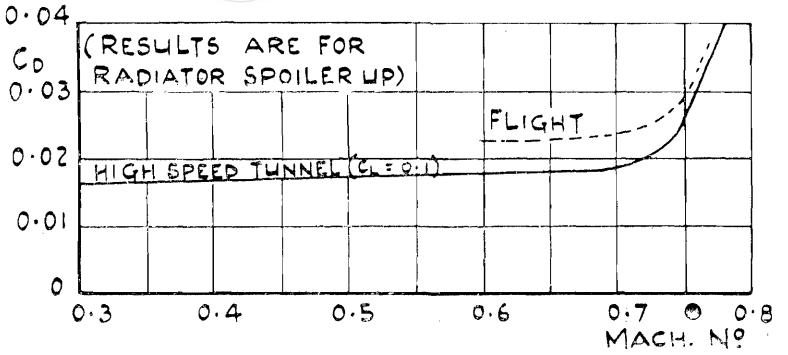

FIG. 171. Drag of Mustang I. (Comparison of flight and tunnel results).

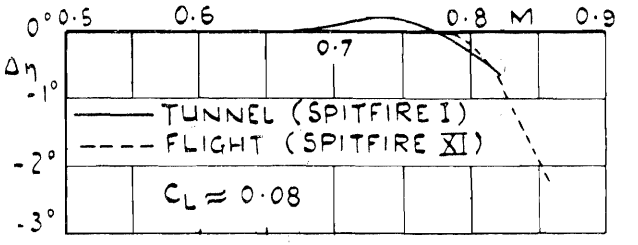

FIG. 173. Change of Elevator Angle to Trim with Mach Number—Spitfire. (Comparison of flight and tunnel results).

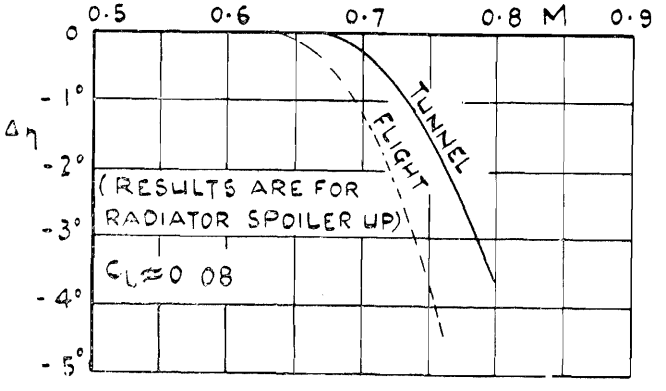

FIG. 172. Change of Elevator Angle to Trim with Mach Number—Mustang I. (Comparison of flight and tunnel results.)

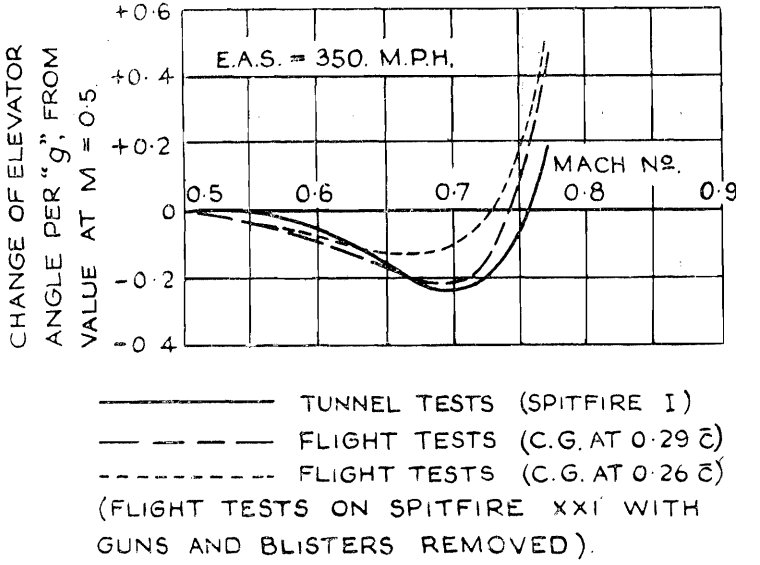

FIG. 174. Elevator Angle per "*g*"—Spitfire. (Comparison of flight and tunnel results).

PRINTED IN GREAT BRITAIN

Publications of the Aeronautical Research Committee

TECHNICAL REPORTS OF THE AERONAUTICAL RESEARCH COMMITTEE—

1934–35 Vol. I. Aerodynamics. 40*s.* (40*s.* 8*d.*)
Vol. II. Seaplanes, Structures, Engines, Materials, etc. 40*s.* (40*s.* 8*d.*)

1935–36 Vol. I. Aerodynamics. 30*s.* (30*s.* 7*d.*)
Vol. II. Structures, Flutter, Engines, Seaplanes, etc. 30*s.* (30*s.* 7*d.*)

1936 Vol. I. Aerodynamics General, Performance, Airscrews, Flutter and Spinning. 40*s.* (40*s.* 9*d.*)
Vol. II. Stability and Control, Structures, Seaplanes, Engines, etc. 50*s.* (50*s.* 10*d.*)

1937 Vol. I. Aerodynamics General, Performance, Airscrews, Flutter and Spinning. 40*s.* (40*s.* 9*d.*)
Vol. II. Stability and Control, Structures, Seaplanes, Engines, etc. 60*s.* (61*s.*)

1938 Vol. I. Aerodynamics General, Performance, Airscrews, 50*s.* (51*s.*)
Vol. II. Stability and Control, Flutter, Structures, Seaplanes, Wind Tunnels, Materials. 30*s.* (30*s.* 9*d.*)

ANNUAL REPORTS OF THE AERONAUTICAL RESEARCH COMMITTEE—

1933–34 1*s.* 6*d.* (1*s.* 8*d.*)
1934–35 1*s.* 6*d.* (1*s.* 8*d.*)
April 1, 1935 to December 31, 1936. 4*s.* (4*s.* 4*d.*)
1937 2*s.* (2*s.* 2*d.*)
1938 1*s.* 6*d.* (1*s.* 8*d.*)

INDEXES TO THE TECHNICAL REPORTS OF THE ADVISORY COMMITTEE ON AERONAUTICS—

December 1, 1936 — June 30, 1939.	R. & M. No. 1850.	1*s.* 3*d.* (1*s.* 5*d.*)
July 1, 1939 — June 30, 1945.	R. & M. No. 1950.	1*s.* (1*s.* 2*d.*)
July 1, 1945 — June 30, 1946.	R. & M. No. 2050.	1*s.* (1*s.* 1*d.*)
July 1, 1946 — December 31, 1946.	R. & M. No. 2150.	1*s.* 3*d.* (1*s.* 4*d.*)
January 1, 1947 — June 30, 1947.	R. & M. No. 2250.	1*s.* 3*d.* (1*s.* 4*d.*)

Prices in brackets include postage.

Obtainable from

His Majesty's Stationery Office

London W.C.2 : York House, Kingsway
[Post Orders—P.O. Box No. 569, London, S.E.1.]

Edinburgh 2 : 13A Castle Street
Birmingham 3 : 2 Edmund Street
Bristol 1 : Tower Lane
Manchester 2 : 39 King Street
Cardiff : 1 St. Andrew's Crescent
Belfast : 80 Chichester Street

or through any bookseller.

S.O. Code No. 23-2222*